FRETTING FATIGUE IN STEEL BOLTED CONNECTIONS

A Thesis Submitted to the

College of Graduate and Postdoctoral Studies

in Partial Fulfillment of the Requirements

for the Degree of Master of Science

In the Department of Civil, Geological and Environmental Engineering

University of Saskatchewan

Saskatoon

By

PEDRO CORDOVA ALCIVAR

PERMISSION TO USE

In presenting this thesis in partial fulfilment of the requirements for a Postgraduate degree from the University of Saskatchewan, I agree that the Libraries of this University may make it freely available for inspection. I further agree that permission for copying of this thesis/dissertation in any manner, in whole or in part, for scholarly purposes may be granted by the professor or professors who supervised my thesis work or, in their absence, by the Head of the Department or the Dean of the College in which my thesis work was done. It is understood that any copying or publication or use of this thesis or parts thereof for financial gain shall not be allowed without my written permission. It is also understood that due recognition shall be given to me and to the University of Saskatchewan in any scholarly use which may be made of any material in my thesis/dissertation.

Requests for permission to copy or to make other use of material in this thesis in whole or part should be addressed to:

Head of the Department of Civil, Geological and Environmental Engineering
57 Campus Drive
University of Saskatchewan
Saskatoon, Saskatchewan S7N 5A9
Canada

OR

Dean
College of Graduate and Postdoctoral Studies
University of Saskatchewan
116 Thorvaldson Building, 110 Science Place
Saskatoon, Saskatchewan S7N 5C9
Canada

ABSTRACT

The steelwork in a potash mineshaft is subjected to repeated lateral loads due to the lateral motion of the cages and skips that transport personnel, ore, and equipment up and down the mineshaft. As a result, the steel assemblies, including their bolted connections, must be designed to prevent failure due to fatigue. However, due to uncertainty regarding the fatigue behaviour of the connections, designers must take a very conservative approach, which could result in an uneconomical design.

The main objective of this research was to determine the fatigue behaviour of slip-critical bolted connections when different bolt types and surface finishes are used. A325 high strength bolts and C50LR Huck tension control bolts were used as the different bolt types. As-received mill scale steel plates (Class A surface finish) and blast-cleaned surfaces with a Cathacoat 302HB coating (Class B surface finish) were used as the different finishes. A digital image correlation system, as well as optical and scanning electron microscopic examination were used to characterize the modes of failure of the specimens.

Bolted connections assembled with the Class A surface finish failed due to fretting fatigue damage and crack initiation took place some distance away from the hole in a partial slip region between a stick region adjacent to the bolt hole and a gross slip region further from the hole where the relative motion between the plates was highest. On the other hand, specimens with the Class B surface finish failed due to bending fatigue caused by the eccentricity between the tension forces in the plates in the single-lap bolted joints, and crack initiation took place at the hole edge where the stress concentration was higher. The bolt type did not have a large effect on the fatigue behaviour, except that the tension in the tension control bolts may have been slightly higher, resulting in a slight improvement in the fatigue life. In general, the fatigue life results were lower than those in the S-N curve given in CSA S16-14, differing from the standard curve by an increasing margin as the stress range increased due to the effects of bending within the specimens.

ACKNOWLEDGEMENTS

I would like to thank my supervisor Dr. Leon Wegner for giving me the opportunity to develop this research project. His support and advice throughout the project encouraged me to execute the experimental program and the preparation of this thesis.

I would like to thank my committee members Dr. Ian MacPhedran and Dr. Moh Boulfiza for their guidance, suggestions and feedback throughout the program.

The financial support provided by the University of Saskatchewan, my supervisor, the Natural Sciences and Engineering Research Council of Canada (NSERC), the companies BHP Billiton Canada Inc., and Stantec Consulting Ltd. is also gratefully acknowledged.

DEDICATION

To my wife Andrea Trivino and daughter Monica Cordova for their support and love.

To my father Pedro Cordova, mother Monica Alcivar, and brother Gabriel Cordova for transmitting me their teachings, experiences and principles for my personal development throughout my life.

TABLE OF CONTENTS

LIST OF TABLES

LIST OF FIGURES

CHAPTER 1

INTRODUCTION

1.1 Background

The steelwork in a typical mineshaft consists of vertical steel guides periodically supported laterally by horizontal bunton sets that consist of a main bunton beam and several cantilevered beams. Bolted connections are commonly used in bunton sets, which are generally constructed with hollow structural sections (HSS). Large cages and skips are used to transport personnel, equipment, and materials such as ore up and down the mineshaft. During the transportation process, the guides and buntons, along with their bolted connections, are subjected to repeated lateral loads due to the lateral motion of the cages and skips. One of the problems encountered in the design of the steelwork is to define the fatigue life of the bolted connections.

When the elements of a steel structure fail statically, they do so usually after experiencing large deformations, because the limit of elasticity has been exceeded; the element can therefore be replaced before fracture occurs. Thus, static failure has the advantage of warning of its presence. On the other hand, fatigue failure takes place when an initiated crack has propagated long enough for its length to become critical, and this happens without much visible deformation. Therefore, it is important to detect an initiated crack to prevent failure. However, in bolted connections, the crack often initiates at the contact interface so that it cannot be detected until it has propagated and grown.

The Canadian steel design standard, CSA S16-14, defines just one S-N curve for the fatigue performance of any type of bolted connection, without taking into account different variables such as the size of bolts, configuration of the connection, bolt type, plate material, etc. A study focused on the fatigue behaviour of slip-critical connections is needed to determine whether this single curve is applicable across the full range of potential values for the several variables found in the bolted connections of mineshafts, especially bolt type and surface finish, in order to ensure the most economical and safe connection designs.

To adequately predict the fatigue behaviour of bolted connections, it is necessary to conduct small scale tests to determine crack initiation sites and their fatigue lives. Most of the studies found in the scientific literature focus on the level of pre-tension applied to bolts as the main variable that can enhance fatigue life in a bolted connection. The influence of other variables, including surface roughness and bolt type, must be determined to develop a more complete understanding of the fatigue behaviour.

According to the Canadian steel design standard, CSA S16-14, cyclic loads do not cause fatigue failure in high-strength bolts when they are loaded in shear. However, the connected plates can suffer unexpected failure due to the induced fretting fatigue phenomenon. Fretting is a complex phenomenon, involving several fields of knowledge, including materials science, mechanical contact and tribology. According to the glossary of terms of ASM International (Davis 1992), fretting fatigue causes damage on the contacting surfaces of a connection when oscillatory displacements of small amplitude occur between the components that are in contact and under pressure. As a consequence, fretting fatigue reduces the strength of assembled components that are subjected to fatigue loads. This can lead to crack initiation and crack propagation, and eventually to fatigue failure.

A number of factors associated with the fretting phenomenon in conjunction with variables related to bolted connections need to be understood for a safe design of bolted connections. The primary variable influencing the fatigue behaviour of bolted connections are the bolt pre-tension and its influence on the fretting fatigue failure behaviour should be understood to improve the fatigue strength of bolted connections. Wagle and Kato (2009) found that lower bolt pretension resulted in fatigue failure of bolted connections at the bolt hole, whereas for higher bolt pretension, fretting induced failure occurred at a certain distance away from the bolt hole. Shankar and Dhamari (2002) confirmed that fretting fatigue caused crack initiation away from the hole edge due to the stress concentration associated with the fretting phenomenon. Benhaddou et al. (2014) investigated the effect of clamping force in double-lap bolted connections and confirmed that lower bolt pre-tension led to bearing of the bolt against the plate and caused failure at the hole edge (net section). Chakherlou et al. (2012) provided the reason for the fretting phenomenon within the contact interface, confirming that frictional forces were induced at the contact interface due to the

relative displacement between the contacting surfaces. They also observed that a higher clamping force improved the fatigue life of bolted connections because it created compressive stresses around the hole.

Furthermore, Kartal et al. (2011) measured the relative displacement close to the contact area using a Digital Image Correlation (DIC) technique and found that fretting was initiated due to the relative displacements within the partial slip region close to the hole edge of the bolted connection. They also recommended that the contacting surfaces be prepared before assembling the connection to have a higher slip coefficient at the contact interface.

This observation was further explored by Reza et al. (2016), who showed that the surface characteristics have a great impact on the fatigue failure of bolted connections. Since the surface roughness is directly proportional to the slip coefficient, contacting surfaces with a higher slip coefficient are always preferred for bolted connections. It was observed that contacting surfaces with a uniform and rough surface profile could reduce the magnitude of the relative displacements and thus reduce the occurrence of fretting wear or fretting fatigue. Although a number of research works have focused on characterizing the fatigue behaviour of bolted connections, many of the important variables such as bolt type and type of contacting surface must still be analyzed to provide a safe design for structures assembled using bolted connections.

1.2 Objectives

The primary objective of this study was to develop a better understanding of the fatigue behaviour and failure mechanisms of slip-critical bolted connections assembled with different types of bolts and the two surface finishes defined in CSA S16-14 (Class A and Class B). Specific sub-objectives include the following:

- To characterize the surface profiles of the as-received Class A and Cathacoat 302HB coated Class B surface finishes and to determine the effect of surface finish on the slip resistance and slip coefficient of bolted connections;
- To determine the influence of surface finish on the fatigue life and failure mechanisms of slip-critical bolted connections, considering Class A and Class B surface finishes;

- To determine the influence of bolt type on the fatigue life and failure mechanisms of slip-critical bolted connections, considering standard high strength bolts (A325) and tension control bolts (C50LR Huck bolts);
- To quantify the fatigue life of single lap joint slip-critical bolted connections at more than three different load levels in order to define the S-N curve for each type of connection, and to compare this with the CSA S16-14 defined S-N curve for Detail Category B;
- To determine the influence of bending, inherent in the single-lap joint specimen, on the fatigue life and failure mechanisms of slip-critical bolted connections; and
- To develop an understanding of the mechanisms of crack initiation for the different types of specimens.

1.3 Scope and Methodology

In this thesis, the fatigue behaviour of bolted connections under fretting conditions was experimentally determined. Different series of fatigue tests were conducted on small single-lap slip critical bolted specimens under different load levels to measure the fatigue life and observe the mechanisms of failure. The two main variables that were studied were the surface finish type and the bolt type. Two different types of faying surfaces (Class A and Class B) and two bolt types (A325 HSB and C50LR Huck tension control bolts) were tested.

Three groups of samples were prepared, and each one was subjected to a number of different stress ranges. The first group consisted of connections using a Class A surface finish and A325 HSB, the second group consisted of connections using a Class B surface finish and A325 HSB, and the third group consisted of connections using a Class B surface finish and C50LR Huck tension control bolts.

For plotting the stress amplitude versus number of cycles to failure (S-N) curves, tests were conducted at more than three stress range levels for each group of specimens. For these tests, the stress ratio (R) and frequency *(f)* of the cyclic load remained constant at 0.0909 and 10 Hz, respectively, to remove any influence of these variables.

During four fatigue tests, a digital image correlation system (Correlated Solutions, Inc, USA) was used to capture images of the bolted specimens in order to determine their

displacements in the directions parallel and perpendicular to the applied load. The measurements were useful to determine the magnitude of the relative motion (slip) between the plates over a fatigue cycle. Also, the strain fields were determined, which then were used to calculate the curvature present in the single lap bolted specimens due to the inherent bending effect.

To understand the fatigue failure mechanisms, it was necessary to observe the damage caused by fretting wear and identify the location of crack initiation. Once the samples failed, their contact surfaces were examined using optical and scanning electron microscopes to identify the different features that occurred due to the fretting phenomenon. In addition, four tests were interrupted, each after a different number of cycles and before the sample failed, in an attempt to determine the crack initiation life.

1.4 Thesis outline

Chapter 1 presents the background about fretting fatigue in bolted connections, the objectives of this research, the scope, and summary of the methodology.

In Chapter 2, the literature review is presented, providing a fairly general compilation of the most important concepts and the necessary theory for the study of fatigue. The literature related to previous studies of fretting fatigue in bolted connections is reviewed to define the variables and methodology for this research.

In Chapter 3, the experimental methods are explained, including a description of the properties of the materials used for the plates, the surface finishes and bolt types, and the design of the test specimens. In addition, the equipment used during the experimental program, including the test machine, the Digital Image Correlation system and the software packages, is presented. Finally, the morphological characterization procedure, equipment and analysis are explained.

Chapter 4 presents the results of the experimental investigations, including the fatigue life measurements and S-N curves, and a comparison of the specimens with the different combinations of variables tested. The chapter also provides a presentation, discussion and analysis of the relative displacements at the contact interface of the bolted connection

samples, the features found during the morphological characterization of the fracture surfaces and contact surfaces and the S-N curves for each specimen type.

Finally, the summary and conclusions of the investigation and recommendations for future work are provided in Chapter 5.

CHAPTER 2

LITERATURE REVIEW

2.1 Introduction

Structural steel members are often assembled using slip-critical bolted connections and these connections typically use high strength bolts for joining the structural members. Structures such as bridges and those within mineshafts are subjected to fatigue loading during their normal operation. In such cases, the slip-critical bolted connections are prone to fatigue failure, which is of critical concern for the safe operation of these structural assemblies. Fisher et al. (1998) stated that civil engineering structures, including mineshaft structures, bridges, crane support structures, stacks and masts, and offshore structures usually fail catastrophically under fatigue loading conditions without any warning. At present, the design methods used to prevent fatigue failure are based on statistical data and, when designed to ensure an adequate margin of safety, the design can be very conservative. Hence, researchers have focused on analyzing the various parameters associated with slip critical bolted connections for understanding their fatigue failure behaviour.

In bolted connections, the shear load is transferred between the connected plates either by bearing of the bolts against the bolt holes or by friction between the plates. Kulak et al. (1987) state that for connections in which the bolts have not been adequately pretensioned, a stress concentration is created in the plate around the bolt hole (net section area) due to load transfer between the plates and the bolt shank by bearing. This can initiate the formation of a crack at the edge of the hole where the bolt and the plate contact each other. Eventually, fatigue failure occurs in the plate due to the repeated impact between the bolt and the plate.

On the other hand, when the bolts have been pretensioned, the applied load is transferred by friction between the plates, which can induce fretting fatigue (Kulak et al. 1987). In this case, there is not a stress concentration around the hole. Instead, cracks develop at the boundary between a stick region near the hole, where the contact pressure is highest, and a slip region some distance from the hole (the partial slip region). This phenomenon is defined as fretting fatigue and must be adequately accounted for to ensure a safe fatigue design. The main factors that affect the fretting fatigue behaviour of bolted connections are bolt

pretension and slip coefficient. According to Kulak et al. (1987), the yield strength of the connected plates does not affect the fretting fatigue life of a bolted connection.

2.2 Slip-critical connections

Slip-critical bolted connections are recommended for structural members that are subjected to fatigue loads. The slip-critical connection is designed to meet a service limit state, in which working loads are not allowed to exceed the slip resistance. Although, theoretically, slip-critical connections are not subjected to shear and bearing loads, these connections must have enough shear and bearing resistance to withstand an overload generated by slip. For structural members assembled with bolted connections, the slip resistance generated at the contact interface depends on the bolt pre-tension and the slip coefficient (k_s). A higher slip coefficient (k_s) or bolt pretension results in improved resistance to relative sliding between the contacting plates and improved fatigue resistance (Kulak et al. 1987). Since the bolt pretension depends on the type of bolt used for slip-critical bolted connections, it is necessary to account for the bolt type used in structural assemblies.

2.2.1 Bolt type

Different types of high strength structural bolts are used in slip-critical bolted connections, which affects the level of applied pretension and the installation process. The installation process ensures that the required minimum level of pretension in the bolt is reached. Additionally, there are no reports of fatigue failures at the contact interface of the bolt head or washer with the connected material (plates). Therefore, it is understood that the geometry of the bolt head, nut or collar and washers may not affect the fatigue behaviour of a bolted connection.

The influence of bolt type in slip-critical bolted connections depends on the level of bolt pretension that the bolts apply to the connection in order to generate slip resistance (Josi et al. 1999). It is clear that a high level of bolt pretension improves the fatigue life of a connection due to the reduced relative displacement between the contacting plates (Josi et al. 1999). The level of pretension applied by a structural bolt depends on the bolt's tensile strength, which is defined by the bolt material's carbon content or the grade of bolt used.

The most common bolt grades are SAE Grade 5 or Grade 8 bolts, which are equivalent to A325 and A490 high strength bolts, respectively. The minimum level of bolt pretension recommended in the CSA S16-14 standard is 70% of the tensile strength of the bolt material (CSA S16-14 2014). As a result, a higher tensile strength leads to a higher level of applied bolt pretension.

A325 standard high strength structural bolts (HSB) (Figure 2.1) are widely used in steel structures. These bolts consist of a head, a shank, and a threaded length. A washer is commonly used on the side of the nut and washers can also be used on the bolt head side. The pretension of these bolts is applied using a turn-of-the-nut method after snug tightening. The amount of turn applied depends on the bolt length and bolt diameter. This method theoretically ensures that at least 70% of bolt pretension is applied to the bolt joint.

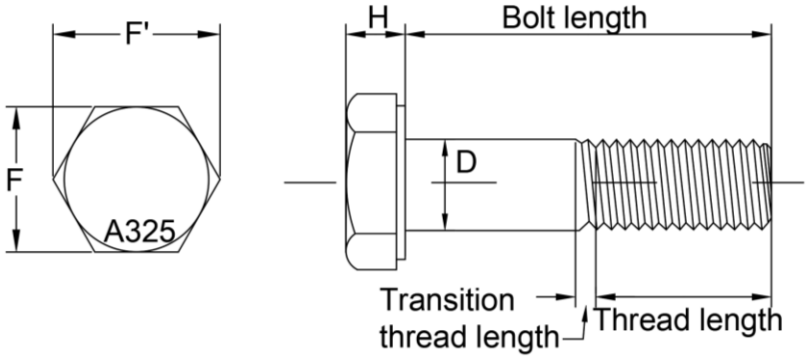

Figure 2.1 ASTM A325 High-strength bolt (based on figure on page 6-176 from CISC 2016).

Tension control bolts are another bolt type that is commonly used in steel structures. Undershute and Kulak (1994) explain that a tension control bolt has a splined end, which extends beyond the threaded length of the bolt. These bolts also have an annular groove between the threaded portion of the nut and the splined end. The installation of these bolts can be carried out using special equipment and the installation procedures may vary from one manufacturer to another.

The C50LR Huck bolt (manufactured by Alcoa Fastening Systems & Rings, USA), shown in Figure 2.2, is one type of tension control bolt that is installed using a special electrically-powered hydraulic tool with a nose assembly. The nose assembly slips over the splined end of the bolt and applies the required level of pretension. Once the required pretension is applied, the bolt snaps off at the annular groove. According to the

manufacturer, this method ensures that a consistent bolt clamping force is applied to the joint.

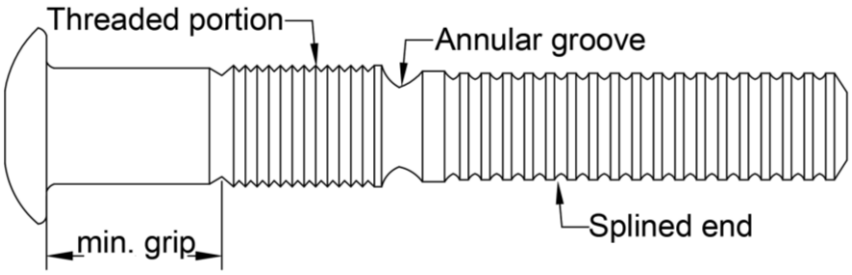

Figure 2.2 C50LR Huck tension control bolt (based on figure on page 4 from Alcoa 2017).

Very little information is available in the scientific literature about the fatigue performance of bolted connections using A325 HSB, and no research study has been found related to the fatigue behaviour of bolted connections using C50LR Huck tension control bolts. As a result, the only source of information available to guide this research project in terms of the expected outcome is CSA S16-14 (2014), which provides a common S-N curve for bolted connections.

2.2.2 Surface finish at the contact interface

Slip-critical connections rely on friction between the assembled plates along the contacting surfaces. The loads applied are transferred from one plate to the other through frictional forces developed between the connected faying surfaces. According to CSA S16-14 (2014), two surface finish types can be used for bolted connection assemblies:

1. Class A surface finish, which is an unpainted clean mill scale steel surface or a blast-cleaned surface coated with a Class A coating; and
2. Class B surface finish, which is an unpainted blast-cleaned steel surface or a blast-cleaned surface coated with a Class B coating.

The only parameter used by CSA S16-14 to differentiate the surface finishes is the slip coefficient (k_s). The slip coefficient is the ratio between slip resistance and pretension applied to the bolts. As recommended by Table 3 of CSA S16-14 (2014), the Class A surface finish provides a slip coefficient of 0.3 and the Class B surface finish provides a slip coefficient of 0.52. The slip coefficient is directly proportional to the roughness of the surfaces. The surface roughness quantifies the level of surface irregularities that can

contribute in developing an anti-slip property in the connection. The friction within the contact interface is caused by the combination of bolt pretension and surface roughness, and a rougher surface profile provides a higher the slip resistance within the slip-critical bolted connection.

The Research Council on Structural Connections (2014) indicates that the slip coefficient (k_s) is not dependent on the pre-tension of the bolt, coating thickness or bolt diameter under static loading conditions. However, they also indicate that the slip coefficient and the bolt pretension are the variables that affect both slip resistance and the failure behaviour of slip-critical bolted connections. Stankevicius et al. (2009) found that the level of pre-tension applied to A325 HSB did not affect the slip coefficient in A588 steel plates with a Class A surface finish. For their experimental specimens, the Class A surface finish consisted of as-received clean mill scale steel plates and degreased clean mill scale steel plates. Degreased plates provided better results for the slip coefficient.

Frank and Yura (1981) tested bolted connections under fatigue loads to determine the difference between uncoated (blast-cleaned surface) and coated specimens. They tested twenty samples in which they used three coatings, including organic zinc, organic zinc with epoxy topcoat, and inorganic zinc. The samples consisted of a long double lap joint with a line of four bolts on one side and two lines of bolts with two bolts per line on the other side. They reported that crack initiation took place at the edge of the hole in coated specimens. Figure 2.3(a) shows that crack initiation took place at the hole edge of the fourth hole of the connection in a specimen that had the organic zinc coating on its blast-cleaned surface and survived 272,030 cycles with a 310 MPa (45 ksi) stress range. Figure 2.3 (b) shows that crack initiation took place at a hole edge of the lowermost row line of two holes in a specimen that had an organic zinc with epoxy topcoat coating over a blast-cleaned surface and was subjected to a 241 MPa (35 ksi) stress range for 462,750 cycles. On the other hand, crack initiation took place at the surface of the gross section due to fretting fatigue in the blast-cleaned specimens. Thus, the blast-cleaned surface specimens demonstrated poorer fatigue life, as shown in Figure 2.4.

(a)

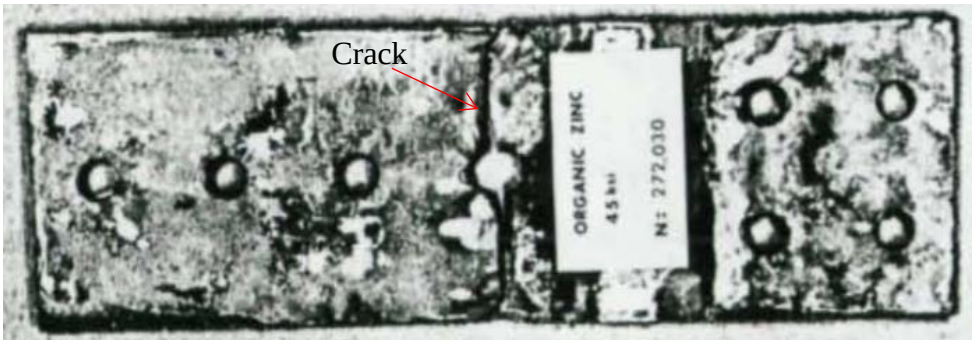

(b)

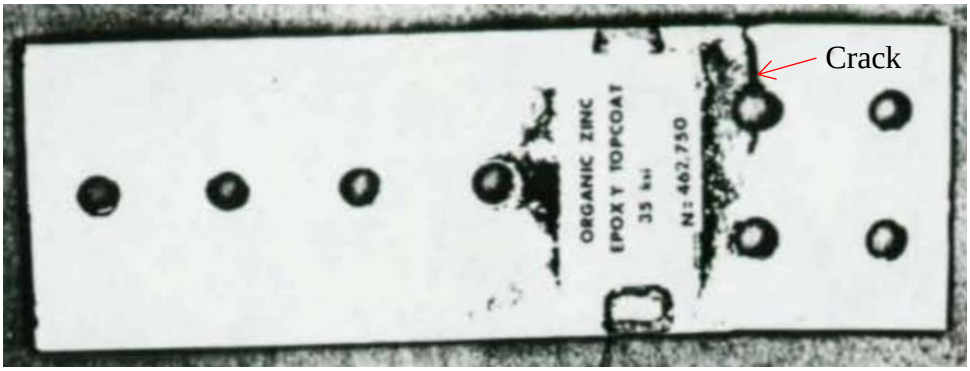

Figure 2.3 Crack initiation in specimens subjected to fatigue tests: (a) Specimen with organic zinc coating after 272,030 cycles at a 310 MPa stress range; and (b) Specimen with organic zinc and epoxy topcoat after 462,750 cycles at a 241 MPa stress range. (Frank and Yura 1981, Images used in accordance with 'Distribution statement' which states 'no restrictions' and 'made available to the public')

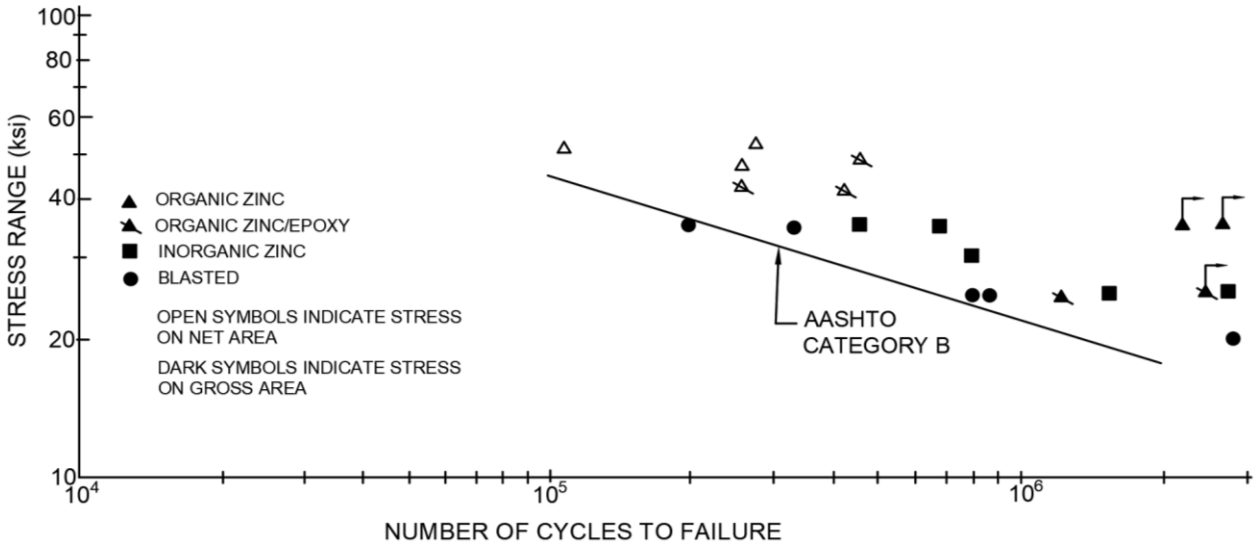

Figure 2.4 Fatigue test results with different surface finishes (based on Figure 89 from Frank and Yura 1981).

Annan and Chiza (2013) explained that the friction coefficient plays a major role in the slip resistance of a slip critical connection. A higher coefficient of friction is desirable for enhancing the strength (slip resistance) of a slip-critical connection, but its effect on fatigue life is not known. It was postulated that a higher slip coefficient can reduce the magnitude of the relative displacement between the plates, thus reducing the fretting effect and increasing the fatigue life. Surface roughness is closely connected to the coefficient of friction, and is therefore expected to affect fatigue failure behaviour. Surfaces with rougher and uniform surface profiles can create an interlocking effect between the two surfaces, thus increasing the coefficient of friction.

Reza et al. (2016) studied the effect of the surface roughness on the fretting fatigue behaviour of double-lap bolted joints. They found that the fretting damage was less severe in coated surfaces and the crack initiation site occurred at the hole edge due to the presence of a stress concentration there. However, for the uncoated specimens, the crack initiation site was found at a distance away from the hole and was caused by fretting fatigue.

2.2.3 Relative displacement in slip-critical connections

Figure 2.5 shows a typical load versus relative displacement curve for a slip-critical bolted connection tested under static tensile loading conditions, and identifies the different stages encountered in such a test (Minguez and Vogwell 2006). At the slip resistance stage, the load is transmitted by friction between the contacting surfaces. During this stage, the contacting plates deform elastically under the applied tensile loads. Once the slip resistance load is reached, the applied tensile load causes slip between the connected plates, which continues until the bolt begins to bear against the plate, at which point the connection becomes a bearing connection. The load is subsequently transferred by bearing of the bolts against the plates until failure occurs.

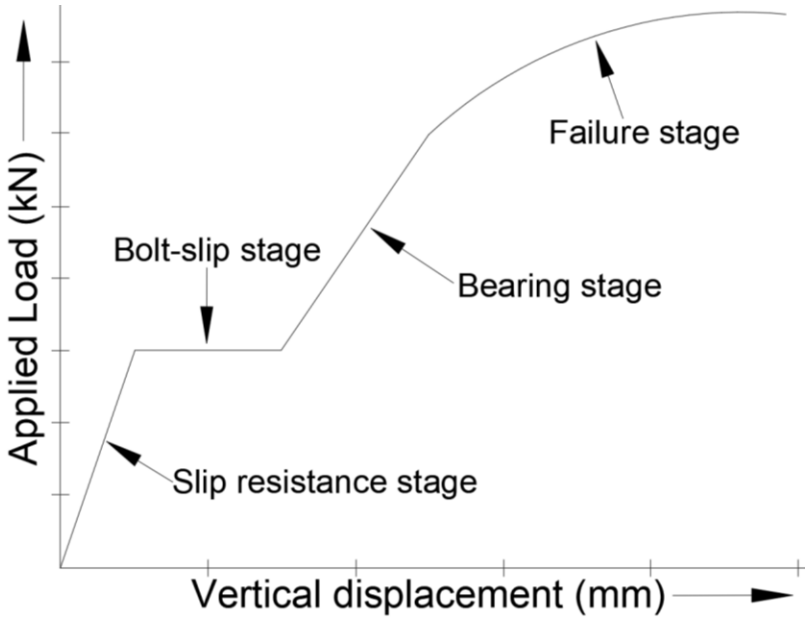

Figure 2.5 Typical load-displacement curve of a slip critical connection (based on Figure 3 from Minguez and Vogwell 2006).

When a slip-critical bolted connection is subjected to fatigue loads lower than its slip resistance, relative displacements of small magnitude will occur at the contact interface of the connected plates, depending on the magnitude of the external cyclic load. The induced relative displacement changes in phase with the applied fatigue loads; i.e., the maximum fatigue load (σ_{max}) induces a maximum relative displacement and the minimum load (σ_{min}) induces a lower relative displacement (Crevoisier et al. 2012). Consequently, the induced frictional force along the contact interface constantly varies between a maximum and a minimum value.

The relative motion between the plates causes fretting fatigue damage at the contact interface and produces stress concentrations at some distance away from the hole edge due to fretting (Xu et al. 2016). The varying relative displacement can be measured using a Digital Image Correlation (DIC) system, such as that shown in Figure 2.6 (Jimenez-Peña et al. 2017). This technique requires high resolution cameras and a data acquisition (DAQ) system for capturing the specimen images with speckle patterns on its surface. The images are analyzed in order to determine the displacement and strain fields in an area of interest of the sample.

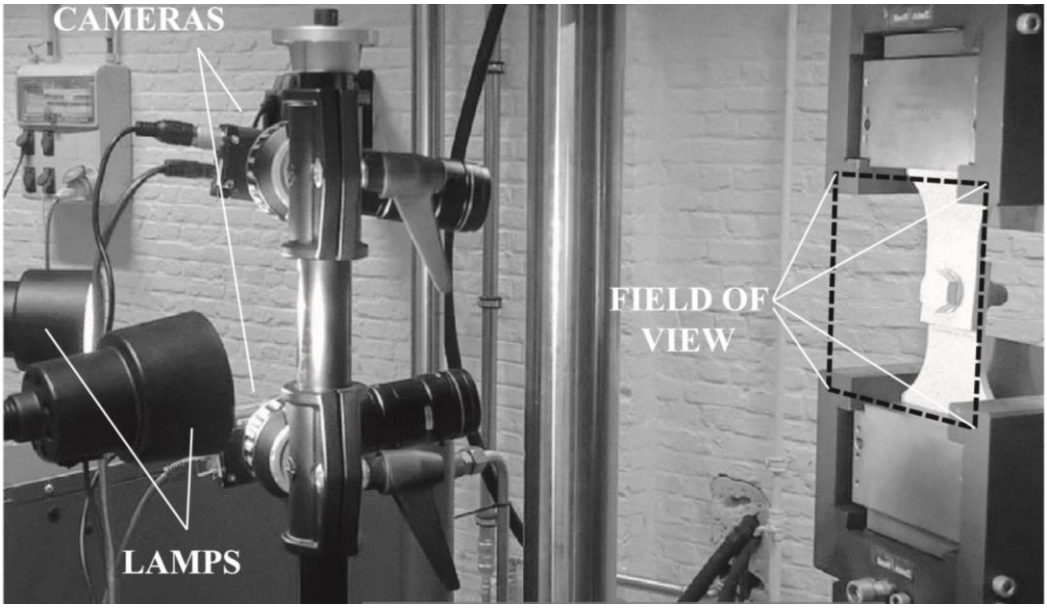

Figure 2.6 DIC set-up to measure the displacements during fatigue tests (Jimenez-Peña et al. 2017).

Figure 2.7 shows an image captured using the DIC technique of a bolted specimen subjected to fatigue loads. The relative displacement between the three plates was determined and Crevoisier et al. (2012) used that information to obtain the frictional properties at the contact interface. Nesládek et al. (2012) used the Digital Image Correlation (DIC) technique to measure the displacements, strains and estimated friction coefficients during fretting fatigue tests. According to them, the DIC technique provided enough information, such as local displacements in the vicinity of the stick-slip interface, and was very useful in calibrating the friction coefficient for a numerical model.

Mello et al. (2017) used the DIC technique to measure the strains during fatigue tests. They stated that DIC results can be biased by producing drift, spatial distortions and magnification uncertainties, which required correction based on the image of a certified grid. In addition, the technique has other disadvantages, such as the dependence on the quality of the images taken during the tests, and difficulties in measuring the deformations with a discontinuity in the specimens. The light necessary for the realization of the tests can be natural light, although sometimes external light sources are used to improve the quality of the images.

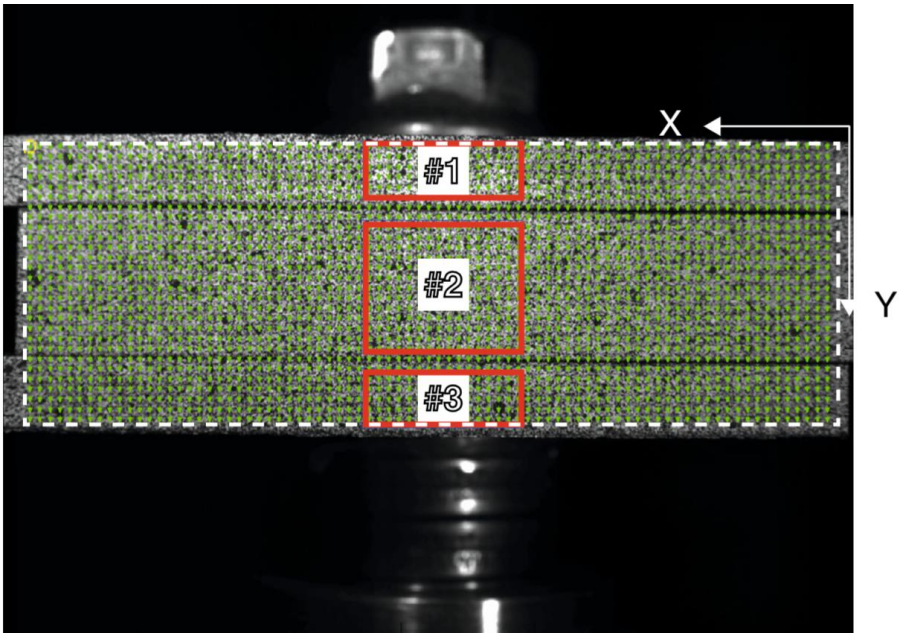

Figure 2.7 Image captured of a bolted specimen using a DIC system during a fatigue test (Crevoisier et al. 2012).

2.3 Fatigue Characterization

2.3.1 Initial considerations

The improvement of the fatigue resistance of a bolted connection is a challenging field due to the numerous factors (around fifty) that affect the fatigue behaviour of bolted connections. Among them, the most important variables are pretension of the bolts, the number of bolts, bolt size, bolt and plate material properties, the coefficient of friction between plates, the frequency of cyclic load, stress amplitude, mean load, and defects in the materials (Minguez and Vogwell 2006). Fatigue failure is one of the most common and complex failure mechanisms experienced in bolted connections due to their complex geometries, which produce stress concentration sites within the connected plates (Xu et al. 2016). Stress concentrations can occur around the drilled hole because of the change in geometry and imperfections introduced during the drilling process (Chakherlou et al. 2010).

2.3.2 Definition of fatigue and cyclic load parameters

According to Hamrock et al. (1999), the fatigue strength of a structural component is the stress level at which fracture occurs after being subjected to a given number of cycles. The number of cycles that are needed to cause fracture at a specific stress level is defined as the

fatigue life (Fisher et al. 1998). Hamrock et al. (1999) also summarizes the main parameters associated with cyclic loading. The stress range (σ_r) is defined as the algebraic difference between the maximum (σ_{max}) and minimum (σ_{min}) applied stresses. The stress amplitude (σ_a) is calculated as half of the stress range, and the stress alternates about the mean stress (σ_m), which is the average between the maximum and minimum stresses applied during a load cycle. These variables are shown in Figure 2.8 for a non-zero mean stress and maximum and minimum tensile stresses.

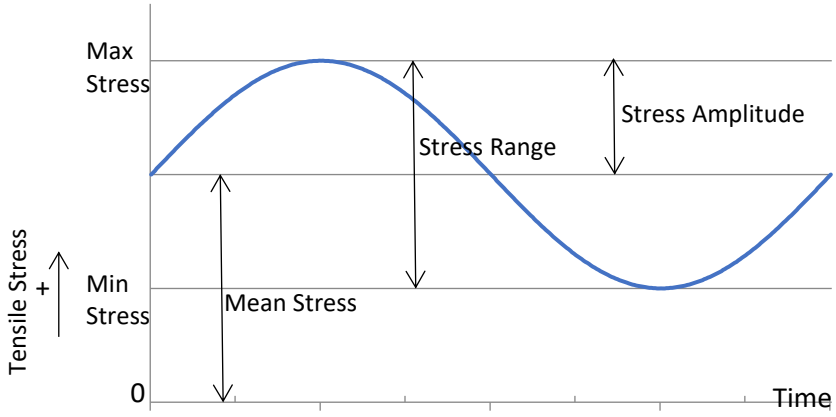

Figure 2.8 Definition of parameters associated with tensile stresses.

The behaviour of a structural component subjected to cyclic loading depends on the type of fatigue regime, such as low cycle fatigue or high cycle fatigue. Low cycle fatigue failure occurs when the applied stress range is high enough to cause plastic strains. The low cycle fatigue test is generally conducted under controlled strain. High cycle fatigue occurs with low stress ranges that cause elastic strains in the structural components. In other words, if the magnitude of the applied stress range is high, the number of cycles to failure will be low, whereas if the magnitude of the applied stress range is low, the number of cycles to failure will be high

According to Woo (2017), there are three different kinds of cyclic loadings used for fatigue testing: reverse stress cycles, repeated stress cycles, and random stress cycles. Stresses that fluctuate symmetrically about a mean stress of zero are termed reverse stress cycles. A repeated stress cycle (shown in Figure 2.8) occurs when the stress amplitude remains constant but the maximum and minimum stresses differ in magnitude. Random

stress cycling occurs when the applied fatigue loading varies randomly in amplitude and frequency with respect to time.

2.3.3 The S-N curve

The results of a series of fatigue tests are plotted in a log-log graph of the stress range versus the number of cycles to failure. Stress range vs. number of cycles to failure (S-N) curves are used to determine the probable fatigue life of a structural element and are based on the average fatigue life of a given type of detail. The S-N curves for different detail categories for structural steel are available in CSA Standard S16-14 and are shown in Figure 2.9. The S-N curve for Detail Category B applies to bolted connections. In order to define the S-N curve of a material, many tests are required to get the number of cycles and apply statistically varied stress ranges, mean stresses, and stress ratios (Fisher 1977).

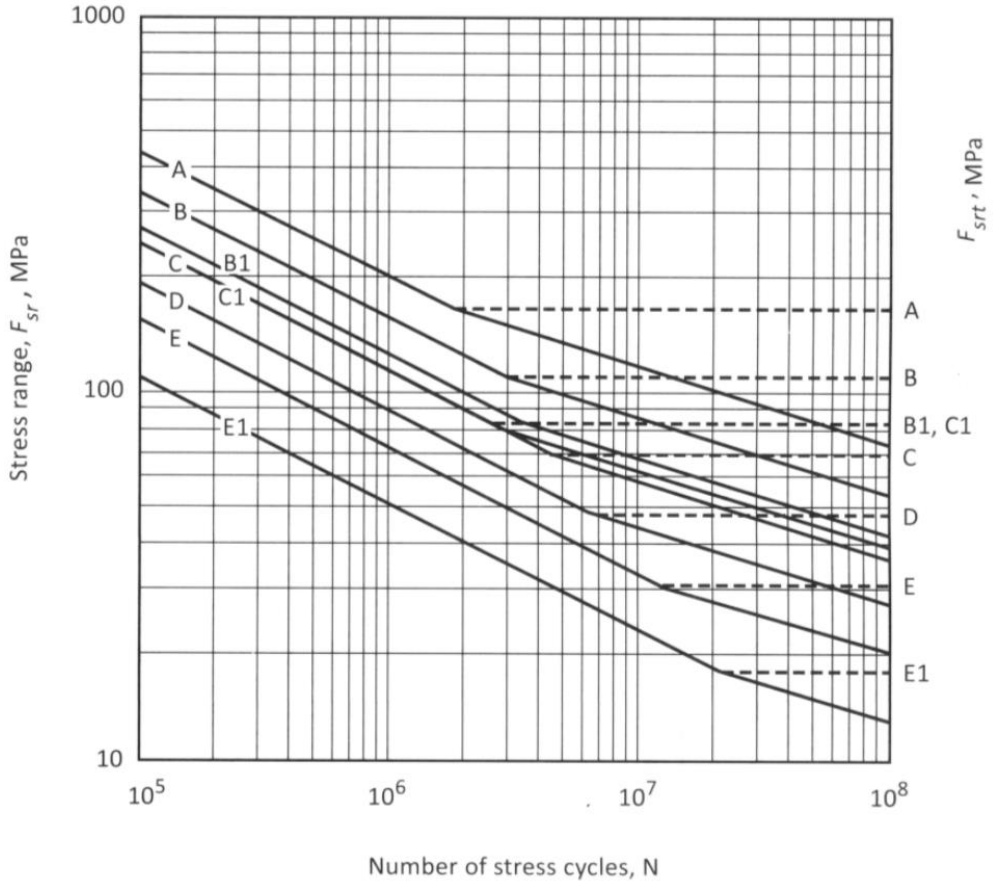

Figure 2.9 S-N curves for different detail categories available in CSA S16-14 and CSA S6-14 (Source: Figure 1, CSA S16-14 – Design of steel structures. © 2014 Canadian Standards Association).

The S-N curve for Detail Category B was developed by the National Cooperative Highway Research Program (NCHRP) sponsored by the American Association of State Highway and Transportation Officials (AASHTO) after conducting fatigue tests on high strength bolted shear splices in a fatigue strength study of steel beams with transverse stiffeners and attachments (Fisher 1977). The test results are shown in Figure 2.10 along with the S-N curve of Detail Category B, which was developed using 5% fractile values with a 95% confidence limit (i.e., 95% of the samples did not fail within the specified number of cycles at the applied stress range) (Fisher 1977). The results are scattered at every stress range. This is due to the different configurations of samples used during the tests. It was also found that the number of bolts in a line does not affect the fatigue behaviour of a bolted connection (Kulak et al. 1987). The data generated by fatigue tests are generally very scattered so that an S-N curve becomes a ‘‘best fit’’ curve of the data (Hertzberg 1996). Therefore, fatigue life and limits are specified in terms of probability. In the AASHTO study (Figure 2.10), the scatter in fatigue life decreased as applied stress range increased.

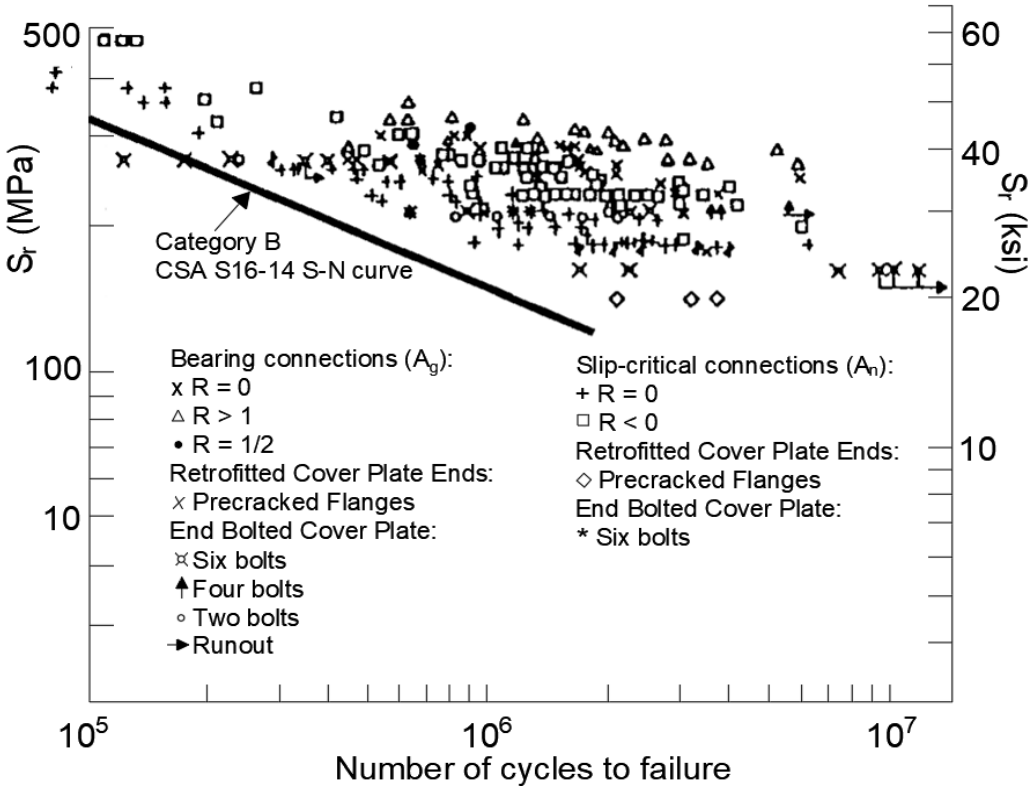

Figure 2.10 Fatigue test results of bolted connections used for the development of the S-N curve for Detail Category B (based on Figure 46 from Fisher et al. 1998. "Copyright © American Institute of Steel Construction. Reprinted with permission. All rights reserved.").

An applied stress range lower than the endurance limit will not cause fatigue failure, regardless of the number of cycles (Hertzberg 1996). Schneider and Maddox (2003) state that the endurance limit is generally defined for materials when the number of cycles to failure exceeds between 2 x 10^6 and 10^7 cycles. At the endurance limit, the stress range of the S-N curve becomes horizontal with respect to the number of cycles. It is also possible that an endurance limit is not present in an S-N curve. In this case, the stress will decrease continually as the number of cycles increases. If there is no endurance limit, fatigue failure will eventually occur regardless of the magnitude of the applied stress.

The fatigue life of a structural element can be determined using the principles of fracture mechanics. Most of the time, this approach is very challenging because the parameters like the size and shape of the initial defect and the stress gradient at the defect should be known in advance (Kulak et al. 1987). As a consequence, experimental fatigue tests are conducted in order to determine the fatigue life of specimens at different stress ranges to obtain the S-N curves.

In order to define the S-N curve, the specimens must be subjected to cyclic stresses at a constant stress range, and the number of cycles to failure must be measured. This procedure must be repeated successively with various stress ranges. Hamrock et al. (1999) explains that the data must be plotted as stress amplitude (S) versus the logarithm of the number of cycles to failure to generate the S-N curve. They also indicate that the results from these tests are very sensitive to the specimen alignment and the frequency of the cycles, which can lead to errors in the results.

In real life situations, the stress range or frequency may vary with time, as stated by Hamrock et al. (1999). This is not the case when fatigue testing is performed in a laboratory setting. The tests can be constant stress or strain controlled, as described by Hertzberg (1996). Stress controlled means that the tests are carried out under load control mode, while in strain controlled tests, the strains are controlled during the experiments. In both cases, cyclic hardening or cyclic softening can occur. Cyclic hardening occurs when the cyclic strain becomes smaller under constant stress amplitude. Cyclic softening implies that the stress to maintain constant strain amplitude decreases with the number of cycles.

The Manual on Statistical Planning and Analysis for Fatigue Experiments (Little and Jebe 1975) recommends that if there is no previous experimental S-N curve, the number of stress levels tested must be between six and eight. For preliminary tests, one or two specimens should be used per stress level. Then, in order to achieve reliable results, between 12 and 24 specimens must be tested, using at least four specimens per stress level. One of the main characteristics of fatigue test results used to define S-N curves is that they are very scattered (Schneider and Maddox 2003), which necessitates the use of replicate specimens. Two main reasons for the variability of the results are slight differences among the samples or the experimental conditions, which may not be carefully controlled during fatigue tests.

2.3.4 Specimen type

Dieter (1961) explains that there are two kinds of fatigue tests for bolted connections:

1. Tests conducted with real geometries; and
2. Tests conducted with simple geometries.

Both kinds of tests try to replicate the behaviour of bolted connections. The tests with real geometries try to replicate the exact behaviour of the structural components assembled with bolted connections when subjected to different stress amplitudes. This kind of test is important because it can simulate the bolted connection's behaviour when subjected to service loads, and this is sometimes necessary to acquire the complete knowledge of the causes of failure and to prevent the occurrence of failure during the service life.

In general, the tests with real geometries are complicated and require the use numerical tools like finite element analysis to identify the stress concentration sites and the strains in the areas of interest. Real geometry tests more difficult to conduct due to a number of requirements to replicate the actual structural behaviour. Wavish et al. (2009) states that tests with complex geometries are limited because they are expensive. There are some cases in which it is possible to simulate the behaviour of a real component using a simple geometry. Consequently, simple geometries are generally used, but it is difficult to replicate the exact behaviour of the real component.

Tests that use specimens with simple geometries can be used to determine the stress concentration sites and the strains in the contact zone, making the procedure relatively

simple. If the simple geometry tests can replicate the loading configuration of the real structure, then these types of experiments can provide sufficiently detailed information for understanding the failure behaviour of the real structure. Kulak et al. (1987) suggested that conducting fatigue tests using simple geometries under controlled conditions using representative variables can provide enough information about the behaviour of the original structural assemblies.

The different types of simple geometry specimens that have been used for fatigue testing of bolted connections found in the scientific literature are summarized in Table 2.1. Aluminum alloys were the focus of most of these investigations because of the importance in aerospace structures. Most of the studies chose to use double-lap bolted connections to avoid the eccentricity that occurs in single-lap connections. Also, most of the authors just used one bolt in the connection. The dimensions of the plates and bolts varied, depending on the plate material, the applied loads and objectives of the studies.

Table 2.2 shows the different levels of bolt tension or bolt torque applied by different authors in their experiments. Most of them found that fatigue life was improved when pre-tension was increased and their results allowed them to find the optimum pre-tension load or tightening torque for improving fatigue life. The optimum level varied depending on the materials used.

Table 2.1: Specimen types used by different authors in fretting fatigue tests of bolted connections.

Reference	Type of specimen	Number of bolts	Plate material	Plate thickness	Bolt Diameter
Maximov et al. (2012)	Single-lap	One	Carbon Steel	12 mm	M12
Jimenes-Pena et al. (2017)	Single-lap	One	High Strength Steel	6 mm	M16
Starikov (2004)	Single-lap	One	Aluminum alloy	3 mm	6 mm
Ferjaoui et al. (2014)	Double-lap	One	Aluminum alloy	4 mm	8 mm
Shankar and Dhamari (2002)	Double-lap	One	Aluminum alloy	3.2 mm	5 mm
Chakherlou et al. (2011)	Double-lap	Two	Aluminum alloy	3.2 mm	M6
Esmaeli et al. (2014)	Double-lap	One	Aluminum alloy	2 mm	M5
Liu et al. (2010)	Reverse double dog bone	Four	Aluminum alloy	7 mm	6 mm
Benhaddou et al. (2014)	Double-lap	One	Aluminum alloy	7.5 mm and 2.5 mm	6 mm
Minguez et al. (2006)	Double-lap	Two	Aluminum alloy	5 mm and 2 mm	M5
Chakherlou et al. (2012)	Double-lap	One	Aluminum alloy	3.2 mm	6 mm
Xu et al. (2016)	Single-lap	Two	Steel	5 mm	M20
Rezgui Maleki et al. (2012)	Single-lap	One	Aluminum alloy	5 mm	6 mm
Hämäläinen et al. (2015)	Double-lap	Two	High Strength Steel	6 mm	M16

Table 2.2: Different levels of clamping force or tightening torque used for tests.

Reference	Number of pre-tension levels or torque	Bolt Diameter
Jimenes-Pena et al. (2017)	Three (58%, 88% and 100% of design preload force)	16 mm
Chakherlou et al. (2011)	Three (0.25 N-m, 2 N-m, 4 N-m)	6 mm
Esmaeli et al. (2014)	Seven (from 1 to 7 N-m)	5 mm
Liu et al. (2010)	Five (from 5 kN to 9 KN)	6 mm
Benhaddou et al. (2014)	Three (5.9 kN, 11.7 kN, 17.6 kN)	6 mm
Minguez et al. (2006)	Four (1 N-m, 2.3 N-m, 3.5 N-m, 8 N-m)	5 mm
Rezgui Maleki et al. (2012)	Eight (from 0 to 8 N-m)	6 mm

2.4 Fretting fatigue in bolted connections

Although there are a number of factors associated with the fatigue failure of bolted connections, the leading failure mechanism consists of fretting induced surface damage, which promotes early crack initiation along the contact interface. Fretting fatigue occurs under a combination of contact pressure due to bold pretension and relative motion between the plates caused by the externally applied fatigue loads (Hämäläinen and Björk 2015). The stress concentration that occurs at the bolt hole under bearing conditions is decreased by bolt pretension (Chakherlou et al. 2007), which results in fretting fatigue stress concentration sites developing at the boundary between the stick and slip regions a certain distance away from the bolt hole. This stress concentration site promotes early crack initiation and subsequent failure, as shown in Figure 2.11.

Benhamena et al. (2011) identified the amplitude of relative displacement and the contact force as the main variables influencing fretting fatigue. This small displacement between the surfaces can induce surface damage that causes nucleation and subsequent propagation of cracks within the contact zone. According to Fisher et al. (1998), the differential strain between the connected plates is highest at the contact interface near the ends of a bolted connection; consequently, crack initiation due to fretting fatigue in slip-critical bolted connections occurs close to the first or last bolt hole in a line.

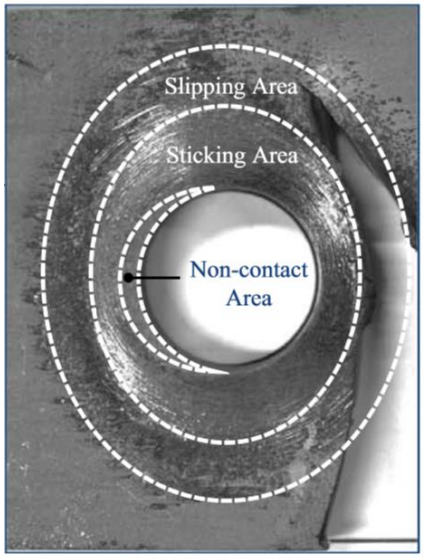

Figure 2.11 Fretting fatigue surface at the hole area, identifying the stick and slip regions and showing the fatigue crack that developed at the boundary between the two regions (Jimenez-Peña et al. 2017).

The induced frictional stresses along the contact interface around the stick and slip regions, as calculated using finite element analysis (FEA), is shown in Figure 2.12 (Jimenez-Peña et al. 2017). The higher stresses are concentrated around the partial slip region at a distance away from the hole edge. Lower stresses (yellow area) are induced in the global slip region where fretting wear takes place. The area around the hole was subjected to compressive stresses due to the clamping force applied by the bolts, which creates the stick region.

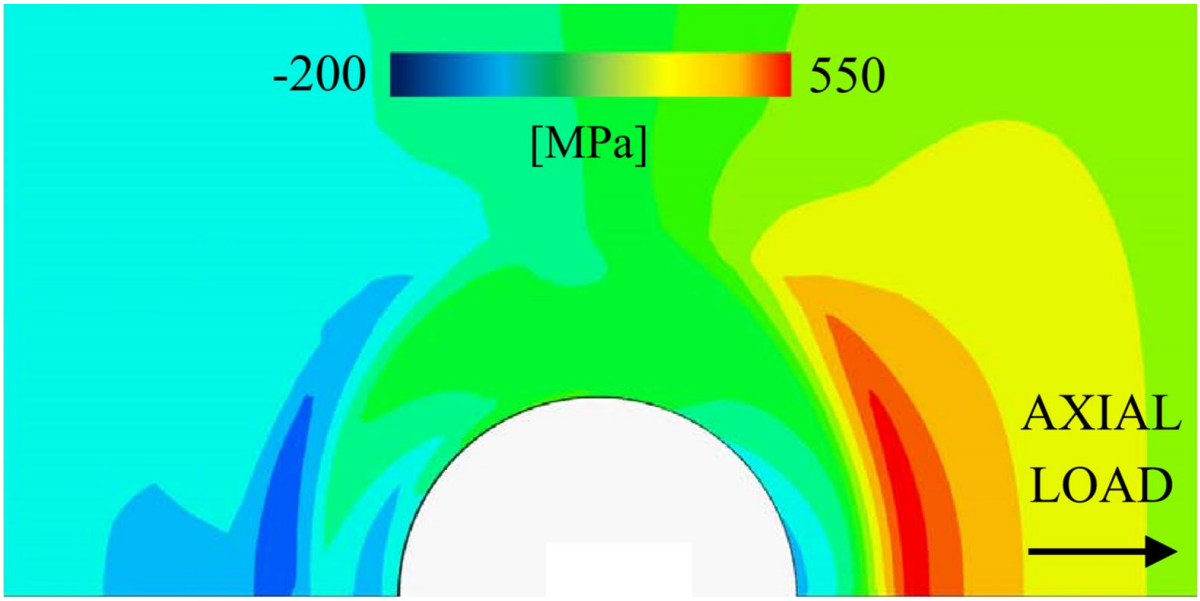

Figure 2.12 Tangential (frictional) stresses in the stick and slip regions around the hole area (Jimenez-Peña et al. 2017).

Fretting fatigue crack initiation sites are usually located at a certain distance away from the first hole of the loaded bolted connection, as seen in Figure 2.13 (Xu et al. 2016). In fretting fatigue, there is generally not only one crack initiation site, but multiple crack initiation sites that nucleate at the partial slip zone where the stress concentration and the fretting damage are higher. The multiple crack initiation sites cannot be detected easily during the experiment with measuring tools (e.g. scanning electron microscope).

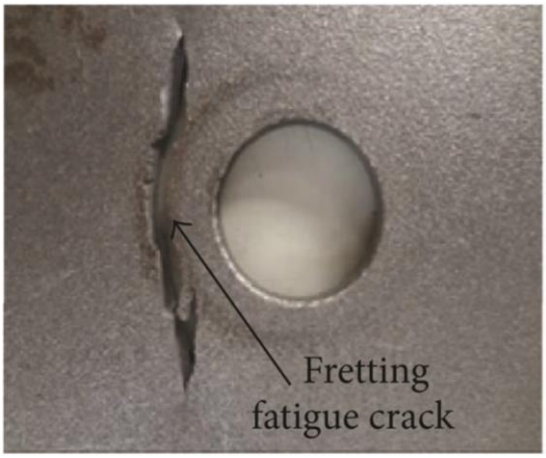

Figure 2.13 Fretting fatigue crack initiation zone in a bolted connection (Xu et al. 2016, CC BY 4.0).

Brown et al. (2007) tested double lap bolted joints with four bolts under fatigue loading conditions. The holes in the specimens were made using different techniques (drilled and punched), and they found that slip critical connections have a better fatigue behaviour than bearing type connections. Also, they found that the hole manufacturing method did not have any influence on the fatigue life of slip-critical connections.

When the contact force between the plates is increased by increasing the bolt pretension, the fatigue life also increases (Benhamena et al. 2011). It has been found that the crack initiation site changes when a pretension load is applied to the bolts. Crack initiation occurs very close to hole edge when the clamping force is low, while it occurs at a certain distance away from the hole due to partial slip when the pretension is high.

Different slip amplitudes can cause different amounts of fretting wear between the surfaces in contact, as shown in Figure 2.14. Shen et al. (2015) showed that as the relative slip amplitude increased, it resulted in earlier crack initiation due to the increased fretting that occurred. In this context, partial slip must be distinguished from gross slip due to their different effects on fretting and crack initiation.

Jiménez-Peña et al. (2017) conducted fatigue tests on bolted connections using different levels of pre-tension, explaining that they did not find enough information in the literature about fretting fatigue within bolted connections. They identified the torque applied to the bolt as the most significant variable that affects the fatigue behaviour of a high strength structural bolted connection. They used single lap bolted-connection specimens with a

single bolt to conduct the tests and designed the specimens according to the Eurocode 3 standard (British Standards Institution 2005). They considered three different torque levels, 58%, 88% and 100% of the design preload, as recommended by the standard. Fatigue failure of the specimens occurred on the contact area and the crack initiation site was always located at the intersection between the stick and slip regions away from the hole. They also concluded that an increase in pre-tension load improved the fatigue life of the specimens.

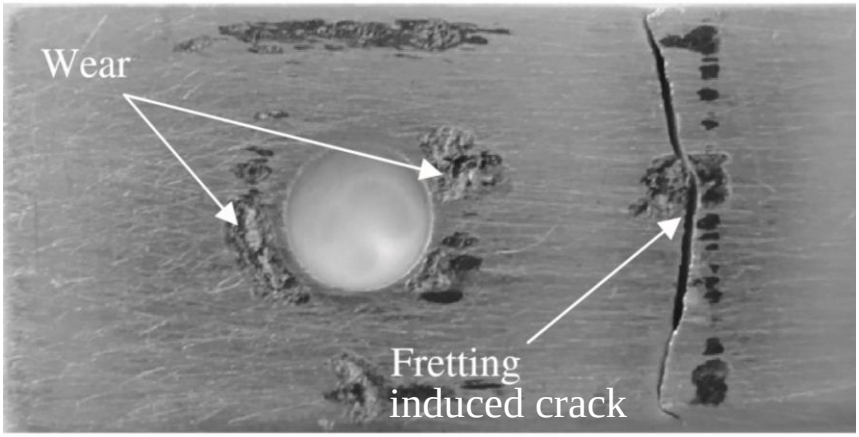

Figure 2.14 Fretting damage on the surface close to the hole edge (Chakherlou et al. 2011).

Esmaeili et al. (2014) observed that an improvement in fatigue strength could be attributed to the increase in frictional forces between the plates and decrease in bearing forces between the bolt and the hole as bolt pretension increased. Also, they believed that the compressive stresses applied by the bolts contributed to a reduction of the concentration of tangential forces at the partial slip region where crack initiation is caused.

Neu (2011) reviewed the different standards related to fretting fatigue and found a small number of testing standards for fretting fatigue. Their research work explained that the main obstacle for developing a standard for fretting fatigue tests was that there are many variables that need to be studied. For conducting experimental fretting fatigue analysis, the only generic standard test method available was developed by the Japan Society of Mechanical Engineers (JSME) in 2002. Neu also explained that ASTM task group E08.05.05 was developing a standard fretting fatigue test method and that their main objective was to define terminology and the means of collecting and reporting data.

In order to understand the fretting failure behaviour of bolted connections, the focus must be on understanding the mechanism of crack initiation and propagation. However, crack initiation sites are difficult to determine during experiments because these are often located within the closed contact interface and not visible during the test (Ferjaoui et al. 2014). Dieter (1961) described the three stages in fretting fatigue failure of bolted connections. First, the crack initiates within the partial slip region on the contact surface. Next, the crack grows or propagates in a direction normal to the applied load. Finally, failure occurs when the crack grows larger than the critical length, and the remaining cross-sectional area decreases.

Two kinds of features can be found on the fracture surface generated by fatigue crack propagation (Hertzberg 1996): striations, which are microscopic parallel lines; and beach marks, which appear in a ring pattern that expand from the origin of the crack. Both of them allow ascertaining the location of the crack tip at some point in time. Also, ratchet lines, which indicate multiple crack initiation sites and fracture planes, are typical of fretting fatigue fracture surfaces, as shown in Figure 2.15. In a ductile material such as steel, the crack propagates by plastic blunting and sharpening at the crack front. The characteristic feature of the fracture surface is the presence of striations, as shown in Figure 2.16. Each striation indicates the successive position of the advancing crack front at the end of each load cycle. The presence of striations on a fracture surface suggests fatigue failure.

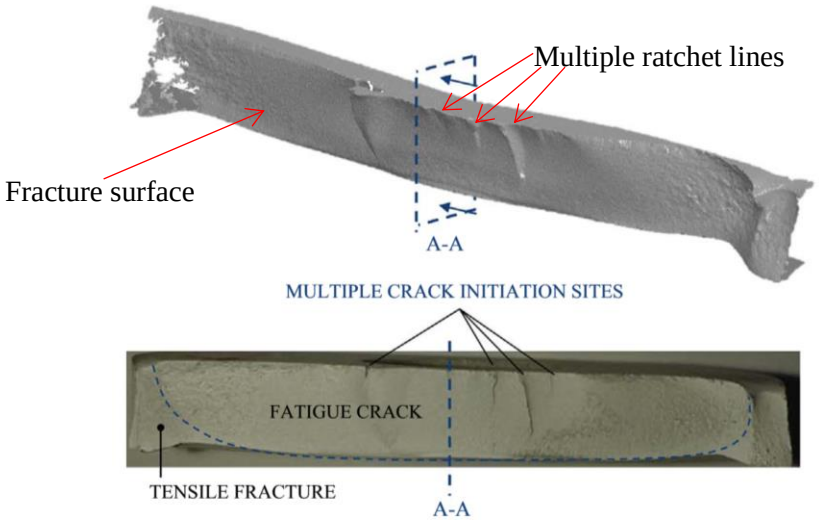

Figure 2.15 Fracture surface analysis of a fretting fatigue failure (Jimenez-Peña et al. 2017).

Hamrock et al. (1999) explained that without any magnification, a surface that has failed by fatigue looks like a brittle failure surface, due to the presence of a planar surface that is generated perpendicular to the applied stress. However, a fatigue failure surface has other features, evident under magnification, to distinguish it from a brittle failure surface.

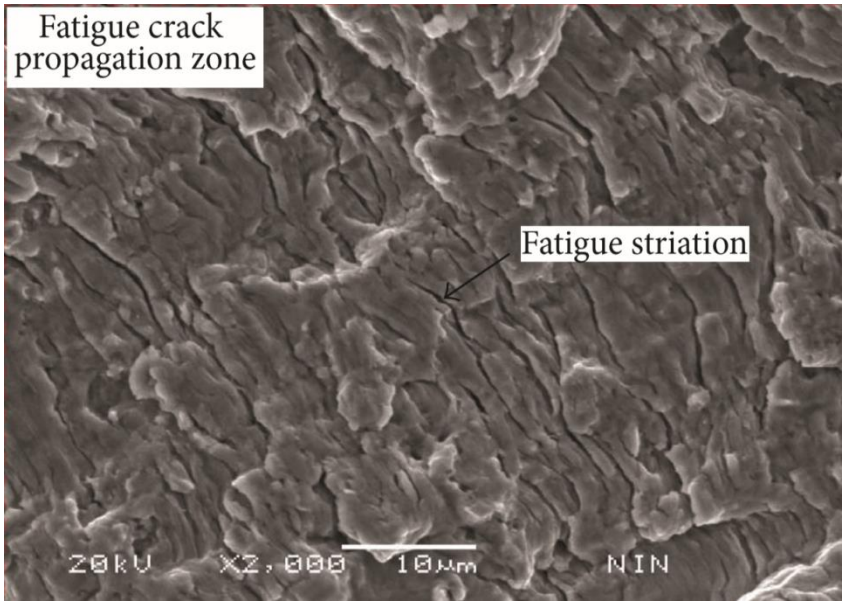

Figure 2.16 Striations found on the fracture surface caused by fretting fatigue (Xu et al. 2016, CC BY 4.0).

The fatigue fracture surface must be analyzed using microscopic images such as the one shown in Figure 2.17. During this analysis, the smooth region and the rough region must be identified. Dieter (1961) described the smooth region as the area in which the initial crack propagation has occurred very slowly. It is smooth because of the friction caused by the relative movement of the fracture surfaces. In the crack propagation zone, crack propagation occurs at a high rate, reducing the cross sectional area of the element (Figure 2.17). The rough region in this figure is the area where ductile failure occurred because the remaining intact cross section was no longer able to resist the load. Normally, the initial cracks cannot be seen by the naked eye. Also, the cyclic loads can produce microscopic superficial discontinuities on the surface that are caused by the constant movement of dislocations.

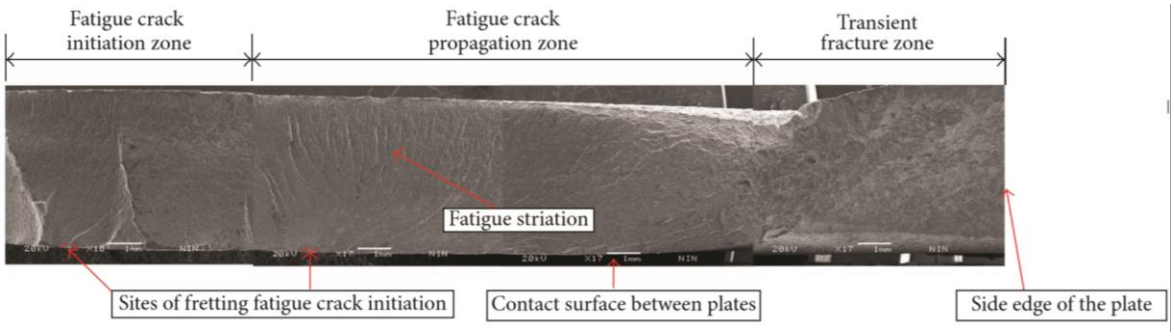

Figure 2.17 Fracture surface zones caused due to a fretting fatigue failure (Xu et al. 2016, CC BY 4.0).

The surface profile and the microstructure of the material that is tested is very important, because any defect will affect the fatigue strength. This is one of the reasons for conducting a microscopic analysis (Ma et al. 2010). It must also be determined if the crack initiated at a pre-existing flaw that was present before cyclic loading was initiated.

2.5 Bending effect in single-lap joints

When tensile loads are applied to a single lap bolted joint, local bending is induced in the connection because the tensile forces in the two plates are not concentric. The longitudinal axes of the connected plates are separated by an eccentricity, as shown in Figure 2.18. The internal bending moment produced by the eccentricity between the lines of action of the applied tensile loads influences the behaviour of the specimen (Ekh and Schon 2005).

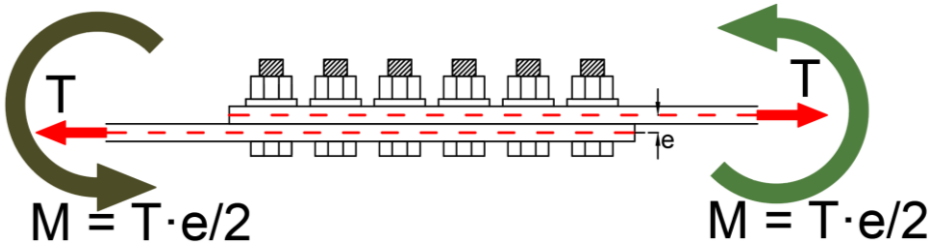

Figure 2.18 Schematic representation (free body diagram) showing the bending moment generated by the eccentricity between the applied tensile loads in a single lap bolted joint specimen.

The tensile strength of single lap joints is reduced by the bending effect when they are loaded by static tensile loads, according to Ekh and Schon (2005). During fatigue testing, Schijve et al. (2009) observed that the secondary bending effect caused the hole edges to come in contact with the shank of the bolt at higher fatigue loads. A similar effect was reported by Evans (1993), who also found that the fretting effect combined with the bending

effect caused crack initiation to occur at the hole edges during fatigue tests, which reduced their fatigue lives.

The bending effect combined with tensile stresses during fatigue testing can increase local stresses at the holes of bolted connections and reduce their fatigue lives, according to Schijve et al. (2009). Out-of-plane displacements due to bending generate higher overall stresses, as shown in Figure 2.19. The combined effects of tensile and bending stresses amplify the stress concentration at the hole of the bolted connection, and the effect increases as the applied stress range increases. The specimen used to generate this graph consisted of a single lap bolted joint with a line of three bolts. The 'tensile + bending' stress corresponds to the stress concentration at the hole edge at the contact interface, where tensile strains are higher. On the other hand, the 'tensile – bending' stress corresponds to the reduction of stress that occurs on the opposite surface of the plate.

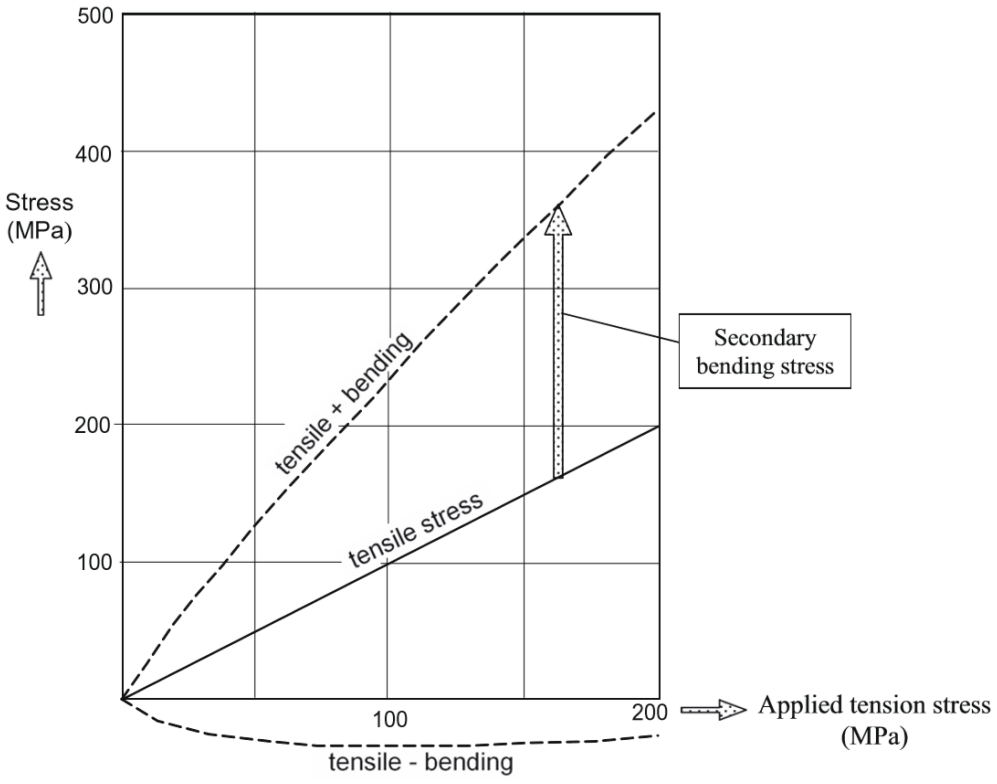

Figure 2.19 Resultant stress due to the bending and tensile stresses in a single lap bolted joint specimen **(**Schijve et al. 2009).

Ekh et al. (2005) measured the lateral displacements of single lap joints subjected to fatigue loading using a digital speckle photography (DSP) technique. The specimens consisted of bearing connections and were assembled with two and four bolts. As shown in Figure 2.20, the magnified deformed shapes of the specimens showed a bending effect. The plate's curvature at the first bolt of the connection was measured and compared for the two specimen types. The value of the maximum curvature for the two-bolt assembly was 0.003 mm^{-1}, whereas the value for four bolt specimens was 0.0015 mm^{-1}. As a result, it was concluded that increasing the number of bolts and the overlap length decreases the bending effect in single lap bolted connections.

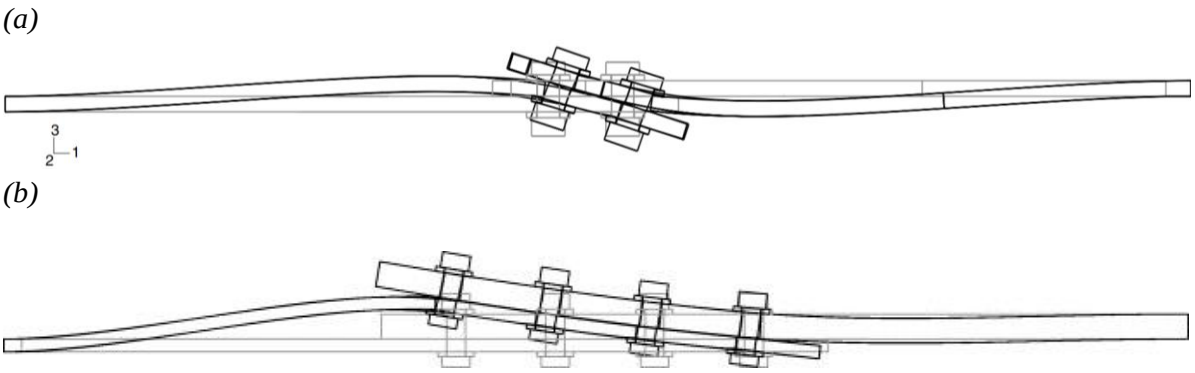

Figure 2.20 Lateral deflections induced by the bending effect in single lap bolted joints, as measured by Ekh and Schön (2005) and Ekh et al. (2005): (a) deflected shape of a specimen with two bolts in a line subjected to an 8 kN load, and (b) deflected shape of a specimen with four bolts in a line subjected to an 18 kN load.

Minguez and Vogwell (2006) studied the influence of the clamping force on the fretting fatigue behaviour of both single-lap and double-lap bolted connections. Nine single-lap samples were tested with very thin plates to minimize the bending effect caused by the asymmetric configuration (shown in Figure 2.21). Thirty-seven samples were tested with the double-lap configuration. They found that the bending moment caused by the distortion of the single-lap joint configuration was the main factor to cause failure. Also, they concluded that specimens with thick plates in double-lap bolted connections benefited more from higher pre-tension loads in terms of improvement in fatigue life than those with thin plates.

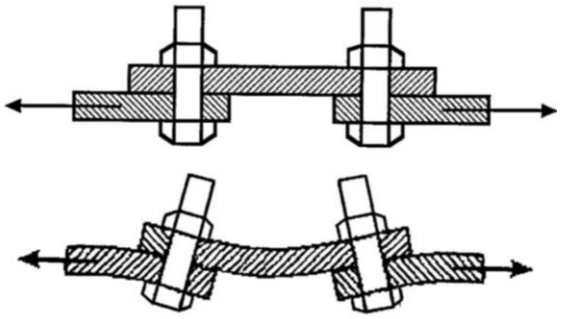

Figure 2.21 Single lap bolted connection deformed by bending (Minguez and Vogwell 2006).

2.6 Summary of Literature review

Fretting fatigue is reported as the main cause of failure in slip-critical bolted connections. Tensile fatigue loads applied to a slip-critical connection generate relative displacements at the contact interface, which produce a tangential or frictional force on the contact surfaces. The pretensioned bolts apply a clamping force, which generates a normal load in the connection between the plates. The stress concentration that is formed due to the combined tangential and normal stresses initiates a crack in the gross section of the connected plates.

Crack initiation occurs along the boundary between a stick region close to the hole, where the maximum clamping pressure exists, and a global slip region further away from the hole. The boundary between the two regions is known as the partial stick-slip region. This region is generally located a certain distance away from the hole. When fretting fatigue occurs, multiple crack initiation sites are generated in the partial slip region due to the relative displacements of small magnitude. The multiple initiated cracks coalesce to form a leading crack, which propagates until the cross section of the plate is reduced so that it cannot resist the applied fatigue loads.

The two most important variables that affect the fatigue behaviour in slip-critical connections are the slip coefficient and the bolt pretension. The focus of most of the scientific studies has been on the bolt pretension and it has been concluded that higher levels of bolt pretension improve the fatigue life of a bolted connection because larger stick regions are created and the magnitude of the relative displacements at the contact interface is reduced. However, it is important to compare the influence of different types of bolts that

apply equal pretension loads on the fatigue behaviour of bolted connections. This comparison would allow the determination of whether the geometry of the bolt head and the method of installation are variables that should be accounted for.

There are not many studies about the influence of the surface finish on the fatigue behaviour of bolted connections. It is reported that coated surfaces have a better behaviour than uncoated surfaces because coatings can reduce surface damage at the contact interface and further delay the crack initiation on the virgin contact surfaces. Because of the limited data available, it is important to study the influence of surface finish on the fatigue behaviour of slip-critical connections, including an investigation of the crack initiation sites, fatigue life, and other relevant parameters.

Double lap bolted joints are preferred over single lap bolted joints because they are symmetric and the load does not generate bending stresses as is experienced in single lap joints. The bending effect is reported to be a stress raiser, which increases the local stress range applied by the tensile fatigue loads. The bending stresses can reduce the fatigue life of the connection and generate crack initiation at the hole edge. However, most of the scientific studies in which single lap bolted specimens were used did not report that the specimens suffered a reduction in fatigue life due to bending stresses.

CHAPTER 3

METHODOLOGY

3.1 Overview

The fretting fatigue failure behaviour of slip-critical single lap joint bolted connections was characterized using an experimental program. The bolted specimens were subjected to quasi-static tensile testing to obtain the slip resistance and to fatigue testing to characterize the fretting fatigue failure behaviour. Two variables were investigated:

1. Type of contact surface finish (Class A and Class B, as defined in CSA S16-14); and
2. Bolt type (ASTM A325 structural high strength bolts (HSB) and C50LR Huck tension control bolts).

A summary of the experimental program is provided in Table 3.1. The A325 HSB were used with Class A and Class B surface finishes and the C50LR Huck tension control bolts were used only with a Class B surface finish. Each type of specimen was tested until failure under several different stress ranges and the total number of cycles to failure was recorded for obtaining the S-N curve. For some of the tests, the displacements between the contact surfaces were measured using a digital image correlation (DIC) system to better characterize the fretting phenomenon at the contact interface. A post failure analysis was carried out using a scanning electron microscope (SEM) and an optical microscope for analyzing the fracture behaviour and the fretting effect. On average, at least three specimens were tested at each stress level. However, higher number of samples was tested at low stress levels where the results were variable with higher coefficients of variation. At stresses closer to the endurance limit, a better estimate was wanted with a higher number of samples.

Table 3.1: Summary of fatigue experimental program

Bolt type	Surface finish	Maximum load (% of slip resistance)	Stress range (σ_{max} - σ_{min}) (MPa)	Number of fatigue samples
A325 High strength bolts (1 bolt)	Class A	64.7%	33.0	1
		3 samples tested under static test to measure slip resistance		
A325 High strength bolts (6 bolts)	Class A	64.6%	103.3	1
		76.4%	122.1	5
		85.2%	136.2	3
		94.0%	150.3	7
		5 samples tested under static test to measure slip resistance		
	Class B	46.9%	122.1	2
		57.8%	150.3	2
		65.0%	169.0	3
		72.2%	187.8	2
		83.1%	216.0	3
		3 samples tested under static test to measure slip resistance		
C50LR Huck tension control bolts (6 bolts)	Class B	44.4%	122.1	2
		54.7%	150.3	8
		61.5%	169.0	4
		68.4%	187.8	3
		6 samples tested under static test to measure slip resistance		
			Number of tests	**63**

3.2 Materials

3.2.1 Plates

3.2.1.1 Grade and size

The specimen plate material, types of surface finish, type of bolts, bolt diameter, type of connection, the specimen geometry, and the number of bolts were chosen based on the literature review combined with preliminary experiments. CSA G20.21 Grade 300W steel was selected for the plate material due to its common use in steel structures. As discussed in Section 3.3.1, the geometry of the plates was defined based on the limit states design requirements of CSA S16-14. The specimen plates had a width of 50.8 mm (2 inches) and thickness of 9.525 mm (3/8 inches). The positions of the holes, minimum edge distance and the pitch were selected in accordance with CSA S16-14 (2014), Clauses 22.3.1 and 22.3.2, and are described further in Section 3.3.

3.2.1.2 Surface finishes

Two types of surface finish were used for the specimen plates. The Class A and Class B surface finishes were chosen according to Table 3 of CSA S16-14 (2014). The Class A surface finish was an as-received unpainted clean mill scale steel surface finish. The Class B surface finish was obtained by applying Cathacoat 302HB (manufactured by International Paint LLC, USA) on the sand blast-cleaned surface, as shown in Figure 3.1. The coating is a reinforced inorganic zinc primer used for cathodic protection of steel structures that also satisfies the slip requirement of a Class B surface finish. The average thickness of the coating is 100 μm according to the manufacturer. The blast-cleaning process of the surface was done at Engineering Shops. The application of the coating on the sample surfaces after they were sand blasted was done by Totally Blasted (Saskatoon) because an industrial facility was needed due to health, safety and environmental standards and regulations.

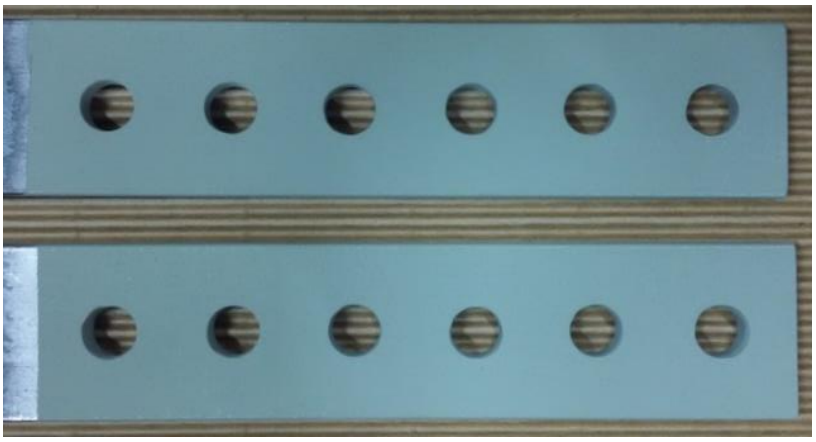

Figure 3.1 Specimen plates with Class B surface finish.

3.2.1.3 Surface characterization

Two parameters were measured for characterizing the surface finish: surface roughness and coefficient of friction. The surface roughness was measured with a Mitutoyo SJ-201 roughness tester available in the Structures Lab. Its fine tip detector quantified the roughness based on the measurement of height profiles of the surface. The tip has a radius of 5 μm, travels a sampling length of 0.25 mm, and one sample length was used for each measurement. As the tip travelled along a straight-line, the undulations of the surface profile were converted into electrical signals, which were then converted into roughness parameters and recorded as shown in Figure 3.2. The roughness was measured in micrometers (μm)

with a precision of ± 0.03 μm. Before carrying out the measurements, the roughness tester was calibrated using a reference specimen.

Figure 3.2 Surface roughness measurement device-Mitutoyo SJ-201.

The parameters used to quantify the surface roughness were:

1. The arithmetic mean deviation of the profile (R_a)
2. The root mean square (RMS) deviation of the profile (R_q)
3. The maximum height of the profile (R_y)
4. The ten-point height of irregularities (R_z).

R_a is the arithmetic mean of the absolute values of the heights and depths measured from the mean line of measurement. R_y provides the sum of the height of the highest point and the depth of the deepest point of the profile. R_z is an overview of the irregularities of the measured surface and is calculated as the sum of the mean values of the five highest points and five deepest points of the profile. R_q is the square root of the mean of the sum of squares of profile deviations from the mean line of measurement. In total, 60 measurements of surface roughness were taken for each type of surface finish.

The coefficients of static and kinetic friction were determined experimentally using coefficient of friction test equipment located in the Physics Lab in the Department of Physics and Engineering Physics at the University of Saskatchewan. The coefficient of static friction was obtained by placing two plates with the required surface finish in contact on an inclining plane as shown in Figure 3.3. The fixed plate was clamped on the slanted surface

and a small plate was placed on top of the fixed plate. Then, the angle of the slanted surface was increased gradually until the small plate started to slide. When sliding occurred, the friction force at the contacting interface was no longer able to resist the component of the plate's self-weight parallel to the inclined plane. On that basis, the coefficient of static friction was determined as the tangent to the angle of inclination ($\mu_s = \tan \theta$). This equation can be obtained by considering force equilibrium parallel and perpendicular to the inclined surface. The coefficient of static friction was measured with a precision of ± 0.009.

Figure 3.3 Coefficient of static friction measurement apparatus.

Since the Class A surface finish was from the as-received material, the surface roughness profile varied along the specimen length. As a result, the number of coefficient of static friction measurements was set to 55. However, the Class B surface finish had a uniform profile due to the coating and hence only 36 measurements were taken to measure the coefficient of static friction.

Similar experiments were carried out to determine the coefficient of kinetic friction, using the experimental set up shown in Figure 3.4. First, the angle of the slanted surface with the fixed plate, θ, was set at 30° for Class A surface finish specimens and at 45° for Class B surface finish specimens. Then, a spark cable holder was mounted onto the slanting surface, a strip of sparking tape was attached to the small plate, and the tape was then connected to a motor. The spark cable holder was then aligned on top of the sparking tape. As the angle of inclination of the slanted surface was high enough so that the small plate was not static, the small plate was placed on top of the fixed plate and it started to slide

down. When the small plate moved, spark marks were created by the spark cable at a rate of 10 Hz to record the change in position of the small plate.

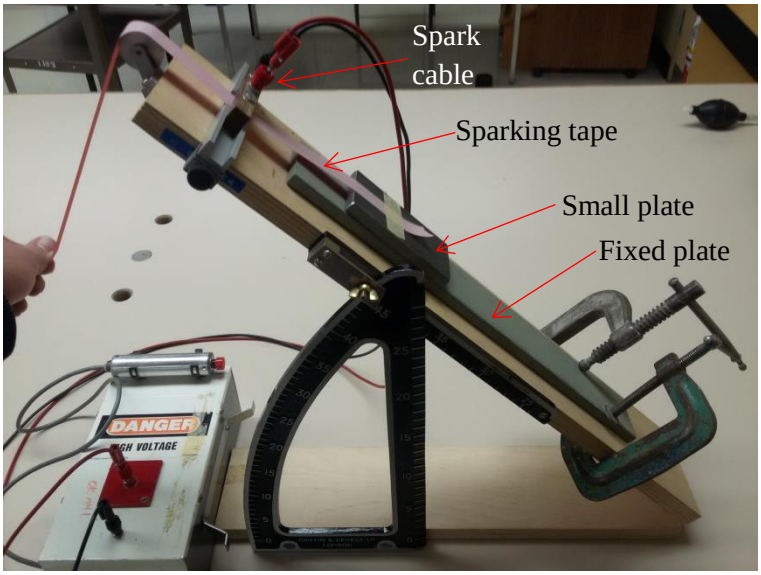

Figure 3.4 Kinetic coefficient of friction measurement.

The distance travelled by the small plate was obtained by measuring the marks on the sparking tape using a ruler and the time taken for the travel was estimated by the sparking frequency. The measured distance and time were used to calculate the initial and final velocities, which were then used to determine the acceleration, a, of the small plate. Finally, the kinetic coefficient of friction (μ_k) was calculated using $\mu_k = \frac{g \sin\theta - a}{g \cos\theta}$, where g is gravitational acceleration. This equation can be obtained by the summation of forces in directions parallel and perpendicular to the inclined surface. In total, 20 measurements were taken for the Class A surface and 15 measurements were taken for the Class B surface. The coefficient of kinetic friction was measured with a precision of ± 0.005.

3.2.2 Bolts

The two bolt types used in this research were ASTM A325 structural high strength bolts (HSB) and C50LR Huck tension control bolts (Alcoa Fastening Systems & Rings, USA). These bolts were chosen due to their common use in slip-critical connections for steel structures and to determine the effect of these bolt types on the fatigue life of bolted connections. Bolts with 12.7 mm (1/2 in.) diameter were selected for the specimen assemblies.

A photograph of an A325 structural high strength bolt, ASTM A563 nut and ASTM F436 washer used for the bolted assemblies is shown in Figure 3.5. This type of bolt with a heavy hex head is equivalent to an SAE Grade 5 bolt and is made of medium carbon steel. These bolts are commonly used in structural steel joints, including typical mineshaft guide-bunton gusset plate assemblies. The specified minimum tensile strength of A325 HSB is 825 MPa and they are usually designed to be pretensioned, in which case they must be pre-tensioned to at least 70% of the bolt tensile strength, as recommended by CSA S16-14. The total length of the bolts was 44 mm with a threaded length of 25 mm.

Figure 3.5 ASTM A325 HS bolt, A563 nut and F436 washer.

The C50LR Huck bolt used for this research was a zinc coated tension control bolt with flanged-3LC collar as shown in Figure 3.6. This type of bolt is equivalent to an SAE Grade 5 bolt made of medium carbon steel and meets the requirements of the ASTM A325 standard. The collar was made of low carbon steel with an inner diameter suitable for a snug fit to the bolt. The bolt has a long pin-tail that is pulled off during installation when the level of pre-tension reaches the design limit. According to the supplier, these bolts are typically pre-tensioned to 70% of the bolt tensile strength. During installation, the collar is locked with the bolt thread as the required bolt pretension is applied using the specified installation tool. The initial bolt length prior to installation was 93 mm with a pintail length of 49.76 mm. The lock grooved (threaded) length of the bolt was 22 mm.

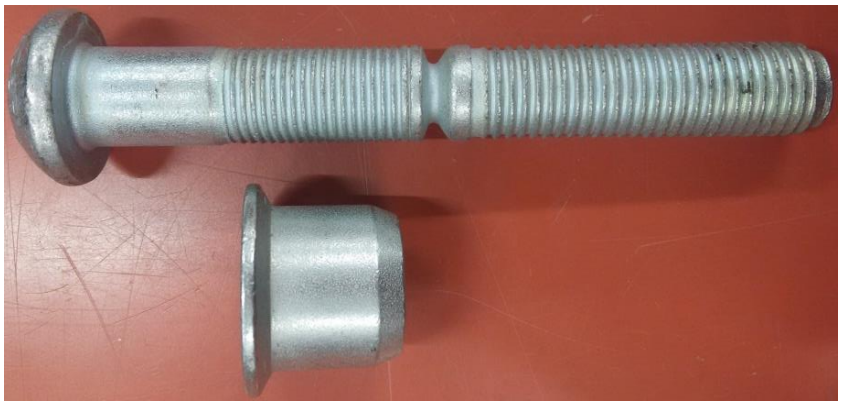

Figure 3.6 C50LR Huck bolt and flanged-3LC collar.

The level of pre-tension was not measured in any bolt. The turn-of-nut-method was used to install the A325 HSB. This approach lengthens the shank and the threaded portion to generate the desired tension and is recommended to reach at least the 70% level of pre-tension by CSA S16-14. The installation procedure for the C50LR Huck tension control bolts shears the pin-tail of the bolt off when the desired level of pre-tension is reached, ensuring that there is a consistent clamping force applied in the connection.

3.3 Bolted Specimens – Design and Fabrication

3.3.1 Specimen Design Considerations

A single-lap bolted connection configuration was chosen for the experiments because this type of connection is commonly found in many structures, including in a typical mineshaft guide-bunton gusset plate assembly. In addition, this type of connection is the one most commonly used in scientific studies of the fretting fatigue behaviour of bolted connections. The single lap joint specimens were designed in such a way that the slip resistance was the controlling factor. The number of bolts for the assembly was also selected based on the theoretical slip resistance, which increases as the number of bolts increases. Consequently, higher fatigue load levels could be applied to investigate the fretting phenomenon within the contact surface when a specimen with a large number of bolts was used. The specimen plates were designed so that they would not fail due to bearing strength, net section fracture at the hole, pull out of the bolt and block shear, as determined by the limit states found in CSA S16-14, and the failure could only occur after the slip-critical bolted connection samples undergo the bolt-slip stage. Also, the distance between the centre

of the hole and the plate edges and the holes' pitch were selected as 25 mm and 35 mm, respectively.

3.3.2 Theoretical Slip resistance

Because the fatigue specimens were intended to represent slip-critical connections, the slip resistance of the specimens played an important role in defining the fatigue load levels to be used for the tests. The slip resistance (V_s) was therefore calculated according to Clause 13.12.2 of CSA S16-14 (2014) as follows,

$$V_s = 0.53 k_s c_s m n A_b F_u \quad (3.1)$$

where

k_s= Slip coefficient of the surface finish recommended by CSA S16-14 (0.3 for Class A and 0.52 for Class B).

c_s = Coefficient that relates the mean slip resistance to a 5% probability of slip, as taken from CSA S16-14 depending on the surface finish and pretension method.

m = Number of faying surfaces

n = Number of bolts

A_b= Area of the bolt

F_u= Tensile strength of the bolt

The calculated values of the slip resistance for different conditions are given in Table 3.2. The calculated slip resistance values were used to select the number of bolts, and then the limit state (shear strength) of the bolts for the slip critical bolted connections was checked. Detailed calculations for specimen design are provided in Appendix A.

Table 3.2: Theoretical slip resistance

Bolt type	Surface finish	k_s	c_s	Slip resistance (kN)
A325 High strength bolt (1 bolt)	Class A	0.30	1.00	16.50
A325 High strength bolt (6 bolts)	Class A	0.30	1.00	99.01
	Class B	0.52	1.04	178.49
C50LR Huck tension control bolt	Class B	0.52	1.04	178.49

3.3.3 Single bolt assembly

The theoretical slip resistance for a single bolt assembly with a Class A surface finish was 16.50 kN. Based on this value, a plate thickness of 4.76 mm was selected and the end distance from the centre of the hole was set at 35 mm. The single bolt slip critical bolted connection assembly is shown in Figure 3.7. The maximum fatigue load of 56% of the slip resistance was selected to test the assembled specimens. However, this load was not sufficient to initiate failure. Hence, a new configuration of the samples was designed with larger number of bolts and a larger plate thickness to obtain a higher slip resistance in the specimens.

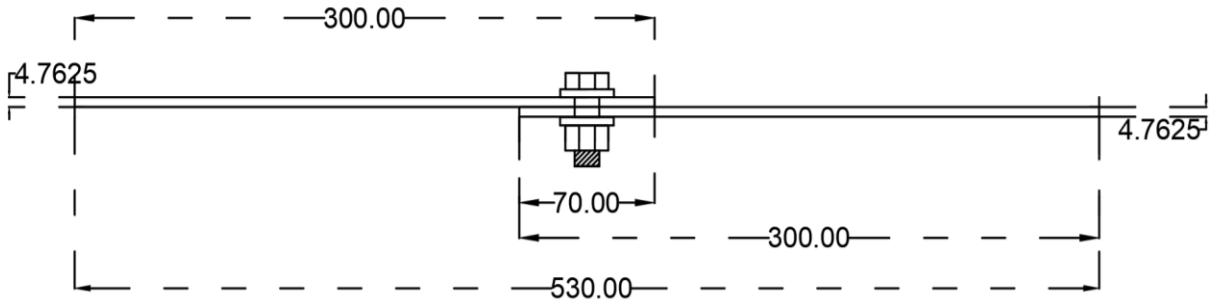

Figure 3.7 Schematic drawing of the **s**ingle bolt assembly (Dimensions are in mm).

3.3.4 Six bolt Assembly

The new configuration was designed with six bolts based on the theoretical slip resistance and was expected to provide sufficient slip resistance while permitting a higher maximum fatigue load. The selected specimen's thickness and geometry are shown in Figure 3.8. The total length of the assembled specimens with A325 HSB and Class A surface finish was 579 mm. The total length was then reduced to 400 mm for the A325 HSB and Class B surface for four experiments to minimize the secondary bending effect. Similarly, the total length of the assembled specimens with tension control bolts and Class B surface finish was set at 400 mm. The overlap length of the connection was kept at 221 mm for all the specimens.

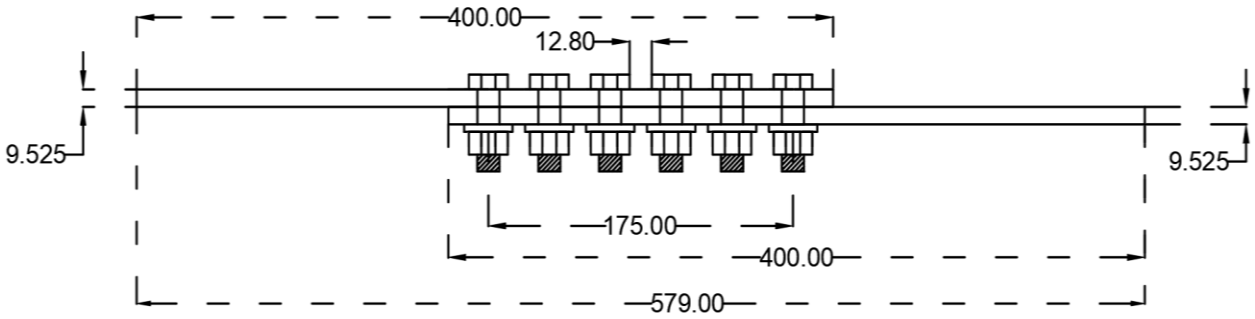

Figure 3.8 Schematic drawing of the six bolt assembly (Dimensions are in mm).

3.3.5 Bolt installation

The A325 HSB were installed using the turn-of-nut method, as described in Clause 23.7.2 of Table 8 of CSA S16-14 (2014), and 1/3 of a turn-of-nut was used. Before assembly, an A563 nut and an F436 washer were inserted onto the bolt and the bolt was then snug-tightened. Then, a red mark was applied to the nut and plate as a benchmark for the rotation and, finally, a 1/3 turn was applied to the nut using a wrench while the head of the bolt was held to prevent rotation. This procedure is designed to achieve a bolt pre-tension equal to 70% of the bolt's tensile strength. Figure 3.9 shows two of the assembled samples using 1/3 of turn-of-nut method.

Figure 3.9 A325 HSB bolted specimens.

For installation of the tension control bolts, a hydraulic tool equipped with a nose assembly was used to install the collar onto the bolt. First, the bolt was inserted into the hole of the plates (Figure 3.10 (a)) and then a collar was slid onto the bolt, as shown in Figure 3.10(b). The next step was to hold the bolt tail using the hydraulic tool (Figure 3.10 (c)). A tensile force was applied to the bolt tail at the same time that a compressive force was applied to the collar. The bolt tail was then sheared off when the maximum pretension load was applied. The collar was deformed by the procedure and locked into the bolt grooves to maintain a uniform pretension load. The only disadvantage of this type of bolt assembly is

that prior to the bolt installation, the specimen plates must be aligned without any misalignment. Once assembled, the bolts can only be removed by splitting the collar. Figure 3.10 (d) shows a specimen assembled with tension control bolts.

(a) *(b)*

(c) *(d)*

Figure 3.10 Huck bolt installation procedure: (a) Bolts placed for installation; (b) Collars placed on the bolts; (c) Nose assembly installing a Huck bolt; and (d) Huck bolts installed on specimens.

3.4 Equipment

3.4.1 MTS 322 Test Frame

The MTS 322 servo hydraulic test machine (Figure 3.11) located in the Materials Lab was used for both tensile and fatigue tests. The test machine is equipped with a load cell with a capacity of 250 kN, a maximum stroke range of -100 to 100 mm, and a maximum testing frequency of 100 Hz. The position of the actuator could be adjusted depending on the length of the sample. The machine is equipped with hydraulic grips, which are used to hold the specimen. The gripping pressure to prevent the slippage was set at 69 MPa. A spacer with the same thickness as the specimen plates was used in the grip to mount the experimental specimens.

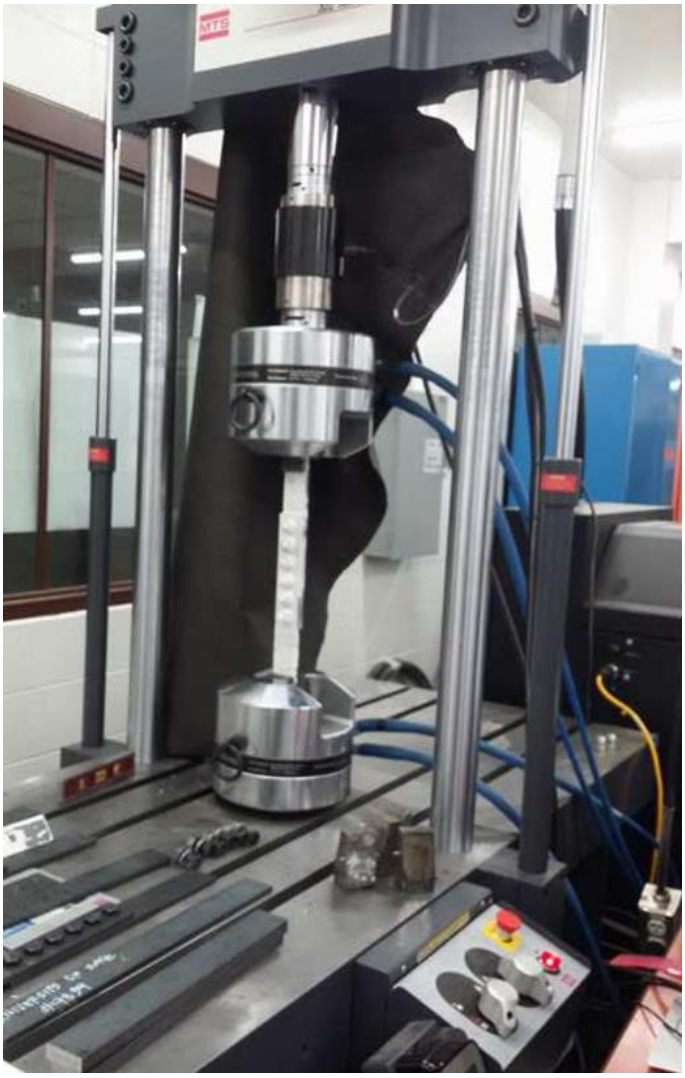

Figure 3.11 MTS 322 Servohydraulic test machine.

3.4.2 MTS Test Suite Software

The MTS test suite software allows the user to design a customized test program. Two test programs were required for the current experimental analysis, one for the tensile tests and the other for conducting fatigue tests. The tensile test program was used to determine the slip resistance of the bolted specimens. The test program recorded both the applied load and the actuator displacement and these data were used to determine the slip resistance. A flowchart that shows the processes used for the tensile static tests can be seen in Appendix B.

The fatigue test program was required to define the necessary steps to perform the tests and also to acquire the desired results. Figure 3.12 shows the processes used for the fatigue tests as a flowchart. The first step before running the fatigue test was to enter the input variables, such as the mean load, the load range, the maximum and the minimum cyclic load, and the test frequency. The test program balanced all the variables to zero before running the test. As the fatigue test started, the test program applied the mean load gradually to the set value and then defined the cyclic loads to be applied to the specimen. During the test, the program acquired the number of cycles, actuator displacements, maximum and minimum fatigue load and the time in seconds, respectively.

The limit detection of axial displacement was set using the test program for two reasons:

1. To stop the machine when the test specimen failed; and
2. To identify the crack initiation by monitoring the change in displacement during the test.

The second limit detection was used during the interrupted tests described below in which a very small change in displacements was monitored and used for checking the crack initiation during the test.

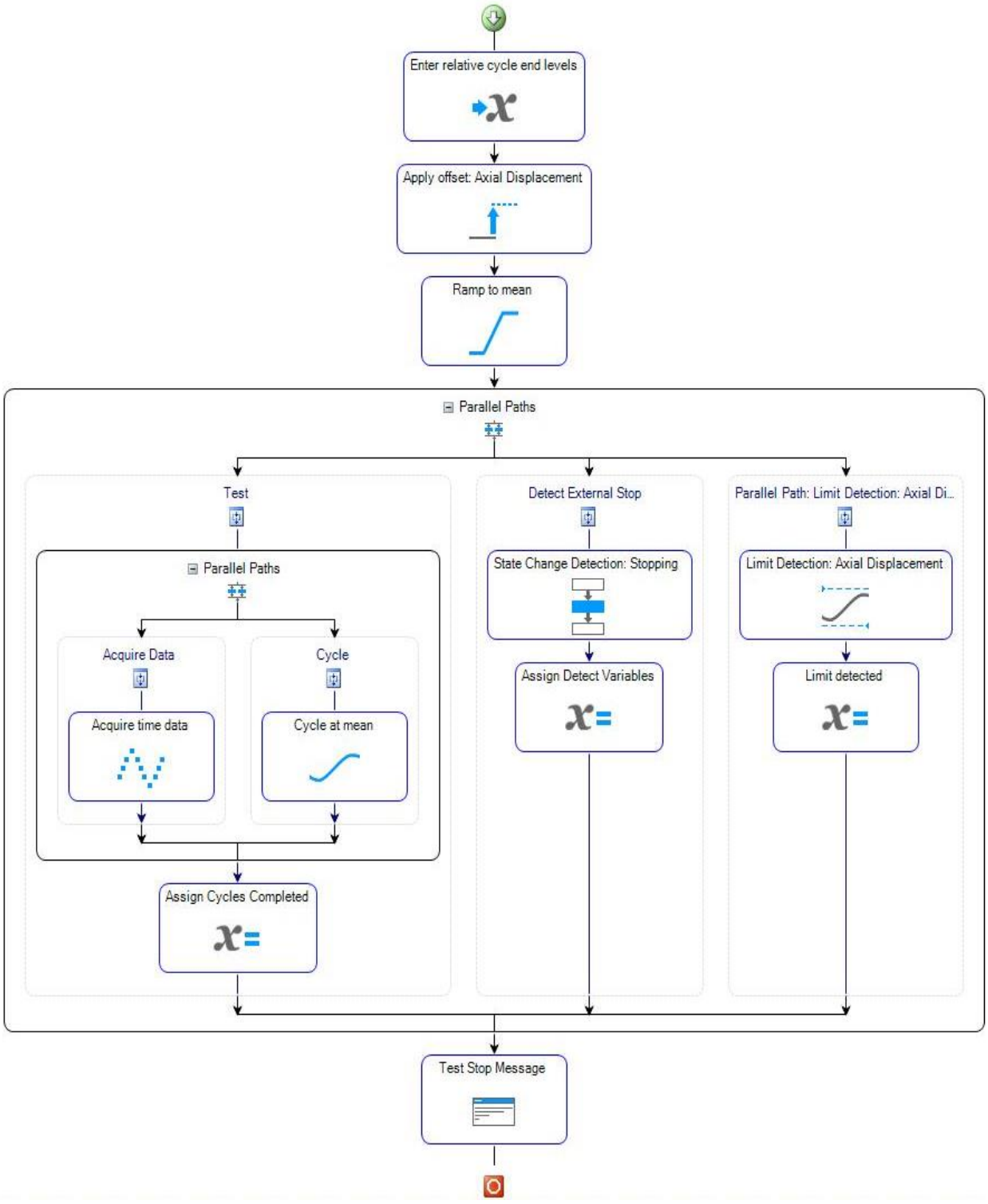

Figure 3.12 MTS Test Suite Software for fatigue testing.

3.4.3 Digital Image Correlation (DIC) system

The Digital Image Correlation (DIC) system from Correlated Solutions, Inc, USA was used to capture specimen images during some of the fatigue tests to measure the relative displacement between the contacting plates in order to better understand the fretting fatigue behaviour. The DIC equipment consisted of a 5 MPixel high-resolution monochrome camera, equipped with an 8 mm f/1.4 compact lens, and mounting accessories for the camera, which included a tripod, aluminum mounting bar, mounting brackets and adjustable accessories. Two software packages, Vic-Snap (version 8, Correlated Solutions, Inc.) and Vic-2D (version 7.2.6, Correlated Solutions, Inc.), were used along with the DIC hardware system. The Vic-Snap software was used for capturing the images during the test and the VIC-2D software was for analyzing the images.

Before using the DIC system for acquiring the images, the specimen's surfaces were prepared with speckle patterns. The specimen surfaces were first coated with white paint before generating the speckle patterns using black paint, as shown in Figure 3.13. For best results, the speckle pattern must be random, non-repetitive, and isotropic with the maximum possible contrast (Jimenez-Peña et al. 2017). This was achieved using a rubber stamp that had been prepared with a random speckle pattern.

Figure 3.13 Speckle pattern DIC sample.

The procedure to capture the images using the DIC technique was initiated by mounting the sample on the testing machine. Then, the high resolution camera was positioned to record images of the area of interest (AOI) without any interference, as shown in Figure 3.14. As is apparent in Figures 3.13 and 3.14, the area of interest was located along the side of the specimens to capture the relative displacement between the plates. The camera was set to suitable focus, brightness, resolution, angle and contrast settings and was connected to the data acquisition system (DAQ) of the DIC prior to capturing images. No external lights were used for capturing the images during the tests. A reference image was

captured before running the test and was used to calculate the displacement profile of the loaded specimens.

After set-up, the DAQ system was connected to the testing machine to capture its load signal. When the DIC system detected the maximum and minimum load values in a fatigue cycle, it triggered the camera to capture the images corresponding to these loads using the Vic-Snap software. The Fulcrum Dialog module of the Vic-Snap software package was used for synchronizing the captured images with the applied load and the number of cycles. For the first 500 cycles, the DIC system was set to detect the load signal and then the rate of acquisition of images was set to every 10 cycles until 10 000 cycles. Finally, the rate of acquisition was set to every 1000 cycles until failure. In total, four samples (identified below) were tested with the DIC system in place to measure the displacements.

Figure 3.14 DIC camera set up to measure the AOI.

Before analyzing the images, the DIC system was calibrated so that the pixels of the images could be converted into length units, in this case millimeters (mm), using Vic-2D software. The images were analyzed by comparing the reference image with the captured images. During the experiments, all of the tested specimens failed close to the first bolt at the top of the specimen where the movable actuator applied the load; the area of interest (AOI) was therefore selected around the first bolt to measure the relative displacement. A

number of points were selected inside the AOI of both the reference and captured images and the Vic-2D software was used to analyze the images to obtain the relative displacements.

The DIC system was used to monitor two samples made with A325 HSB and Class B surface finish and two samples made with C50LR Huck tension control bolts and Class B surface finish when they were subjected to stress ranges of 150 MPa and 169 MPa. The displacements in directions parallel and normal to the applied load provided evidence about the relative displacements at the contact interface of the plates. The displacements of many locations (points) inside the area of interest were analyzed to better understand the fretting fatigue behaviour of the specimens.

3.5 Experimental Procedure

3.5.1 Tensile test procedure

Tensile tests were carried out to determine the slip resistance of the slip-critical bolted connections and were necessary to verify the theoretical values of the slip resistance. The tests were run under load control with a loading rate of 0.5 kN/s. The test set up is shown in Figure 3.15. As the load was applied, the relative displacement between the plates reached a maximum when the bolts began bearing against the plates, and then the specimen failed.

The relative displacement between the plates was measured using laser displacement sensors (ILD1320-50, Micro-Epsilon, USA) capable of measuring displacements with a precision of ± 60 µm. As shown in Figure 3.15, a wood stick was glued to the end of each plate for measuring the plate displacements using the sensor's beam. The displacement of the wood sticks was equal to the displacement of the individual plates and was acquired at a rate of 10 Hz. The difference between the displacement readings of the two sensors was defined as the relative displacement between the plates. The relative displacements and the corresponding load were used to determine the experimental slip resistance. In total, 17 samples were tested to measure slip resistance, as shown in Table 3.3. Three single bolt assembly specimens were tested during the preliminary experiments. Five specimens for A325 HSB with Class A surface finish, three specimens for A325 HSB with Class B surface

finish, and six specimens for tension control bolts with class B surface finish were tested to obtain the slip resistance.

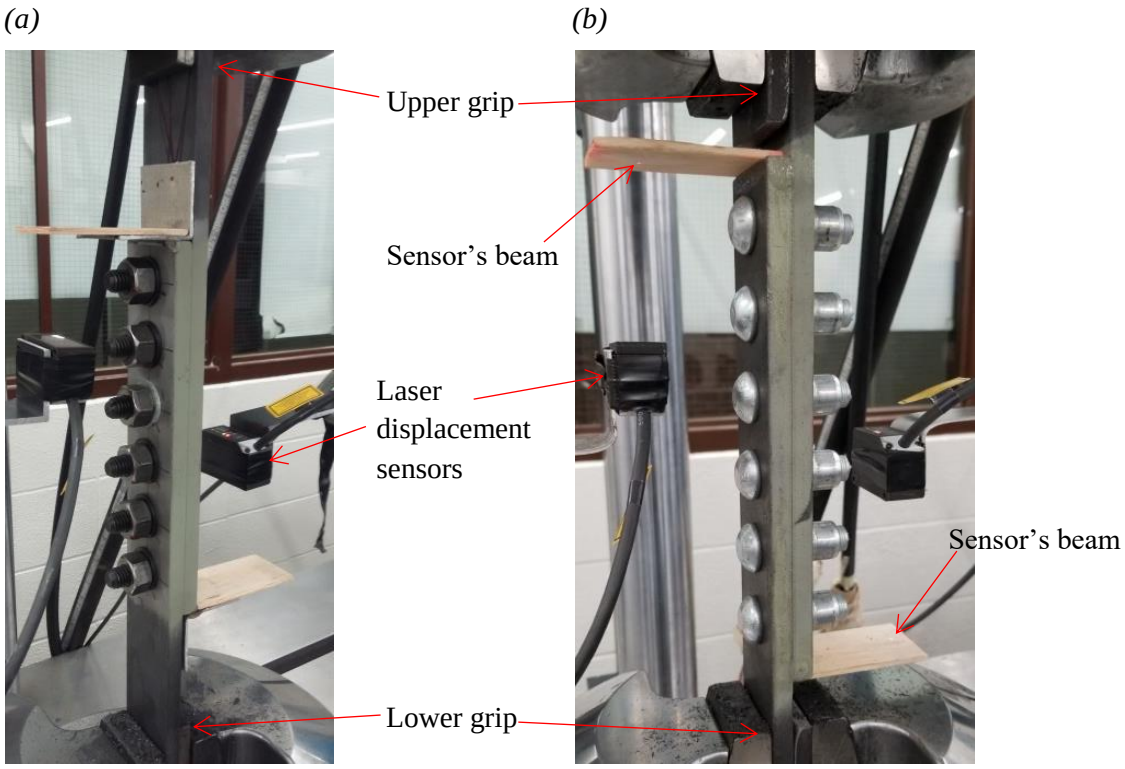

Figure 3.15 Tensile test set up. *(a) High strength structural bolts; (b) Tension control bolts.*

Table 3.3: Number of samples for the slip resistance tests

Bolt type	Surface finish	Number of samples
A325 High strength bolt (1 bolt)	Class A	3
A325 High strength bolt (6 bolts)	Class A	5
	Class B	3
C50LR Huck bolt (6 bolts)	Class B	6

3.5.2 Fatigue test procedure

Since there is no standard procedure for conducting fretting fatigue tests on bolted connections, the test parameters were chosen based on the literature and the slip resistance results. Table 3.4 summarizes the parameters used for the fatigue tests, including the maximum load in a fatigue cycle (specified as a percentage of slip resistance), the corresponding maximum stress based on the gross area of the plate, stress range and number of samples. The fatigue tests were conducted under load control mode.

As explained before, a single bolt specimen was tested first. This test was carried out with a maximum cyclic stress (σ_{max}) of 37 MPa and a minimum stress (σ_{min}) of 4 MPa, resulting in a stress range (σ_r) of 33.1 MPa and stress ratio (R) of 0.11. The test was conducted at a loading frequency (*f*) of 10 Hz. The stresses were calculated as the ratio between the applied load and the gross section area. The specimen did not fail due to the low fatigue load and the test was stopped at 1,527,876 cycles. After the test, the specimen's contact surfaces were examined and no fretting wear was found.

For the six bolt assembly, a stress ratio (R) of 0.0909 and frequency (*f*) of 10 Hz were selected, based on the literature. The specimens were tested until failure to obtain the S-N curve, although for a few specimens the tests were stopped after 8 million cycles without failure. Since a large variation in the number of cycles to failure was expected, a total of 45 samples with different combinations of test parameters were tested to obtain the S-N curves. As shown in Table 3.4, 16 samples with the combination of A325 HSB and Class A surface finish, 12 samples with the combination of A325 HSB and Class B surface finish, and 17 samples with the combination of Huck tension control bolt-Class B surface finish were tested to characterize the fretting fatigue behaviour.

Table 3.4: Fatigue test parameters

Bolt type	Surface finish	Maximum load (% of slip resistance)	Maximum Stress (σ_{max}), MPa	Stress range (σ_{max} - σ_{min}) (MPa)	Fatigue test: Number of samples
A325 High strength bolt (6 bolts)	Class A	64.68%	113.67	103.33	1
		76.44%	134.33	122.12	5
		85.26%	149.83	136.21	3
		94.08%	165.33	150.30	7
	Class B	46.99%	134.33	122.12	2
		57.83%	165.33	150.30	2
		65.06%	186.00	169.09	3
		72.29%	206.67	187.88	2
		83.14%	237.67	216.06	3
C50LR Huck Tension control bolt (6 bolts)	Class B	44.48%	134.33	122.12	2
		54.75%	165.33	150.30	8
		61.59%	186.00	169.09	4
		68.44%	206.67	187.88	3
				Total	45

In addition, four samples with the combination of A325 HSB and Class A surface finish were tested to estimate when crack initiation occurred. These tests were carried out with the limit displacement detection feature enabled in the fatigue test program. When the actuator displacement exceeded a value corresponding to the expected value under the applied cyclic load, the MTS test program stopped the test and the specimen was removed to study the crack initiation behaviour. The number of cycles at which the test stopped was defined as the number of cycles to crack initiation. These four tests were carried out with a stress range (σ_r) of 150 MPa.

The fatigue test load levels were selected based on

1. The endurance limit of the bolted connections as defined in CSA S16-14; and
2. Achieving between 40% and 95% of the slip resistance of the individual combinations.

The minimum stress range values were selected as per the CSA S16-14 endurance limit (110 MPa) for any bolted connection. As such, stress ranges (σ_r) of 103 MPa and 122 MPa were chosen as the lowest values of the cyclic loads. Then the stress ranges were increased further based on the slip resistance of the individual combinations. The applied fatigue load levels for the individual combinations are given in Table 3.4.

Four load levels were used to test the connections assembled with A325 HSB and Class A surface finish shown in Figure 3.16(a). The stress ranges 103 MPa and 122 MPa were used to find its endurance limit. The stress ranges 136 MPa and 150 MPa, with loads below the slip resistance, were tested to define higher levels in the S-N curve. The sample shown in Figure 3.16(b) consisted of the combination of A325 HSB and Class B surface finish and was tested under five stress levels.

The stress range of 122 MPa was used to find the fatigue limit for this bolted connection. The other four stress ranges tested, 150 MPa, 169 MPa, 187 MPa and 216 MPa, were used to determine their fatigue behaviour under high stresses and define the S-N curve. The samples made with C50LR Huck tension control bolts and Class B surface finish shown in Figure 3.16(c) were tested under four stress levels. The stress range 122 MPa was used to

verify the endurance limit and the other three stress ranges, 150 MPa, 169 MPa and 187 MPa, were used to determine their fatigue life and define the S-N curve.

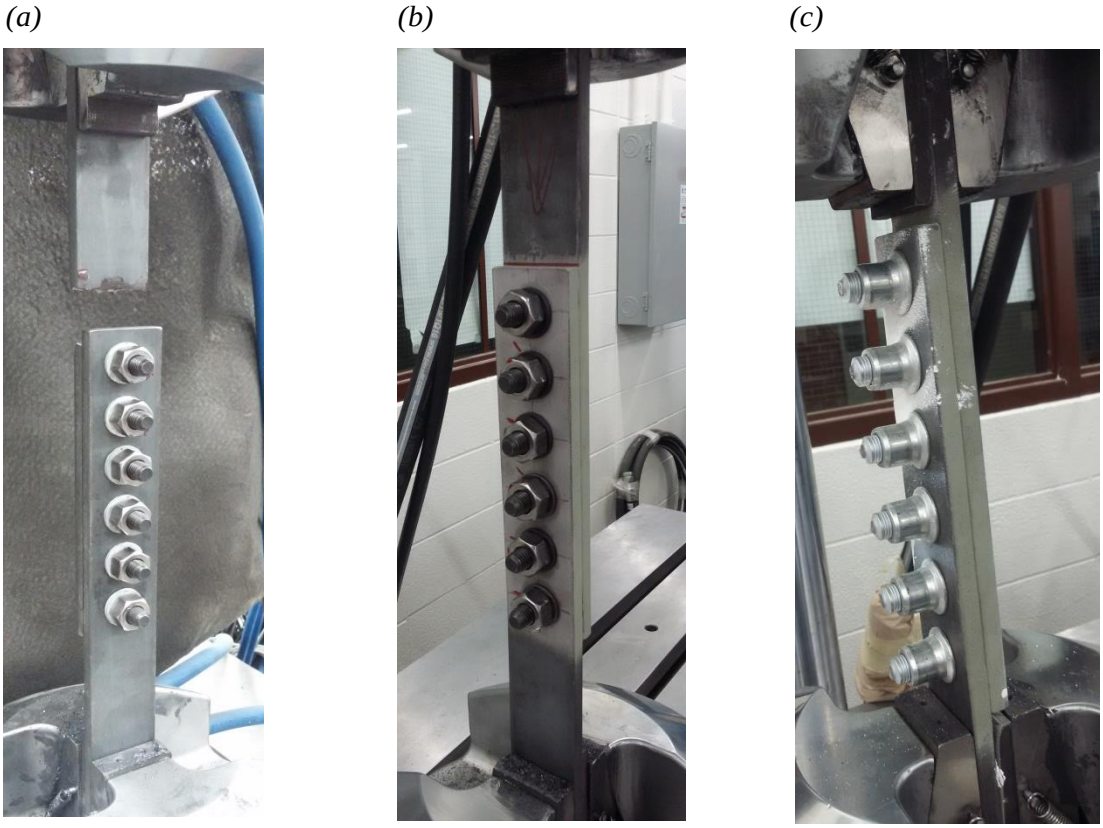

Figure 3.16 Fatigue test set up: (a) Post-failure sample made with A325 HSB and Class A surface finish; (b) Sample made with A325 HSB and Class B surface finish; and (c) Sample made with C50LR Huck bolts and Class B surface finish.

3.6 Morphological Characterization

3.6.1 Initial considerations

One of the difficulties with the bolted connection experiments was that crack initiation and propagation could not be observed since the contact area was hidden between the plates. Post-failure morphological characterization was therefore required to understand the failure behaviour of the tested specimens. Both a stereo microscope and a scanning electron microscope (SEM) were used to examine the contact surfaces and the fracture surfaces of the specimens. These observations were used to characterize the fretting phenomenon, crack initiation and crack propagation behaviour.

3.6.2 Stereo Microscope Examination

The stereo microscope (SZMT2, Optika microscopes, USA) was used for examining all the tested samples. The magnification that could be used was between 3.5X and 90X, depending on the working distance and the use of auxiliary objectives. A 1.3 MPixel digital camera connected to the microscope was used to capture the images and the images were analyzed using AmScope software (AmScope v3.7.13522, USA). Surface cracks could be detected using 7X and 30X total magnification, depending on the desired field of view. The lowest magnification of 7X was used to inspect the contact interface and also to examine the partial slip region around the hole, whereas the highest magnification of 30X was used to observe micro surface cracks, debris, ratchet lines and the crack initiation sites.

3.6.3 Scanning Electron Microscope Examination

The scanning electron microscope (SEM) (JSM-6010LV, JEOL USA Inc.) was used to examine the contact interface and the fracture surfaces. The magnification range used with this microscope was in the range of 30X to 5000X. In-Touch-Scope software (JEOL USA v1.02, Inc.) was used to adjust focus, contrast and brightness of the images for the different magnifications. The samples were cut with a cold saw into 16 mm x 29 mm pieces to mount them on the scanning table, as shown in Figure 3.17. The samples were cleaned using alcohol before mounting onto the holder using conductive tape. Low magnification was used to inspect the whole area of the fracture surface of the specimen to decide on the focus area for higher magnification. Then a higher magnification of 2000X was used to examine the crack initiation sites and crack propagation path on the fracture surface.

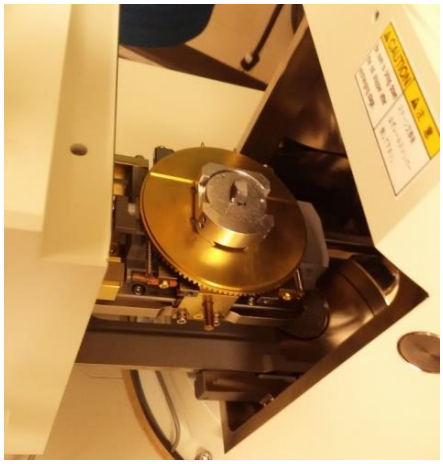

Figure 3.17 SEM sample holder.

CHAPTER 4

RESULTS AND DISCUSSION

4.1 Introduction

This chapter presents the experimental results and discusses the fatigue behaviour of the slip-critical bolted connections. The chapter starts with the results of the surface characterization of the two types of surfaces considered, and then focuses on the results of tests to measure the slip resistance of the bolted connections with different bolt types and surface finishes. The fatigue test results are presented and discussed next, first by presenting the fatigue life of the slip-critical bolted connections in terms of S-N curves, considering the different types of observed fatigue behaviours. Then, the observed fatigue behaviours are characterized for different specimens using examination of the contact interfaces, and relative displacement of the samples, and lastly by investigating the crack initiation sites.

4.2 Surface characterization

4.2.1 Surface roughness

Four parameters, R_a, R_y, R_z and R_q, as defined in Chapter 3, were measured for characterizing the surface roughness. The mean, standard deviation and coefficient of variation of the measured values were calculated and are given in Table 4.1. Detailed results for each test are included in Appendix C.

The results show that the surface roughness parameters for the Class B surface finish were higher than for the Class A surface finish, and that the Class B surface finish was more uniform with higher peaks and deeper valleys on its surface (i.e., rougher surface) due to the coating. This conclusion is validated by analyzing the individual surface parameters. R_a represents the arithmetic mean deviation of the surface profile from the mean surface. The R_a value of 1.490 μm for the Class B surface finish was three times higher than that of the Class A surface finish (0.493 μm), confirming a rougher surface profile for the Class B surface.

Table 4.1: Surface Roughness Measurements

		Ra (µm)	Rq (µm)	Ry (µm)	Rz (µm)
Class A surface finish	**Mean value**	0.493	0.613	2.723	1.870
	Standard deviation	0.187	0.225	1.007	0.823
	Coefficient of variation	38.03%	36.77%	36.99%	44.05%
Class B surface finish	**Mean value**	1.490	1.870	8.217	5.526
	Standard deviation	0.277	0.358	2.351	1.977
	Coefficient of variation	18.61%	19.13%	28.61%	35.78%

Similarly, R_q represents the root mean square (RMS) of the surface profile deviation. The R_q mean value for the Class B surface finish was three times higher than that of the Class A surface finish, which again confirmed the rougher surface profile for the Class B surface. The coefficients of variation of R_a and R_q were lower for the Class B surface finish, which indicates that the Class B surface finish was more uniform.

Considering the R_y parameter (maximum height of the profile), the mean value for the Class B surface (8.217 µm) was three times higher than that of the Class A surface (2.723 µm), which showed that there were higher peaks and deeper valleys in the Class B surface. Moreover, half of the R_y value corresponds roughly to the height of the highest peak or the depth of the deepest valley of the surface profile; for Class A this value was 1.361 µm and for Class B it was 4.109 µm, demonstrating that the class B surface finish had a rougher surface profile compared to Class A. Relatively high values of the coefficient of variation of the R_y parameter confirms that the magnitude of the highest peak or the deepest valley for both surface finishes varied with location.

In addition, R_a can be compared to the half of the R_y value for the individual surface finishes to identify whether the surfaces have a large number of peaks and valleys similar to the highest peak and deepest valley. The half R_y value for the Class A surface finish (1.361 µm) is 2.76 times higher than the R_a parameter (0.493 µm). Similarly, for the Class B surface finish, the half R_y value of 4.109 µm is also 2.76 times higher than the mean value of the R_a parameter of the Class B surface finish (1.490 µm). This indicated that the highest peaks and the deepest valleys do not dominate either of the surface finishes.

A similar behaviour was also observed in the R_z parameter, which represents the five highest peaks and five lowest valleys on a surface profile. The difference between the R_z

parameters of both surface finishes was also of the order of three times. By comparing the R_a and R_z parameters for the individual surfaces, it can be determined whether the surfaces had high or low values of heights and depths on the surface profile. The R_z value for the Class A surface finish was almost four times higher than the R_a value, suggesting that there were a large number of small peaks and valleys compared to the five highest peaks and deepest valleys. For the Class B surface finish, the R_z value was also almost four times higher than the R_a parameter. This indicated that most of the peaks and valleys in the Class B surface finish were generally smaller than the five highest peaks and deepest valleys. Higher values of the coefficient of variation were present in the R_z parameter, which indicated that the values of the five highest peaks or deepest valleys were not same at different locations on the same surface.

Overall, the Class B surface finish had a surface roughness that was approximately three times higher than that of the Class A surface finish. In addition, the Class B surface finish had a more uniform surface profile compared to the Class A surface finish. The surface roughness characterization was very useful for quantifying the difference between the two surface finish types. Surface roughness may be a helpful parameter to consider when developing an efficient slip resistance in bolted connections.

4.2.2 Coefficient of friction

The coefficients of static and kinetic friction were measured for both types of surface finish and are provided in Table 4.2. The mean values, the standard deviations and the coefficients of variation were calculated from the measurements. Detailed results for each test are included in Appendix D.

The coefficient of static friction (μ_s) for the Class A surface finish was in the range of 0.249 to 0.344, with a mean value of 0.288. The values of μ_s for the Class B surface finish were in the range of 0.752 to 0.932, with a mean value of 0.840. The mean value of the coefficient of static friction (μ_s) for the Class B surface was 3.68 times higher than that of the Class A surface finish. This is largely due to the rougher Class B surface finish compared to the Class A surface finish, as discussed in the previous section.

Table 4.2: Coefficient of friction

	Class A surface finish		Class B surface finish	
	Static (μ_s)	**Kinetic (μ_k)**	**Static (μ_s)**	**Kinetic (μ_k)**
Mean value	0.288	0.261	0.840	0.730
Standard deviation	0.028	0.008	0.052	0.024
Coefficient of variation	9.74%	2.9%	6.24%	3.35%

The value of coefficient of kinetic friction (μ_k) for the Class A surface finish was in the range of 0.253 to 0.278, with a mean value of 0.261, whereas for the Class B surface, the coefficient of kinetic friction varied from 0.701 to 0.758, with a mean value of 0.730. The coefficient of variation for the coefficient of kinetic friction for both surface finishes was lower than that for the coefficient of static friction. Similarly, the mean value of the coefficient of kinetic friction (μ_k) of the Class B surface finish was 2.80 times higher than that for the Class A surface finish, similar to what was observed for the coefficient of static friction.

As a result, the Class B surface finish is considered to be rougher than the Class A surface finish with a higher coefficient of static friction. The coefficient of static friction results are consistent with the surface roughness measurements presented in the previous section because the Class B surface finish was observed to be approximately three times rougher than the Class A surface finish. In addition, the coefficient of variation of the friction measurements was slightly higher in the results for the Class A surface finish, which also corresponds to greater variability in the surface roughness.

Overall, the measurements of surface roughness and coefficients of friction confirmed that the Class B surface finish was approximately three times rougher and more uniform than the Class A surface finish due to surface preparation and surface coating. The coated Class B surface finish therefore increased the coefficient of friction and surface roughness within the contact interface of the single lap joint bolted specimens.

4.3 Slip resistance

The slip resistance was generated by friction forces within the contact interface of the single lap joint bolted specimens and was induced by the contact pressure between the plates caused by bolt pre-tension combined with the coefficient of friction between the material

surfaces. The applied bolt pre-tension was assumed to be a minimum of 70% of the bolt's tensile strength (F_u) of 53 kN, according to Table 7 of CSA S16-14.

Figure 4.1 shows typical load vs relative displacement curves for the experimental slip resistance tests for each combination of bolt type and surface finish. The relative displacement was measured as the difference between the laser displacement sensor readings for the corresponding axial load. As the load was applied, the bolt pretension combined with the slip coefficient resisted the external load by inducing a frictional force within the contact interface. This frictional force increased linearly with respect to the externally applied load before reaching a maximum slip resistance value. This stage was defined as the slip resistance stage.

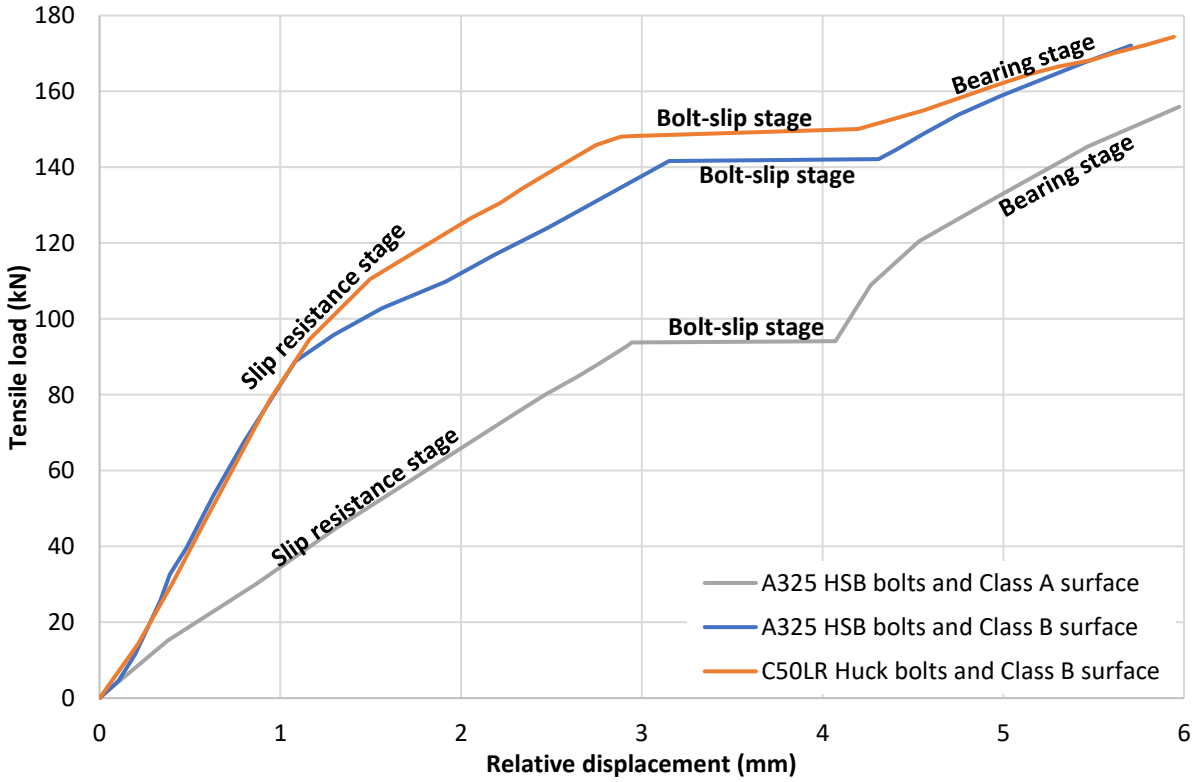

Figure 4.1 Typical load-displacement curves of the slip resistance tests.

As discussed earlier, the Class B surface finish had a higher surface roughness and a higher coefficient of friction than the Class A surface finish. As a result, samples made with the Class B surface finish had a higher slip resistance than the samples made with the Class A surface finish. Furthermore, the samples made of tension control bolts with Class B

surface finish had a slightly higher slip resistance than samples assembled with A325 HSB and Class B surface finish. This might be due to a higher clamping force applied by the C50LR Huck tension control bolts, but this could not be confirmed.

During the slip resistance stage, the slope of the curve for connections that used the combination of A325 HSB and Class A surface finish was constant. Therefore, the relative motion of the plates for these specimens was stable during this stage and they did not suffer significant sliding along the contact interface or loss in the level of pre-tension in the bolts.

For the samples assembled with a Class B surface finish and A325 HSB, the slip resistance initially increased linearly with respect to the applied load. However, the slope then decreased as a loss of slip resistance occurred before reaching a maximum value of slip resistance. The loss of slip resistance during the second part of the slip resistance stage might be the result of friction loss within the contact interface. This might be due to the removal of parts of the surface coating as the relative displacement induced wear on the contacting surfaces.

Similar behaviour was observed for the combination of C50LR Huck tension control bolts and Class B surface finish. During the initial stage, the slip resistance increased linearly with respect to the applied load with a relatively high slope and then loss of slip resistance, manifested by a reduction in slope, occurred due to friction loss before reaching a maximum slip resistance value.

Figure 4.2 shows an image of the contact surfaces of a sample with the combination of A325 HSB and Class B surface finish after testing, where the surface damage due to the removal of the coating can be seen. This observation is consistent with friction loss within the contact interface due to the relative displacement during the slip resistance stage, although most of the surface damage likely occurred during the slip stage.

Once the maximum slip resistance was reached, the slip-critical connections moved into a bolt-slip stage, during which the friction force between the plates remained constant. After more than 1 mm of slip, the bolts began to bear against the plates and the connections became bearing connections. During the bearing stage, the applied load was carried by the plates and the bolts, and friction no longer played a significant role.

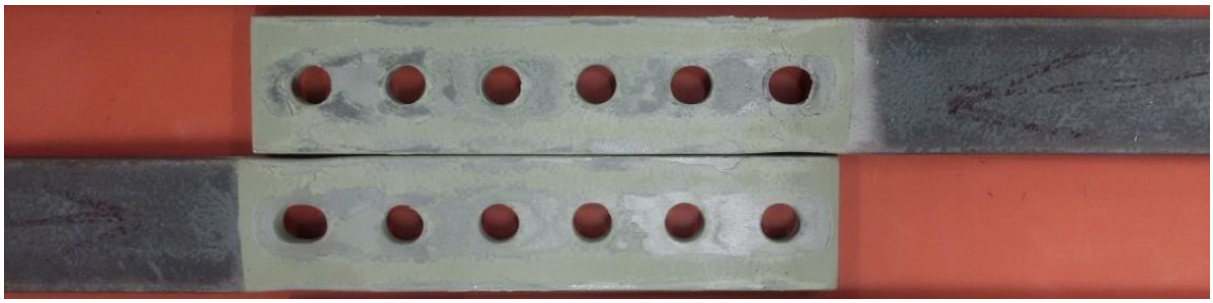

Figure 4.2 Camera image of the contact interface of a specimen with A325 HSB and Class B surface finish after static testing showing wear of the surface finish.

Figure 4.3 shows the experimentally measured mean slip resistance of the three types of slip-critical bolted connections tested, in which the error bars correspond to the standard deviations. Detailed results for each test are included in Appendix E. The mean values of the slip resistance of samples made with A325 HSB and Class A surface finish, A325 HSB and Class B surface finish, and C50LR Huck tension control bolts and Class B surface finish were 93 kN, 138 kN, and 146 kN, respectively. The higher value of the error bars for the combination of A325 HSB and Class A surface finish was a result of larger deviations in the experimental results. The lowest standard deviation corresponds to the samples assembled with C50LR Huck tension control bolts and Class B surface finish. The differences between the mean values for all three specimen types were found to be statistically significant at the 95% confidence limit (see Appendix F).

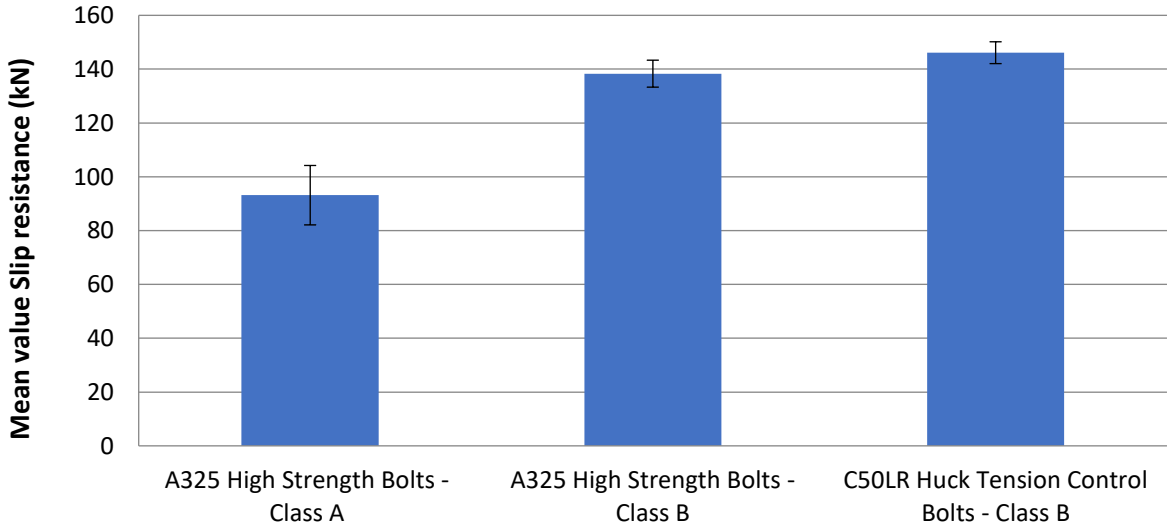

Figure 4.3 Slip resistance, as measured experimentally. The theoretical slip resistance, as recorded in Chapter 3 was higher than these values.

In general, the experimental slip resistance values were lower than the theoretically calculated values for all the samples. The experimental mean slip resistance of the A325 HSB and Class A surface finish combination was approximately 94% of the theoretical value, for the A325 HSB and Class B surface finish combination it was 78% of the theoretical value, and for the C50LR Huck tension control bolts and Class B surface finish combination it was 82% of the theoretical value.

The slip coefficient (k_s) represents the constant of proportionality between the friction force within the contact interface between the bolted plates and the normal force between the plates. The amount of friction that can be generated between two surfaces is proportional to the surface roughness, and a higher slip coefficient produces a higher resistance to relative sliding and therefore slip resistance. The slip coefficient (k_s) was calculated using the slip resistance results and assuming that the bolts reached a level of pre-tension of 70% of their tensile strength. In other words, the values of slip resistance that were determined and presented in Figure 4.3 were divided by 53 kN, which is the value specified by CSA S16-14. The results are shown in Figure 4.4. Detailed results are included in Appendix G.

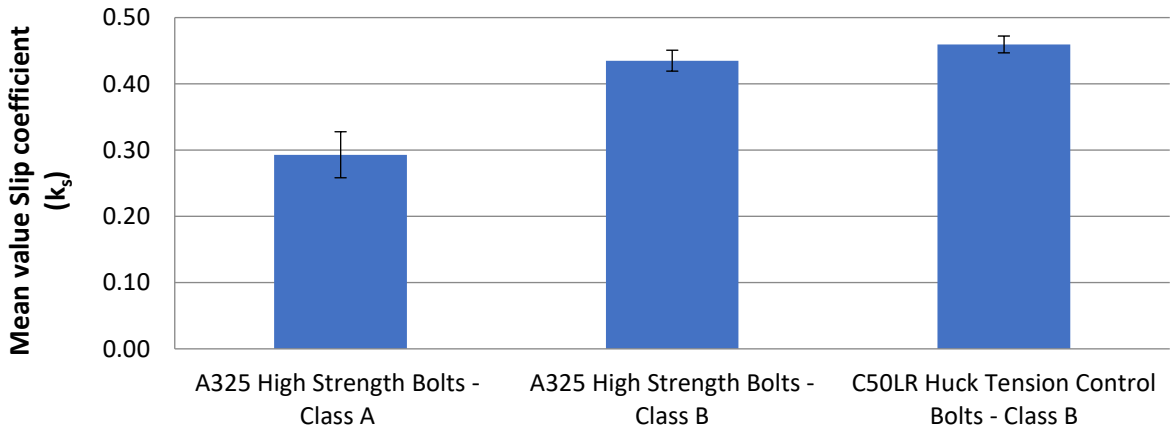

Figure 4.4 Slip coefficient (k_s) calculated using the slip resistance results.

For the Class A surface finish, the mean value of the experimental slip coefficient (0.293) was 97% of the theoretical value of 0.30 specified in CSA S16-14. Conversely, for the Class B surface finish, the mean experimental values of k_s were 84 to 88% of the theoretical value of 0.52 specified by CSA S16-14. During the slip resistance stage, part of the coating was removed from one of the plates at the contact interface, due to the relative displacement between the clamped plates, which broke the interlocked surface asperities of

the coated surface. These effects caused a slip coefficient k_s that was lower than the one recommended by CSA S16-14.

The effect of bolt pre-tension on the slip resistance can be identified by comparing the results of the A325 HSB and Class B surface finish combination with those of the C50LR Huck tension control bolts and Class B surface finish combination. It is clear from the results that the C50LR Huck tension control bolts provided a higher and consistent clamping force, which resulted in a higher slip resistance in comparison with the A325 HSB bolted samples.

4.4 Fatigue life (S-N curves)

4.4.1 Overview

The slip critical bolted connections were tested under fatigue loading conditions to measure the fatigue life and characterize the fatigue failure behaviour. Table 4.3 summarizes the test results, including the fatigue test parameters, the number of cycles experienced, the failure mode (fretting or bending, as discussed later), the location of crack initiation (at the hole edge or a certain distance from the hole above the uppermost bolt in the connection), and for which samples the DIC technique was used to capture images. The combination of Class A surface finish with A325 HSB were named as A series, Class B surface finish with A325 HSB were named as B series, and Class B surface finish with C50LR Huck bolts were coded as C series.

The stress range versus number of cycles to failure (S-N curve) results for 41 fatigue tests are plotted in Figure 4.5 along with the S-N curve for detail category B (slip-critical bolted connections) from CSA S16-14. Eight samples (all with Class A surface) failed due to fretting fatigue, while 8 samples did not fail after 8 million cycles. The latter group was assumed to be representative of the endurance limit. The remaining samples failed due to bending fatigue, although evidence of fretting was also apparent. CSA S16-14 indicates that the detail-category B S-N curve should not be used if bending is induced in an axially loaded bolted connection. However, the Canadian Highway Bridge Design Code (CSA S6-14) recommends that the S-N curve can be plotted with a combination of bending and axial load.

Table 4.3: Fatigue test results

Stress range (MPa)	Sample	Number of cycles	Failure Mode	Crack initiation zone	DIC measurements
103.3	A1-A325-103	3,500,713	No Failure	-	-
122.12	A2-A325-122	3,709,575	Fretting	Away from hole	-
	A3-A325-122	8,002,185	No Failure	-	-
	A4-A325-122	7,608,877	No Failure	-	-
	A5-A325-122	1,425,162	Fretting	Away from hole	-
	A6-A325-122	8,495,372	No Failure	-	-
	B1-A325-122	8,132,741	No Failure	-	-
	B2- A325-122	8,564,976	No Failure	-	-
	C1-C50LR-122	7,727,804	No Failure	-	-
	C2-C50LR-122	8,000,000	No Failure	-	-
136.21	A7-A325-136	2,054,222	Fretting	Hole edge	-
	A8-A325-136	2,607,685	Fretting	Away from hole	-
	A9-A325-136	1,928,344	Fretting	Away from hole	-
150.3	A10-A325-150	937,892	Fretting	Away from hole	-
	A11-A325-150	1,309,628	Fretting	Away from hole	-
	A12-A325-150	931,312	Fretting	Away from hole	-
	A13-A325-150	914,215	Interrupted tests for crack initiation	Away from hole	-
	A14-A325-150	1,317,177			-
	A15-A325-150	972,135			-
	A16-A325-150	1,425,084			-
	B3- A325-150	7,515,227	Bending	Hole edge	-
	B4- A325-150	8,474,936	No Failure	-	-
	B5- A325-150	874,463	Failed Inside grip	-	X
	C3-C50LR-150	1,489,342	Bending	Hole edge	-
	C4-C50LR-150	1,307,330	Bending	Hole edge	-
	C5-C50LR-150	1,082,560	Bending	Hole edge	-
	C6-C50LR-150	1,097,196	Bending	Hole edge	-
	C7-C50LR-150	1,170,318	Bending	Hole edge	-
	C8-C50LR-150	1,516,033	Bending	Hole edge	-
	C9-C50LR-150	1,215,972	Bending	Hole edge	-
	C10-C50LR-150	1,255,384	Bending	Hole edge	X
169.09	B6-A325-169	313,546	Bending	Hole edge	-
	B7-A325-169	368,417	Bending	Hole edge	-
	B8-A325-169	349,697	Bending	Hole edge	X
	C11-C50LR-169	366,743	Bending	Hole edge	-
	C12-C50LR-169	382,764	Bending	Hole edge	-
	C13-C50LR-169	325,597	Bending	Hole edge	-
	C14-C50LR-169	351,185	Bending	Hole edge	X
187.88	B9-A325-187	142,362	Bending	Hole edge	-
	B10-A325-187	139,516	Bending	Hole edge	-
	C15-C50LR-187	155,061	Bending	Hole edge	-
	C16-C50LR-187	168,025	Bending	Hole edge	-
	C17-C50LR-187	166,332	Bending	Hole edge	-
216.06	B11-A325-216	67,972	Bending	Hole edge	-
	B12-A325-216	72,396	Bending	Hole edge	-
	B13-A325-216	70,900	Bending	Hole edge	-

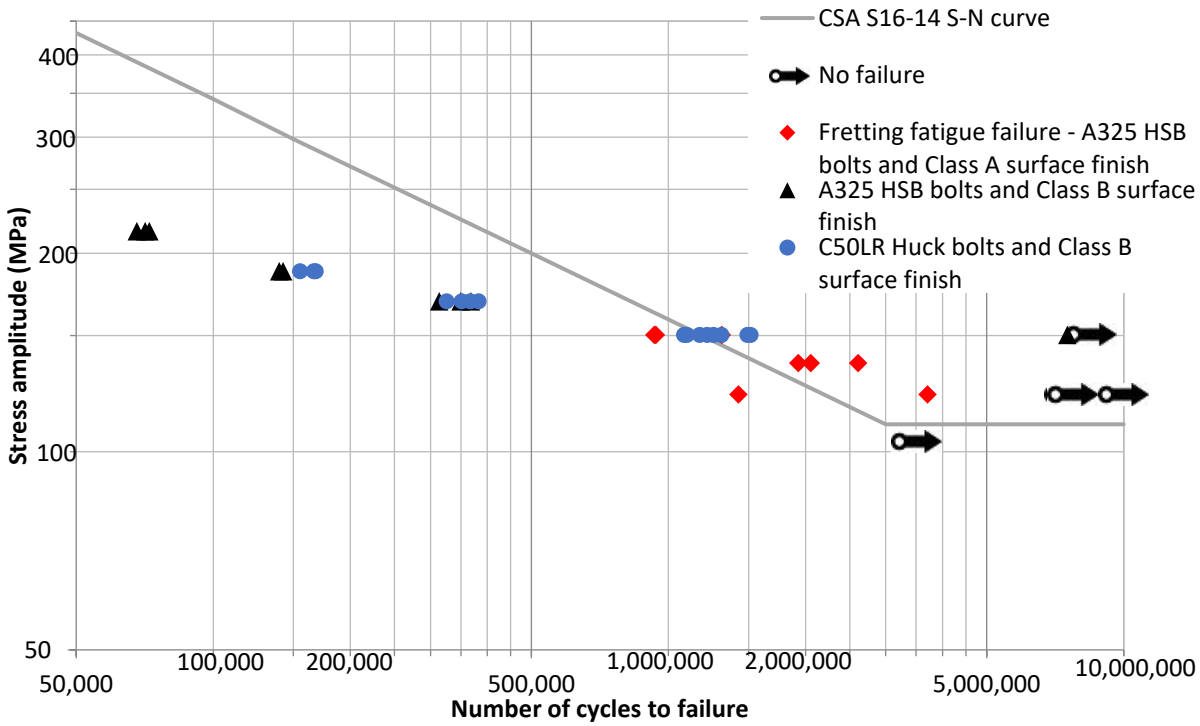

Figure 4.5 Fatigue life of every sample tested, plotted with the CSA S16-14 S-N curve for Detail Category B.

4.4.2 Class B surface and A325 HSB

The A325 HSB and Class B surface finish samples experienced a combination of secondary bending and fretting fatigue, but failure was initiated by bending fatigue. The S-N results for these samples are plotted in Figure 4.6. In this figure, the experimental results are compared with the S-N curve for detail category B given by CSA S16-14. At high stress ranges (216, 187 and 169 MPa), the number of cycles to failure for the eight specimens tested were significantly lower than the number of cycles predicted by CSA S16-14. This is believed to be due to the secondary bending load that was acting along with the fretting effect. Secondary bending resulted in crack initiation at a separate location at the hole edge and led to the failure of the specimens. From the results, it can be concluded that at high stress range levels, the crack that formed due to bending fatigue initiated and began propagating earlier than fretting initiated cracks and led to a lower number of fatigue life cycles. The S16-14 S-N curve did not account for the secondary bending effects. The stress ranges in the S16-14 S-N curve should include bending stresses according to Clauses 26.1 and 26.3.1.

Considering the lower fatigue stress ranges, three samples were tested at a stress range of 150 MPa (one of which failed in the grip) and another two samples were tested at a stress range of 122 MPa. One specimen at the 150 MPa stress range and both at the 122 MPa stress range did not fail and the tests were stopped after 8 million cycles. The two specimens at the 122 MPa stress range had different lengths (579 mm and 400 mm) and both samples did not fail. This suggests that the total length of the specimen did not affect the fatigue failure behaviour of the bolted connections.

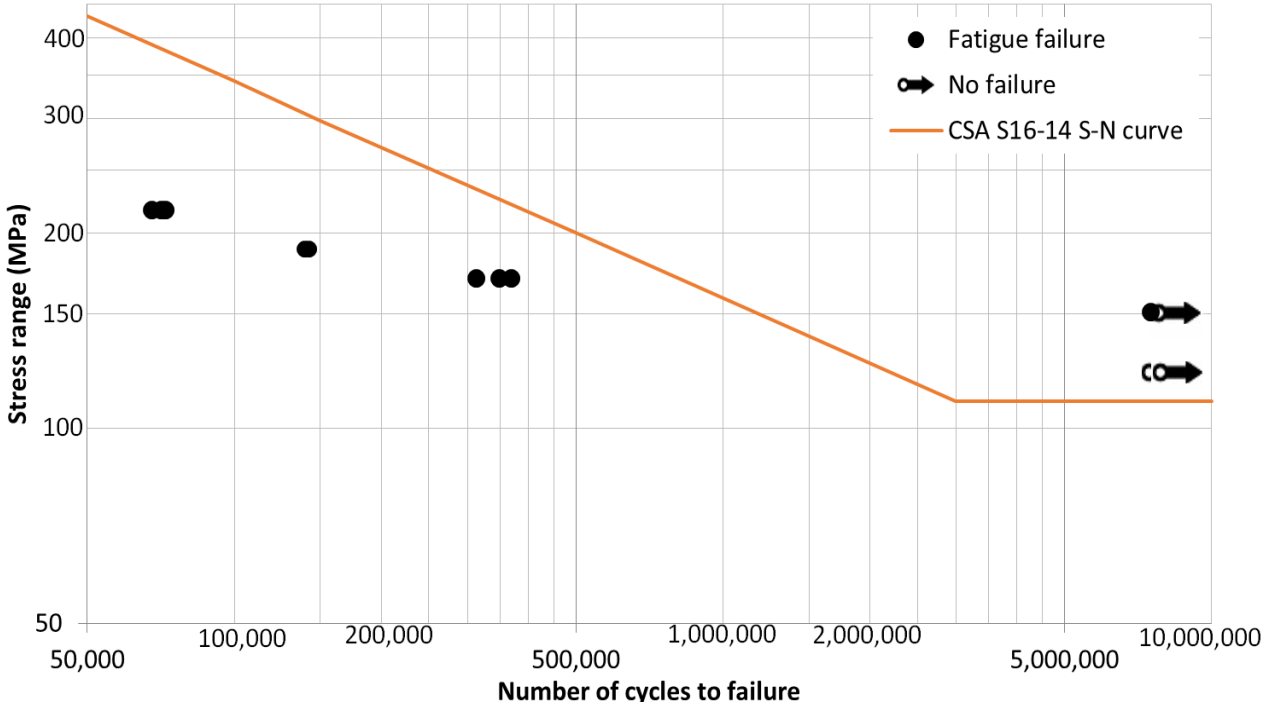

Figure 4.6 Fatigue life test results of samples using A325 HSB and Class B surface finish.

There is a large difference between the experimental results and the CSA S16-14 S-N curve for the 150 and 122 MPa stress ranges. Specimen B3-A325-150 failed at 7.5 million cycles, whereas specimen B4-A325-150 did not fail and the test was stopped after 8.5 million cycles, even though both were tested at the 150 MPa stress range. Specimens B1-A325-122 and B2-A325-122, tested at the 122 MPa stress range, did not fail after 8.5 million cycles. However, the CSA S16-14 standard S-N curve fatigue life for a stress range of 150 MPa is around 1.5 million cycles and for the 122 MPa stress range it is around 3 million cycles, much lower than the experiment results. Moreover, the stress range of

122 MPa can be considered to lie below the endurance limit based on the experimental results for samples with a Class B surface finish and A325 HSB.

The 5% fractile values for fatigue life were also calculated based on the experimental results, and are shown in Table 4.4. These were used to generate the experimental S-N curve for comparison with CSA S16-14, as shown in Figure 4.7. The two curves intersect at a stress range of 135 MPa and fatigue life of approximately 1.7 million cycles. The experimental endurance limit was assumed to be 122 MPa because two samples did not fail at that stress level after more than 8 million cycles were applied. 122 MPa is higher than the endurance limit for detail category B found in Table 10 of CSA S16-14 (110 MPa).

Table 4.4: 5% fractile values of fatigue life for samples with Class B surface and A325 HSB

	Number of cycles to failure				
Stress range (MPa)	**Number of samples**	**Mean value**	**Standard deviation**	**Coefficient of variation**	**5% fractile values**
150.30	1	7,515,227		8.50% (assumed)	6,878,756
169.09	3	343,887	27,893	8.11%	298,002
187.88	2	140,939	2,012	1.43%	137,629
216.06	3	70,423	2,250	3.20%	66,721

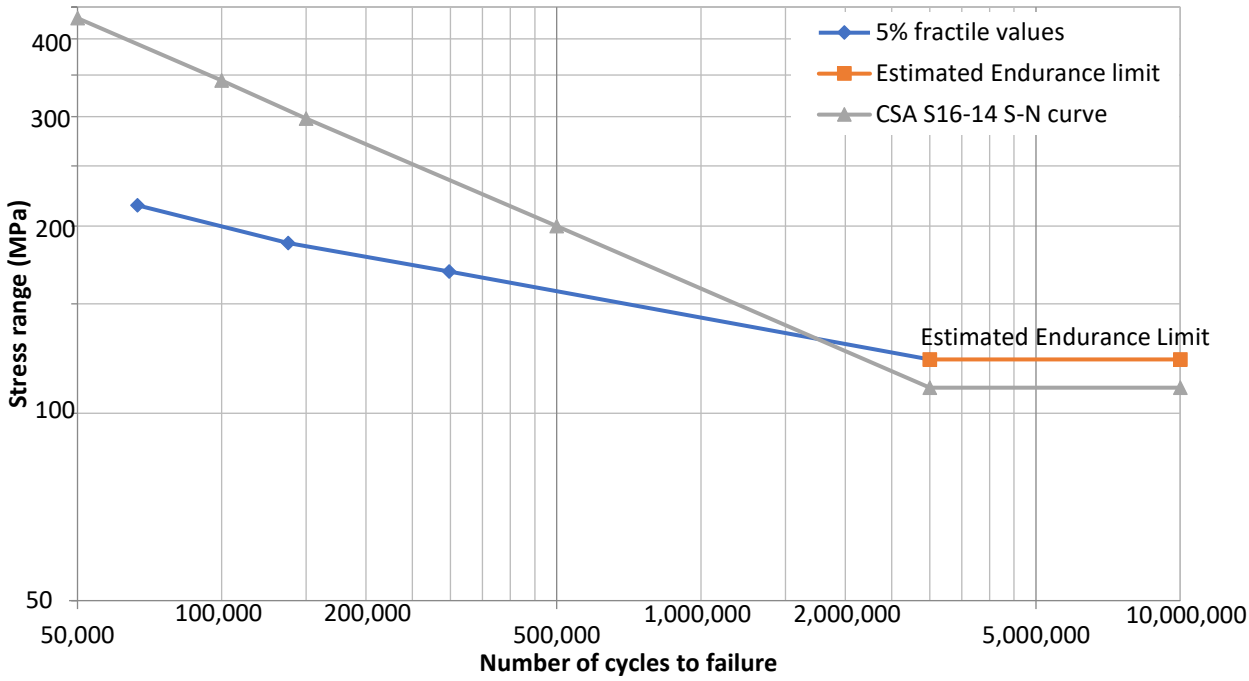

Figure 4.7 S-N curve of specimens assembled with A325 HSB and Class B surface finish.

The lowest coefficient of variation values were found for the two highest stress ranges (187 and 216 MPa). Schijve et al. (2009) also observed that the secondary bending effect reduced the fatigue life at higher stress range levels in single lap joint test specimens. At the lower stress range levels, it appears that the fatigue lives of the single lap joint specimens were increased by the coating on Class B surface finish samples. The 5% fractile value result for the 150 MPa stress range was not taken in consideration to plot the S-N curve due to insufficient data because just one sample failed at that stress level.

4.4.3 Class B surface and C50LR Huck bolts

Four stress ranges were selected for the tests conducted with C50LR Huck tension control bolts and Class B surface finish and these specimens were coded with letter 'C'. The total specimen length for these specimens was kept at 400 mm, with an overlap length of 175 mm, based on the previous analysis results. Three specimens were tested at 187 MPa, four specimens at 169 MPa, eight at 150 MPa, and two at 122 MPa.

The S-N curve results are plotted in Figure 4.8 along with the CSA S16-14 curve for detail category B. Similar behaviour to that experienced for samples with A325 HSB was observed at the higher stress range levels. The experimental fatigue lives for the 187 and 169 MPa stress ranges were lower than the S-N curve given by CSA S16-14. This is likely due to the bending effect, as discussed above. At the lower stress range level of 150 MPa, the fatigue lives were in the range of 1 to 1.5 million cycles. However, at the 122 MPa stress range level, the specimens did not fail and the tests were stopped after 8.5 million cycles. Based on the results, it was concluded that specimens with a combination of Class B surface and C50LR Huck bolts had an endurance limit of 122 MPa, which is higher than the CSA S16-14 standard S-N curve.

The 5% fractile values for fatigue life based on the experimental results are provided in Table 4.5. As was observed for samples with standard high strength bolts, the coefficients of variation at the two highest stress levels were low, whereas that at the 150 MPa stress range is relatively high. The 5% fractile value of fatigue life at the 150 MPa stress range was lower than that given in CSA S16-14.

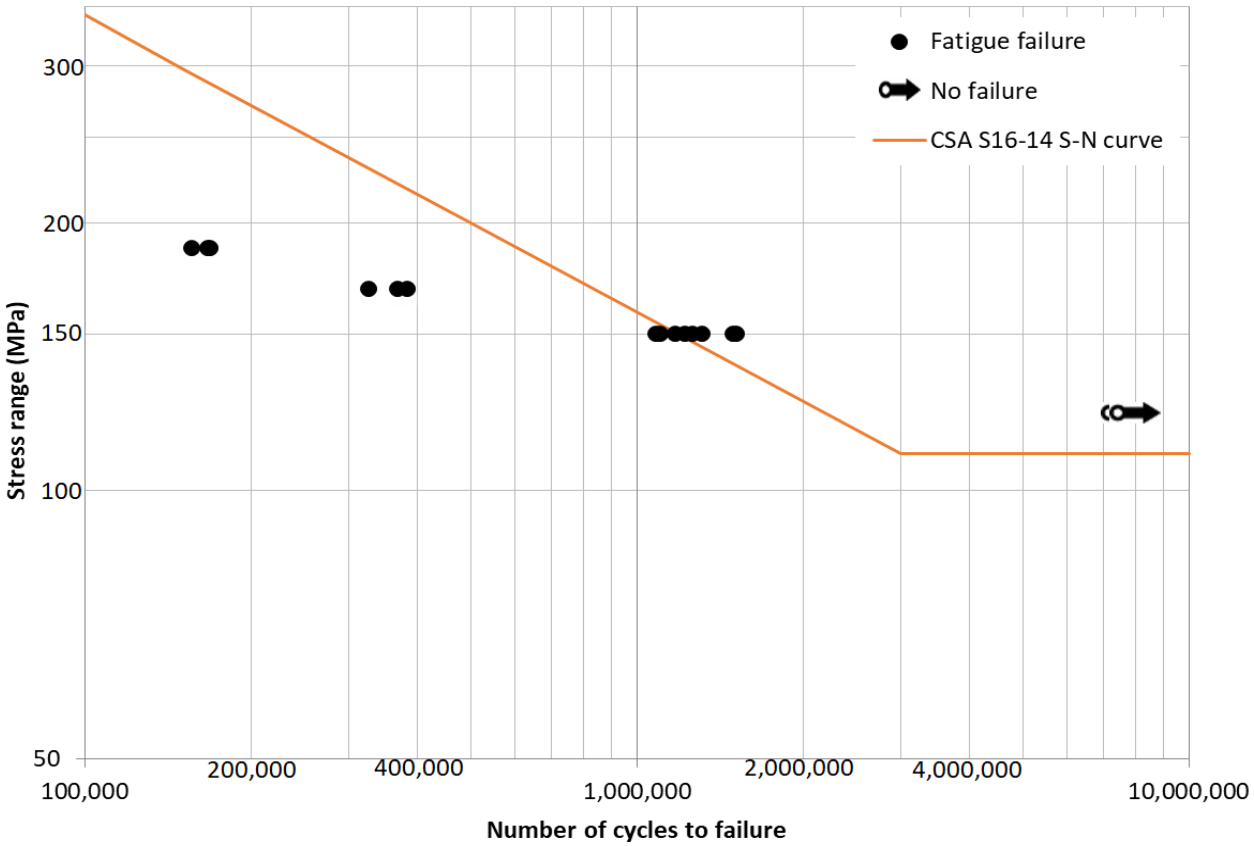

Figure 4.8 Fatigue life test results of samples using Huck C50LR bolts and Class B surface finish.

Table 4.5: 5% fractile values of fatigue life for samples with Class B surface and C50LR Huck bolts

		Number of cycles to failure			
Stress range (MPa)	**Number of samples**	**Mean value**	**Standard deviation**	**Coefficient of variation**	**5% fractile values**
150.30	8	1,266,767	163,889	12.94%	997,170
169.09	4	356,572	24,344	6.83%	316,526
187.88	3	163,139	7,047	4.32%	151,547

The experimental S-N curve for these samples, including the estimated endurance limit, is shown in Figure 4.9. This S-N curve is different from the CSA S16-14 S-N curve, especially at the highest stress levels. The curves intersect just below the 150 MPa stress range. In addition, the endurance limit of the CSA S16-14 S-N curve is conservative because it is lower than the results from the tests. The difference can again be attributed to the fact that the CSA S16-14 S-N curve does not account for bending.

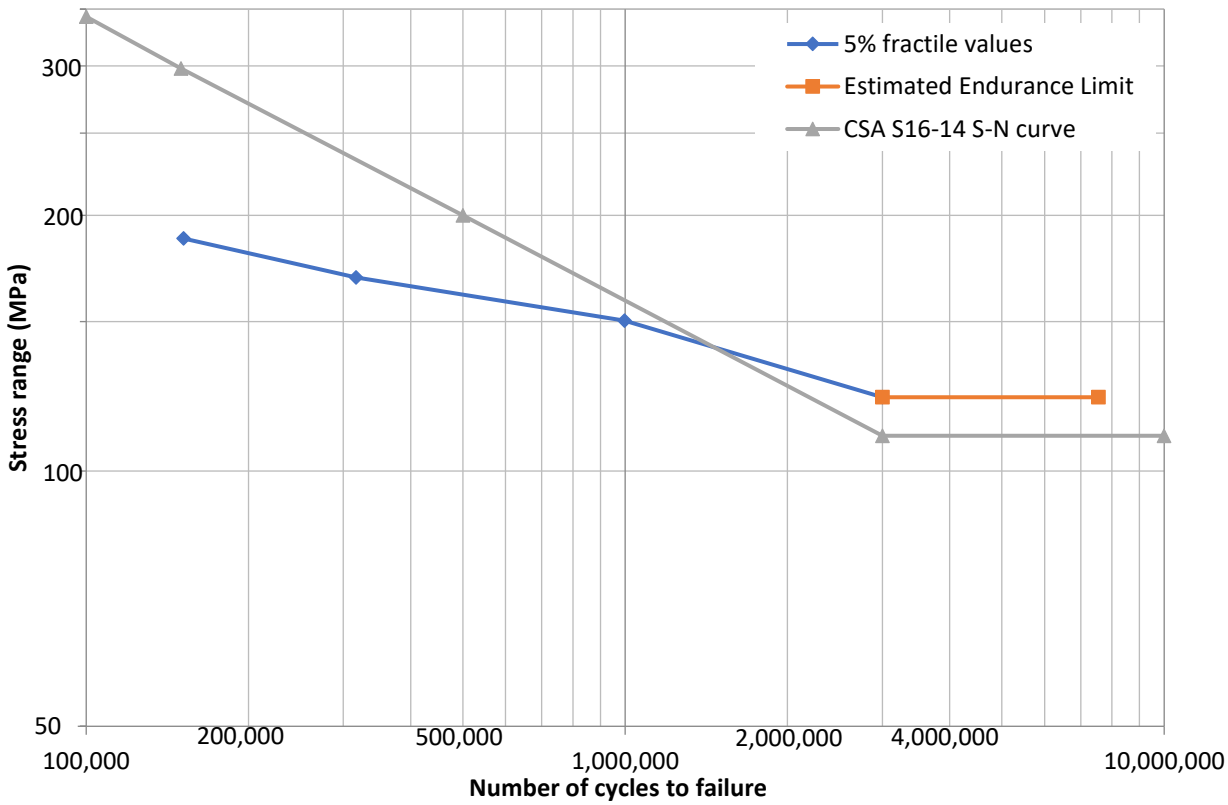

Figure 4.9 S-N curve of specimens with C50LR Huck bolts and Class B surface finish.

4.4.4 Class A Surface Samples

Specimens with a Class A surface finish and A325 HSB failed due to fretting fatigue. In total, sixteen samples were tested at four different stress ranges (103, 122, 136, 150 MPa). Only one sample was tested at the 103 MPa stress range and the specimen did not fail. The test was stopped after 3.5 million cycles. Five specimens were tested with a 122 MPa stress range, of which three specimens did not fail after 8.5 million cycles, while the remaining two failed by fretting fatigue after 1.4 million and 3.7 million cycles, respectively. At higher stress range levels, three specimens were tested with a 136 MPa stress range and another seven specimens were tested at the 150 MPa stress range. With the exception of the interrupted tests, these all failed due to fretting fatigue. The experimental stress range versus number of cycles to failure (S-N) is shown in Figure 4.10 along with the S-N curve from CSA S16-14.

At the 136 MPa stress range, the experimental fatigue life was higher than that given in CSA S16-14. However, for the 150 MPa stress range, the experimental fatigue lives were

scattered around the value provided by CSA S16-14; three samples had higher fatigue lives than those given by CSA S16-14, while another four specimens had lower fatigue lives. Similar variability was also seen at lower stress ranges as well. At the 122 MPa stress range, one sample (A5-A325-122) failed at 1.4 million cycles, another (A2-A325-122) at 3.7 million cycles and the last three specimens did not fail even after 7.6 million cycles. However, the endurance limit given by CSA S16-14 is 110 MPa. The experimental results show that the stress range of 122 MPa could be considered as the endurance limit for these samples. The reason behind the higher endurance limit might be due to the surface preparation, which is important according to Stankevicius et al. (2009).

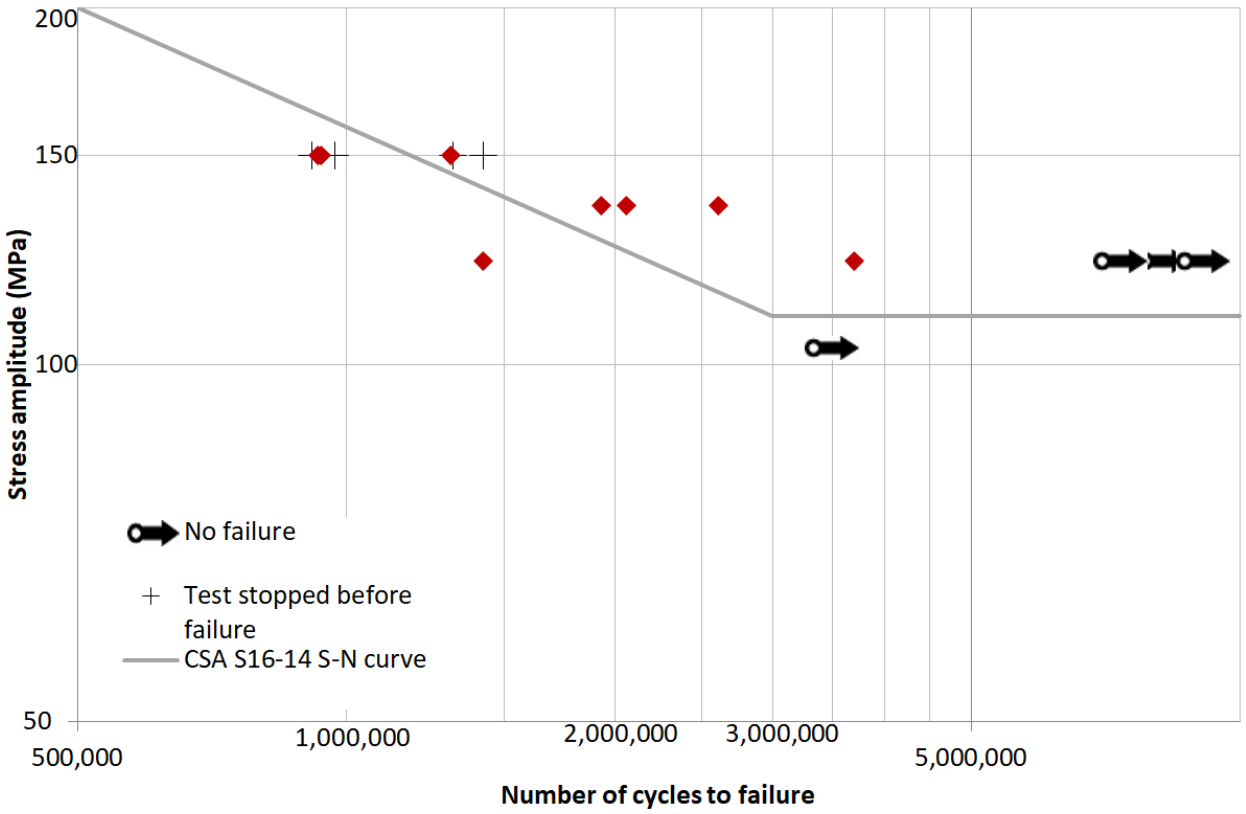

Figure 4.10 Fatigue life test results for samples using A325 HSB and Class A surface finish.

The 5% fractile values for this set of specimens are given in Table 4.6. This table also shows that the fatigue life results are scattered for all three stress ranges. At the 136 MPa stress range, the difference between the maximum and minimum fatigue life is almost 700,000 cycles. However, the lowest coefficient of variation is found at the same stress level. For the 150 MPa stress range, the fatigue lives are scattered, with a mean value of

1.1 million cycles but a 5% fractile value of 0.7 million cycles, which is lower than the fatigue life expected from the CSA S16-14 S-N curve. However, the number of samples at each stress level is relatively small.

Table 4.6: 5% fractile values of fatigue life for samples with A325 HSB and Class A surface finish

		Number of cycles to failure			
Stress range (MPa)	**Number of samples**	**Mean value**	**Standard deviation**	**Coefficient of variation**	**5% fractile values**
122.12	2	2,567,369	1,615,324	62.92%	
136.21	3	2,196,750	361,403	16.45%	1,602,243
150.30	3	1,059,611	216,546	20.44%	703,392

The S-N curve for the 5% fractile values is shown in Figure 4.11. The experimental endurance limit is higher than the S-N curve from CSA S16-14. Both curves intersect at the 136 MPa stress range with a similar fatigue life of approximately 1.6 million cycles. However, for the 150 MPa stress range, the experimental fatigue life is lower than the S-N curve given by CSA S16-14. This is believed to be due to the bending effect, as discussed above.

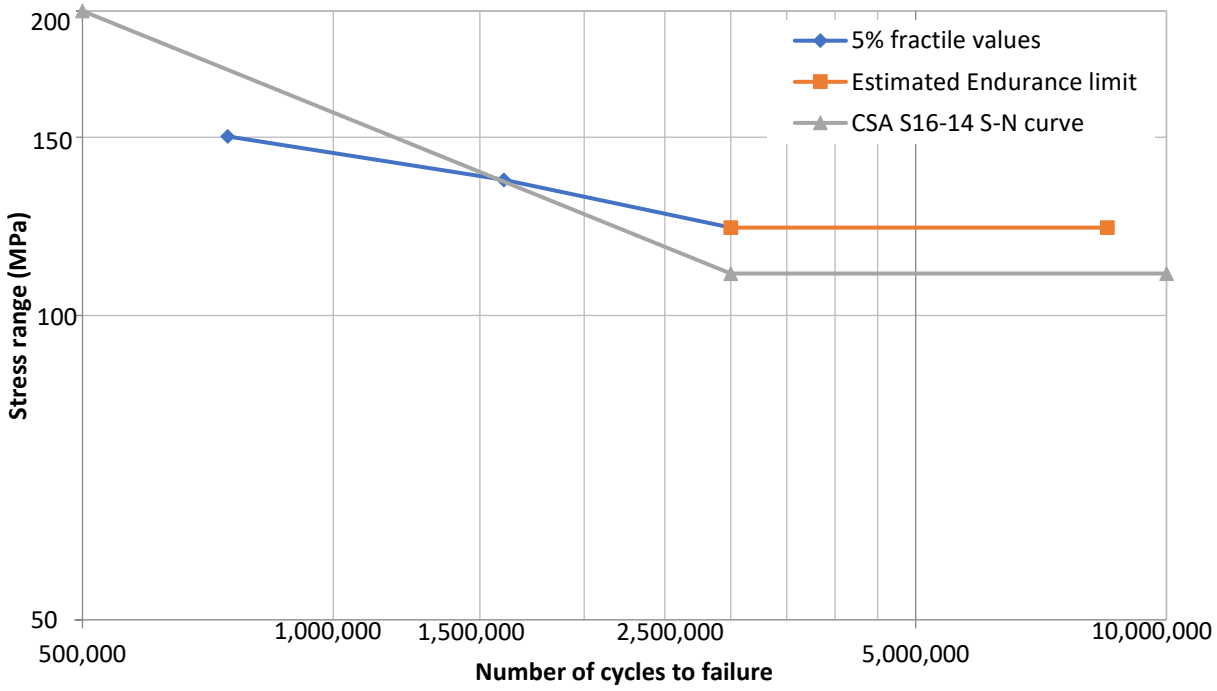

Figure 4.11 Experimental S-N curve based on the 5% fractile values for fatigue life for samples that consisted of Class A surface finish and A325 HSB.

4.4.5 Influence of surface finish and bolt type on fatigue life

One of the objectives of this research project was to compare the performance of specimens with two different surface finishes and two different bolt types (A325 HSB and Huck C50LR). The mean S-N curves of all specimens, along with the S-N curve from CSA S16-14, are plotted in Figure 4.12. At the 150 MPa stress range, specimens with the Class A surface finish samples showed lower fatigue lives compared to those with the Class B surface finish. The mean fatigue life at the 150 MPa stress range for Class A surface finish with A325 HSB was approximately 1.06 million cycles, while specimens with Class B surface finish and C50LR Huck bolts had a mean fatigue life close to 1.27 million cycles. However, the difference is not statistically significant at the 90% level of confidence. Only one specimen with Class B surface finish and A325 HSB failed, and it survived more than 7.5 million cycles. Similar behaviour was observed at the 122 MPa stress range, i.e., no Class B surface finish specimens failed after approximately 8 million cycles whereas two Class A surface finish specimens failed at 1.4 and 3.7 million cycles.

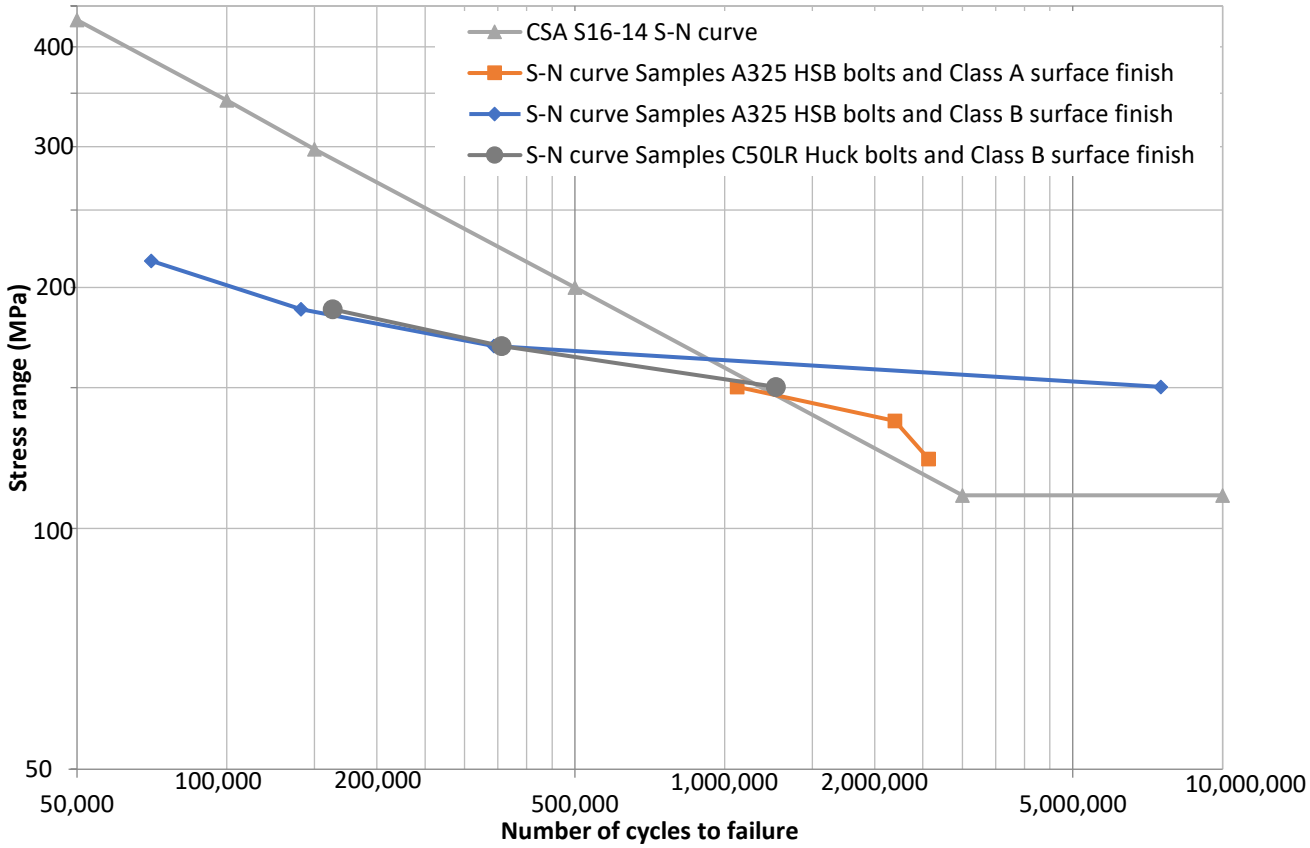

Figure 4.12 S-N curve of each type of specimen using the mean fatigue life values.

Considering the influence of bolt type, specimens with the Class B surface finish and C50LR Huck bolts had slightly higher fatigue lives compared to those with the A325 HSB at the higher stress ranges. However, the difference was not statistically significant at the 169 MPa stress range, and an insufficient number of samples was tested at the 188 MPa stress range to draw a definitive conclusion. If the difference was real, the reason could be the slightly higher level of pre-tension applied by the tension control bolts. However, this could not be confirmed, since the bolt pretension was not measured.

The specimens were grouped according to their failure mode (i.e., fretting fatigue or bending fatigue) and S-N curves corresponding to each of these groups, along with individual data points, are plotted in Figure 4.13. Samples that did not experience failure were not included in this analysis, except that they were used to estimate the endurance limit, and specimen B3-A325-150 was excluded as an outlier for bending failure at the 150 MPa stress range. It appears that the trend followed by these two groups is similar. The main difference between the two groups is that only specimens with a Class A surface finish experienced failure by fretting fatigue.

Fretting fatigue controlled the failure behaviour and fatigue life of the bolted connections made with Class A surface finish. On the other hand, bending controlled the failure behaviour and fatigue life of specimens with the Class B surface finish. If specimens made with the Class B surface finish had not experienced the bending effect, failure would have been delayed until fretting produced crack initiation and eventual failure. Therefore, bending reduced the fatigue life in most cases. The coating on the Class B surface finish samples prevented or at least delayed the occurrence of fretting fatigue failure such that samples coated with the Class B surface finish demonstrated a better fatigue behaviour and longer fatigue life than uncoated samples with a Class A surface finish.

It appears that the coating played a major role in the fretting fatigue behaviour of samples with a Class B surface finish. Severe damage had to occur to the coating before cracks developed in the underlying base material. Additional surface cracks might be developed on the virgin contact surfaces once the coating is completely removed due to fretting wear but the delay associated with removal of the coating, might have increased the number of fatigue cycles before the specimen failed.

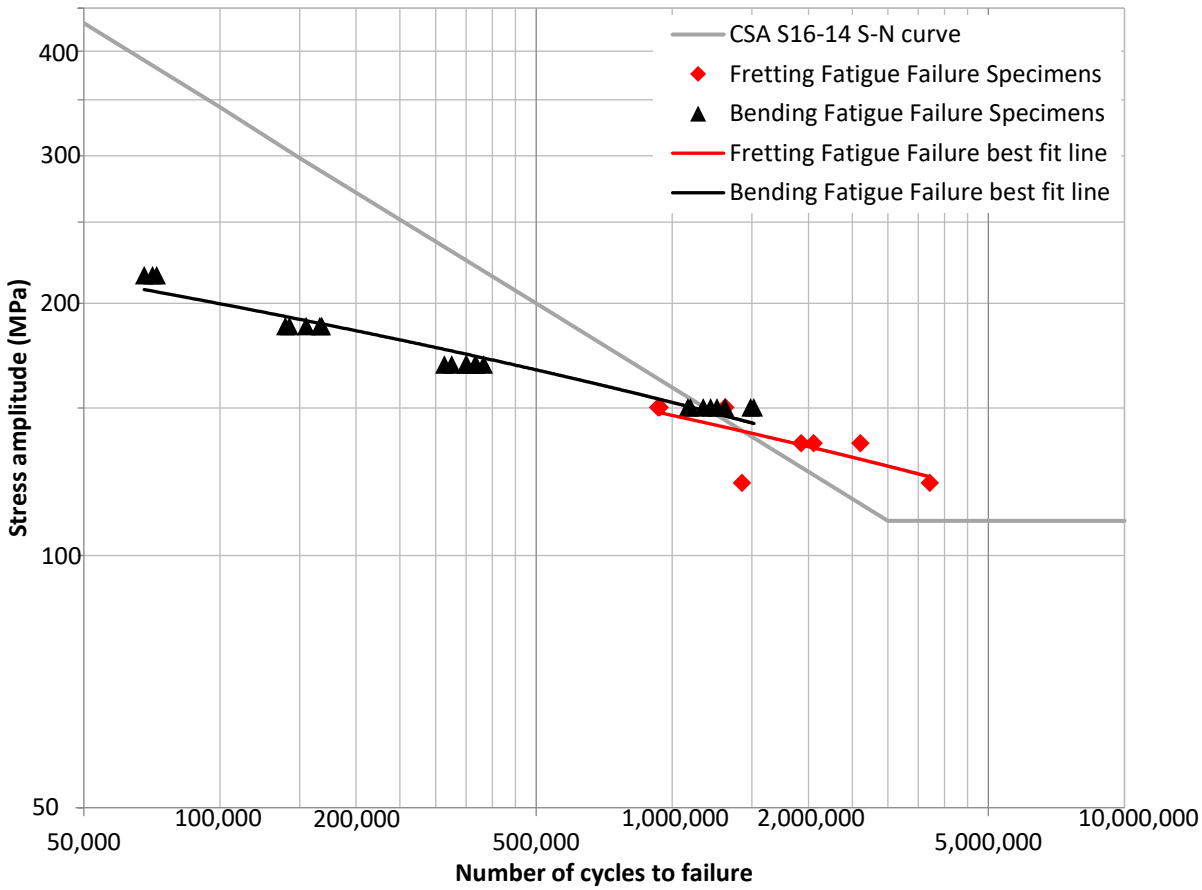

Figure 4.13 Mean S-N curves and fatigue life results plotted according to the type of failure.

4.4.6 Accounting for bending effects

The S-N curves plotted in the previous sections considered only axial tensile stresses when calculating the stress range. In order to account for the additional stresses due to bending caused by eccentric loading and second order effects in the single lap joint specimens, the curvature values were measured during four fatigue tests using the DIC system, as described in Section 4.5. Table 4.7 shows the maximum curvature values that were obtained for each sample and the total stress that was applied to the sample as a result of the combined bending and tensile stresses. For these calculations, the bending moment (ΔM) was calculated using the measured curvature values $\left(\frac{d^2y}{dx^2}\right)$ as $\Delta M = \frac{d^2y}{dx^2} EI$. Then, the bending stress $(\Delta\sigma_b)$ was calculated as $\Delta\sigma_b = \frac{(\Delta M)(y)}{I}$, in which y is half of the plate thickness, I is the moment of inertia, and E is the Young's modulus.

Table 4.7: Total stress range including bending effects

Sample	Stress range (MPa)	Curvature (mm^{-1})	Bending moment (kN-mm)	Bending stress (MPa)	Total stress (MPa)
B5-A325-150	150	0.000095	69.80	90.87	241
B8-A325-169	169	0.000174	126.97	165.30	334
C10-C50LR-150	150	0.000082	60.03	78.15	228
C14-C50LR-169	169	0.000167	122.47	159.44	328

The bending stresses increased the total stress by 52% to 60% at the 150 MPa axial stress range, while they were high enough to double the stress range at the 169 MPa axial stress range. The data points for these specimens, using the revised total stress ranges, are plotted with the CSA S16-14 S-N curves in Figures 4.14 and 4.15. Although the data set is very small, the revised data points indicate that the specimens had a longer fatigue life than expected by the CSA S16-14 S-N curve for detail category B. It should be noted, though, that the 5% fractile values would bring the data points closer to the standard S-N curves.

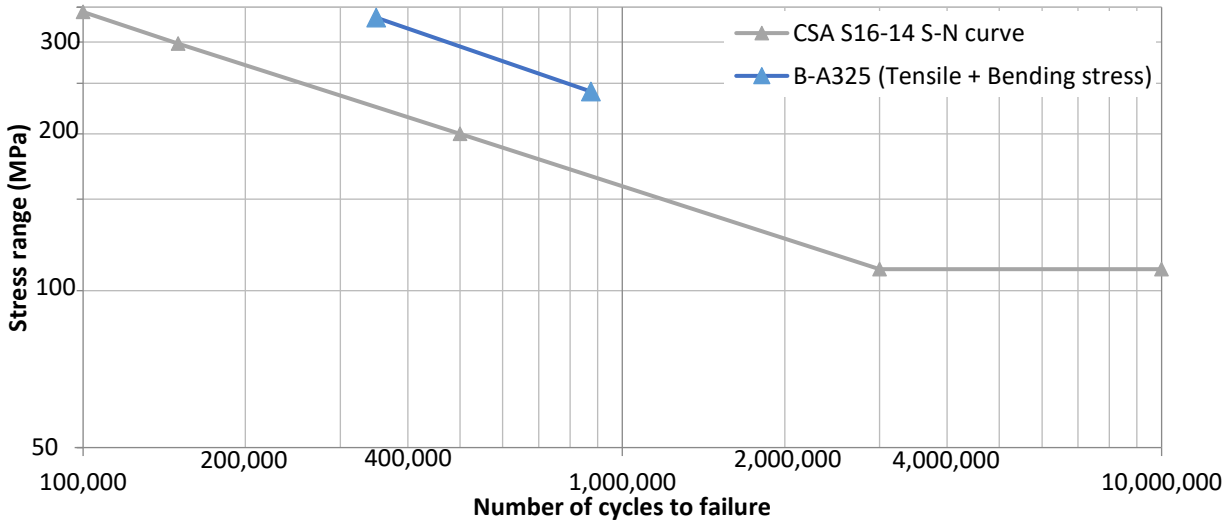

Figure 4.14 Experimental data points based on the total stress values for fatigue life for samples that consisted of Class B surface finish and A325 HSB.

If a designer had to calculate the stress range of a single lap bolted connection, including the effects of bending, it would not be possible to have access to curvature measurements. The designer would have to do an elastic analysis and use the principles of mechanics of materials to calculate the bending stresses that may result due to joint eccentricities as

recommended by Clause 26.3.1 in CSA S16-14. This approach is applied to the experimental data in the following paragraph.

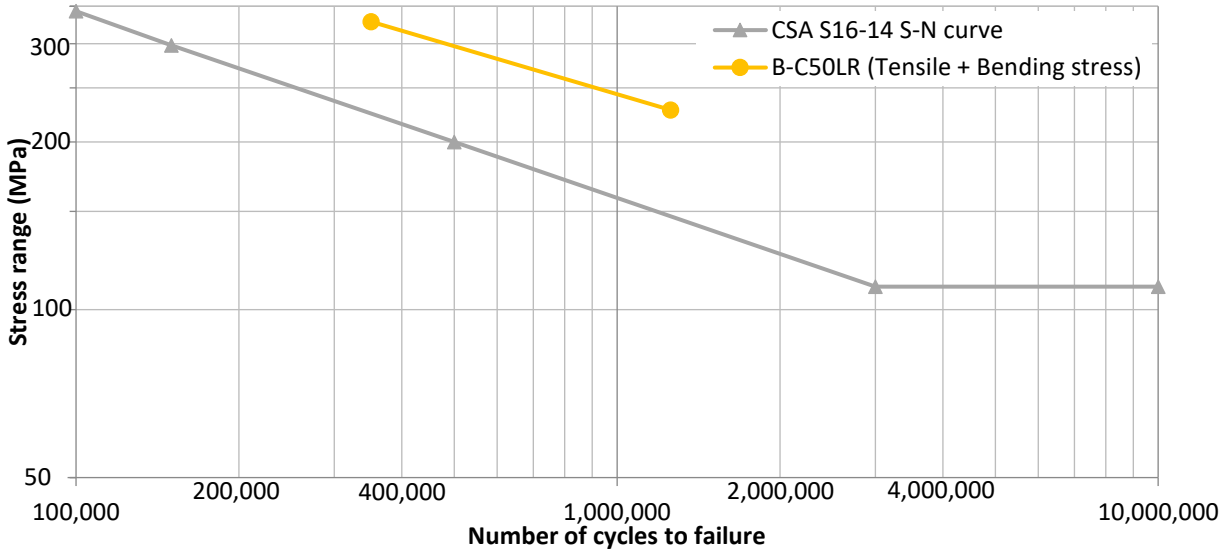

Figure 4.15 Experimental data points based on the total stress values for fatigue life for samples that consisted of Class B surface finish and C50LR Huck bolts.

Using the free body diagram shown in Figure 2.18, the primary bending moment due to the eccentricity between the plates can be determined as $M = (P)\left(\frac{t}{2}\right)$ when the plates are undeformed. The bending moment range in a fatigue test is then $\Delta M = (\Delta P)\left(\frac{t}{2}\right)$ where ΔP is the axial load range.

The nominal stress range due to axial tension alone is $\Delta\sigma = \frac{\Delta P}{A} = \frac{\Delta P}{wt}$, in which $\Delta P = (\Delta\sigma)(w)(t)$.

The bending moment range can be rewritten as $\Delta M = (\Delta\sigma)(w)\left(\frac{t^2}{2}\right)$.

The bending stress range can then be calculated as $\Delta\sigma_b = \frac{(\Delta M)(y)}{I}$. Substituting ΔM leads to $\Delta\sigma_b = \left[(\Delta\sigma)(w)\left(\frac{t^2}{2}\right)\right]\left(\frac{t}{2}\right)\left(\frac{12}{wt^3}\right) = 3\Delta\sigma$, and therefore the total stress range, including both axial and bending stresses is: $\Delta\sigma_{tot} = \Delta\sigma + \Delta\sigma_b = 4\Delta\sigma$

The total stress should therefore be calculated as four times the nominal axial stress range according to the first order analysis results. This is very conservative and would result

in a connection design with dimensions substantially greater than necessary. For example, if a 150 MPa nominal stress range were applied, it would result in a total stress range of 600 MPa. A 676 MPa total stress range would be calculated if a 169 MPa nominal stress range were applied. These total stresses are substantially higher than the yield strength of the plates. Therefore, the total stresses calculated by the first order elastic analysis are clearly higher than what was experienced by the specimens, since no yielding was observed. The second order effects tend to mitigate the bending stresses.

The fatigue life results that were plotted in Figure 4.5 using the nominal axial stress ranges have been plotted in Figure 4.16 using the total stresses ($\Delta\sigma_{tot} = 4\Delta\sigma$). As a result, the data lie well above the S-N curve for detail category B from CSA S16-14, and are unrealistic. A designer should not use this method to quantify the stress range applied to a single lap bolted connection since it is extremely conservative.

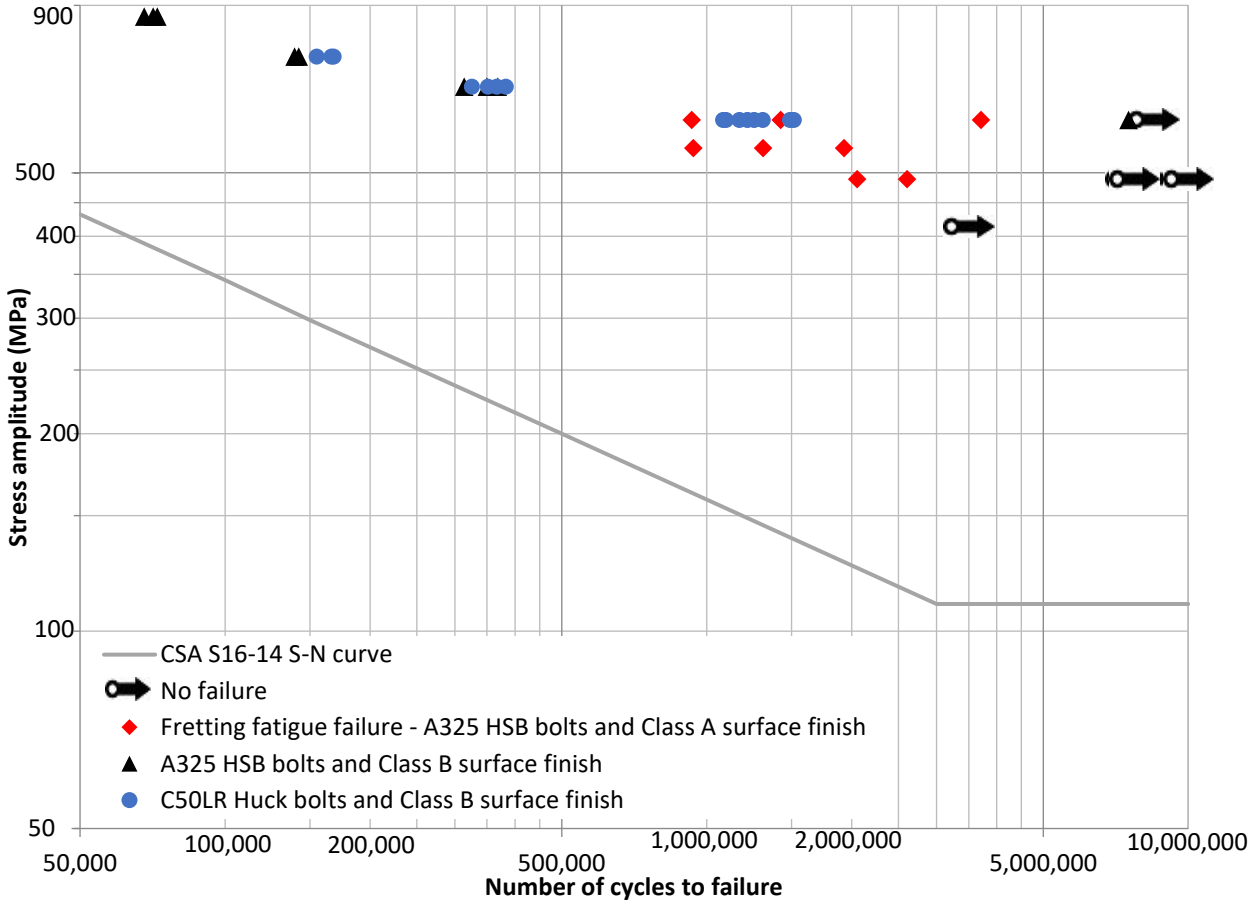

Figure 4.16 Fatigue life of every sample tested, plotted with total stresses determined by a first order analysis.

4.5 Fatigue Characterization

4.5.1 Overview and initial considerations

In general, two different types of fatigue failure behaviour were observed: fretting fatigue and bending fatigue. These were discussed in Chapter 2 and physical evidence for the two behaviours is presented in this section. The specimens with Class B and Class A surface finishes exhibited different fatigue failure behaviours for the same bolt type (A325 HSB). Specimens with the Class B surface finish showed signs of fretting fatigue but failed due to bending fatigue regardless of the bolt type. On the other hand, specimens with a Class A surface finish primarily failed due to the fretting fatigue phenomenon. As a result, this section is organized by specimen type, first considering specimens with a Class B surface finish, and then those with a Class A surface finish.

As discussed in Chapter 3, images were captured during four of the fatigue tests using the DIC system. Then, the Vic-2D software was used to measure the displacements parallel to the applied load (in the plane of the plates) and perpendicular to the applied load (out of the plane of the plates) in the vicinity of the uppermost bolt where the failure occurred. A representative DIC image of the area of interest is shown in Figure 4.17, defining some of the terminology and locations used in the presentation and discussion of the results.

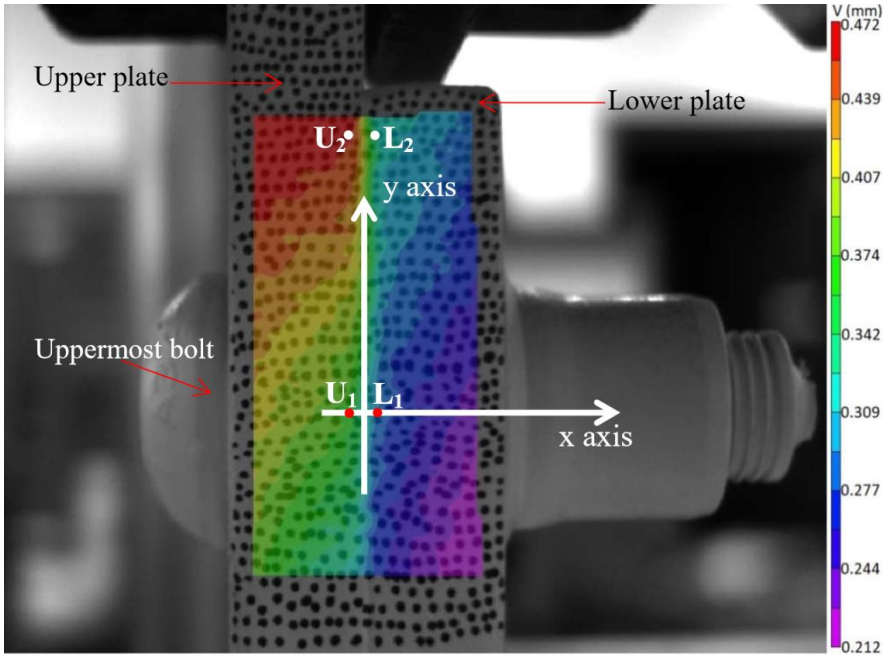

Figure 4.17 Representative DIC image, defining the upper and lower plates and x- and y-axes.

Points U_1 and L_1 on the upper and lower plates, respectively, are located on the visible edge of the sample along the bolt axis adjacent to the contact surface and were used to determine the relative displacement of the plates parallel to the load. Points U_2 and L_2 on the upper and lower plates, respectively, are located close to the top end of the lower plate. These points were used to determine the relative displacement of the plates along the contact interface some distance from the bolt. It should be noted that the DIC system could not capture images of the fatigue tests during the first several hundred cycles because it took time for the system to synchronize with the testing machine due to the high rate of cyclic loading used. As a consequence, the displacements were accurately calculated starting several hundred cycles after the beginning of the test in the analysis using Vic-2D software. Therefore, displacement data were not recorded during the earliest parts of each fatigue test.

4.5.2 Class B surface: Combined Fatigue

4.5.2.1 Class B Surface with A325 HSB

As described below, the specimens prepared with a Class B surface finish experienced a combination of secondary bending and fretting fatigue at the contact surfaces. Evidence from the relative displacements obtained from the Digital Image Correlation (DIC) system along with microscopic observations suggest that fretting wear occurred during the test but that bending effects were responsible for crack initiation and eventual failure of the specimen.

150 MPa stress range

The measured maximum and minimum displacements parallel to the applied load at points U_1 and L_1 for specimen B5-A325-150 are plotted in Figure 4.18(a). The specimen was subjected to a fatigue stress range (σ_r) of 150 MPa. It can be seen that the maximum and minimum cyclic displacements near the contact interface stabilized to relatively constant values within the first 575 cycles. The stabilized minimum displacements in a cycle for the upper and lower plates were 0.43 mm and 0.38 mm, respectively, indicating that there was a permanent displacement of just under 0.4 mm in the lower plate when the specimen was nearly unloaded, due to the settling-in of the sample at the lower grip.

(a)

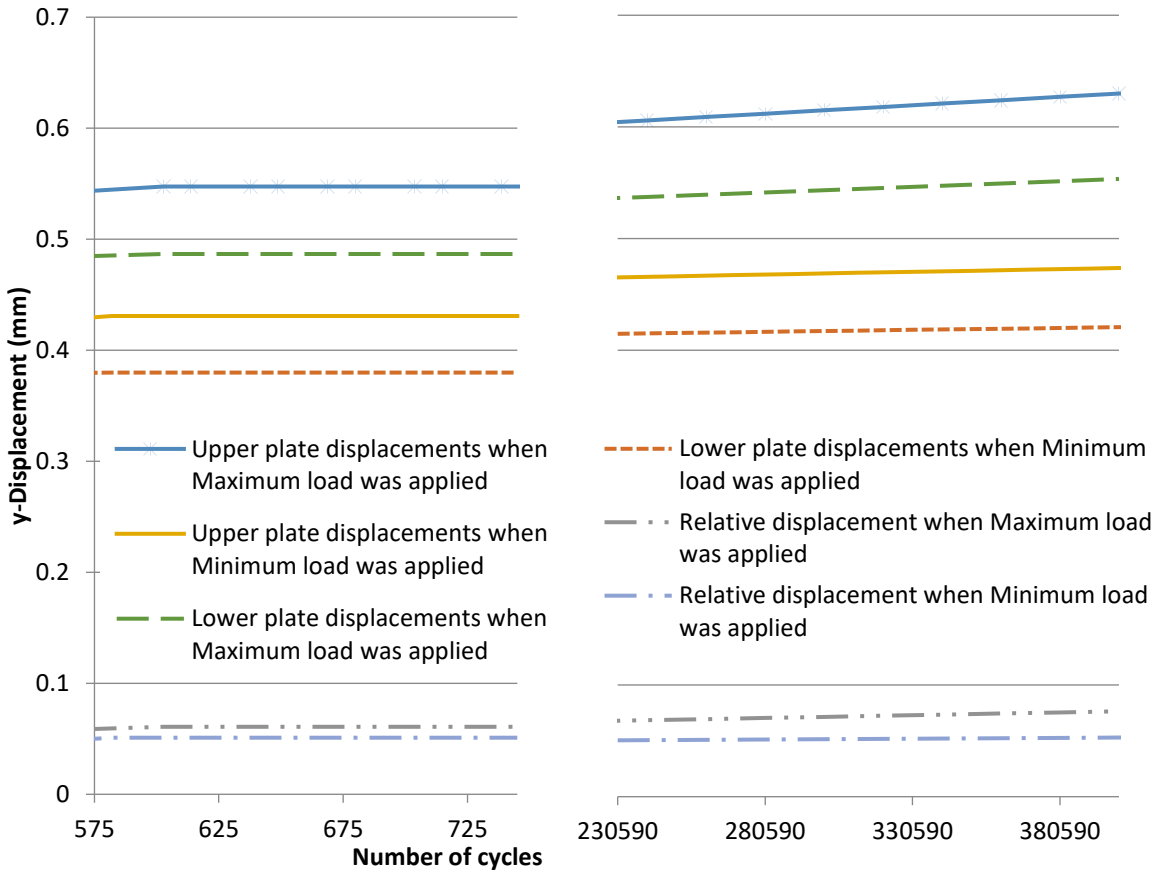

(b)

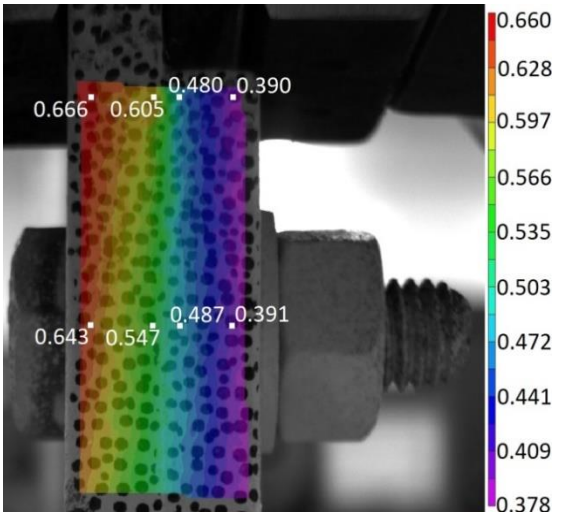

(c)

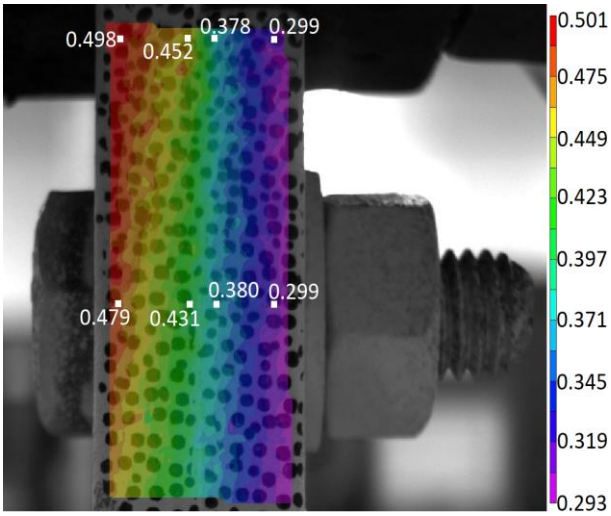

Figure 4.18 Displacements parallel to the applied load (y axis) in sample B5-A325-150: (a) Graph of the maximum, minimum, and relative displacements in the upper and lower plates along the bolt axis; (b) measured peak displacements at the 739th fatigue cycle; and (c) minimum displacements at the 745th fatigue cycle in the y direction (mm).

The minimum relative displacement at the bolt axis was equal to 51 μm, which corresponds to settling-in effects between the two plates. After stabilization, the relative motion between the plates over a cycle was 9.8 μm on the exposed surface along the bolt axis. A gradual increase in the maximum and minimum displacements is also noted over the first 400,000 cycles. Part of this may be caused by additional displacement within the lower grip. The relative motion between the plates over a cycle increased gradually to 20 μm after 400,000 cycles, likely due to increased fretting wear.

Figure 4.18(b) shows the maximum y-displacements captured from a DIC image along the bolt axis and at the top edge of the lower plate during the 739th fatigue cycle. The relative displacement between the plates at the bolt axis was 60 μm and at the top edge of the lower plate was 0.125 mm. Figure 4.18(c) shows the y-displacements captured when the minimum load of the cycle was applied during the 745th fatigue cycle. The relative displacement between the plates at the bolt axis was 51 μm and at the top end of the lower plate was 74 μm. The relative motion between the plates over a fatigue cycle was therefore 9 μm and 51 μm at the bolt axis and top end of the lower plate, respectively. The relative motion likely removed parts of the coating and then caused damage to the surface of the plates. The images also show the displacement field of the entire region and they look similar for both the minimum and the maximum load.

The normal strain in the y-direction for sample B5-A325-150 when the maximum cyclic load was applied during the 739th cycle was calculated by the DIC system and is shown in Figure 4.19(a). The strain field shows that the whole specimen in this region was in tension, but it was not uniform. The maximum strain is located in the upper plate close to the contact interface approximately 5 mm below the top edge of the lower plate. This indicates that the bending suffered by the specimen was highest at this location. The curvature was calculated as the derivative of the strain values along cross sections parallel to the x-axis in the upper plate and is shown in Figure 4.19(b). The maximum value of curvature is located 3.48 mm below the top edge of the lower plate. The presence of curvature in the specimen indicates that the bending effect was present in this sample. A bending moment of 69.8 kN-mm and the bending stress of 90.87 MPa were calculated using the maximum curvature value. The

tensile and bending stresses resulted in a total stress of 240.87 MPa. This increase of applied stress decreased the expected fatigue life of the specimen.

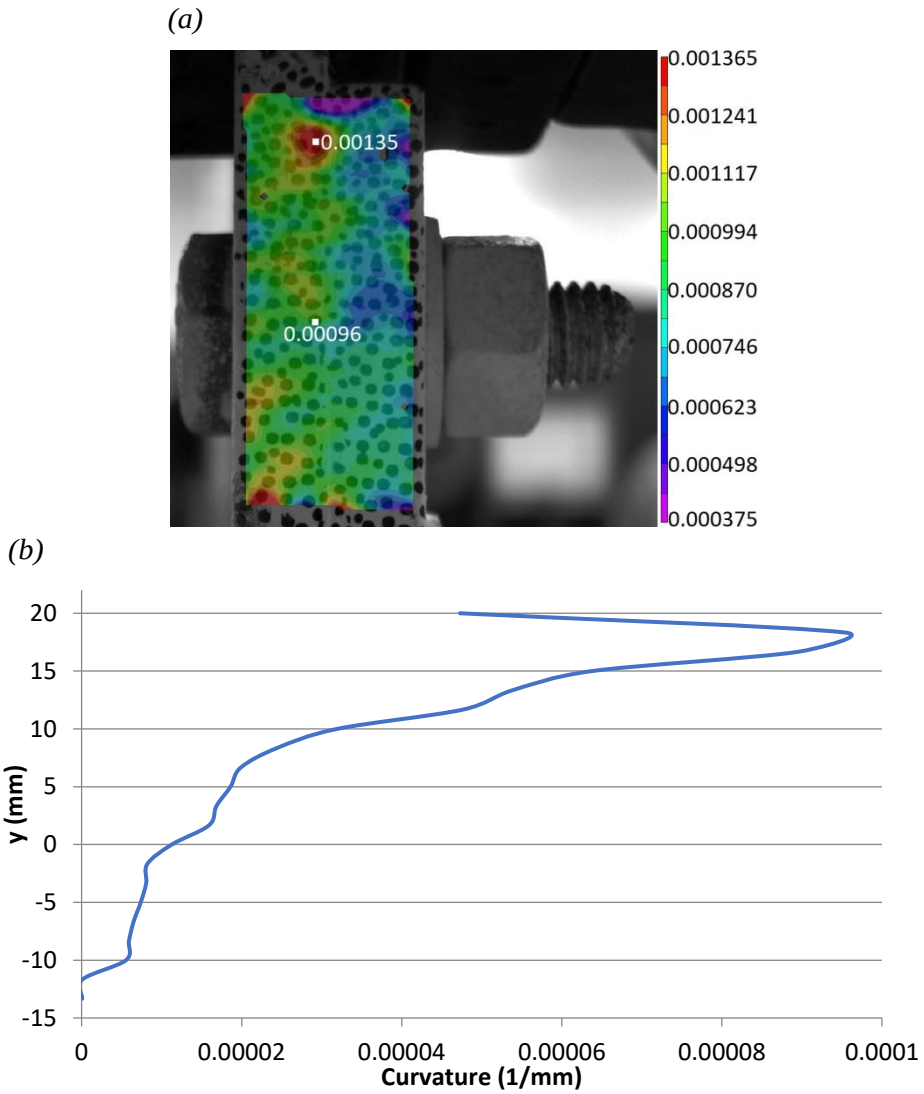

Figure 4.19 Bending analysis results in sample B5-A325-150: (a) Normal strains parallel to the applied load (y axis); and (b) curvature calculated in the upper plate.

Figure 4.20 shows an optical microscope image of the contact surface of the lower plate of specimen B3-A325-150 above the first bolt hole. Apparent on this image are the stick, global slip and partial stick-slip regions. In the stick region, there was no relative displacement between the plates and the coating remained intact. This region was located around the hole edges. The global slip region, which resulted from the plates slipping with

respect each other, can be seen a certain distance away from the bolt hole. Global slip in this region led to fretting wear, and thus the surface coating was almost completely removed.

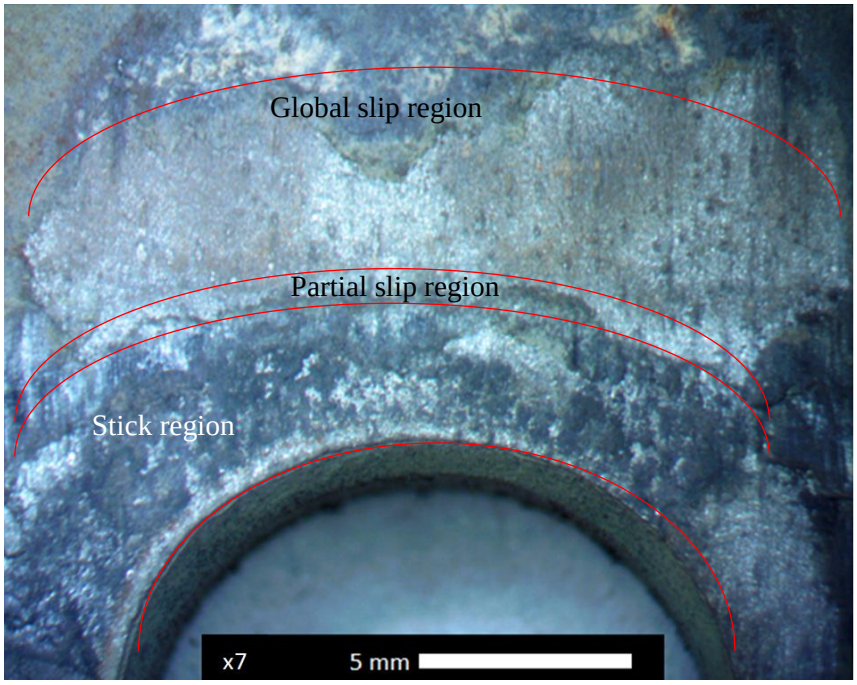

Figure 4.20 Optical microscopic image of the stick-slip regions at contact interface of sample B3-A325-150.

The partial slip-stick region can be seen at the boundary between the stick and global slip regions; as described in Chapter 2, this region generally acts as a stress raiser due to the higher frictional force within the region. The resultant surface damage is shown in the SEM micrograph of Figure 4.21. Due to the higher relative displacements, the global slip region featured complex surface characteristics, as shown in Figure 4.22. Ploughing lines indicate the direction of the relative motion and also the presence of higher frictional forces. The oxidised particles are generated by the partial slip fretting wear, which is again the result of a higher frictional force at the contact interface. In addition, a number of micro cracks are apparent; these nucleated due to relative displacement within the global slip region. These surface characteristics demonstrate that the Class B surface finish with A325 HSB was subjected to fretting fatigue. The micro-cracks were very small, with a maximum length of approximately 17 μm and could have eventually propagated into a leading crack if there had been no bending effect at the first hole of the bolted assembly.

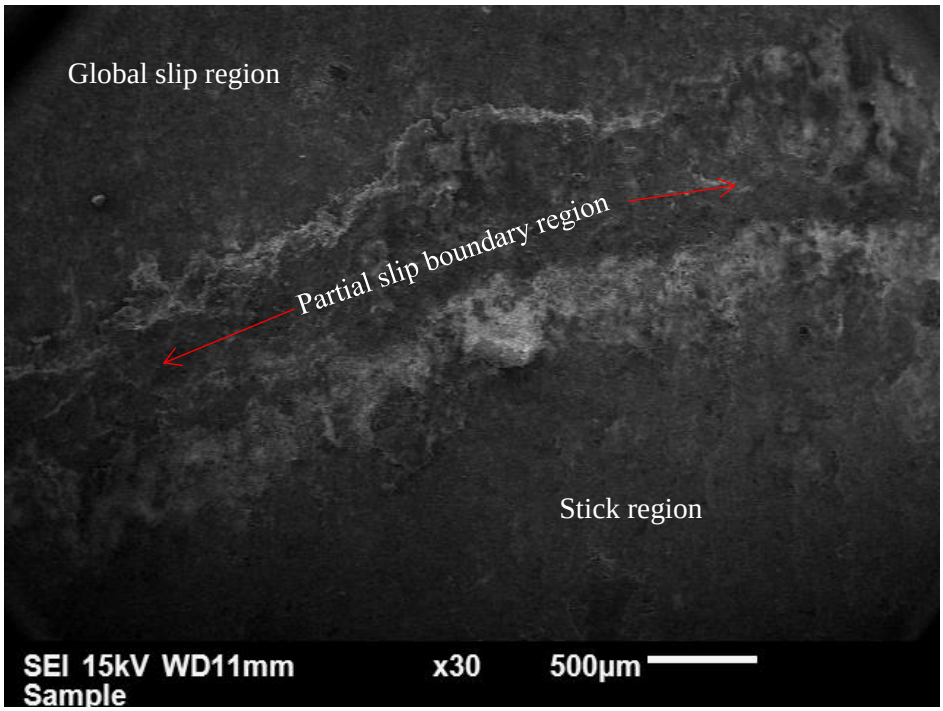

Figure 4.21 SEM micrograph of the partial stick-slip region for sample B3-A325-150.

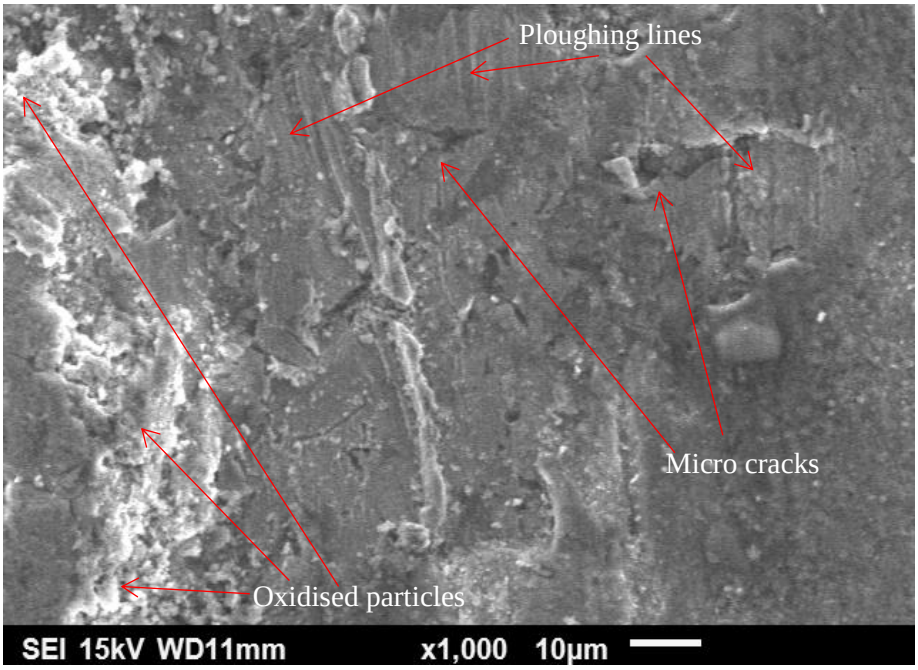

Figure 4.22 SEM micrograph of the global-slip region of the lower plate for sample B3-A325-150.

The displacements perpendicular to the loading direction (out-of-plane displacement) were measured in an attempt to better understand the secondary bending effect. The secondary bending was induced as a consequence of the load eccentricity that occurs in a

single lap joint specimen, as discussed in Chapter 2. It results in an out-of-plane displacement of the specimen. The measured out-of-plane displacements for specimen B5-A325-150 are shown in Figure 4.23(a).

(a)

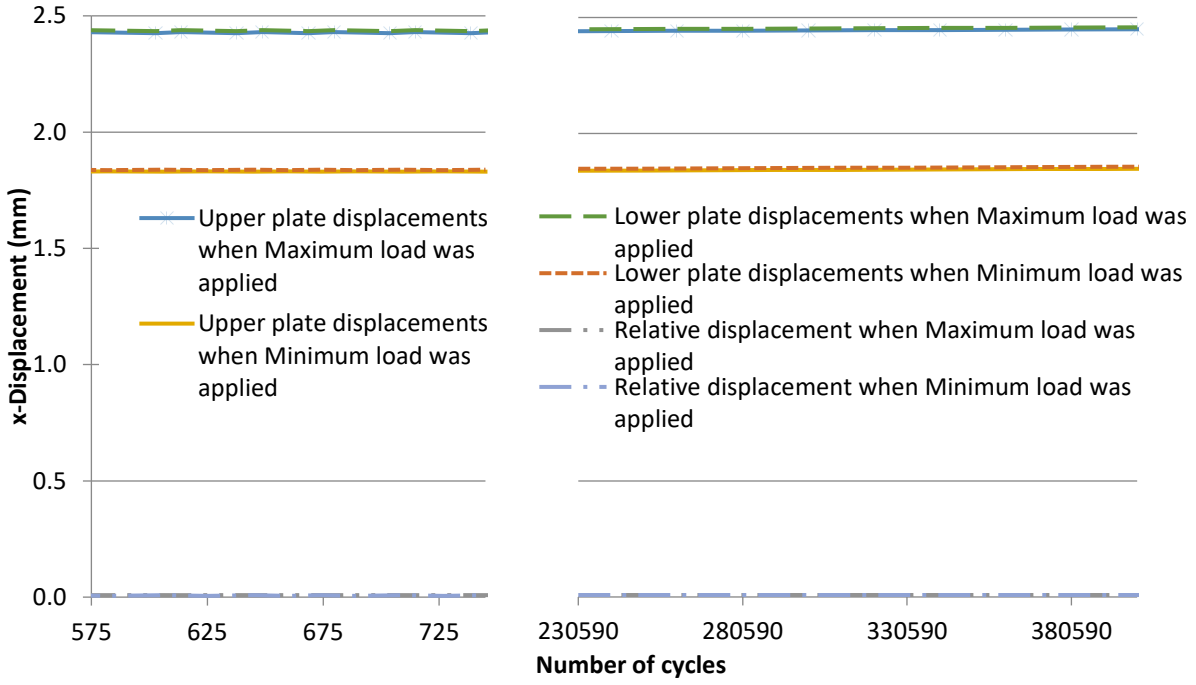

(b)

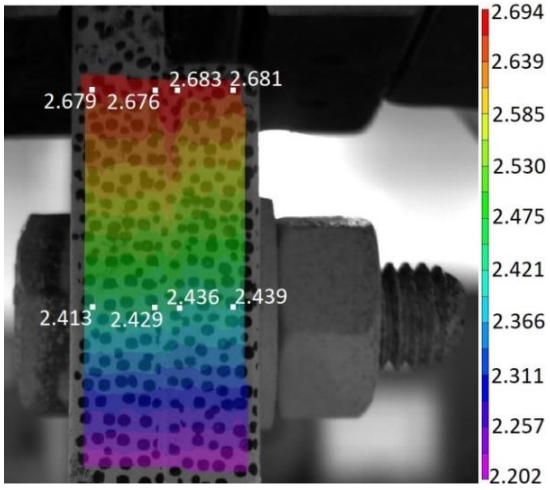

Figure 4.23 Displacements perpendicular to the applied load (x-axis) in sample B5-A325-150: (a) Graph of the maximum, minimum, and relative displacements in the upper and lower plates along the bolt axis; and (b) measured peak displacements at the 739th fatigue cycle.

Both plates displaced approximately the same amount as the loading cycles were applied during the fatigue test. The out-of-plane displacement increased during the settling in period and reached a stabilized value by approximately 500 cycles. The maximum and minimum displacements of both plates were 2.43 mm and 1.83 mm, respectively. At the same time, due to the bending effect, the contacting plates moved relatively opposite to each other and developed a gap with maximum and minimum values in a cycle of 8.5 μm and 5.4 μm, respectively. The out-of-plane displacements at the bolt axis appear to show that the plates were not in full contact due to the secondary bending effect, at least along the visible edge, possibly preventing or reducing the development of fretting damage. Figure 4.23(b) shows a DIC image of the stabilized maximum out-of-plane displacements for sample B5-A325-150. These displacements were a consequence of the bending effect that is believed to be the cause of bending fatigue failure in the specimen. Specimen B5-A325-150 experienced a maximum out-of-plane displacement of 2.4 mm at the first hole of the sample and a 7 μm gap between the plates at the contact interface along the entire exposed edge.

169 MPa stress range

Similar behaviour was observed for specimens subjected to a higher stress range of 169 MPa (sample B8-A325-169). As shown in Figure 4.24(a), the upper and lower plate displacements at points U_1 and L_1 for the 169 MPa stress range were three times higher than for the specimen tested with the 150 MPa stress range (Figure 4.18(a)). The maximum and minimum displacements close to the contact interface stabilized to relatively constant values within the first 595 cycles. The stabilized minimum displacements for the upper and lower plates were 1.52 mm and 1.33 mm, respectively, indicating that there was a permanent displacement lower than 1.33 mm in the lower plate when the specimen was nearly unloaded, due to the settling-in of the sample at the lower grip. The stabilized minimum relative displacement was measured as 0.186 mm, which corresponds to settling-in effects between the two plates as also occurred in specimen B5-A325-150. At the 823rd cycle, the change in relative displacement between the plates over a cycle was 13 μm on the visible edge of the contact interface along the bolt axis. This change in the relative displacement is just 3.2 μm higher than in specimen B5-A325-150 due to the higher fatigue loads applied to specimen B8-A325-169. The maximum and minimum displacements of both plates

increased gradually over the first 300,000 cycles. Consequently, the relative slip between the plates during a cycle increased to 23 μm after 290,000 cycles.

(a)

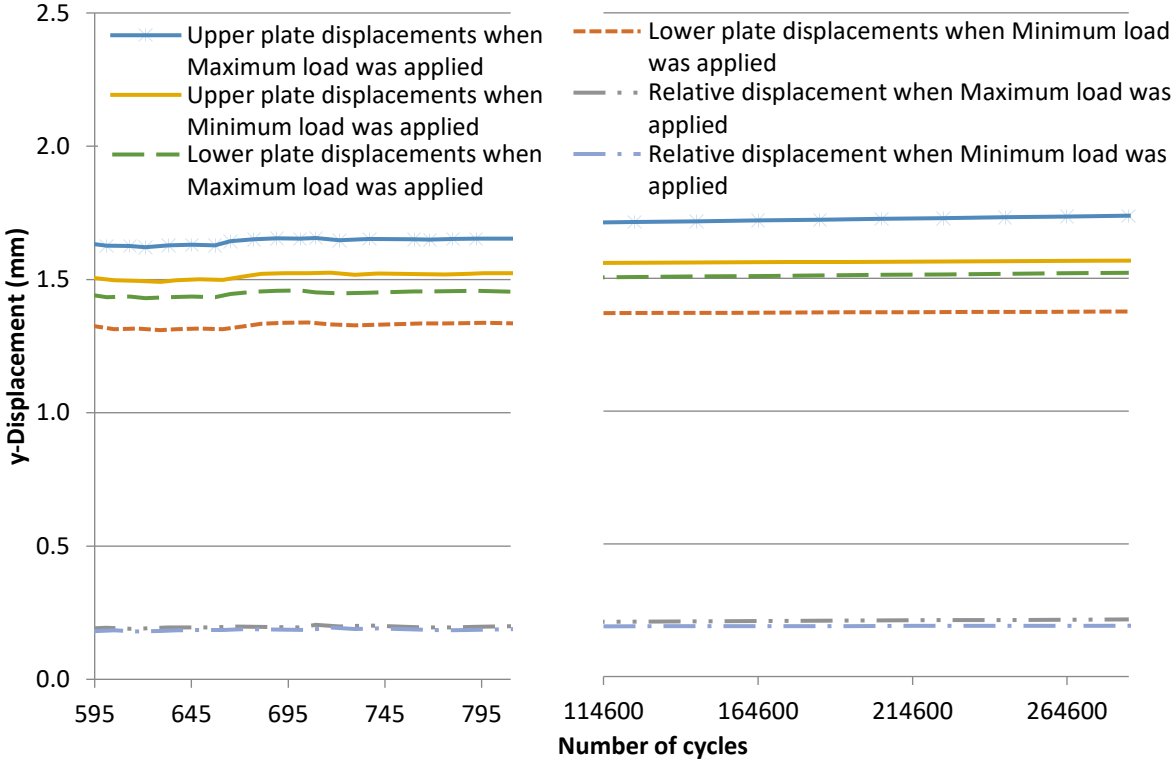

(b)

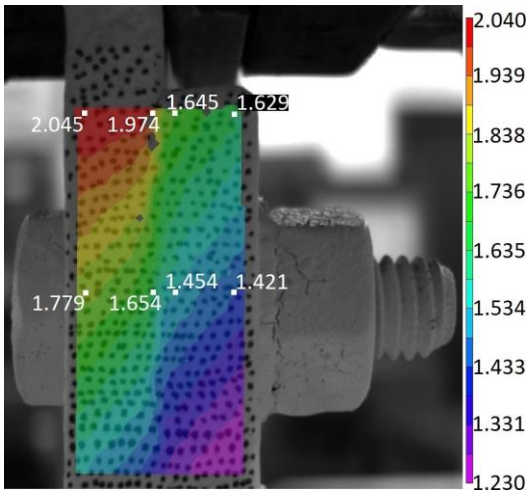

(c)

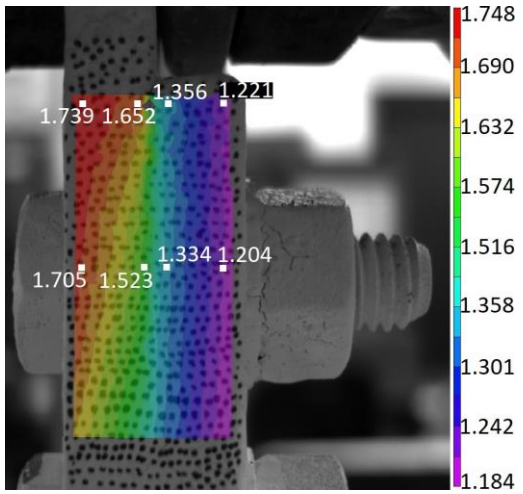

Figure 4.24 Displacements parallel to the applied load (y axis) in sample B8-A325-169: (a) Graph of the maximum, minimum, and relative displacements in the upper and lower plates along the bolt axis; (b) measured peak displacements at the 812th fatigue cycle; and (c) minimum displacements at the 823rd fatigue cycle in the y-direction (mm).

The maximum stabilized displacements for specimen B8-A325-169 in the direction parallel to the applied load during the 812th fatigue cycle, as captured from the DIC image, are shown in Figure 4.24(b). These displacements are at least three times higher than the displacements obtained for specimen B5-A325-150 (Figure 4.18(b)), which was subjected to the lower stress range of 150 MPa. The relative displacement at the contact interface near the hole section was 0.20 mm. In addition, the measured relative displacement between the upper end of the lower plate and the upper plate was 0.329 mm. The displacements caused to specimen B8-A325-169 by the minimum cyclic load can be seen in Figure 4.24(c). The relative displacement at the bolt axis was 0.189 mm and at the upper end of the lower plate it was 0.296 mm. The relative motion between the plates over a fatigue cycle was therefore 11 μm along the bolt axis and 33 μm at the upper end of the lower plate. The relative motion would be expected to cause fretting damage to the surface.

The normal strains in the y-direction along the visible edge of sample B8-A325-169 when the maximum load was applied is shown in Figure 4.25(a). The peak strain value is located at the top of the upper plate at the contact interface approximately 3 mm below the top edge of the lower plate; the values are generally higher than those of sample B5-A325-150 (Figure 4.19(a)). The corresponding curvatures in the upper plate are shown in Figure 4.25(b). The maximum value of curvature is located approximately 5 mm below the top edge of the lower plate and is more than 80% higher than that of sample B5-A325-150 (Figure 4.19(b)). As a result, bending had a greater effect on specimens subjected to a 169 MPa stress range. This would explain why the fatigue life of these specimens fell well below the CSA S16-14 S-N curve, whereas the fatigue life of specimens tested at the 150 MPa stress range did not. The maximum curvature value was used to calculate the bending moment as 126.97 kN-mm and the bending stress as 165.30 MPa. This resulted in a total stress of 334.30 MPa.

At the higher stress range of 169 MPa, the contacting surfaces were subjected to more fretting wear due to the larger in-plane relative motion parallel to the applied load, which caused global slip over the entire contact area near the bolt. This led to a complete elimination of the partial slip region. Figure 4.26(a) shows the area above the uppermost hole of the lower plate, in which the partial slip region cannot be identified between the

global slip and the stick regions. The coating has suffered severe damage due to fretting wear in the global slip region. If the bending effect had not been present in the specimen, it is believed that in a higher number of cycles the coating could have been removed completely and as a result, a crack could have been initiated in a partial slip region.

(a)

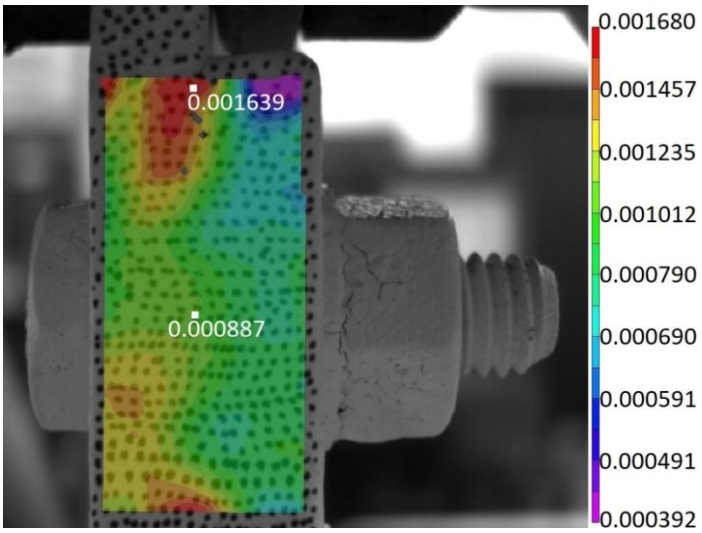

(b)

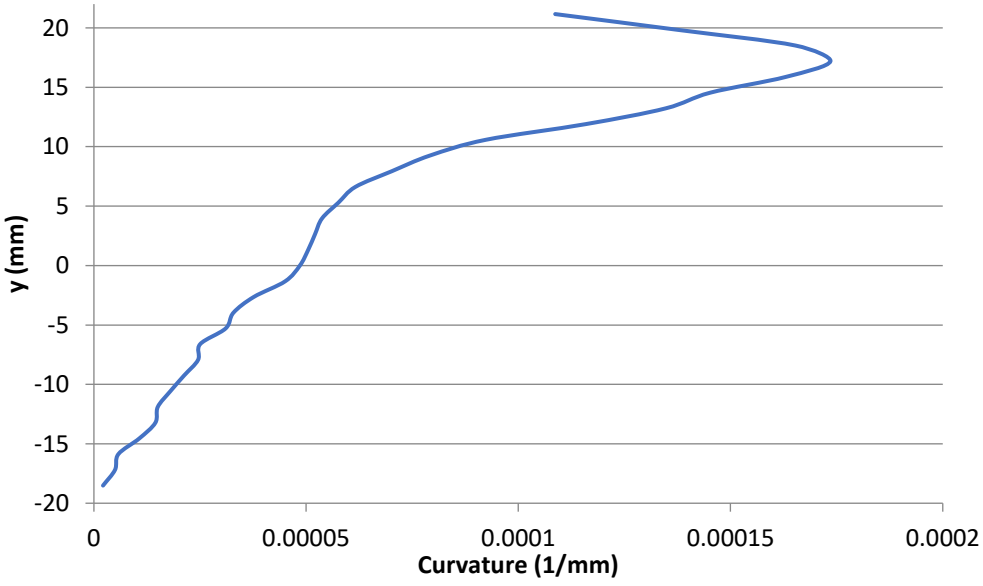

Figure 4.25 Bending analysis results in sample B8-A325-169: (a) Normal strains parallel to the applied load (y-axis); and (b) Curvature along the specimen edge.

Figure 4.26(b) shows the area around the lowermost hole of the lower plate, in which the stress concentration was higher like in the uppermost hole of the upper plate due to the secondary bending effect. An initiated crack at the hole due to the stress concentration can be seen under the coating in the stick region. The damage on the surface is severe, as seen on the coating surface in the global slip region.

(a) *(b)*

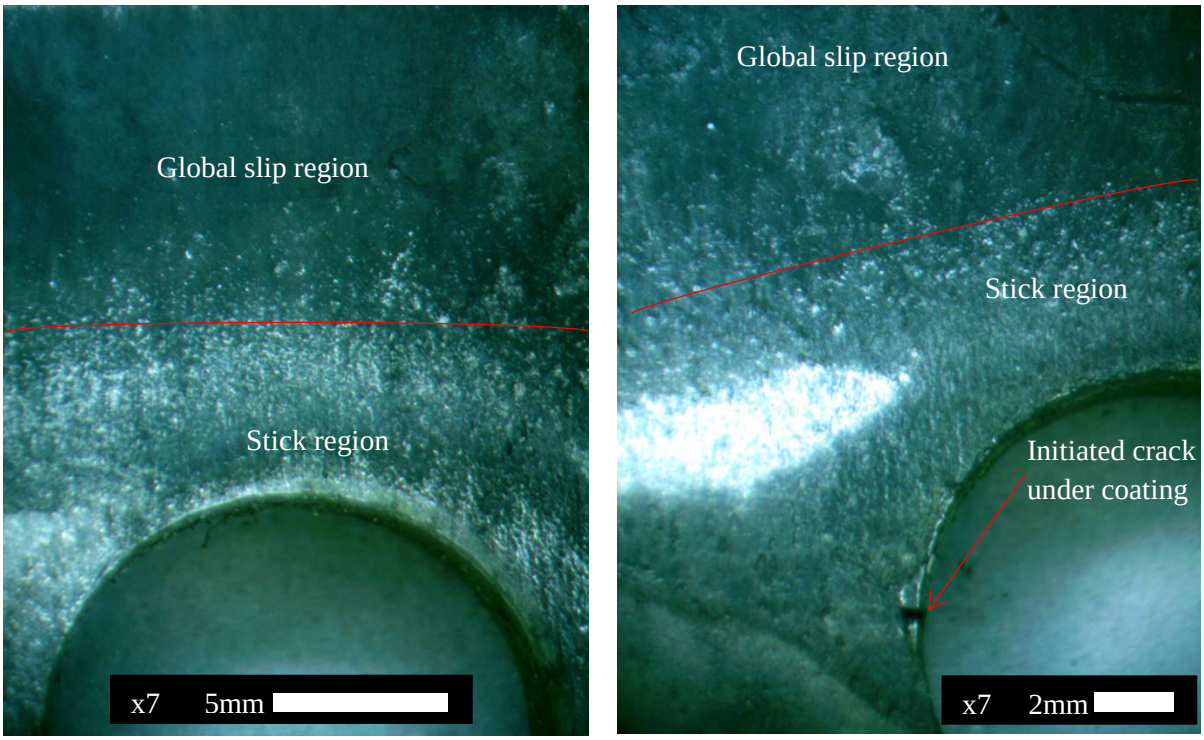

Figure 4.26 Optical micrograph of contact interface area of sample B8-A325-169: (a) in the vicinity of the uppermost hole for the lower plate; and (b) in the vicinity of the lowermost hole for the lower plate.

In addition, the higher levels of global slip caused more damage to the contacting surfaces, as shown in Figure 4.27. Ploughing lines parallel to the applied load confirmed that the large displacements removed the stick-slip region and the contact surfaces were subjected to global slip, fretting wear and surface damage. The results for samples subjected to even higher stress ranges than 169 MPa were similar.

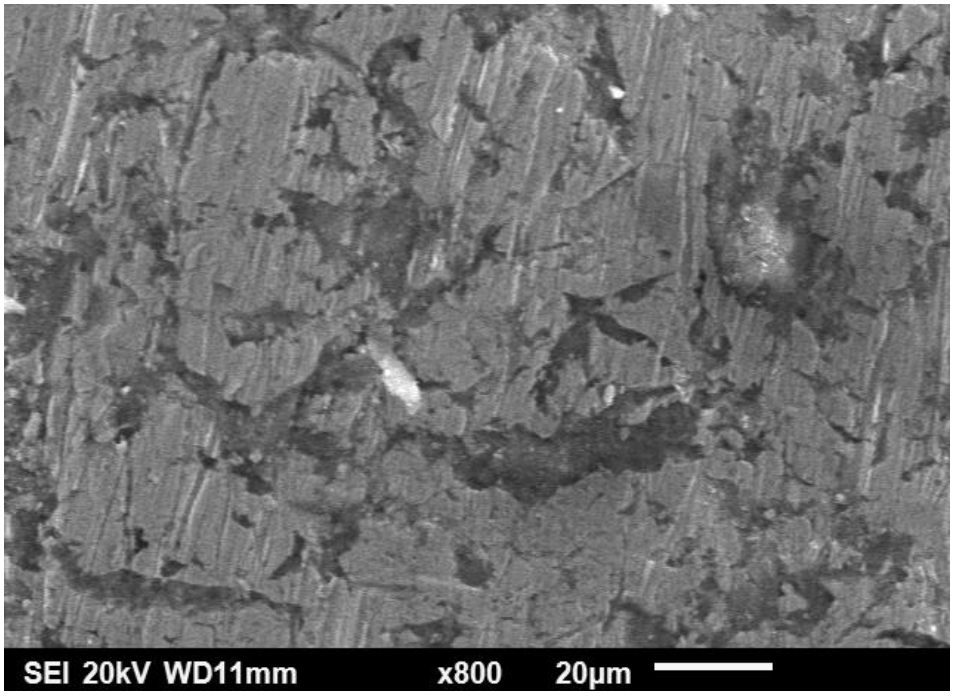

Figure 4.27 SEM micrograph of the surface damage in the global slip region on sample B8-A325-169.

The out-of-plane displacements were also measured for sample B8-A325-169, which was subjected to a stress range of 169 MPa. Similar to sample B5-A325-150, the displacements reached a stabilized value after 550 cycles, as shown in Figure 4.28(a). The maximum lateral displacements for the upper and lower plates were 3.16 mm and 3.23 mm, respectively, and the minimum lateral displacements were 2.45 mm and 2.47 mm, respectively. This indicated that there was a gap with maximum and minimum values of 67 μm and 22 μm between the plates. The gap was at least four times larger than that for the sample subjected to the 150 MPa stress range (B5-A325-150).

The stabilized maximum out-of-plane displacements for sample B8-A325-169 are shown in Figure 4.28(b) on a DIC image. It is clear that the out-of-plane displacements due to the secondary bending effect were higher in B8-A325-169 than B5-A325-150 (Figure 4.23(b)) due to higher fatigue loading. When the maximum load was applied, the sample experienced a maximum cyclic horizontal displacement of 3.2 mm and a gap of 58 μm at the contact interface along the bolt axis at the visible edge. This sample failed after only 0.35 million cycles.

(a)

(b)

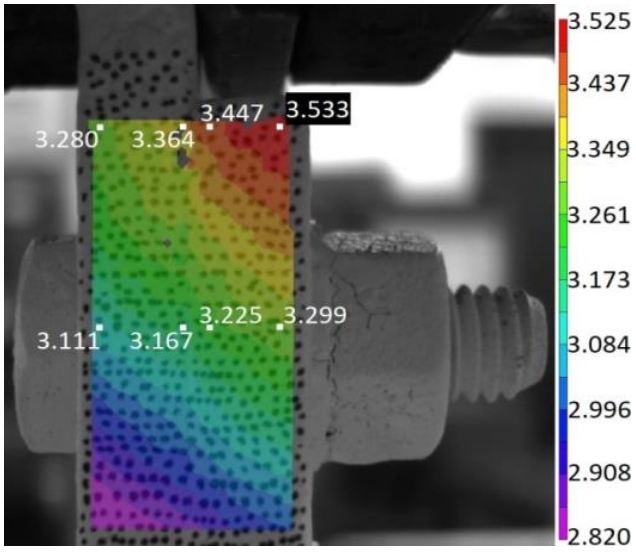

Figure 4.28 Displacements perpendicular to the applied load (x-axis) in sample B8-A325-169: (a) Graph of the maximum, minimum, and relative displacements in the upper and lower plates along the bolt axis; and (b) measured peak displacements at the 812th fatigue cycle.

Figure 4.29 shows a schematic drawing of the displaced shapes of samples B5-A325-150 and B8-A325-169 corresponding to peak loads at load cycles 739 and 812, respectively. These plots were drawn using the measurements obtained from the captured DIC images. In

addition to the out-of-plane displacements, these plots show that the samples also experienced rotation, amounting to 0.66° for B5-A325-150 and 0.74° for B8-A325-169, as measured at the first hole of the sample's upper plate. The existence of rotation is consistent with bending effects.

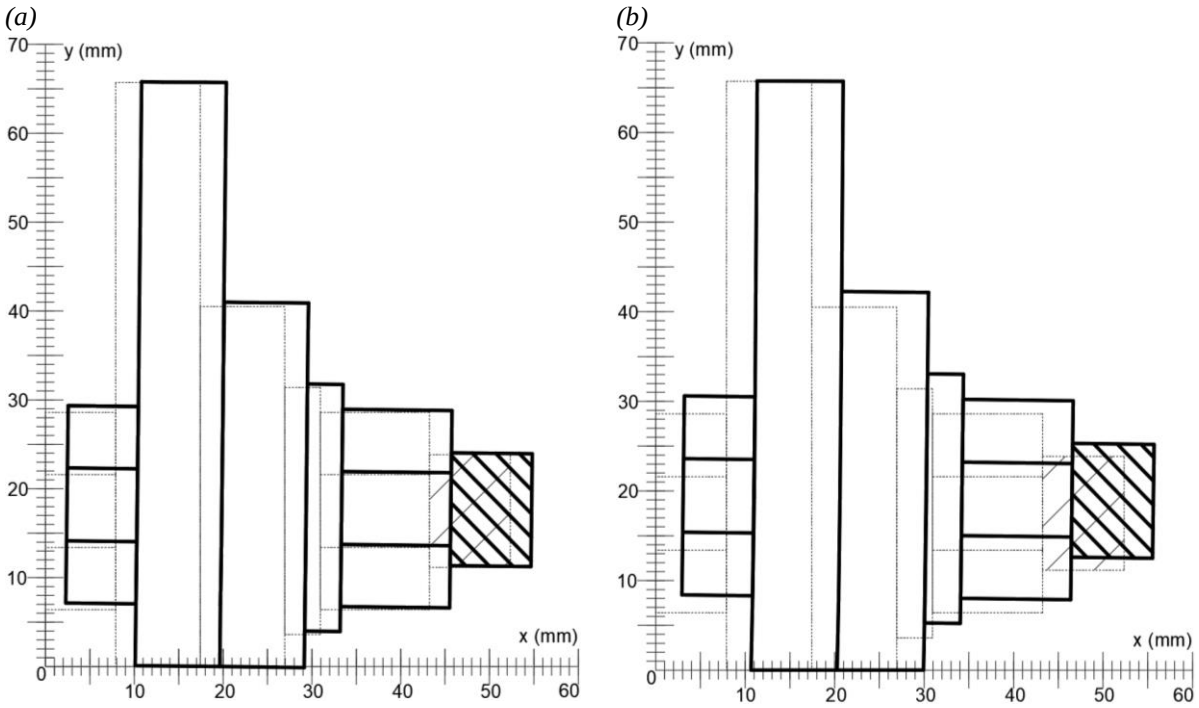

Figure 4.29 Displaced shapes at the maximum cyclic load of samples tested with different stress ranges: (a) Sample B5-A325-150 at 739 cycles, and (b) Sample B8-A325-169 at 812 cycles.

4.5.2.2 Class B surface with C50LR Huck tension control bolts

The effect of using C50LR Huck bolts on the fretting fatigue phenomenon was analysed by measuring the relative displacement close to the first bolt of the contacting plates for these samples, as well as examining the contact surfaces. The fatigue life results were similar to the combination of Class B surface finish and A325 HSB as seen in Table 4.3. A combination of fretting fatigue and the secondary bending effect was seen in C50LR Huck bolted connections.

<u>150 MPa stress range</u>

The displacements parallel to the applied load (in-plane displacement) measured on either side of the contact surface along the bolt axis using DIC images at points U_1 and L_1 for

sample C10-C50LR-150, tested at the 150 MPa stress range, are shown in Figure 4.30(a). After an initial settling-in period of less than 500 cycles, the displacements reached stabilized values. The minimum displacements in a cycle in the upper plate and lower plate were 0.46 mm and 0.43 mm, respectively, indicating that there was a permanent displacement of just over 0.4 mm at the minimum load due to settling-in effects at the lower grip. The minimum relative displacement was 36 μm, which corresponds to settling-in effects between the plates. The relative motion between the plates over a fatigue cycle was 8 μm initially and increased slightly to 11 μm at 440,000 cycles, most likely caused by increased fretting wear. A gradual increase in the minimum and maximum displacements also occurred over the first 440,000 cycles.

The maximum displacements for sample C10-C50LR-150 in the 777th cycle are shown as a DIC image in Figure 4.30(b). The displacement distributions for specimens with C50LR Huck and A325 HSB are slightly different at the 150 MPa stress range, as can be seen by comparing Figures 4.18(b) and 4.30(b).

The relative displacement between the plates at the top edge of the lower plate was 98 μm, which is more than two times higher than the relative displacement along the first bolt axis (44 μm). In addition, these displacements are lower than those seen in Figure 4.18(b) (0.125 mm and 60 μm, respectively). This is believed to be due to the higher clamping force applied by the C50LR Huck bolts.

The displacements caused by the minimum load of the cycle can be seen in Figure 4.30(c). The relative displacement at the bolt axis was 36 μm, which is lower than the relative displacement for specimen B5-A325-150 in Figure 4.18(c). It is likely that the C50LR Huck bolts applied a higher pretension load, which reduced the relative displacement when the minimum load of the cycle was applied. This relative displacement corresponds roughly to a permanent offset between the plates, most of which occurred during the initial settling-in process.

The normal axial strain field on the visible edge of specimen C10-C50LR-150 when the maximum cyclic load was applied is shown in Figure 4.31(a). The peak strain value is located in the upper plate near the interface just below the upper end of the lower plate,

similar to other samples already discussed. This is consistent with the bending effect in the upper plate. The peak strain value and the strain at the bolt axis are slightly lower than in sample B5-A325-150 (Figure 4.19).

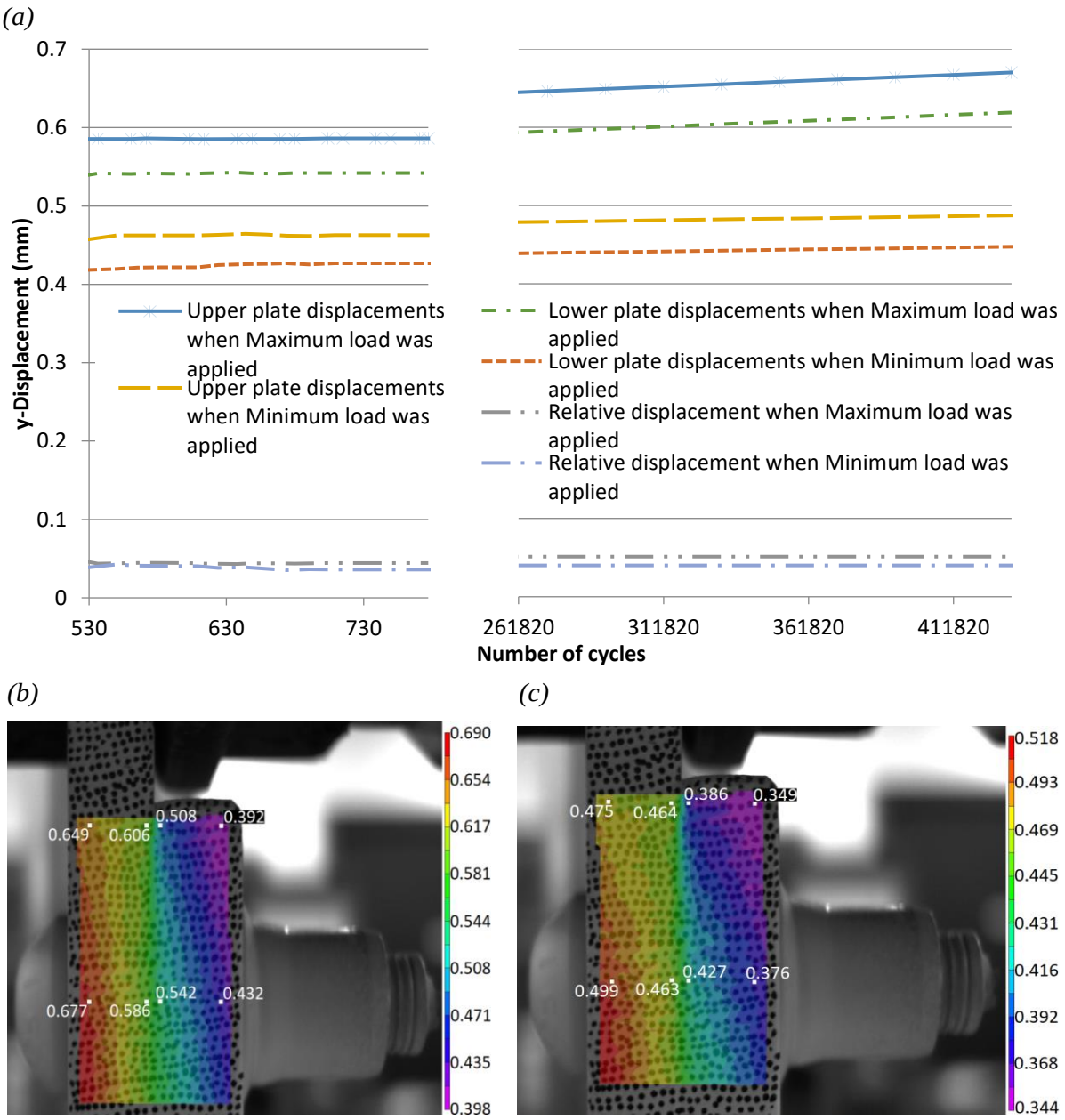

Figure 4.30 Displacements parallel to the applied load (y-axis) in sample C10-C50LR-150: (a) Graph of the maximum, minimum, and relative displacements in the upper and lower plates along the bolt axis; (b) measured peak displacements at the 777th fatigue cycle; and (c) minimum displacements at the 779th fatigue cycle in the y direction (mm).

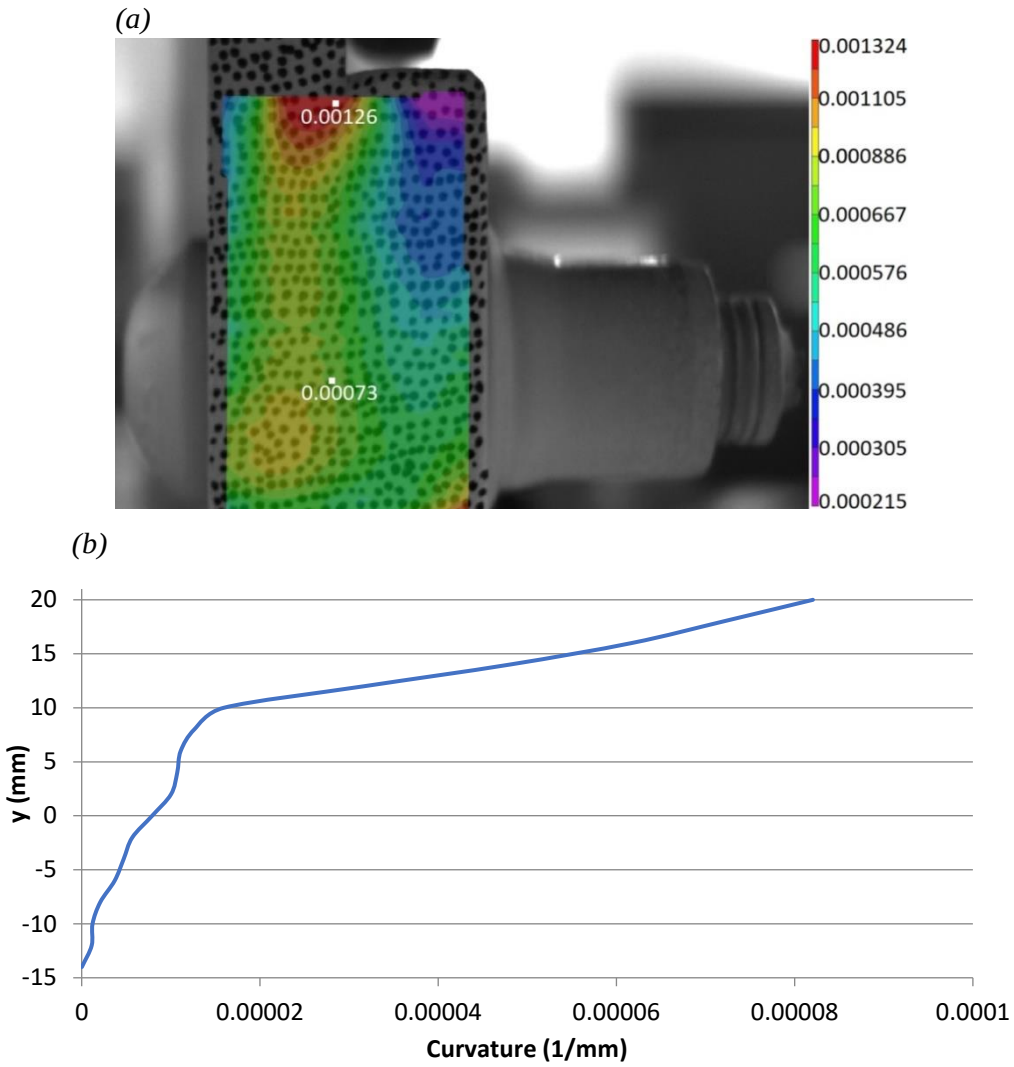

Figure 4.31 Bending analysis results in sample C10-C50LR-150: (a) Normal strains parallel to the applied load (y axis); and (b) Curvature in the upper plate along the specimen edge.

The curvature in the upper plate of sample C10-C50LR-150 is shown in Figure 4.31(b). The maximum value of the curvature is located at the top of the upper plate and its value is slightly lower than that in specimen B5-A325-150 (Figure 4.19). Although the values of the curvature are relatively low, its presence indicates that the secondary bending effect was present in this specimen. However, these values were measured at the visible edge of the specimens. The low curvature values are believed to have caused higher stress concentration at the hole edge due to the tensile and bending stresses. A bending moment of 60.03 kN-mm and a bending stress of 78.15 MPa were calculated using the maximum curvature value. As

a result, a total stress of 228.15 MPa was applied to the specimen instead of the 150 MPa and this reduced the fatigue life of the specimen.

The higher clamping force applied by the Huck bolts also resulted in larger stick regions around the bolt hole area, with small partial slip regions close to it. It may also have induced a larger global slip area away from the bolted contact area. This phenomenon can be seen on an optical microscope image of sample C8-C50LR-150, as shown in Figure 4.32(a). This image was taken on the lower plate near where the uppermost bolt was located. The stick region is apparent around the bolt hole, where the coating remained attached to the surface due to the higher clamping force applied by the C50LR Huck bolts. The coating of the upper plate in which failure occurred at the hole edge remained attached to the coating of the lower plate, and this image shows the back of the coating that had been attached to the upper plate. This explains the metal like colour in the stick region instead of the original green colour of the coating. In the gross slip area, the coating was removed from the contacting surfaces away from the hole due to the fretting wear, and some wear pits can be seen on the surface. At the boundary between the stick and gross slip regions, a smaller partial slip region is apparent.

Figure 4.32(b) shows similar features in the area around the hole of the uppermost bolt of the lower plate for specimen C4-C50LR-150. Wear pits can be seen in the global slip region where fretting wear removed the coating. The coating remained attached to the surface in the stick region, but remained stuck to the upper plate when the sample was dismantled. At the boundary between the regions, cracks can be seen in the coating in the partial slip region.

An SEM image of an area in the partial slip region of the upper plate for sample C8-C50LR is shown in Figure 4.33. The partial slip region is not as evident as in Figure 4.21 because specimen C8-C50LR-150 was subjected to 6 million fewer cycles than sample B3-A325-150. The partial slip region of sample C8-C50LR-150 was located some distance away from the hole, where a number of micro cracks were nucleated, as shown in the higher magnification SEM image in Figure 4.34. These micro cracks had a mean length of 7 μm.

Additionally, surface damage and oxidised particles were found in the surrounding area caused by the relative slip.

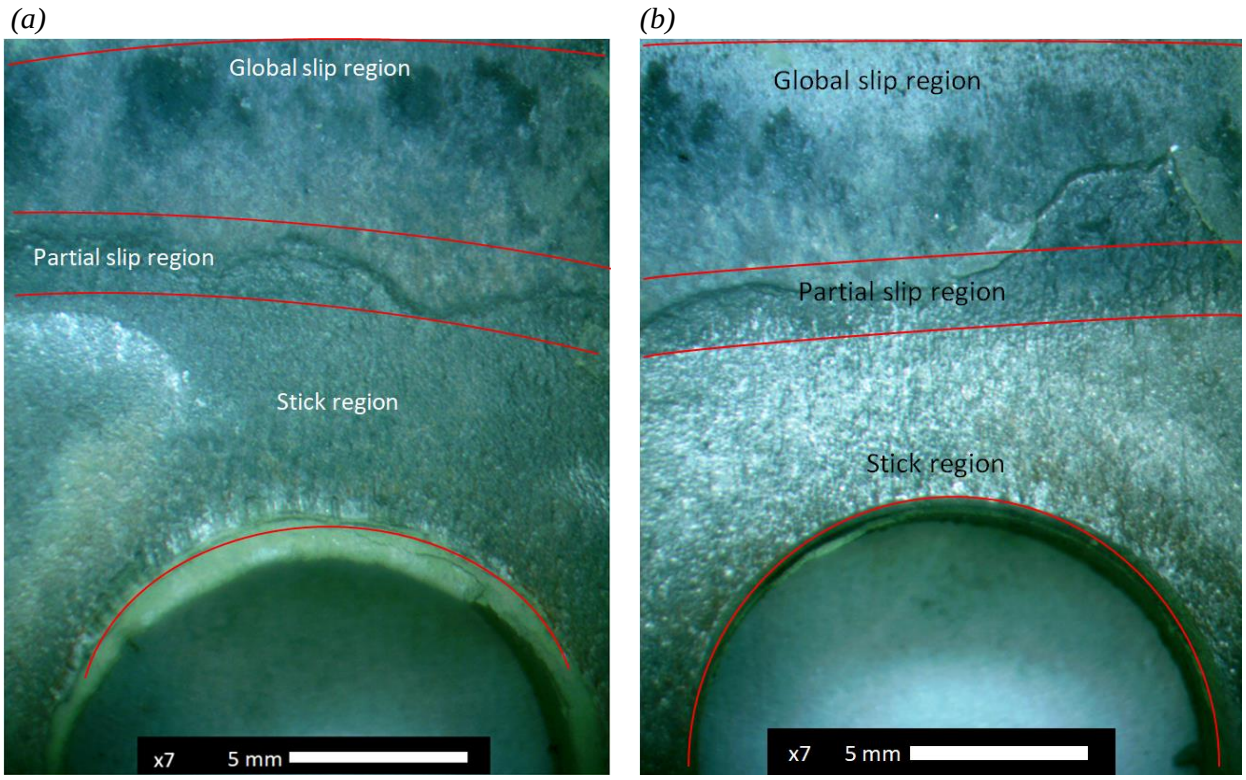

Figure 4.32 Optical microscopic image of the stick-slip regions at the contact interface of: (a) sample C8-C50LR-150 and (b) sample C4-C50LR-150.

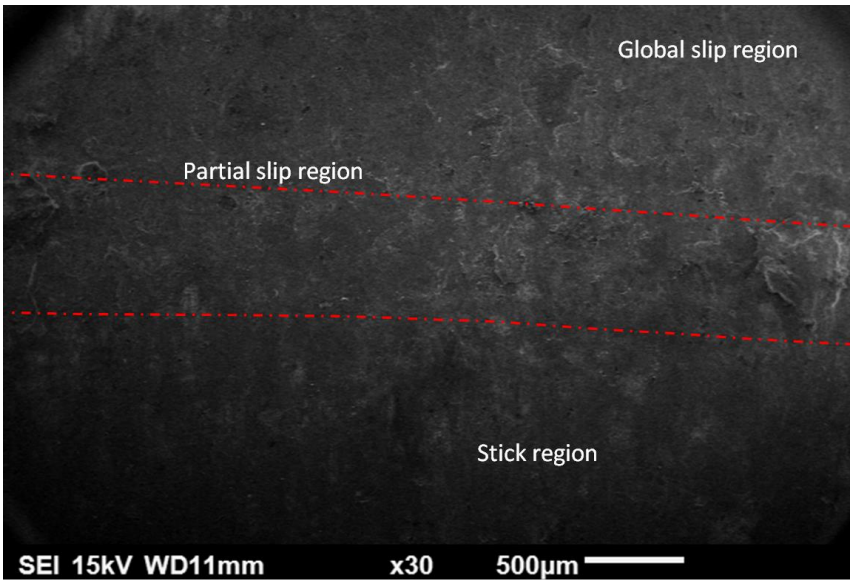

Figure 4.33 SEM micrograph of the boundaries of the partial slip region at the contact interface of sample C8-C50LR-150.

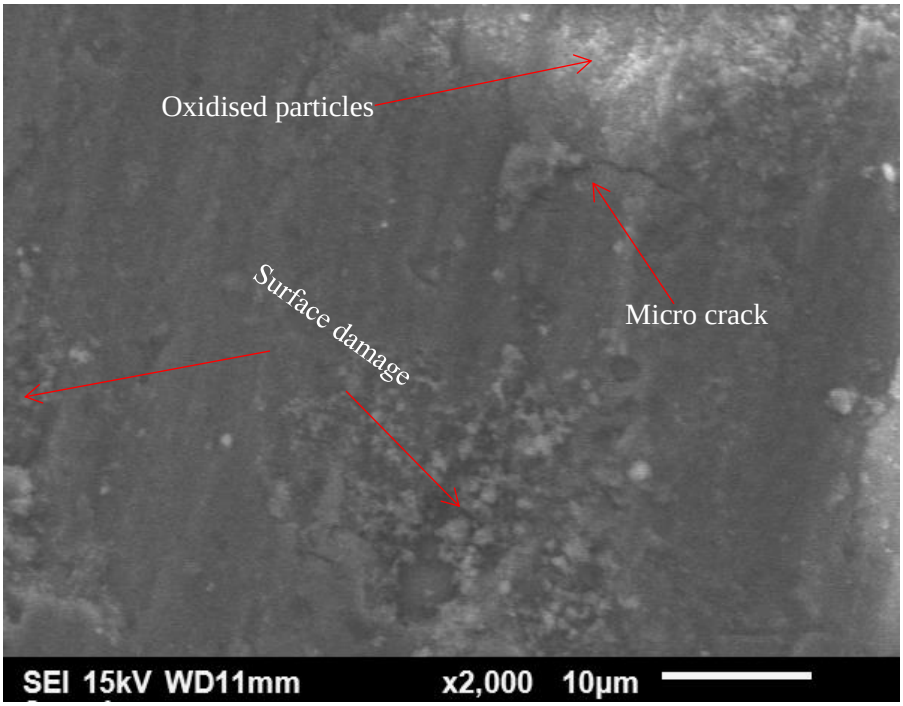

Figure 4.34 SEM micrograph of the partial slip region, showing a micro-crack on the surface of sample C8-C50LR-150.

The displacements normal to the applied load (out-of-plane displacements) for sample C10-C50LR-150 are presented in Figure 4.35(a). The displacements increased initially before stabilizing after 480 fatigue cycles. The mean displacement of the upper plate was 2.135 mm and the lower plate mean displacement was 2.12 mm. Consequently, there was a gap of 15 µm at the contact interface along the visible edge of the sample.

The out-of-plane displacement field at the maximum load for sample C10-C50LR-150 is shown in Figure 4.35(b). The highest out-of-plane displacement was located at the top of the sample. The out-of-plane displacement along the bolt axis was approximately 2.7 mm, which is 0.23 mm higher than the sample assembled with HSB (B5-A325-150) in Figure 4.23(b). The gap between the plates at the centerline of the bolt on the visible edge of the sample was 1 µm, which is seven times smaller than the sample assembled with A325 HSB (sample B5-A325-150). This is believed to be the result of the C50LR Huck tension control bolts having higher bolt preload than the A325 HSB.

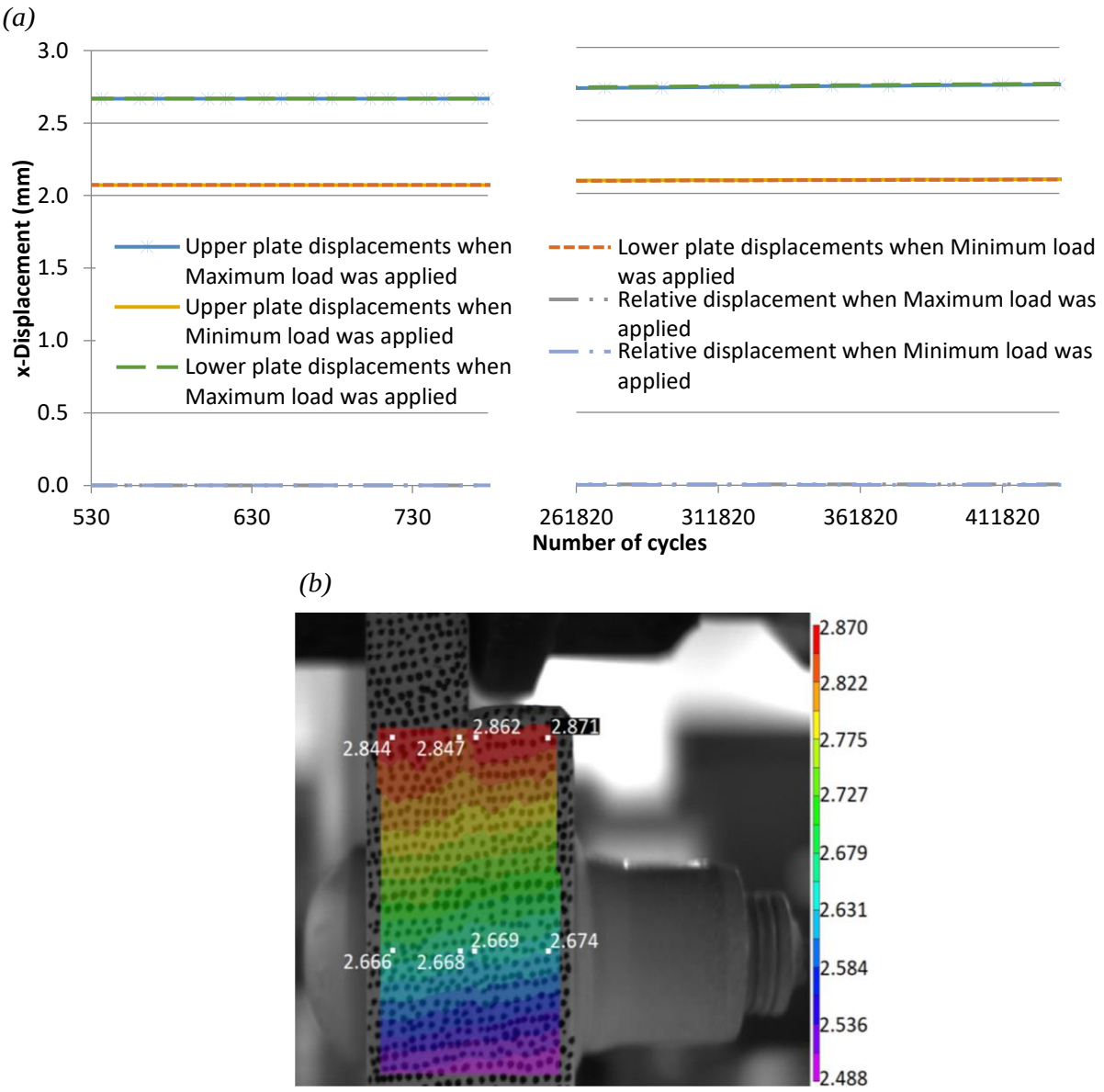

Figure 4.35 Maximum displacements in the x-direction measured in sample C10-C50LR-150. (a) Graph of the maximum, minimum and relative displacements in the upper and lower plates along the bolt axis; and (b) measured peak displacements in the x direction at the 777th cycle (mm).

169 MPa stress range

The displacements parallel to the applied load at points U_1 and L_1 for sample C14-C50LR-169, which had a Class B surface finish with C50LR Huck tension control bolts with a higher stress range of 169 MPa, are shown in Figure 4.36(a). The displacements reached stabilized values around 580 fatigue cycles. The minimum displacement of the upper plate was 1.439 mm while that of the lower plate was 1.297 mm. This shows that

there was a permanent displacement of approximately 1.3 mm when the specimen was nearly unloaded, due to the settling-in of the sample. The minimum relative displacement at the 795th cycle was 0.14 mm, which corresponds to settling-in effects between the plates, similar to the specimens discussed above.

(a)

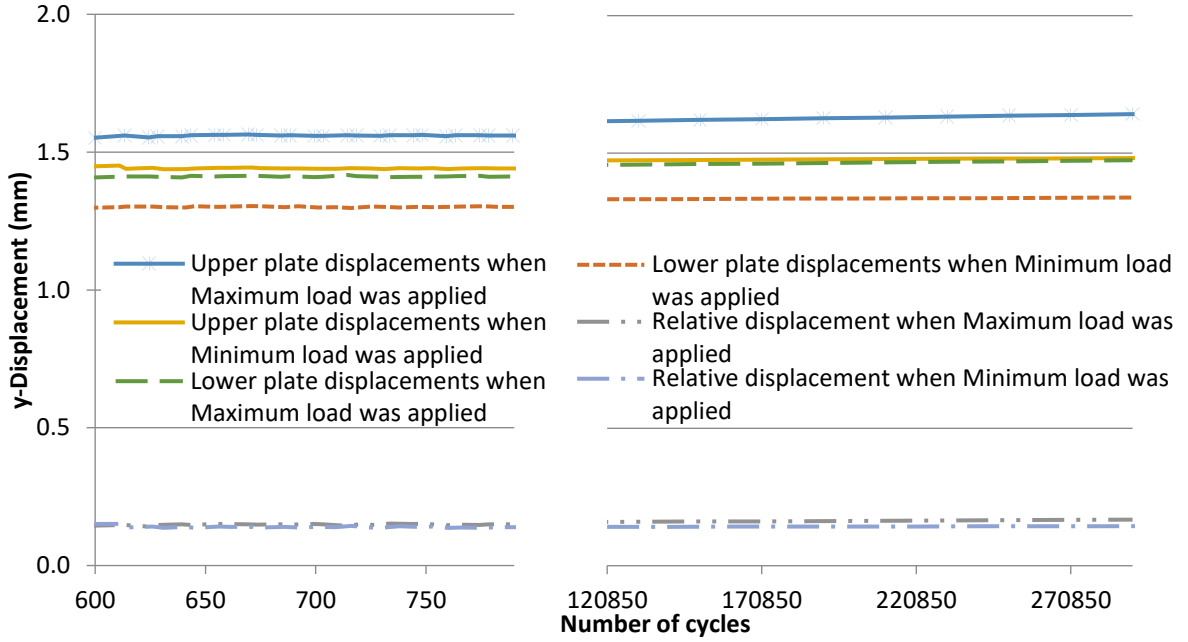

(b) *(c)*

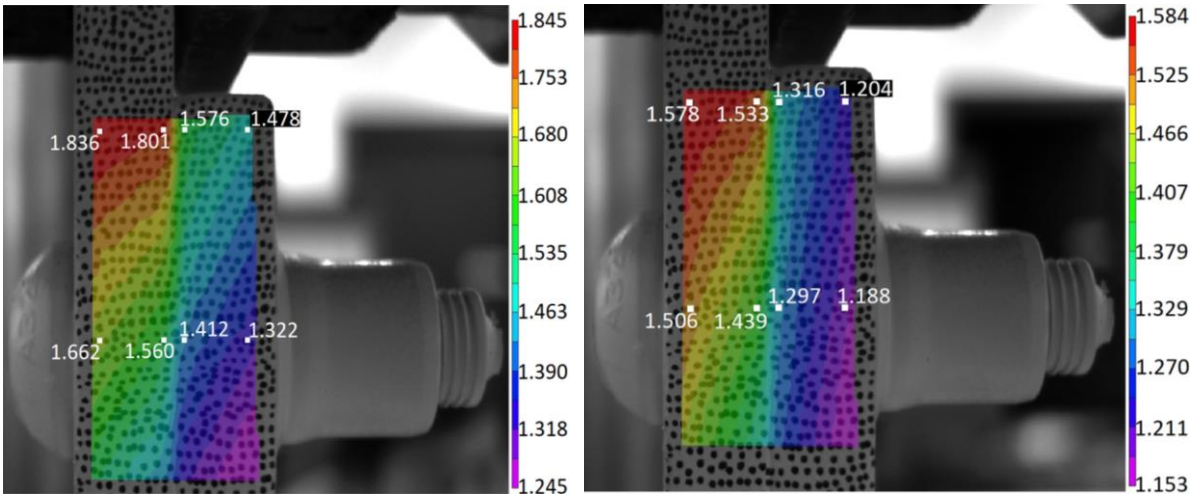

Figure 4.36 Displacements parallel to the applied load (y axis) in sample C14-C50LR-169: (a) Graph of the maximum, minimum, and relative displacements in the upper and lower plates along the bolt axis; (b) measured peak displacements at the 793rd fatigue cycle; and (c) displacements at the 795th fatigue cycle in the y direction (mm).

Between the 793rd and the 795th cycle, the amount of slip that occurred on the exposed surface of the specimen along the bolt axis over a cycle was 10 μm, which is believed to have caused fretting damage within the contact interface. The maximum and minimum displacements of the plates increased steadily over the first 300,000 cycles. Consequently, the relative slip between the plates during a cycle increased to 23 μm after 300,000 cycles. The relative displacement values are very similar to those of specimen B8-A325-169, 13 μm at the 823rd cycle, and 23 μm after 290,000 cycles.

The distribution of the maximum displacements along the edge of the sample is shown in Figure 4.36(b), which is also similar to that of the sample assembled with A325 HSB (Figure 4.24(b)). The maximum displacement was located at the top of the upper plate. This distribution of displacements is consistent with the combined effects of slip and bending. The relative displacement at the contact interface at the bolt axis was 0.148 mm and at the top edge of the lower plate was 0.225 mm, respectively. These values are slightly lower than the sample B8-A325-169 (0.2 mm and 0.329 mm, respectively).

The displacements caused in sample C14-C50LR-169 when the minimum load of the cycle was applied are shown in Figure 4.36(c). The distribution of the displacement field is similar to that observed for specimen B8-A325-169 in Figure 4.24(c), with lower values of displacement. The relative displacement at the bolt axis was 0.142 mm and at the edge of the lower plate was 0.217 mm. These displacements are lower than those of sample B8-A325-169 (0.189 mm and 0.297 mm, respectively). These values probably correspond to the settling-in displacements of the sample.

The axial normal strains along the visible edge of specimen C14-C50LR-169 when the maximum cyclic load was applied are shown in Figure 4.37(a). The maximum strain values occur in the upper plate and extend from the bolt axis close to the contact interface between the plates upward and slightly away from the interface. The peak strain value is at the top of the upper plate inside of the AOI and unlike the other specimens, the strain is also high at the bolt axis. Thus, this specimen had a different behaviour than sample B8-A325-169 although the peak strain values at the top of the upper plate were similar.

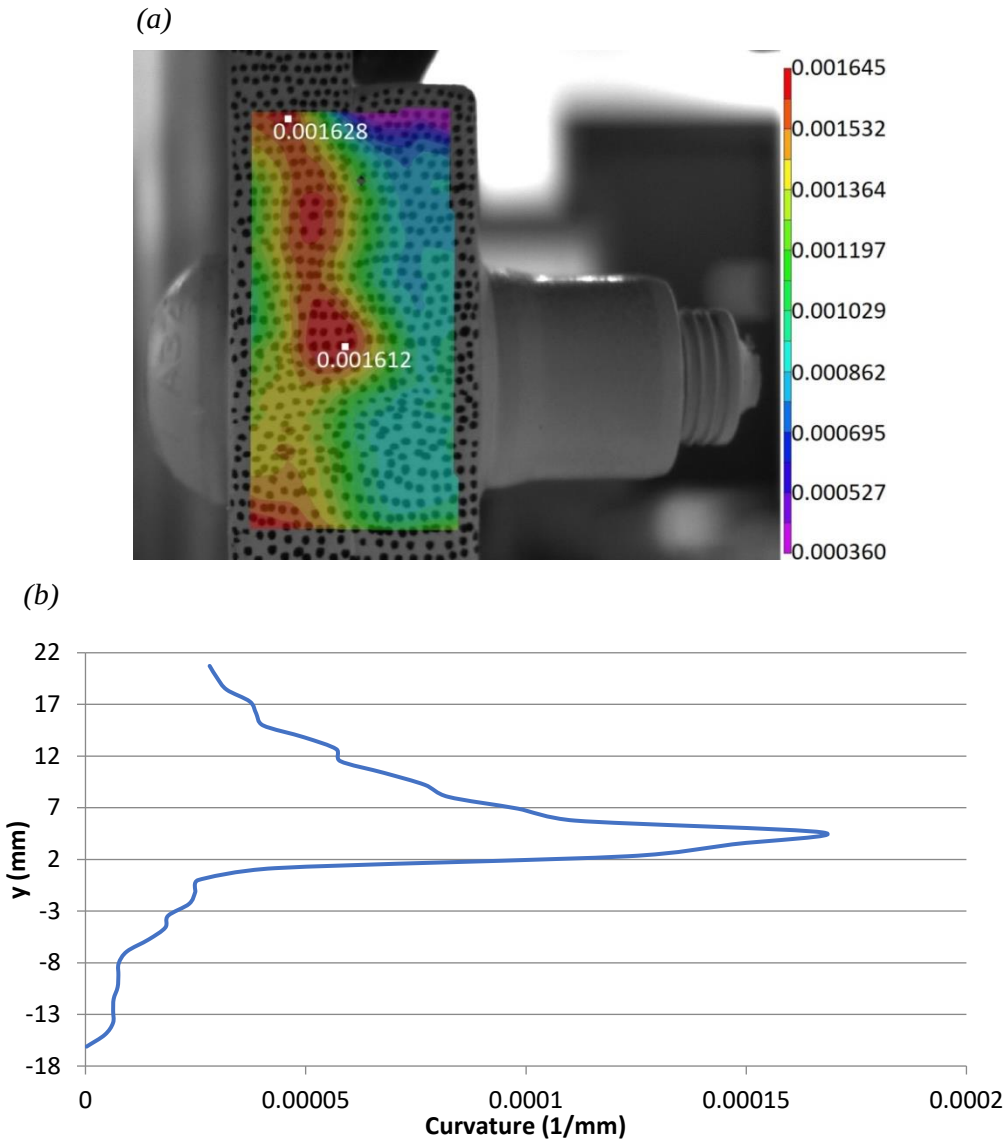

Figure 4.37 Bending analysis results in sample C14-C50LR-169: (a) Normal strains parallel to the applied load (y-axis); and (b) Curvature along the specimen edge in the upper plate.

The curvature in the upper plate of sample C14-C50LR-169 along the visible edge is shown in Figure 4.37(b). In this case, the maximum curvature occurred along the bolt axis, which is different from that of sample B8-A325-169; the peak values are similar but they occur at different places. The reason for this is unknown. The higher values of curvature in Specimens B8-A325-169 and C14-C50LR-169 compared to Specimens B5-A325-150 and C10-C50LR-150 demonstrates that the secondary bending effect was more pronounced in specimens subjected to the 169 MPa stress range. Again, this explains why the fatigue life of specimens tested at the 169 MPa stress range fell well below the CSA S16-14 S-N curve.

The maximum curvature value was used to determine the bending moment value of 122.47 kN-mm and a bending stress of 159.43 MPa. The total stress applied to the sample resulted in 328.44 MPa, which caused a low fatigue life.

Optical microscopic images of the contact surface of sample C14-C50LR-169 in the region above the bolt hole are shown in Figure 4.38 and look similar to samples assembled with A325 HSB subjected to the 169 MPa stress range (Figure 4.26). Fretting wear and micro-cracks were found on the surface, the global and stick regions could be identified, and the partial slip region was located between them, as shown in Figure 4.38(a). For these images, the coating that was attached to the surface in the stick region was intentionally removed to inspect the area. In the partial slip region, a wear pit can be seen, which was caused by the stress concentration (tangential and normal forces) on the surface where cracks could have initiated. Also, fretting wear can be seen in the global slip region, caused by the high relative displacements.

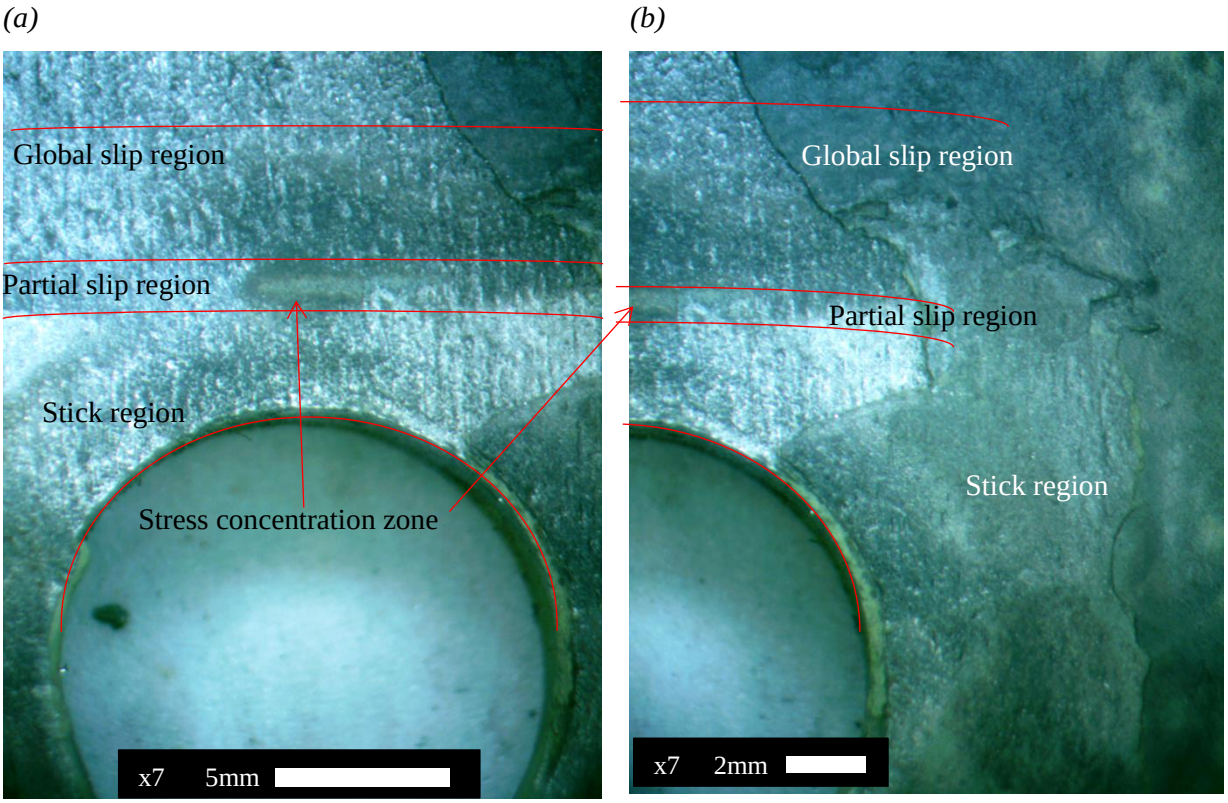

Figure 4.38 Contact interface of sample C14-C50LR-169: (a) Partial stick-slip regions above the hole; and (b) Partial stick-slip regions around the hole.

Figure 4.38(b) shows similar features on the contact surface around the hole of sample C14-C50LR-169. It can be seen that the surface in the stick region has suffered minor damage. The coating located close to the global slip region shows major damage but less severe than that of sample B8-A325-169 in Figure 4.26. The coating of the upper plate was attached to the coating of the lower plate in the stick region. Some surface damage was found along with ploughing lines parallel to the applied load, as shown in Figure 4.39. The large displacements caused by the 169 MPa stress range caused gross slip on the surface to produce the surface wear related damage.

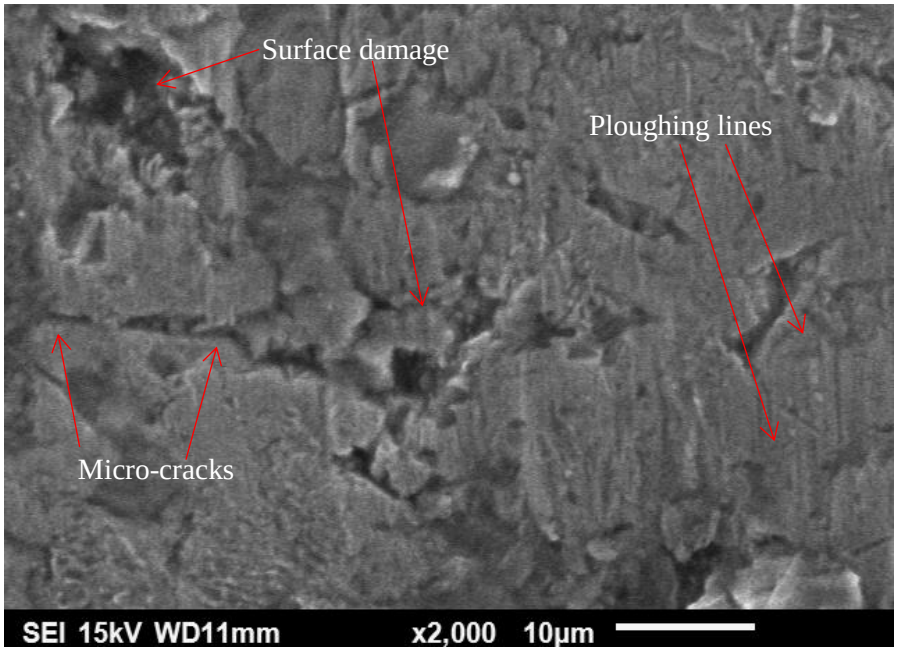

Figure 4.39 SEM micrograph of the gross slip region, showing fretting damage at the contact interface of sample C14-C50LR-169.

The measured out-of-plane displacements for sample C14-C50LR-169 are presented in Figure 4.40(a). Both plates deflected by similar amounts, with maximum displacements in the upper and lower plates along the bolt axis adjacent to the interface of 3.176 mm and 3.181 mm, respectively. The gap between the plates at the bolt axis was therefore 5 µm. As discussed before, if a similar gap existed within the sample (i.e. not only on the surface), it would be responsible for the reduced fretting damage at the contact interface. The higher out-of-plane displacements also increased the possibility of stress concentration sites at the hole, causing crack initiation and fracture in the form of bending fatigue.

(a)

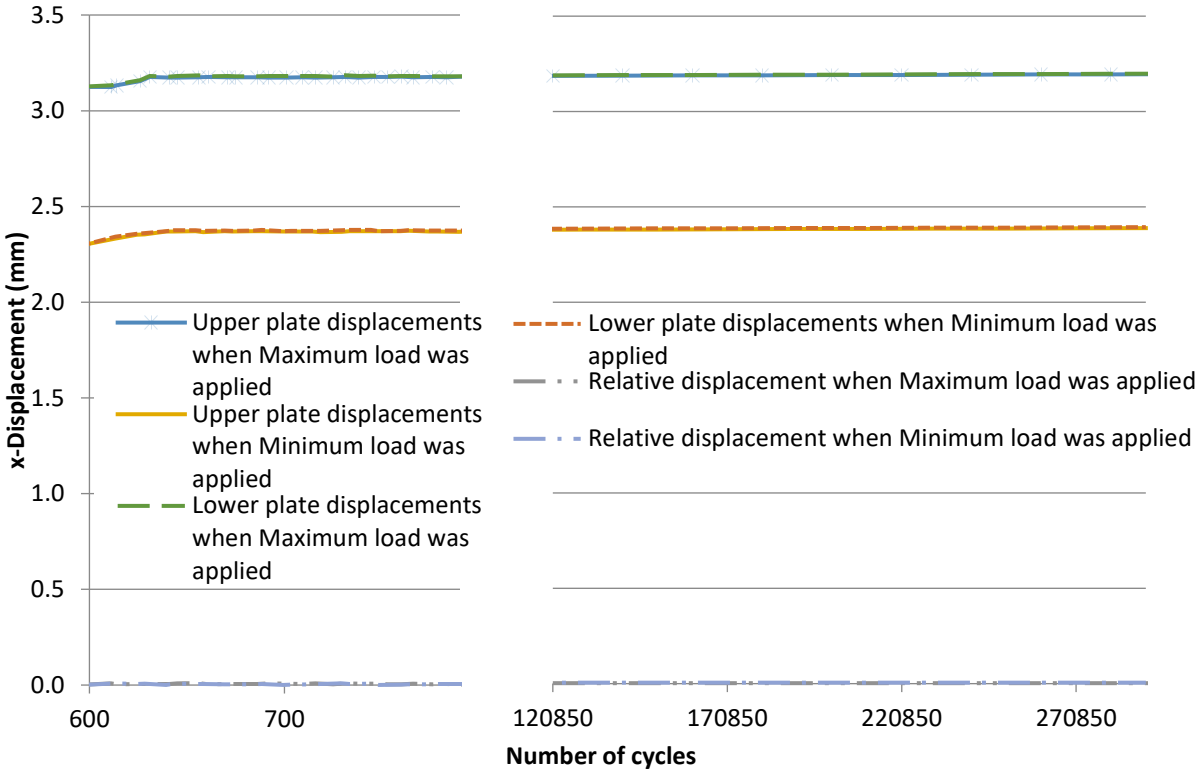

(b)

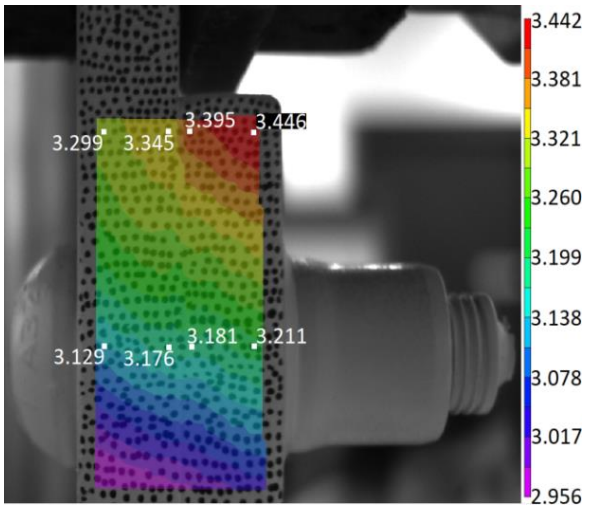

Figure 4.40 Displacements perpendicular to the applied load (x-axis) in sample C14-C50LR-169: (a) Graph of the maximum, minimum, and relative displacements in the upper and lower plates along the bolt axis; and (b) measured peak displacements at the 795th fatigue cycle.

The distribution of the maximum displacements and their values at various points in the area of interest are shown in Figure 4.40(b). The maximum out-of-plane displacement in

sample C14-C50LR-169 was similar to that of B8-A325-169 HSB (Figure 4.28(b)). A gap of 5 μm was present at the specimen surface near the first bolt, which was eleven times smaller than the gap present in the sample B8-A325-150 (58 μm). This is evidence that the tension control bolts were able to apply a higher pre-tension to the connection. Moreover, a gap of 50 μm was present at the top end of the lower plate, an observation consistent with secondary bending.

An analysis was undertaken to better understand the secondary bending effect in samples with Class B surface and C50LR Huck tension control bolts. The secondary bending effect was similar to that observed for the samples assembled with Class B surface finish and A325 HSB. A schematic representation of the out-of-plane displacements measured using the DIC images for samples C10-C50LR-150 and C14-C50LR-169 are shown in Figures 4.41(a) and 4.41(b), respectively. A small amount of rotation (twisting) (0.63° for sample C10-C50LR-150 and 0.77° for sample of C14-C50LR-169) was present along the axis of the first bolt of the assembled bolted specimens, which is also consistent with secondary bending.

It can be seen from the above results that the specimens with Class B surface finishes were predominantly subjected to the combined effect of fretting fatigue and secondary bending. The bending effect resulted in stress concentration sites in the upper plate around and above the first bolt of the connection. The samples tested at the lower stress range levels (i.e., an applied fatigue load lower than half the yield stress), exhibited more fretting damage characteristics on the contacting surface. At higher stress range levels, the secondary bending effects were more dominant as compared to fretting fatigue behaviour and it is possible that the larger gaps between the plates at the higher load reduced the fretting effects. The reason behind the predominant bending failure for specimens with a Class B surface finish could be due to the coating on these contacting surfaces, which delayed fretting fatigue crack initiation long enough for crack initiation due to bending to occur. As the relative displacement between the contacting plate surfaces induced a frictional force, it caused fretting wear on the contacting surfaces, and the surface coating was removed in the gross-slip region. As fretting continued, it caused new microcracks to nucleate on the virgin uncoated surface. Even though the fretting continued to cause further damage on the

contacting surfaces, the secondary bending effect initiated a crack at the bolt hole due to the stress concentration sites and led to failure.

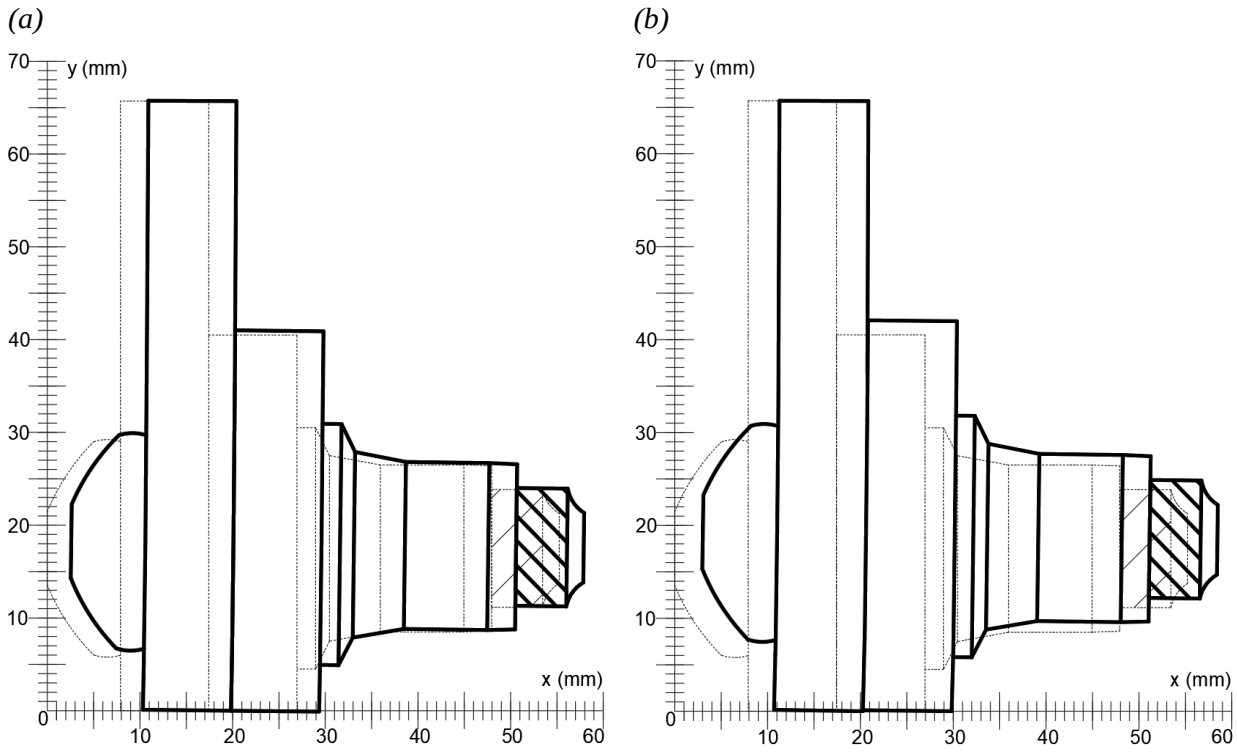

Figure 4.41 Displaced shapes at maximum cyclic loads of samples tested with different stress ranges: (a) Sample C10-C50LR-150 at 777 cycles, and (b) Sample C14-C50LR-169 at 795 cycles.

4.5.3 Class A surface: Fretting Fatigue

Since both A325 HSB and C50LR Huck tension control bolt specimens with Class B surface finishes showed similar fretting fatigue features on their contact surfaces, it was assumed that specimens with the Class A surface finish and A325 HSB might also exhibit similar fretting fatigue behaviour at the contact interface. The results confirmed that specimens with a Class A surface finish and A325 HSB experienced fretting fatigue failure.

In these samples, crack initiation took place due to severe fretting damage at the contact interface and then the cracks propagated to final failure. Although the relative displacements were not measured using the DIC technique for these samples, based on the stereo microscope and scanning electron microscope (SEM) images, the slip behaviours were likely similar to Class B surfaces. The contact interface was examined to analyse the fretting

phenomenon (fretting wear, slip behaviour, surface micro cracks) and the fractured surface was analysed to understand the crack initiation and crack propagation behaviour.

Two samples, A10-A325-150 and A12-A325-150, were selected for analysing the fretting fatigue failure behaviour; photographs of the contact surfaces after failure are shown in Figure 4.42. The area around the first and the sixth hole of the plates suffered severe fretting damage, while the contact interface between the second and the fourth holes experienced less surface damage.

The surface characteristics of the specimens with Class A surface finish and A325 HSB were very similar. Due to the applied bolt preload, the contacting surfaces exhibited stick, partial slip and global slip regions, as shown in Figure 4.43(a). The stick regions around the hole experienced minimal surface damage due to fretting. However, the partial stick-slip regions, located a certain distance away from the first hole, exhibited severe surface damage and fretting wear (Figures 4.43(a) and (b)).

Figure 4.42 Contact interface of samples A10-A325-150 and A12-A325-150 after fretting fatigue failure.

Figure 4.43(c) shows the contact interface of Sample A10-A325-150 in the vicinity of the failure surface. The cracks nucleated at multiple locations away from the bolt hole due to fretting. The nucleation of microcracks was the result of a higher frictional force at the boundary between the stick and global slip regions (i.e. in the partial stick-slip region). The

higher frictional forces induced stress concentration sites around the stick-slip regions and promoted the nucleation of multiple microcracks. These microcracks coalesced into a leading crack before initiating final failure.

(a) *(b)*

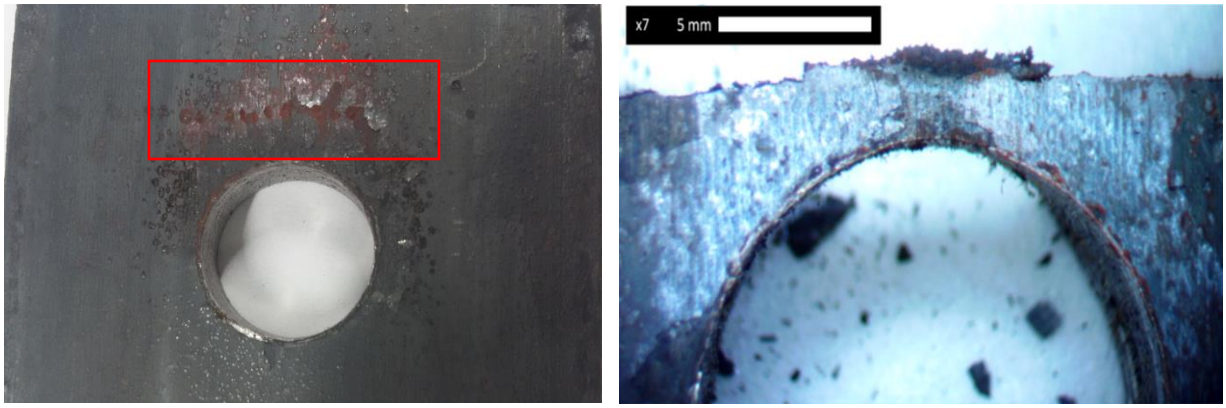

(c)

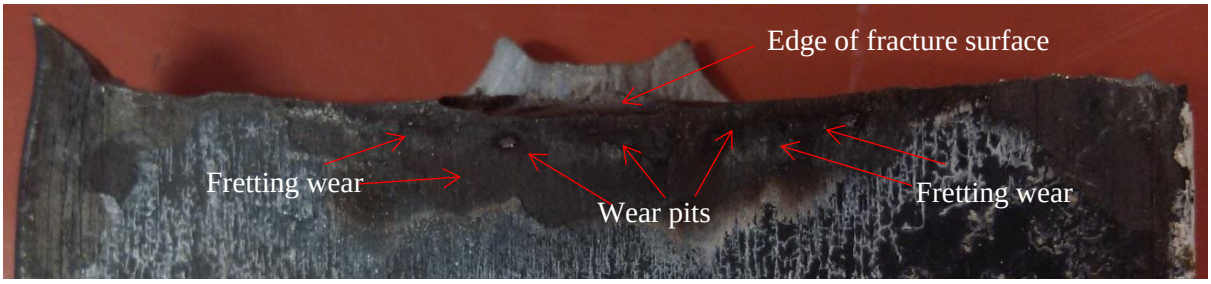

Figure 4.43 Optical images of fretting fatigue damage: (a) Fretting fatigue damage in sample A8-A325-136; (b) Fretting failure of sample A12-A325-150, and (c) Contact surface of sample A10-A325-150 near the location of fracture.

The partial slip-stick regions of different specimens made with Class A surface finish were identified in the optical microscopic images shown in Figure 4.44. The images show the area above the uppermost hole of each lower plate that was in contact with the upper plate where fretting fatigue failure occurred. Samples A10-A325-150 and A11-A325-150 (in Figures 4.44(a) and 4.44(b), respectively) show the most damage on the surface due to the higher applied load and higher stress concentration in the partial slip region. The global slip region in both samples is covered by debris caused by the relative slip between the plates, whereas the stick region in both specimens shows no apparent damage. Multiple crack initiation sites and final fracture occurred in the partial slip regions in the upper plate.

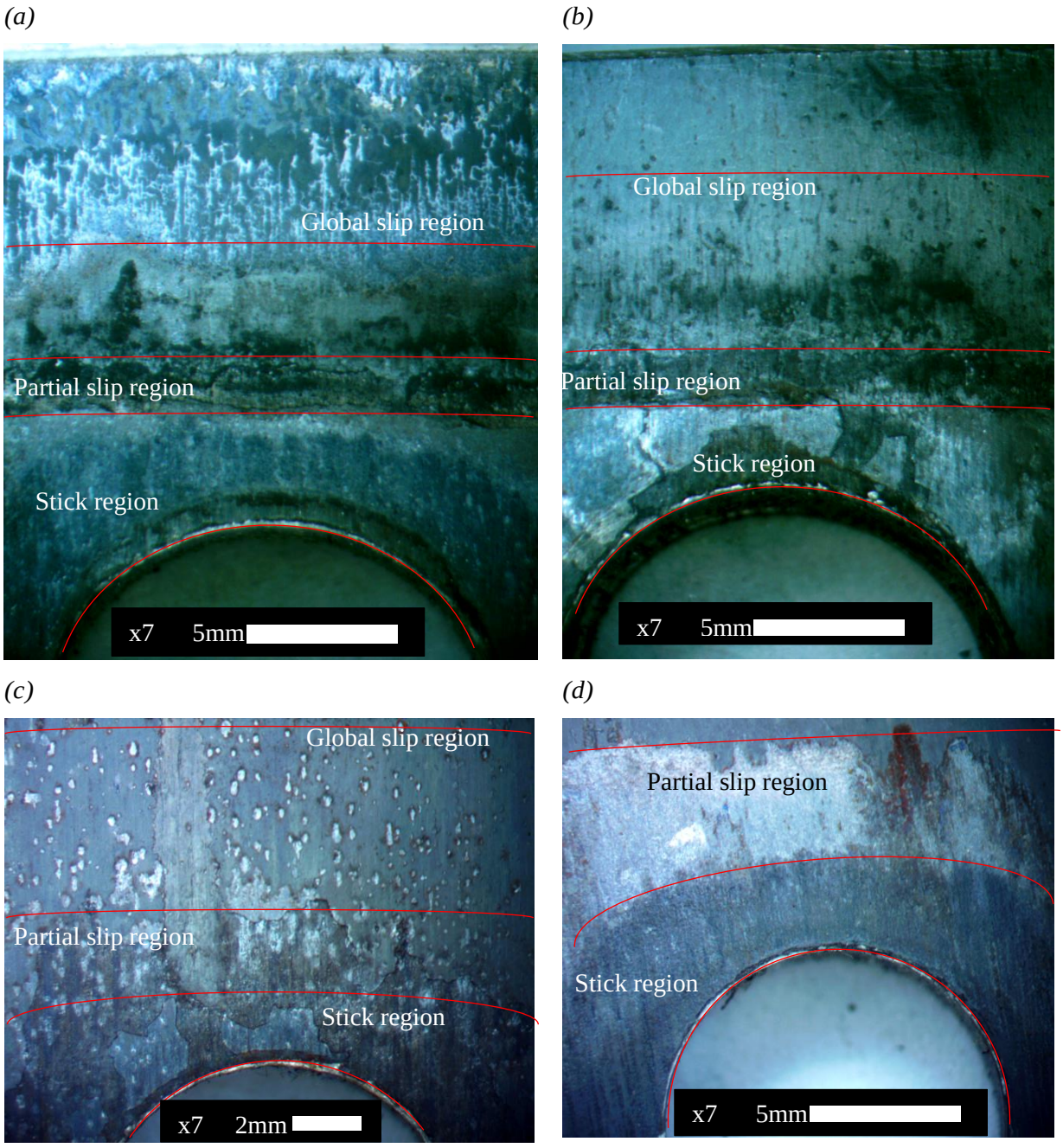

Figure 4.44 Partial slip-stick regions of fretting fatigue damaged surfaces: (a) Sample A10-A325-150; (b) Sample A11-A325-150; (c) Sample A7-A325-136; and (d) Sample A2-A325-122.

Figure 4.44(c) shows the surface of sample A7-A325-136, which was subjected to the stress range of 136 MPa and had a fatigue life of 2.6 million cycles. The surface damage in the global slip region was severe in the form of fretting wear pits. The stress concentration in the partial slip region was lower than in specimens subjected to the 150 MPa stress range. Similarly, the stress concentration in the partial slip region of sample A2-A325-122, which

was subjected to a stress range of 122 MPa was even lower, which as a result caused less damage in the global and partial slip regions, as shown in Figure 4.44(d).

Figure 4.45 shows surface deterioration in the partial stick-slip regions in the upper plate of sample A12-A325-150. The red arrow points to the intersection of two propagating cracks (ratchet mark) in which the lower crack propagated further and joined with another crack. The yellow ellipse shows severe surface damage close to the fracture surface. Additional fretting damage is seen in Figure 4.46. The fretting micro cracks (identified with red arrows) were found on the surface, oriented normal to the direction of the applied load. Typical microscopic wear debris particles were also found all over the surface, appearing as bright small particles within the closed yellow ellipse. Ploughing lines that indicate the sliding direction on the surface are also found on the surface in Figure 4.46. These were generated by the relative motion between the contacting plates at the contact interface. The path of the lines shows irregularities, such as micro-discontinuities or surface damage caused by fretting wear. The ploughing lines are shown at higher magnification in Figure 4.47.

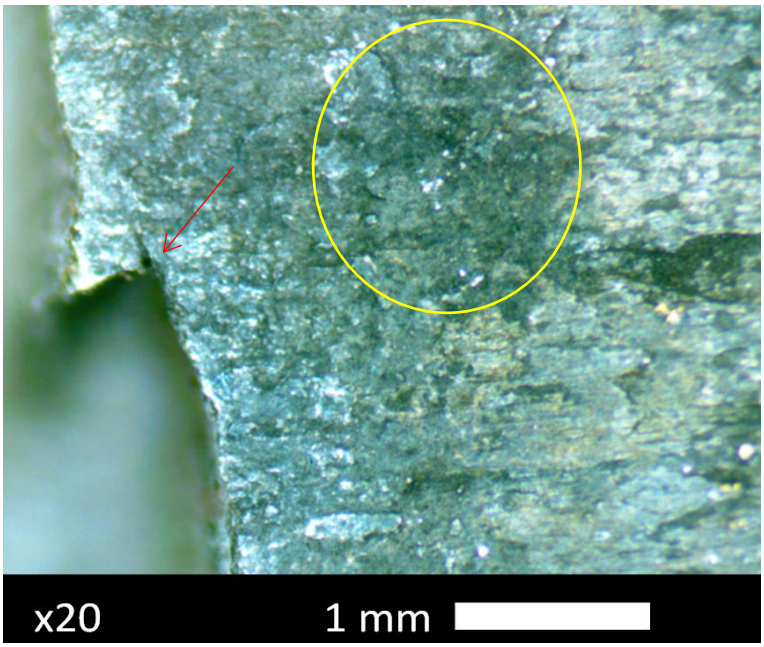

Figure 4.45 Contact interface of the upper plate of sample A12-A325-150 observed using the Stereo microscope.

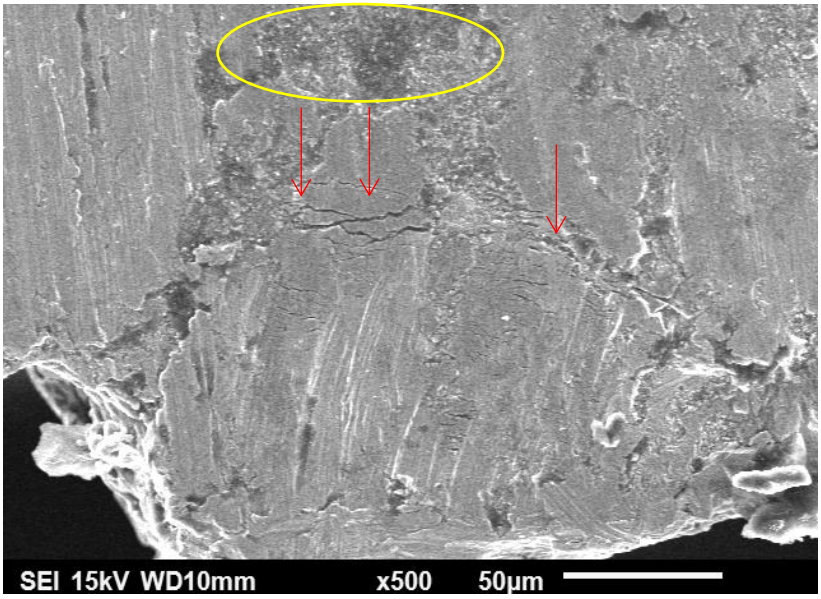

Figure 4.46 SEM image of micro cracks parallel to the fracture edge in the upper plate of sample A12-A325-150.

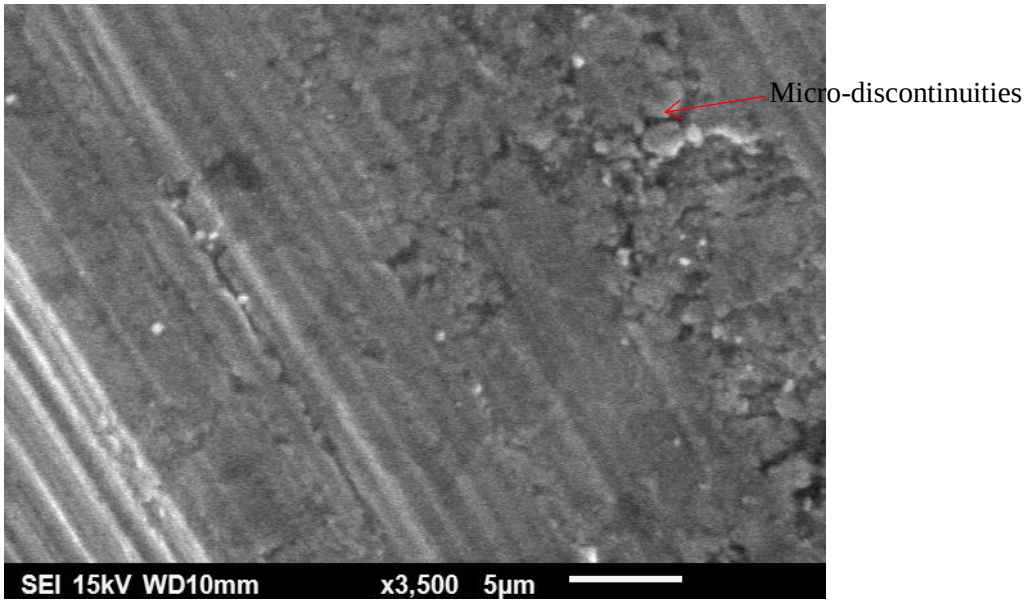

Figure 4.47 High magnification SEM image showing ploughing lines on the contact interface on the upper plate of sample A12-A325-150.

The measurement of relative displacements as well as microscopic examination demonstrated that the Class B surfaces assembled with both A325 HSB and C50LR Huck bolts were subjected to a combination of fretting and bending fatigue, while the Class A surface experienced predominantly fretting fatigue. The relative displacements parallel to

the applied load (in-plane displacement) between contacting plates with the Class B surface finish promoted the fretting damage and the eccentric loading inherent in the single lap joint specimens, which caused out-of-plane displacements, produced the secondary bending effect. The gap that formed between the contacting plates along the edge of the specimens due to the secondary bending may have extended closer to the bolt hole within the specimen, which could have prevented continuous fretting damage from occurring and allowing bending failure. Similar behaviour was observed by Ekh et. al (2005) and Schijve et al. (2009). They explained that the secondary bending effect increased the stress concentration during fatigue loading and that it could certainly change the failure mode of the bolted connection.

4.6 Crack initiation

4.6.1 Class B surface

As discussed before, the relative displacement between the contacting plates induced frictional forces and caused the formation of stick-slip regions, where a number of micro cracks nucleated. Some of these microcracks were intercepted by the continued fretting wear and subsequently cracks induced by secondary bending became a leading crack. Since the plates with Class B surfaces were coated with the Cathacoat 302HB coating, microcracks were prevented on the surface until the coating was delaminated by the fretting wear. The subsequent fretting cycles produced new virgin surfaces and the fretting process started. During these periods, the secondary bending induced additional cracks around the hole edges normal to the direction of the fatigue load due to the stress concentration sites. These microcracks coalesced into a leading crack and led to final fracture.

Evidence for the behaviour described above could be seen in all specimens with Class B surface finishes within the contact interface around the first hole. The crack initiation sites observed for these specimens are shown schematically as zones A and B in Figure 4.48. Zone A is a region of stress concentration adjacent to the hole edge, where secondary bending amplified the stresses, while Zone B is the region of fretting damage and wear.

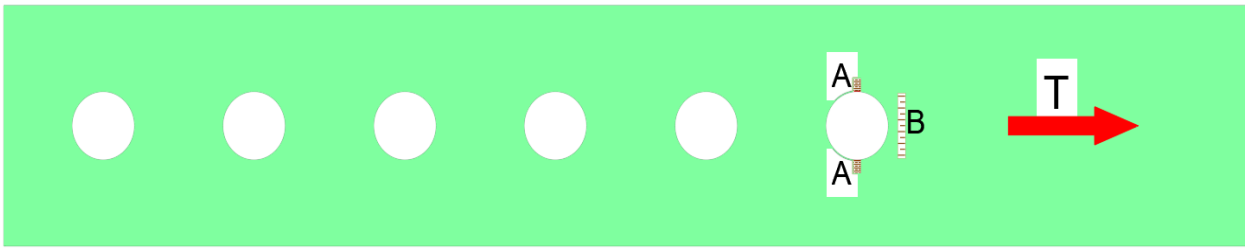

Figure 4.48 Crack initiation sites found in Class B surface finish bolted specimens.

An SEM image of the crack initiation location (Zone A) from sample C8-C50LR-150, subjected to a stress range of 150 MPa, is shown in Figure 4.49. The initiated crack apparently changed direction from parallel to the relative motion to become a crack propagating perpendicular to the applied load, as seen from the crack propagation path. Similar behaviour was also observed for sample B3-A325-150, also subjected to a stress range of 150 MPa, where the crack was initiated at edge of the hole due to the bending effect, as shown in the optical microscopic image in Figure 4.50. The first crack occurred at the right side of this image, in the quadrant close to the edge where the stress concentration was higher. Interestingly, no damage was found below the hole.

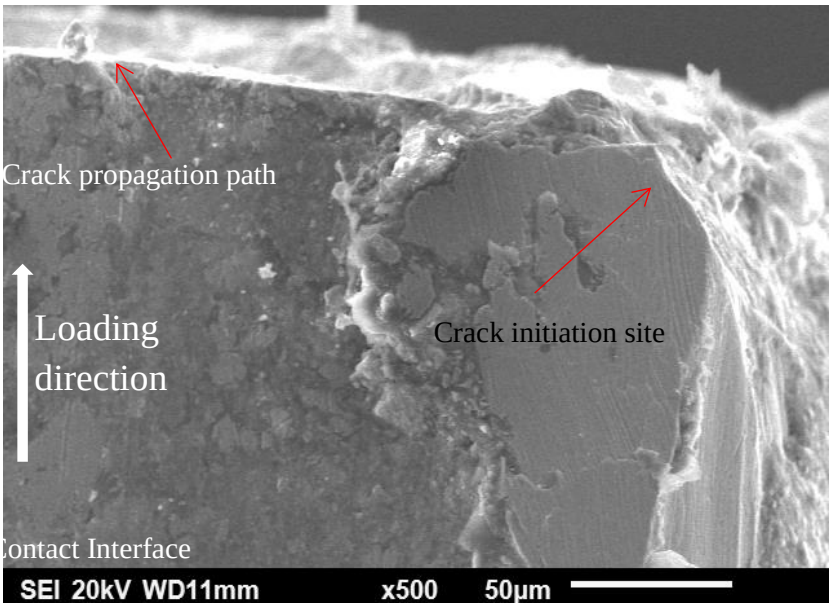

Figure 4.49 Crack initiation site at the edge of the hole of the upper plate of sample C8-C50LR-150.

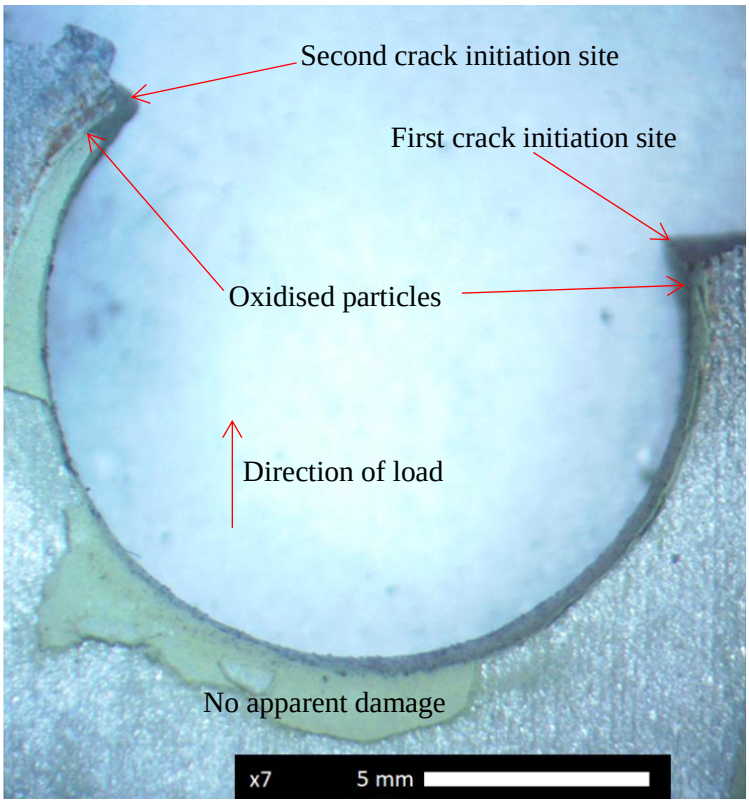

Figure 4.50 Optical microscopic image of the contact interface of the upper plate of sample B3-A325-150, showing the crack initiation sites.

Figure 4.51 shows an SEM image of Zone A in Specimen B3-A325-150 after failure, identifying the point of crack initiation at the edge of the hole. Although fretting wear removed the coating and nucleated a number of microcracks on the surface of this specimen in Zone B, the influence of bending resulted in the formation of a leading crack at the hole edge. An additional crack initiation site can be seen at a distance of 0.67 mm from the edge of the hole, likely caused by combined effects of bending and fretting.

The crack propagation behaviour for sample B3-A325-150 can be seen in Figure 4.52. It should be noted that this specimen had to be cut to fit into the SEM, explaining the two separate pieces on either end of the photograph. The crack propagation area of the leading crack was bigger than the secondary crack path, but the presence of the secondary propagation path shows that the secondary crack was also propagating along with the leading crack. However, the crack with the higher stress intensity factor propagated at a faster rate and resulted in final failure.

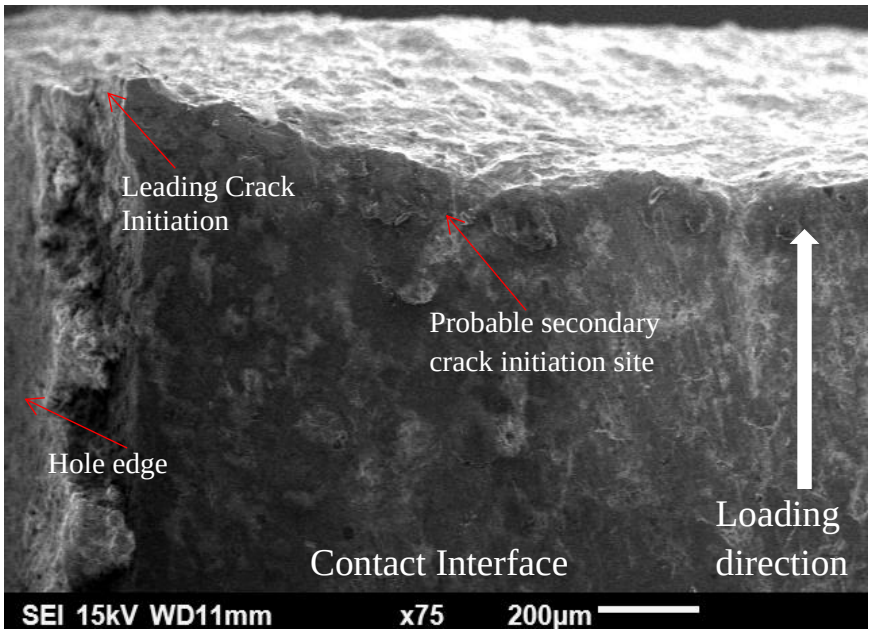

Figure 4.51 Crack initiation site at the edge of the hole in the upper plate of sample B3-A325-150.

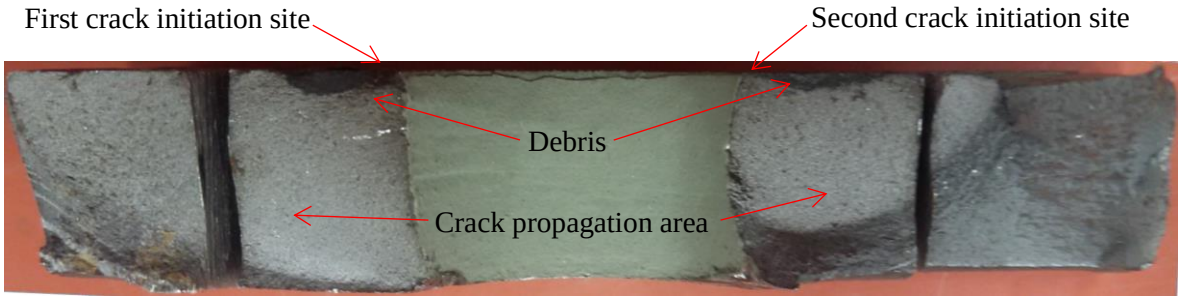

Figure 4.52 Camera image of fracture surface of sample B3-A325-150.

At a higher stress range of 169 MPa, there were no apparent crack initiation sites within Zone B, indicating that there was no appreciable fretting effect on crack initiation. Instead, the specimens failed due to strictly flexural stresses, as can be seen from sample C13-C50LR-169 (Figure 4.53). This sample had a relatively short fatigue life (325,597 cycles), which means that the number of fatigue cycles was not enough to cause severe fretting damage. However, Figure 4.53 shows that the relative slip between the plates removed the coating close to the hole; the coating remained attached to the other contacting plate. The specimen did not fail at the crack initiation site shown in Figure 4.53 because it failed at the hole of the other plate.

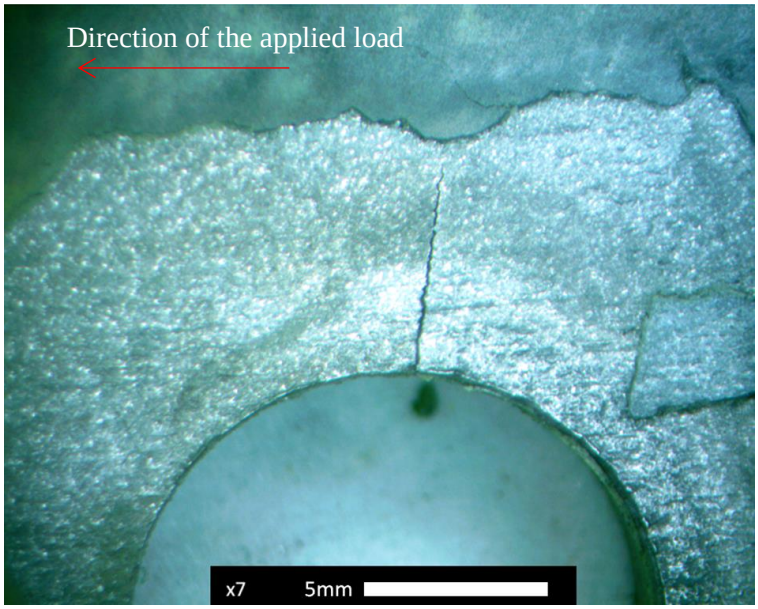

Figure 4.53 Optical image of the surface of the lower plate of sample C13-C50LR-169 showing a crack that initiated at the stress concentration site of the hole.

Three short samples, B5-A325-169 to B7-A325-169, were tested with a 169 MPa stress range and all these samples had similar fatigue lives and modes of failure. Similar behaviour was observed for both short and long specimens. Five long samples were tested at the highest stress range levels of 187 MPa and 216 MPa, and all these specimens also failed due to the effects of secondary bending.

4.6.2 Class A surface

4.6.2.1 Fretting fatigue crack initiation sites

Specimens with the Class A surface and A325 HSB predominantly failed due to fretting fatigue. The specimens failed close to the first bolt but some distance away from the hole edge, where the fretting behaviour was more active. The specimens with Class A surface finish suffered severe fretting fatigue damage at the contact interface, especially in Zone B, identified in Figure 4.54. As discussed in Section 4.5.3, the partial stick slip action in this region induced micro cracks, which coalesced into a leading crack that propagated to cause final failure.

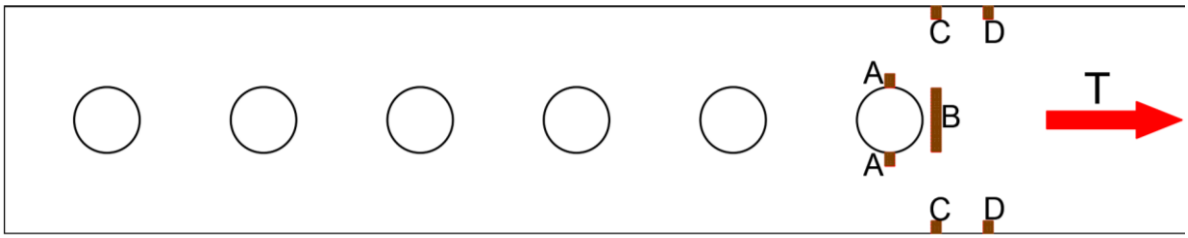

Figure 4.54 Crack initiation sites found in specimens with Class A surface finish and A325 HSB.

Specimens A10-A325-150, A11-A325-150 and A12-A325-150, tested at the 150 MPa stress range, failed due to fretting fatigue with crack initiation sites in Zone B of the contact interface. Samples A2-325-122 and A5-A325-122 were subjected to a 122 MPa stress range and failed after 3.7 million cycles and 1.4 million cycles, respectively, with crack initiation sites in Zone B. Specimens A7-A325-136 to A9-A325-136, with a stress range of 136 MPa, failed due to fretting fatigue with crack initiation sites located in Zone B and Zone A.

Although these specimens experienced both fretting fatigue and secondary bending, all the Class A surface specimens failed due to fretting fatigue. The fretting fatigue failure was initiated by the frictional force induced by the relative displacement between the contacting plates. Since the Class A surface finish was not coated, the stick-slip region, which was located between the stick and global slip regions within the contact interface, was subjected to severe fretting that induced stress concentration sites and crack initiation well before the secondary bending effect initiated cracks. The induced microcracks in the stick-slip regions then coalesced into a leading crack and formed a propagating crack. There were a number of microcracks due to the secondary bending at locations A, C and D, but these did not lead to a propagating crack prior to fretting fatigue causing failure.

Figure 4.55(a) shows the fracture surface of sample A12-A325-150, which failed due to fretting fatigue. Figure 4.55(b) shows a magnified view of the fracture area. Microscopic ratchet lines can be seen, indicating that multiple microscopic cracks nucleated. There were a number of crack initiation sites, which formed the ratchet lines seen in these figures.

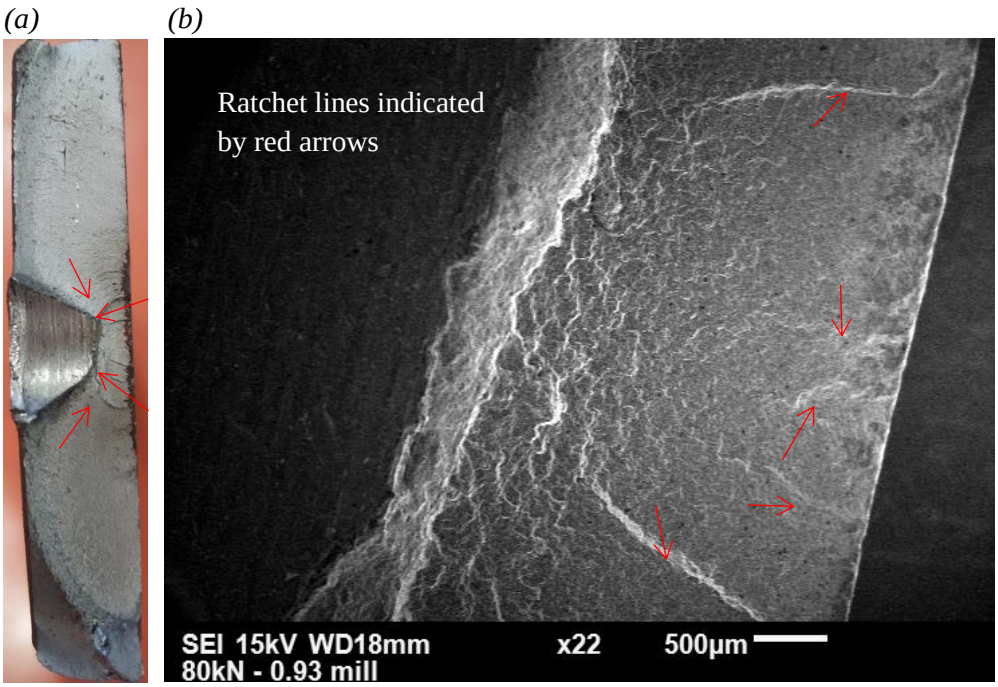

Figure 4.55 Fracture surface of sample A12-A325-150, showing ratchet lines indicative of multiple crack initiation sites: (a) Photograph of the fracture surface; and (b) SEM micrograph showing microscopic ratchet lines.

Figure 4.56 shows the fracture surface of sample A10-A325-150. The fracture surface has three main regions: the rather dull, predominantly flat fatigue crack propagation area; the rough residual fracture area; and the crack initiation sites where wear pits can be seen. The residual fracture area resulted from the final catastrophic rupture. The fatigue crack propagation area developed during the cyclic growth of the fatigue cracks that had started at the contact interface of the bolted plates.

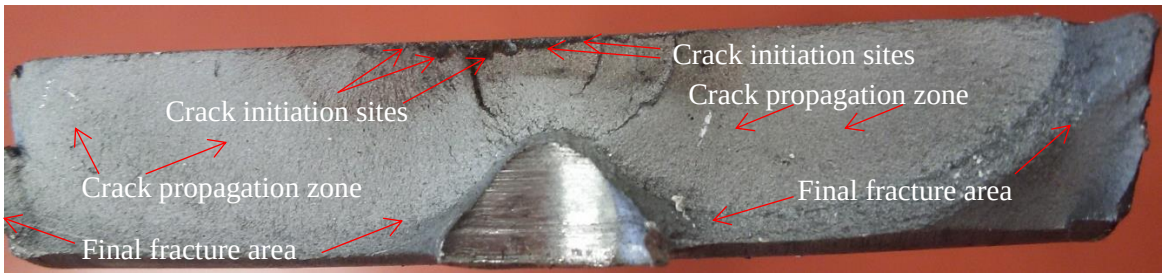

Figure 4.56 Camera image of the fracture surface of sample A10-A325-150.

At least four fracture planes with different angles can be seen at the edge of the fracture surface shown in Figure 4.57, which corresponds to specimen A12-A325-150. This

indicates that multiple cracks nucleated and coalesced together, forming ratchet lines along the fracture surface. This figure also shows severe surface damage in the fretting zone. The red arrows indicate the intersection points of multiple cracks (ratchet steps) within a very short distance.

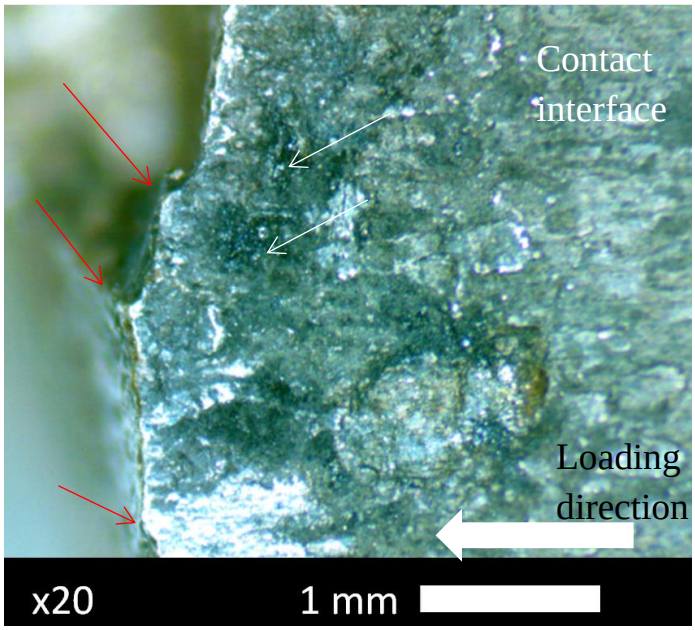

Figure 4.57 Optical microscopic image of the edge of the fracture surface showing ratchet marks in sample A12-A325-150.

Some of the multiple crack initiation sites found in sample A12-A325-150 can be seen in an SEM image of the fracture surface shown in Figure 4.58. They are surrounded by ratchet lines separated by less than 0.2 mm indicating the approximate distance between crack initiation sites. The ratchet lines also show the direction of crack propagation. Overall, the fractured surface looks smooth due to the rubbing between the fracture surfaces as the crack propagated before specimen failure occurred.

Some of the initiated cracks initially grew at an angle before turning perpendicular to the applied load (Figure 4.59). This phenomenon confirmed that fretting action initiated the cracks due to the combination of normal and frictional forces acting at the contact interface. The fretting induced high frictional forces, which caused the initiated crack to propagate under Mode-II loading. As a result, the crack initially grew at an angle from the contact interface. Once the crack moved away from the influence of the frictional force at the contact interface, it turned in direction and propagated further under the influence of Mode-I

loading. Evidence for this phenomenon can be seen along the edge of the fracture surface. The initiated cracks were at an angle and then propagated perpendicular to the external fatigue load.

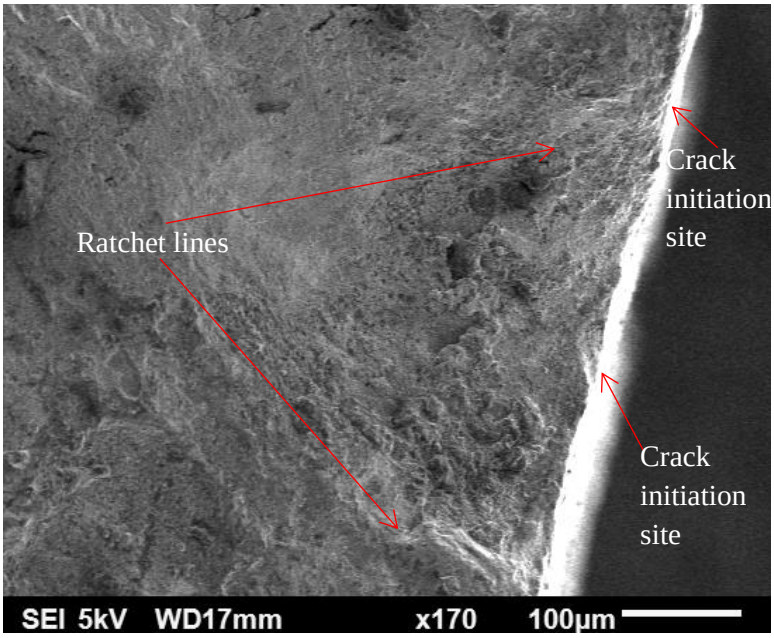

Figure 4.58 SEM image of the fracture surface of sample A12-A325-150, showing crack initiation sites and ratchet lines.

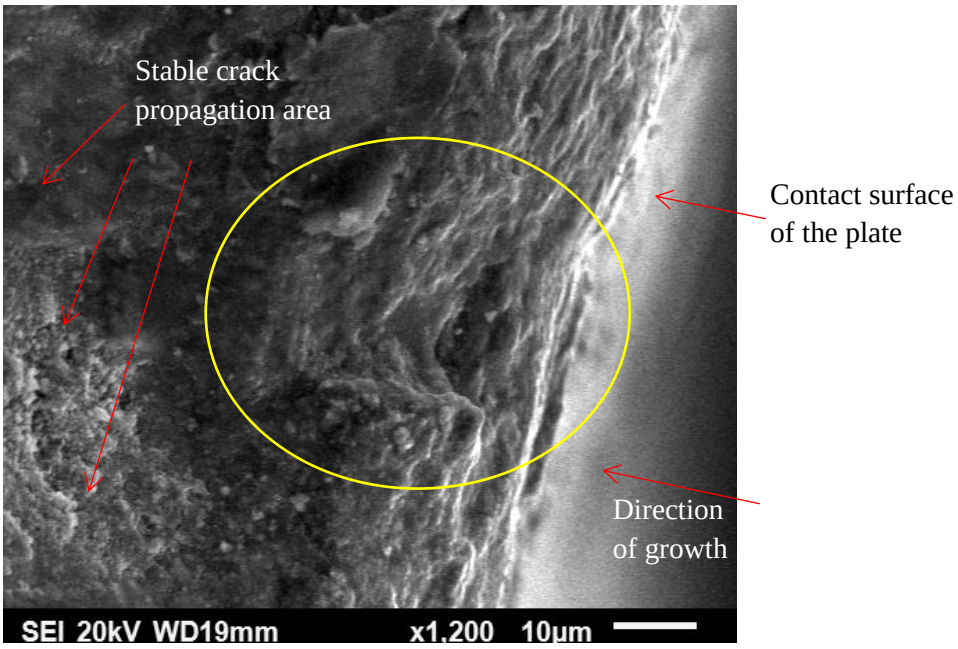

Figure 4.59 High magnification SEM image of the fracture surface near the contact surface of sample A12-A325-150, showing a crack that initiated at an angle to the surface.

Striations are one of the main features that can be found in the crack propagation zone of a fracture surface under fatigue loading. Each striation indicates the position of the crack tip at a cycle of applied load. Striations were observed at different locations of the crack propagation area in sample A12-A325-150 and are shown in Figures 4.60 and 4.61. These striations demonstrate that stable crack propagation occurred once the crack was subjected to Mode-I loading, as shown in Figure 4.60. The space between the striations in this location was between 0.4 μm and 0.8 μm.

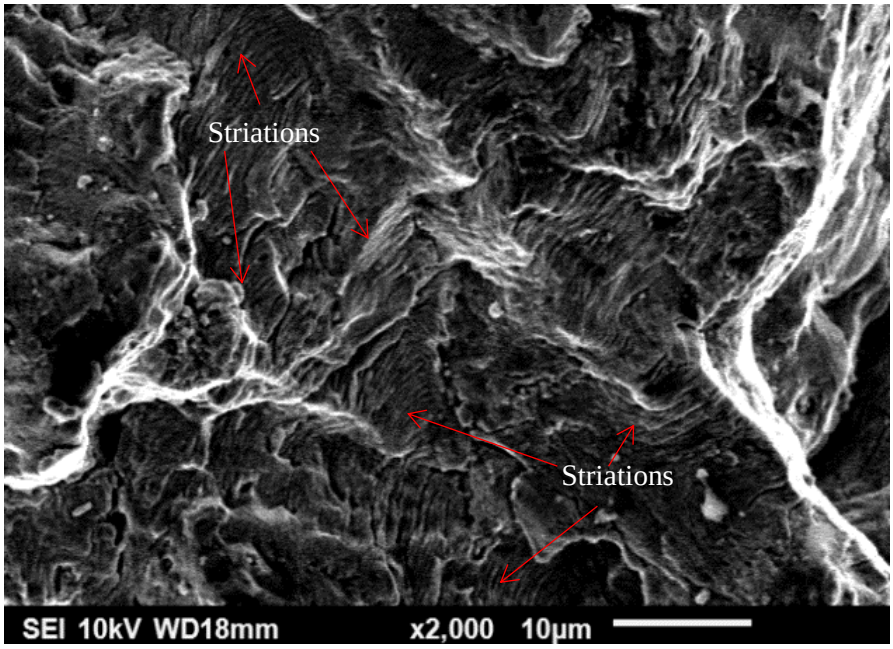

Figure 4.60 SEM micrograph showing striations close to the contact interface in Sample A12-A325-150.

Striations were also found in the area close to the zone of final fracture shown in Figure 4.61. The space between the striations in this zone was between 0.13 μm and 0.18 μm, indicating that there was a steady crack propagation when the crack length was smaller than the critical crack length. When the crack reached the critical length, crack propagation became unstable and led to complete failure. Some spaces can also be seen between the striations, which are cracks caused by local stresses after the main crack has passed, as described by Milella (2013).

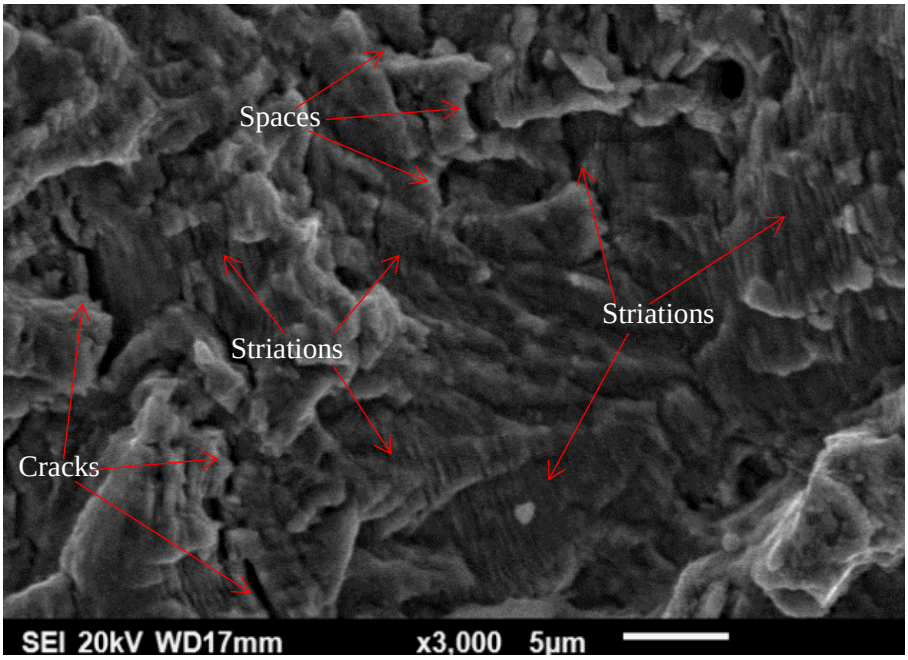

Figure 4.61 SEM micrograph of the fracture surface of sample A12-A325-150 showing striations far from the contact interface.

4.6.2.2 Crack initiation life

In order to estimate the number of cycles required for crack initiation, four samples with a Class A surface finish were tested at the 150 MPa stress range. The tests were interrupted when the MTS software detected an actuator displacement that exceeded an expected value, as explained in Chapter 3. This stress range level was selected because the specimens tested with this stress range (A10-A325-150 to A12-A325-150) had failed due to fretting fatigue. When the fatigue tests were stopped, the corresponding number of cycles was defined as the number of cycles for crack initiation. The crack initiation cycles for these samples varied from 0.91 to 1.4 million cycles and the remaining number of cycles to failure was assumed to correspond to crack propagation. Table 4.8 shows the number of cycles for crack initiation.

Table 4.8: Results of interrupted fatigue tests

Stress range (MPa)	Sample	Number of cycles	Failure mode
150.3	A13-A325-150	914,215	Interrupted tests for crack initiation
	A14-A325-150	1,317,177	
	A15-A325-150	972,135	
	A16-A325-150	1,425,084	

The crack initiation sites in these four interrupted tests were also different from the ones that occurred in the previous tests which were caused primarily by fretting fatigue. The crack initiation of three samples, A14 to A16, took place at the edge of the plate, which is illustrated as Zone C in Figure 4.54. This was caused by the misalignment of the grips and the fretting damage occurred at the border of the plates in the contact interface. In sample A13, crack initiation took place at the border of the upper plate that was in contact with the upper corner of the lower plate, shown as Zone D in Figure 4.54. This was caused by the rubbing action of the sharp corner over the plate. Also, it took the lowest number of cycles, 0.915 million, for crack initiation to occur in this sample.

The mean fatigue life value specimens made with A325 HSB and Class A surface finish at the 150 MPa stress range was 1,059,611, as seen in Table 4.6. The mean value of the number of cycles to crack initiation in Table 4.8 was 1,157,153 cycles. As a result, the mean value of cycles required to crack initiation was higher than the mean fatigue life of the samples. This observation, combined with the different crack initiation sites and the high standard deviation of both the crack initiation and fatigue life results did not allow a determination of the fraction of the fatigue life that corresponded to crack initiation.

There was an attempt to determine the number of cycles of crack propagation by determining the number of striations present on the fracture surface. According to Bulloch and Callagy (2010), the mean fatigue striation spacing can be used to predict the crack growth rate with a precision of ±2% to 35%. The spacing between the striations of the samples was in the range of 0.1 μm and 1 μm, indicating that the crack growth rate was also variable along the fracture surface, similar to the findings of Connors (1994). For example, in specimen A12-A325-150, the mean spacing between the striations was 0.37 μm, which could be used to estimate the number of cycles that the crack took to propagate.

During the crack initiation stage, fatigue striations are not produced on the fracture surface, as described by DeVries et al. (2010). Striation counting was done into the plate thickness dimension. As a result, it is estimated that crack propagation for specimen A12-A325-150 took place during the last 25,743 cycles. For specimens A10-A325-150 and A11-A325-150, the mean striation spacing was 0.32 μm and 0.36 μm, respectively. The crack for these specimens propagated for an estimated 29,527 and 26,458 cycles. These estimated

values indicate that almost 8% of the fatigue life was taken for crack propagation in specimens subjected to the 150 MPa stress range.

4.7 Summary of results

The surface roughness and the coefficient of friction measurements showed that the Class B surface finish was three times rougher than the Class A surface finish. As a result, the slip resistance of specimens with a Class B surface finish was 49 to 57% higher than that of specimens with a Class A surface finish. The measured slip resistances were used to determine appropriate load levels to use for fatigue tests, to ensure that slip loads were not exceeded. The measured slip coefficients (k_s) were smaller than the values recommended by CSA S16-14, reaching 94% of the code specified value for Class A surface finish and only 84 to 88% of the code specified value for Class B surface finish.

Specimens assembled with the two bolt types used in the experiments (A325 High strength bolts and C50LR Huck tension control bolts) showed small differences in behaviour. Only specimens with a Class B surface finish were prepared with both bolt types, and the slip resistance of specimens with tension control bolts was slightly higher, most likely due to a higher clamping force. Although the clamping force (bolt tension) was not measured, other evidence supports this hypothesis. A thinner gap between the plates along the visible edge of the surface of the specimens occurred due to the bending effect when tension control bolts were used, according to the measurement of displacements using the DIC system. Specimens with tension control bolts also had less relative slip between the plates in a fatigue cycle compared to those assembled with A325 high strength bolts.

All the samples that consisted of A325 HSB and Class A surface finish failed due to fretting fatigue. The fatigue life at stress levels over the endurance limit was within the range of the CSA S16-14 defined S-N curve for Detail Category B. Crack initiation took place some distance away from the uppermost hole of the connection. It was caused by the stress concentration in the partial stick-slip region of tangential and normal stresses.

All samples made with a Class B surface finish, including those with A325 HSB and Huck C50LR bolts, failed due to bending fatigue. The fatigue life fell close to the CSA S16-14 S-N curve for Detail Category B at the 150 MPa stress range level, but fell below the

curve by an increasing margin as the stress range increased. Failure always occurred at the uppermost hole of the connection where the maximum stress concentration was present. Some fretting damage was found in samples subjected to the lower stress ranges, which had fatigue lives that were long enough to cause damage on the surface. The coating played a major role in preventing fretting damage in the base metal during the application of the fatigue load until it was partially removed by fretting action as was observed by Reza et al. (2016). In addition, the bending curvatures in the upper plate of specimens tested at higher stress ranges were substantially higher than those at lower stress ranges, showing that the bending effect increased with increasing stress range, which led to the development of larger gaps between the plates along the visible edge, which may have reduced the development of fretting damage.

CHAPTER 5

CONCLUSIONS AND RECOMMENDATIONS

5.1 Summary of work

The research described in this thesis was focused on characterizing the fretting fatigue behaviour and failure mechanisms of slip-critical bolted connections assembled with different surface finishes (Class A and Class B) and different bolt types (A325 high strength bolts and C50LR Huck tension control bolts).

First, both Class A and Class B surface finishes were characterized using surface roughness measurements and then the static and kinetic coefficient of friction values were determined. The plates with Class A and Class B surface finishes were then assembled with A325 HSB and C50LR tension control bolts and tested to obtain the slip resistance.

The slip-critical bolted connections were then experimentally tested to determine their fatigue lives and define the S-N curves, and to characterize the fretting fatigue and fatigue failure behaviour. The S-N curves for the different combinations of variables were obtained from the experimental results and compared with the S-N curve given in the CSA S16-14 and CSA S6-14 standards for bolted connections.

The failure behaviour was further examined by using a DIC technique to measure both in-plane and out-of-plane displacements and relative displacements between the contacting surfaces close to the uppermost bolt of the connection, where the failure was generally initiated. In addition, contact and fracture surfaces of the specimens were examined using optical and scanning electron microscopes to study the fretting damage, crack initiation, and crack propagation.

5.2 Conclusions

5.2.1 Surface profile

Based on the results, the Cathacoat 302HB coated Class B surface finish was found to have a rougher and more uniform surface profile than the as-received Class A surface finish. The mean slip resistance of the Class B surface finish specimens was 1.7 times higher than

the mean slip resistance provided by Class A surface finish specimens, and the experimental slip coefficients (k_s) values were lower than the values recommended by CSA S16-14 and CSA S6-14, reaching 84 to 97% of code values.

5.2.2 Effect of surface finish

All specimens showed evidence of fretting wear and damage due to the relative slip between the contacting surfaces. However, the specimens assembled with a Class A surface finish predominantly failed due to fretting fatigue initiated failure and those with a Class B surface finish failed due to the effects of bending, which occurs in single-lap joint specimens.

Both scanning electron and optical microscope post-failure images of the contact and fracture surfaces confirmed that crack nucleation and subsequent crack propagation in specimens with a Class A surface finish and A325 HSB occurred due to the stress concentration in the partial stick-slip region of the contact surface some distance from the bolt hole. Conversely, specimens with a Class B surface finish assembled with A325 HSB and C50LR Huck tension control bolts failed due to bending fatigue. Although fretting damage was induced due to the relative motion between the plates, the coating on the Class B surface finish prevented fretting initiated failure so that crack initiation and propagation due to the stress concentration caused by the bending effect at the bolt holes became the governing mode of failure.

5.2.3 Effect of bolt type

The slip resistance provided by the C50LR Huck tension control bolts was slightly higher than that provided by the A325 HSB, which may have been due to a slightly higher clamping force. From the analysis of the DIC images, it was also observed that the specimens assembled with C50LR Huck bolts had smaller gaps and slightly lower magnitudes of relative motion between the contacting plates at the visible edge of the specimens.

It is believed that the small differences between the fatigue lives of specimens with the two bolt types can also be attributed to a slightly higher bolt pretension developed with the C50LR Huck bolts. Otherwise, the fatigue failure behaviour of specimens assembled with

both bolt types was similar. Therefore, it can be concluded that the type of bolt does not affect the fatigue behaviour of a slip-critical bolted connection, as long as they apply the same magnitude of clamping force.

5.2.4 S-N curves

The S-N curves obtained from the experimental results differed from the S-N curve for Detail Category B given in CSA S16-14 and CSA S6-14 for bolted connections. The results were similar at the 150 MPa stress range but they deviated by an increasing margin as the stress range increased. The difference can be attributed to the bending effect. At high stress ranges, the bending effect controlled the crack initiation and failure. The experimental results showed an endurance limit of approximately 122 MPa, which was higher than the value of 110 MPa given in the CSA S16-14 and CSA- S6-14 standards.

5.2.5 Effect of bending

The measured displacements using the DIC technique confirmed that a small gap was induced between the contacting plates due to the bending of the samples, particularly those subjected to higher stress ranges. Although the bending effect was present on both surface types, the Class A surface finish samples all failed due to fretting fatigue, while the coated Class B specimens failed due to bending fatigue. DIC measurements also confirmed the presence of curvature within the upper plate, which promoted the development of stress concentration sites at the hole edge of the first bolt of the connection, leading to bending fatigue at that location.

5.2.6 Mechanisms of crack initiation

The relative displacements measured with the DIC system helped to confirm that there was relative motion between the plates parallel to the applied load, which was the main reason for the development of fretting damage on the contact surfaces. Crack initiation within the contact interface of samples with a Class A surface finish was caused by the stress concentration that developed within the stick-slip region some distance away from the edge of the hole. Multiple cracks were nucleated in these regions and then propagated approximately perpendicular to the applied load. For the samples with a Class B surface finish, crack initiation occurred at the edge of the hole due to the development of a stress concentration that resulted from bending.

5.3 Recommendations for future work

The following recommendations for future work can be considered:

i. The experimental analysis could be further extended to determine the fatigue life of bolted connections with materials of different yield stress and different surface coatings.

ii. It would also be beneficial to analyze the effect of varying surface treatments such as shot peening or laser-peening on the fatigue life.

iii. The effect of different specimen configurations, such as double-lap joints and different overlap lengths, on the fatigue life and fretting fatigue failure behaviour could be analyzed. It is believed that double-lap joint specimens should be used instead of single-lap joint bolted connection specimens. Also, the bolt pretension should be measured in order to eliminate its uncertainty.

iv. The effect of misalignment between the grips of the fatigue test machine need to be analyzed to understand the additional secondary bending effects on the fatigue specimens.

v. This study could also be extended to different numbers of bolts, plate thicknesses, and plate geometries to include varying bolt configurations.

vi. Some sort of analytical or numerical method could be used in order to relate the conditions at the crack initiation sites to those on the surface where measurements are made.

vii. The measurement of the slip coefficient (k_S) must be done by the experimental method recommended in Annex A of the RCSC Specification for structural joints using high-strength bolts (RCSC 2014).

viii. The DIC technique was useful to understand the fatigue test results. It should be used for every specimen tested under fatigue. Also, in order to improve the measurements, the test frequency should be as low as 1 Hz so that useful parameters such as the hysteresis loop can be determined.

REFERENCES

Alcoa Fastening System & Rings. 2017. C50L Huckbolt brochure. 8 pages.

Annan, C.D., Chiza, A. 2013. Characterization of slip resistance of high strength bolted connections with zinc-based metallized faying surfaces. Engineering Structures, Vol.56, pp.2187-2196.

Benhamena, A., Amrouche, A., Talha, A., Benseddiq, N. 2011. Effect of contact forces on fretting fatigue behavior of bolted plates: Numerical and experimental analysis. Noureddine Tribology International, April 2012, Vol.48, pp.237-245.

Benhamena, A., Talha, A., Benseddiqc, N., Amrouche, A., Mesmacquec, G., Benguediabf, M. 2010. Effect of clamping force on fretting fatigue behaviour of bolted assemblies: Case of couple steel–aluminium. Materials Science & Engineering A, 2010, Vol.527(23), pp.6413-6421.

Benhaddou, T., Chirol, C., Daidie, A., Guillot, J., Stephan, P., Tuery, J.P. 2014. Pre-tensioning effect on fatigue life of bolted shear joints. Aerospace Science and Technology, July 2014, Vol.36, pp.36-43.

British Standards Institution (BSI). BS EN 1993-1-8:2005. Eurocode 3: design of steel structures–Part 1–8: design of joints. London. 2005.

Brown, Lubitz, Cekov, Frank, Keating. 2007. Evaluation of Influence of Hole Making Upon the Performance of Structural Steel Plates and Connections. Center for Transportation Research The University of Texas at Austin.

Bulloch, J.H., Callagy, A.G. 2010. A detailed study of the relationship between fatigue crack growth rate and striation spacing in a range of low alloy ferritic steels. Engineering Failure Analysis, 2010, Vol.17(1), pp.168-178.

Canadian Institute of Steel Construction. 2016. Handbook of Steel Construction, 11th Edition, 1092 p.

Chakherlou, T.N., Miezajanzadeh, M., Vogwell, J., Abazadeh, B. 2010. Investigation of the fatigue life and crack growth in torque tightened bolted joints. Aerospace Science and Technology, 2011, Vol.15(4), pp.304-313.

Chakherlou, T.N., Oskouei, R.H., Vogwell, J. 2007. Experimental and numerical investigation of the effect of clamping force on the fatigue behaviour of bolted plates. Engineering Failure Analysis, 2008, Vol.15(5), pp.563-574.

Chakherlou, T.N., Razavi, M.J., Aghdam, A.B., Abazadeh, B. 2011. An experimental investigation of the bolt clamping force and friction effect on the fatigue behavior of aluminum alloy 2024-T3 double shear lap joint. Materials and Design, 2011, Vol.32(8), pp.4641-4649. Figure 2.14 Reprinted from Materials and Design, Volume 32, Issues 8–9, Chakherlou, T.N., Razavi, M.J., Aghdam, A.B., Abazadeh, B., An experimental investigation of the bolt clamping force and friction effect on the fatigue behavior of aluminum alloy 2024-T3 double shear lap joint, Pages 4641-4649, Copyright (2011), with permission from Elsevier.

Chakherlou, T.N., Razavi, M.J., Aghdam, A.B. 2012. On the variation of clamping force in bolted double lap joints subjected to longitudinal loading: a numerical and experimental investigation. Strain, February 2012, Vol.48(1), pp.21-29.

Connors, W. C. 1994. Fatigue Striation Spacing Analysis. Materials Characterization, 1994, Vol.33(3), pp.245-253.

Crevoisier, J., Swiergiel, N. , Champaney, L., Hild, F. 2012. Identification of In Situ Frictional Properties of Bolted Assemblies with Digital Image Correlation. Experimental Mechanics, 2012, Vol.52(6), pp.561-572. Figure 2.7 Experimental mechanics by Society for Experimental Mechanics (U.S.) Reproduced with permission of SAGE

PUBLICATIONS LTD in the format Thesis/Dissertation. Figure 2.7 Reprinted from Experimental Mechanics, Volume 52, Issue 6, Crevoisier, J., Swiergiel, N. , Champaney, L., Hild, F., Identification of In Situ Frictional Properties of Bolted Assemblies with Digital Image Correlation., Pages 561–572, Copyright (2012), with permission from Springer Nature.

CSA. 2014. CSA-S16-14, Design of Steel Structures. Canadian Standards Association, Mississauga, ON.

CSA. 2014. S6-14, Canadian Highway Bridge Design Code. Canadian Standards Association (CSA), Mississauga, ON, Canada.

Davis, J. R. 1992. ASM Materials Engineering Dictionary. ASM International. Materials Park, Ohio. 557 pages.

DeVries, P., Ruth, K., Dennies, D. 2010. Counting on Fatigue: Striations and Their Measure. Journal of Failure Analysis and Prevention, 2010, Vol.10(2), pp.120-137.

Dieter, G. 1961. Metallurgy and metallurgical engineering series. McGraw Hill Book Company, New York, 644 p.

DiMatteo, N. 1997. ASM Handbook: Fatigue and Fracture Vol. 19. ASM International. Materials Park, Ohio. (Jan. 1 1997) 1057p.

Ekh, J., Schön, J. 2005. Effect of secondary bending on strength prediction of composite, single shear lap joints. Composites Science and Technology, 2005, Vol.65(6), pp.953-965. Figure 2.20(a) Reprinted from Composites Science and Technology, Volume 65, Issue 6, Ekh, J., Schön, J., Effect of secondary bending on strength prediction of composite, single shear lap joints., Pages 953-965, Copyright (2005), with permission from Elsevier.

Ekh, J., Schön, J., Melin, L. G. 2005. Secondary bending in multi fastener, composite-to-

aluminium single shear lap joints. Composites Part B, 2005, Vol.36(3), pp.195-208. Figure 2.20(b) Reprinted from Composites Part B: Engineering., Volume 36, Issue 3, Ekh, J., Schön, J., Melin, L. G., Secondary bending in multi fastener, composite-to-aluminium single shear lap joints., Pages 195-208, Copyright (2005), with permission from Elsevier.

Esmaeili, F., Zehsaz, M., and Chakherlou, T.N. 2014. Experimental Investigations on the Effects of Torque Tightening on the Fatigue Strength of Double-lap Simple Bolted and Hybrid (Bolted/Bonded) Joints. Strain, Vol.50(4), pp.347-354.

Evans, R. L. 1993. The influence of secondary bending on fatigue life improvement in bolted joints. Department of Defence of Australia. Defence, science and technology organisation. Aeronautical research laboratory. Melbourne, Victoria. Research report 14, 32 pages.

Ferjaoui, A., Yue, T., Abdel Wahab, M., Hojjati-Talemi, R. 2014. Prediction of fretting fatigue crack initiation in double lap bolted joint using Continuum Damage Mechanics. International Journal of Fatigue, Vol.73, pp.66-76.

Fisher, J., Kulak, G., and Smith, I. 1998. A Fatigue Primer for Structural Engineers. National Steel Bridge Alliance, Chicago, USA, 130 pages.

Fisher, J. W. 1977. Bridge fatigue guide design and details. American Institute of Steel Construction, Chicago, USA. 63 pages.

Frank and Yura. 1981. An experimental study of bolted shear connections. The University of Texas at Austin. 230 pages.

Guo, R., Duan, R., Mesmacque, G., Zhang, L., Amrouche, A., Guo, R. 2008. Fretting fatigue behavior of riveted Al 6XXX components. Materials Science & Engineering A, 2008, Vol.483, pp.398-401.

Hämäläinen, and Björk. 2015. Fretting fatigue phenomenon in bolted high-strength steel

plate connections. Steel Construction, Vol.8(3), pp.174-178.

Hamrock, B.J., Schmid, S.R., and Jacobson, Bo. 1999. Fundamentals of machine elements. 2nd. ed., McGraw Hill Higher Education, New York, USA, 926 p.

Hertzberg, R.W. 1989. Deformation and Fracture Mechanics of Engineering Materials. 3rd. ed., John Wylie and Sons, New York, 680 p.

Jayaprakash, M., Mutoh, Y., Yoshii, K. 2011. Fretting fatigue behavior and life prediction of automotive steel bolted joint. Materials and Design, 2011, Vol.32(7), pp.3911-3919.

Jiménez-Peña, C., H. Talemi, R., Rossi, B., Debruyne, D. 2017. Investigations on the fretting fatigue failure mechanism of bolted joints in high strength steel subjected to different levels of pre-tension. Tribology International, Vol.108, pp.128-140. Figures 2.6, 2.11, 2.12 and 2.15 Reprinted from Tribology International, Volume 108, Jiménez-Peña, C., H. Talemi, R., Rossi, B., Debruyne, D., Investigations on the fretting fatigue failure mechanism of bolted joints in high strength steel subjected to different levels of pre-tension., Pages 128-140, Copyright (2017), with permission from Elsevier.

Josi, G., Grondin, G., and Kulak, G. 1999. Fatigue of bearing-type shear splice. Structural Engineering Report No. 227. University of Alberta. Department of Civil and Environmental Engineering.

Kartal, M.E., Mulvihill, D.M., Nowell, D., Hills, D.A. 2011. Measurements of pressure and area dependent tangential contact stiffness between rough surfaces using digital image correlation. Tribology International, 2011, Vol.44(10), pp.1188-1198.

Kulak, Fisher and Struik. 1987. Guide to design criteria for bolted and riveted joints. 2nd. ed. American Institute Of Steel Construction, Inc, Chicago, 350 p.

Little, R.E., and Jebe, E.H. 1975. Manual on statistical planning and analysis for fatigue

experiments. American Society for Testing Materials, Special Technical Publication 588. Subcommittee E09.06 on Statistical Aspects of Fatigue.

Liu, J., Kang, J.X., Yan, W.Z., Wang, F.S., Yue, Z.F. 2010. Prediction of fatigue performance of fastener holes with bolt clamping force based on critical plane approach. Materials Science & Engineering A, Vol.527(15), pp.3510-3514.

Ma, X., Shi, H. J., Gu, J. 2010 In-situ scanning electron microscopy studies of small fatigue crack growth in recrystallized layer of a directionally solidified superalloy. Materials Letters, Vol.64(19), pp.2080-2083.

Maximov, J.T., Duncheva, G.V., Ganev, N. 2012. Enhancement of fatigue life of net section in fitted bolt connections. Journal of Constructional Steel Research, July 2012, Vol.74, pp.37-48.

Mello, A.W., Nicolas, A., Sangid, M. D. 2017. Fatigue strain mapping via digital image correlation for Ni-based superalloys: The role of thermal activation on cube slip. Materials Science & Engineering A, Vol.695, pp.332-341.

Milella, P.P. 2013. Morphological aspects of fatigue crack formation and growth. Fatigue and Corrosion in Metals, pp.73-108.

Minguez, J.M., Vogwell, J. 2006. Effect of torque tightening on the fatigue strength of bolted joints. Engineering Failure Analysis, Vol. 13, Issue 8, pp. 1410-1421. Figure 2.21 Reprinted from Engineering Failure Analysis., Volume 13. Issue 8, Minguez, J.M., Vogwell, J., Effect of torque tightening on the fatigue strength of bolted joints., Pages 1410-1421, Copyright (2006), with permission from Elsevier.

Nesládek, M., Španiel, M., Jurenka, J., Růžička, J., Kuželka, J. 2012. Fretting fatigue – Experimental and numerical approaches. International Journal of Fatigue, Vol.44, pp.61-73.

Neu, R.W. 2011. Progress in standardization of fretting fatigue terminology and testing. Tribology International, 2011, Vol.44(11), pp.1371-1377.

Research Council On Structural Connections (RCSC). 2014. Specification for Structural Joints Using High-Strength Bolts. AISC, Chicago, 98 pages.

Reza, H. O., Mohammad, R. B., Raafat N. I. 2016. Surface Characterizations of Fretting Fatigue Damage in Aluminum Alloy 7075-T6 Clamped Joints: The Beneficial Role of Ni–P Coatings. Materials, 01 February 2016, Vol.9(3), p.141.

Rezghi Maleki, H., and Abazadeh, B. 2012. Fretting Fatigue behavior of Bolted Single Lap Joints of Aluminum alloys. Proceedings of World Academy of Science, Engineering and Technology. International Journal of Mechanical and Mechatronics Engineering Vol:6, No:8, 2012.

Schijve, J., Campoli, G., Monaco, A. 2009. Fatigue of structures and secondary bending in structural elements. International Journal of Fatigue, 2009, Vol.31(7), pp.1111-1123. Figure 2.19 Reprinted from International Journal of Fatigue, Vol 31, Issue 7, Schijve, J., Campoli, G., Monaco, A., Fatigue of structures and secondary bending in structural elements., Pages 1111-1123, Copyright (2009), with permission from Elsevier.

Schneider, C. R. A. and Maddox, S.J. 2003. Best practice guide on statistical analysis of fatigue data. International Institute of Welding. Cambridge, UK.

Shankar, K., and Dhamari, R. 2002. Fatigue behaviour of aluminium alloy 7075 bolted joints treated with oily film corrosion compounds. Materials and Design, Vol.23(2), pp.209-216.

Shen, F., Hu, W., Voyiadjis, G., Meng, Q. 2015. Effects of fatigue damage and wear on fretting fatigue under partial slip condition. Wear, 15 September 2015, Vol.338-339, pp.394-405.

Stankevicius, J., Kulak, G. L., Georg, J., and Grondin, G. Y. 2009. Measurement of slip coefficient for grade ASTM A588 steel. Structural engineering report SER 268 | SER-ID SER268. DOI: https://doi.org/10.7939/R3BN0H.

Starikov, R. 2004. Fatigue behaviour of mechanically fastened aluminium joints tested in spectrum loading. International Journal of Fatigue, 2004, Vol.26(10), pp.1115-1127.

Undershute, S., Kulak, G. L. 1994. Strength and installation characteristics of tension-control bolts. Department of Civil Engineering, University of Alberta, 104 p.

Wagle, S. and Kato, H. 2009. Ultrasonic detection of fretting fatigue damage at bolt joints of aluminum alloy plates. International Journal of Fatigue, 2009, Vol.31(8), pp.1378-1385.

Wavish, P.M., Houghton, D., Ding, J., Leen, S.B., Williams, E.J., and Mccoll, I.R. 2009. A multiaxial fretting fatigue test for spline coupling contact. Fatigue & Fracture of Engineering Materials & Structures, Vol.32(4), pp.325-345.

Woo, S. 2017. Reliability Design of Mechanical Systems: A Guide for Mechanical and Civil. Springer International Publishing, Korea, 316 p.

Xu, Y., Sun, Z., and Zhang, Y. 2016. Experimental and Numerical Investigations of Fretting Fatigue Behavior for Steel Q235 Single-Lap Bolted Joints. Advances in Materials Science and Engineering, Vol.2016, 10 pages.

APPENDIX A: SPECIMEN DESIGN

The limits states that were calculated so that the specimen fulfills the requirements by CSA S16-14 are shown here.

The plate material chosen was 300W (44W) steel:

Yield strength: 300 MPa.

Ultimate strength: 440 MPa.

Plate thickness: 9.53 mm (3/8 inch)

Plate width: 50.8 mm (2 inches).

The ½ inch A325 high strength bolt had a cross sectional area of 127 mm^2.

The ultimate tensile strength of this bolt was 825 MPa.

The hole diameter was 14.7 mm which is 2 mm bigger than the bolt diameter.

The number of bolts chosen for the connection was six.

Clause 22.3.1: Minimum pitch: 2.7 time the bolt diameter: 34.29 mm (1.35 inch)

Clause 22.3.2: Minimum edge distance was 22.225 mm (7/8 inch).

Clause 22.3.4: Minimum end distance when more than two bolts in a line parallel to the direction of the load: 22.225 mm (7/8 inch)

The bolt length chosen was 44.45 mm (1.75 inch).

Bolts Shear strength:

$V_r = 0.6nmA_bF_u = 0.6(6)(1)(127\ mm^2)(825\ MPa) = 377.19\ kN$

Bolts Bearing strength:

$B_r = 3ntdF_u = 3(6)(9.53\ mm)(12.7\ mm)(825\ MPa) = 958.06\ kN$

Plates Tensile Strength:

$T_r = A_gF_y = (50.8\ mm)(9.53\ mm)(300\ MPa) = 145.16\ kN$

Plates net section fracture strength:

$T_r = A_{ne}F_u = (50.8\ mm - 14.7\ mm)(9.53\ mm)(440\ MPa) = 151.30\ kN$

Block shear:

$$T_r = U_t A_n F_u + 0.6 A_{gv} \frac{(F_y + F_u)}{2} =$$

$$T_r = (1)\left(\frac{(50.8-14.7)(9.53)}{2}\right)(440\ MPa) + 0.6\big((5(34.29) + 22.225)(9.53)\big)\frac{(300+440)}{2}$$

$$T_r = 494.33\ kN$$

Pull out of the bolt:

$$T_r = 0.6 A_{gv} \frac{(F_y + F_u)}{2} = 0.6\left((2)\big((5(34.29) + 22.225)(9.53)\big)\right)\frac{(300+440)}{2}$$

$$T_r = 837.36\ kN$$

Slip resistance:

$$V_s = 0.53 c_s k_s m n A_b F_u$$

Class A surface finish:

$$V_s = 0.53(1)(0.3)(1)(6)(127\ mm^2)(825\ MPa) = 99.01\ kN$$

Class B surface finish:

$$V_s = 0.53(1.04)(0.52)(1)(6)(127\ mm^2)(825\ MPa) = 178.49\ kN$$

APPENDIX B: SLIP RESISTANCE TEST PROGRAM

The procedure followed in the MTS Multipurpose Elite software for running the tensile static tests to determine the slip resistance is shown below.

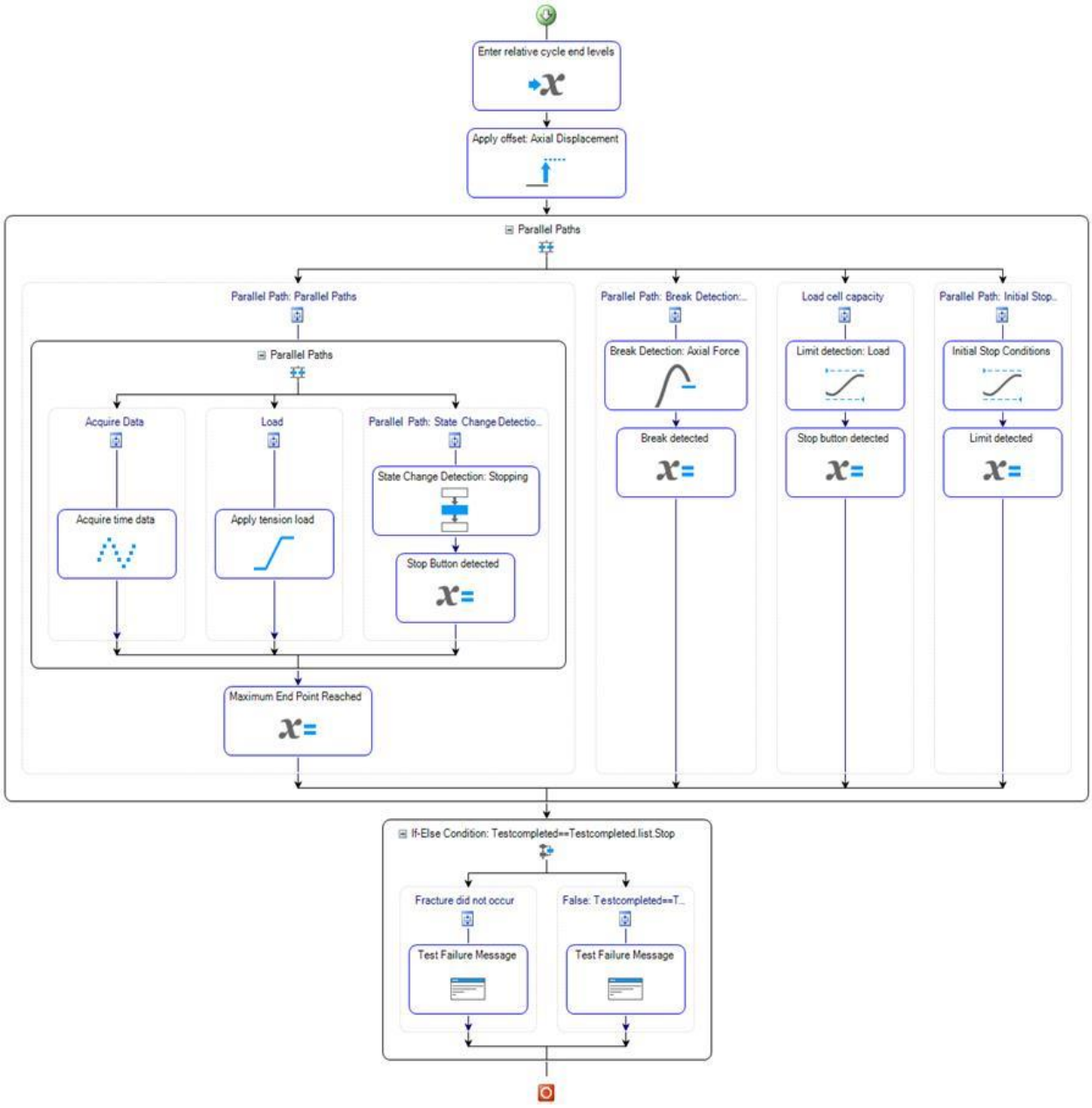

APPENDIX C: SURFACE ROUGHNESS MEASUREMENTS

Class A surface finish:

No.	Ra (µm)	Ry (µm)	Rz (µm)	Rq (µm)	No.	Ra (µm)	Ry (µm)	Rz (µm)	Rq (µm)
1	0.61	3.65	2.52	0.82	31	0.55	3.96	2.44	0.74
2	0.3	2.34	1.24	0.42	32	0.5	2.38	1.47	0.59
3	0.38	2.18	1.48	0.46	33	0.34	2.02	1.48	0.42
4	0.33	1.8	1.27	0.41	34	0.52	3.42	1.82	0.65
5	0.49	3.04	2.3	0.62	35	0.32	1.59	1.07	0.37
6	0.4	2.53	1.44	0.52	36	0.64	3.03	2.65	0.83
7	0.68	4.19	2.51	0.92	37	0.84	3.86	2.98	0.95
8	0.47	3.22	1.88	0.64	38	1.02	4.65	4.35	1.25
9	0.8	4.54	2.5	1.05	39	0.31	1.97	1.37	0.41
10	1.1	4.44	3.84	1.27	40	0.37	1.63	1.05	0.45
11	0.6	3.26	1.9	0.75	41	0.26	1.73	1.22	0.34
12	0.38	1.83	1.36	0.47	42	0.63	3.7	2.37	0.76
13	0.44	5.7	4.01	0.66	43	0.25	1.8	1.23	0.32
14	0.8	5.66	4.12	1.01	44	0.41	1.86	1.64	0.51
15	0.54	2.68	2.11	0.64	45	0.54	2.53	1.75	0.66
16	0.6	2.85	1.77	0.75	46	0.35	1.69	1.03	0.41
17	0.42	2.38	1.23	0.56	47	0.46	2.37	1.55	0.55
18	0.52	2.32	1.69	0.6	48	0.3	1.76	1.13	0.37
19	0.38	1.87	1.22	0.44	49	0.32	1.87	1.12	0.4
20	0.39	1.87	1.16	0.46	50	0.63	2.75	2.13	0.72
21	0.65	2.93	2.12	0.77	51	0.5	2.55	1.8	0.6
22	0.43	2.32	1.29	0.57	52	0.4	2.1	1.56	0.49
23	0.57	3.33	2.66	0.74	53	0.3	1.99	1.04	0.42
24	0.45	2.35	1.8	0.55	54	0.65	3.67	3.01	0.8
25	0.92	4.19	3.28	1.09	55	0.31	1.74	1.14	0.38
26	0.28	1.86	1.08	0.35	56	0.56	3.48	2.18	0.72
27	0.6	3.04	2.22	0.75	57	0.3	1.71	1.14	0.37
28	0.53	2.8	1.92	0.63	58	0.37	2.03	1.4	0.48
29	0.31	1.79	1.09	0.39	59	0.4	2	1.31	0.48
30	0.27	1.58	0.99	0.33	60	0.56	3.01	1.74	0.69
Mean	0.52	2.95	2.00	0.65		0.46	2.50	1.74	0.57
Standard deviation	0.19	1.11	0.88	0.23		0.18	0.85	0.76	0.21

Class B surface finish:

No.	Ra (µm)	Ry (µm)	Rz (µm)	Rq (µm)	No.	Ra (µm)	Ry (µm)	Rz (µm)	Rq (µm)
1	1.88	15.82	14.4	3.05	31	1.78	9.32	6.88	2.19
2	2.41	11.53	9.3	2.89	32	1.81	11.3	6.58	2.3
3	1.35	7.8	5.48	1.79	33	1.81	10.33	7.25	2.23
4	1.33	6.01	3.82	1.64	34	1.3	7.34	4.72	1.71
5	1.34	20.41	13.58	2.11	35	1.23	7.74	5.28	1.57
6	1.27	8.35	4.72	1.68	36	1.1	7.51	3.61	1.43
7	1.41	6.44	5.01	1.66	37	1.23	6.35	4.45	1.47
8	1.3	8.54	5.15	1.65	38	1.17	5.05	4.09	1.42
9	2.07	10.29	7.52	2.53	39	1.57	6.94	6.06	1.85
10	1.6	10.55	7.42	2.16	40	1.29	8.14	5.78	1.69
11	1.66	7.85	6.33	1.92	41	1.46	7.28	3.8	1.8
12	1.07	5.02	3.95	1.27	42	1.53	8.17	6.38	1.83
13	1.33	8.84	5.03	1.73	43	1.17	6.27	3.93	1.61
14	1.03	5.61	3.48	1.25	44	1.58	9.17	5.02	1.95
15	1.55	8.27	4.66	1.95	45	1.4	8.24	5.09	1.81
16	1.6	7.76	6.16	1.86	46	1.25	8.34	5.02	1.67
17	1.55	6.45	4.38	1.81	47	1.93	10.56	9.13	2.45
18	1.74	8.57	5.24	2.07	48	1.44	6.14	4.3	1.67
19	1.44	7.14	4.55	1.73	49	1.16	6.87	3.64	1.51
20	1.26	6.4	3.97	1.53	50	1.31	8.23	5.31	1.76
21	1.02	5.29	4	1.34	51	1.71	9.11	5.25	2.13
22	1.39	7.11	5.07	1.72	52	1.69	8.25	6.76	2.11
23	1.25	6.48	4.33	1.49	53	1.33	8.04	4.85	1.67
24	1.43	6.39	4.04	1.66	54	1.45	6.96	4.58	1.81
25	2.25	9.24	6.1	2.74	55	1.51	8.33	5.85	1.93
26	1.6	7.6	4.9	1.93	56	1.67	8.84	5.46	2.05
27	1.69	9.34	5.6	2.21	57	1.66	9.05	5.38	2.08
28	1.74	8.84	5.05	2.15	58	1.37	8.37	5.27	1.71
29	1.77	9.59	7.3	2.19	59	1.47	7.14	4.98	1.78
30	1.72	8.51	5.85	2.06	60	1.22	7.44	4.09	1.58
Mean	1.54	8.53	5.88	1.93		1.45	8.03	5.29	1.83
Standard deviation	0.33	3.10	2.56	0.44		0.23	1.36	1.21	0.27

APPENDIX D: COEFFICIENT OF FRICTION MEASUREMENTS

Coefficient of static friction: Class A surface finish.

$\mu_s = \tan(\theta)$

No.	θ	μ_s	No.	θ	μ_s	No.	θ	μ_s	No.	θ	μ_s
1	17	0.3057	15	16	0.2867	29	17	0.3057	43	17.5	0.3153
2	15	0.2679	16	18	0.3249	30	16	0.2867	44	16	0.2867
3	15.5	0.2773	17	18	0.3249	31	14	0.2493	45	14	0.2493
4	17	0.3057	18	17	0.3057	32	15	0.2679	46	15	0.2679
5	15	0.2679	19	19	0.3443	33	16	0.2867	47	14.5	0.2586
6	16.5	0.2962	20	16	0.2867	34	15	0.2679	48	15	0.2679
7	15	0.2679	21	16.5	0.2962	35	16	0.2867	49	15	0.2679
8	19	0.3443	22	16	0.2867	36	14	0.2493	50	17	0.3057
9	14.5	0.2586	23	18	0.3249	37	19	0.3443	51	19	0.3443
10	14.5	0.2586	24	14	0.2493	38	16.5	0.2962	52	19	0.3443
11	14	0.2493	25	16	0.2867	39	17	0.3057	53	18	0.3249
12	14	0.2493	26	15	0.2679	40	14.5	0.2586	54	17	0.3057
13	15	0.2679	27	15	0.2679	41	17	0.3057	55	16	0.2867
14	15.5	0.2773	28	15	0.2679	42	17	0.3057			
Mean	15.54	0.2782		16.39	0.2944		16.00	0.2869		16.38	0.2943
Standard deviation	1.39	0.0264		1.44	0.0274		1.40	0.0265		1.67	0.0318

Coefficient of static friction: Class B surface finish.

No.	θ	μ_s	No.	θ	μ_s	No.	θ	μ_s
1	40.5	0.8541	13	41	0.8693	25	41.5	0.8847
2	39	0.8098	14	37.5	0.7673	26	38	0.7813
3	42.5	0.9163	15	41.5	0.8847	27	38	0.7813
4	38	0.7813	16	39.5	0.8243	28	42	0.9004
5	40.5	0.8541	17	40	0.8391	29	38.5	0.7954
6	40	0.8391	18	38.5	0.7954	30	41	0.8693
7	43	0.9325	19	38.5	0.7954	31	37.5	0.7673
8	38.5	0.7954	20	41	0.8693	32	41	0.8693
9	38	0.7813	21	37	0.7536	33	39.5	0.8243
10	41	0.8693	22	39.5	0.8243	34	41.5	0.8847
11	42.5	0.9163	23	38.5	0.7954	35	43	0.9325
12	40	0.8391	24	39	0.8098	36	43	0.9325
Mean	40.29	0.8491		39.29	0.8190		40.38	0.8519
Standard deviation	1.74	0.0525		1.41	0.0411		1.99	0.0597

Coefficient of kinetic friction: Class A surface finish.

$$\mu_k = \frac{g \sin\theta - a}{g \cos\theta}$$

No.	a (m/s^2)	μ_k	No.	a (m/s^2)	μ_k	No.	a (m/s^2)	μ_k
1	2.557802	0.2556	8	2.577031	0.2532	15	2.576115	0.2533
2	2.544988	0.2572	9	2.542895	0.2575	16	2.550534	0.2565
3	2.535999	0.2584	10	2.526101	0.2596	17	2.533835	0.2586
4	2.445804	0.2697	11	2.575402	0.2534	18	2.50629	0.2621
5	2.540456	0.2578	12	2.571132	0.2539	19	2.507396	0.2620
6	2.429376	0.2718	13	2.546447	0.2570	20	2.448351	0.2694
7	2.405381	0.2748	14	2.379074	0.2781			
Mean	2.49	0.2636		2.53	0.2590		2.52	0.2603
Standard deviation	0.06	0.0081		0.07	0.0088		0.04	0.0056

Coefficient of kinetic friction: Class B surface finish.

No.	a (m/s^2)	μ_k	No.	a (m/s^2)	μ_k	No.	a (m/s^2)	μ_k
1	0.862112	0.7081	6	0.535071	0.7492	11	0.915031	0.7014
2	0.915365	0.7014	7	0.532497	0.7495	12	0.512349	0.7521
3	0.519799	0.7511	8	0.890568	0.7045	13	0.904458	0.7027
4	0.463464	0.7582	9	0.528478	0.7500	14	0.85889	0.7085
5	0.528526	0.7500	10	0.486027	0.7554	15	0.85746	0.7086
Mean	0.66	0.7337		0.59	0.7417		0.81	0.7147
Standard deviation	0.21	0.0268		0.17	0.0210		0.17	0.0212

APPENDIX E: SLIP RESISTANCE MEASUREMENTS

	Slip Resistance (kN)		
	A325 High Strength Bolts		C50LR Huck Bolts
	Class A	Class B	Class B
	78.28	141.76	149.42
	104.80	132.58	141.03
	93.38	140.65	149.96
	96.16		143.01
			143.45
			149.84
Mean value Slip resistance (kN)	93.15	138.33	146.12
Standard deviation (kN)	11.045	5.013	4.055
Coefficient of variation	11.86%	3.62%	2.77%

Load-displacement curves:

A325 High strength bolts and Class A surface finish specimens:

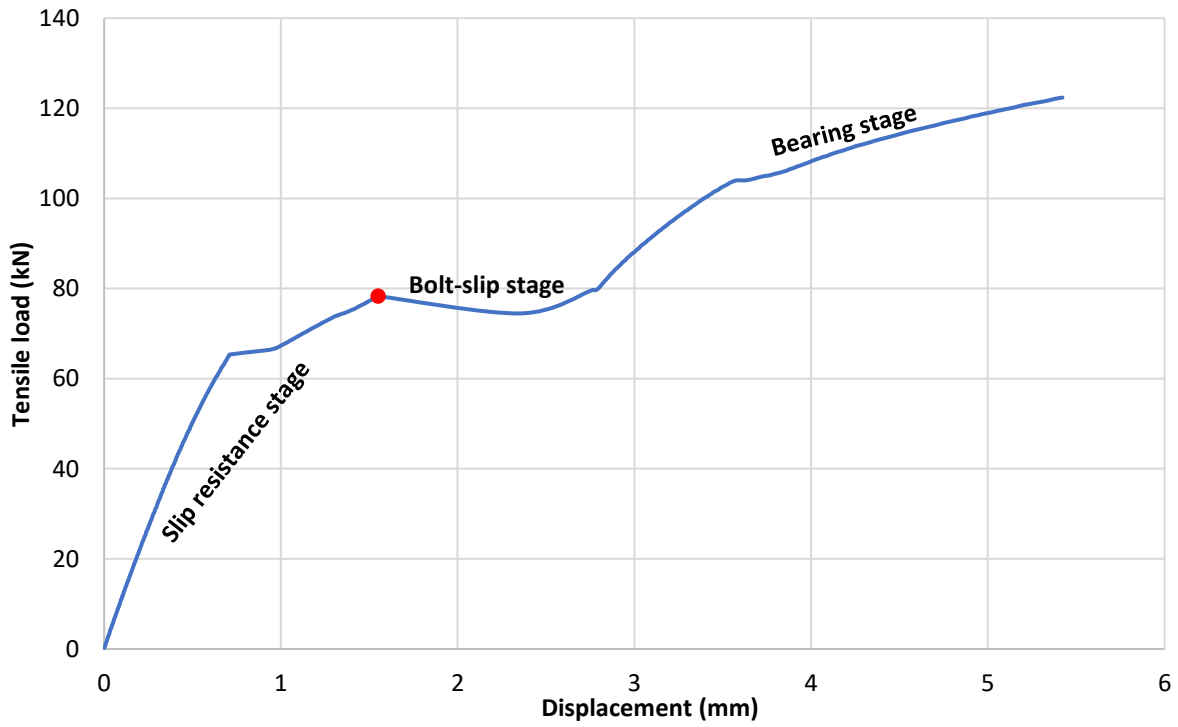

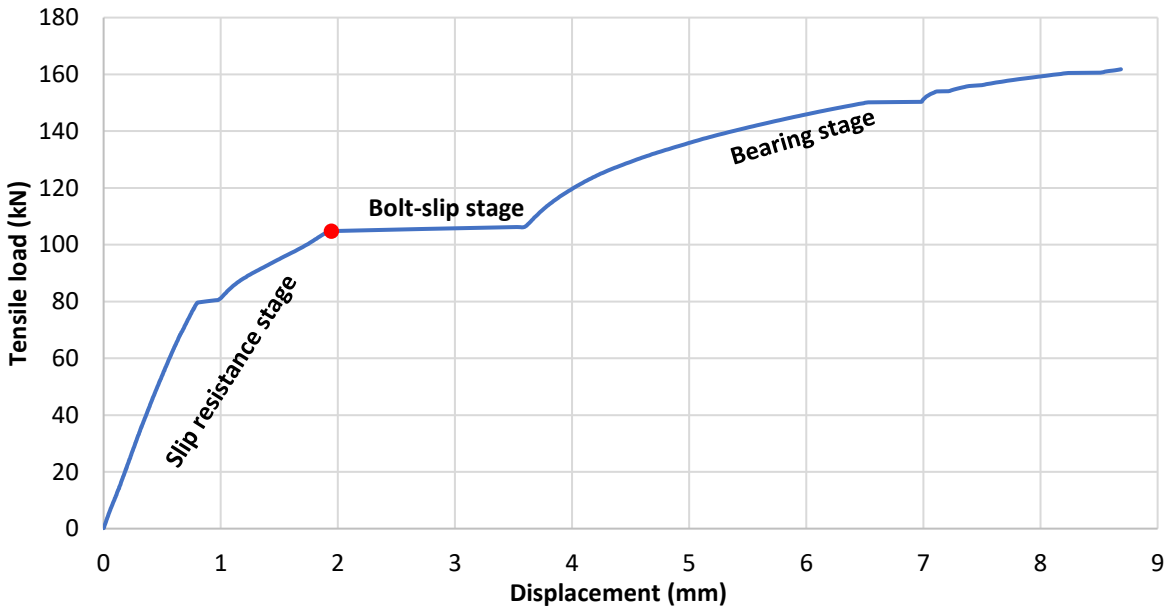
Tensile load (kN)
180
160
140
120
100
80
60
40
20
0
0
1
2
3
4
5
6
7
8
9
Displacement (mm)
Slip resistance stage
Bolt-slip stage
Bearing stage

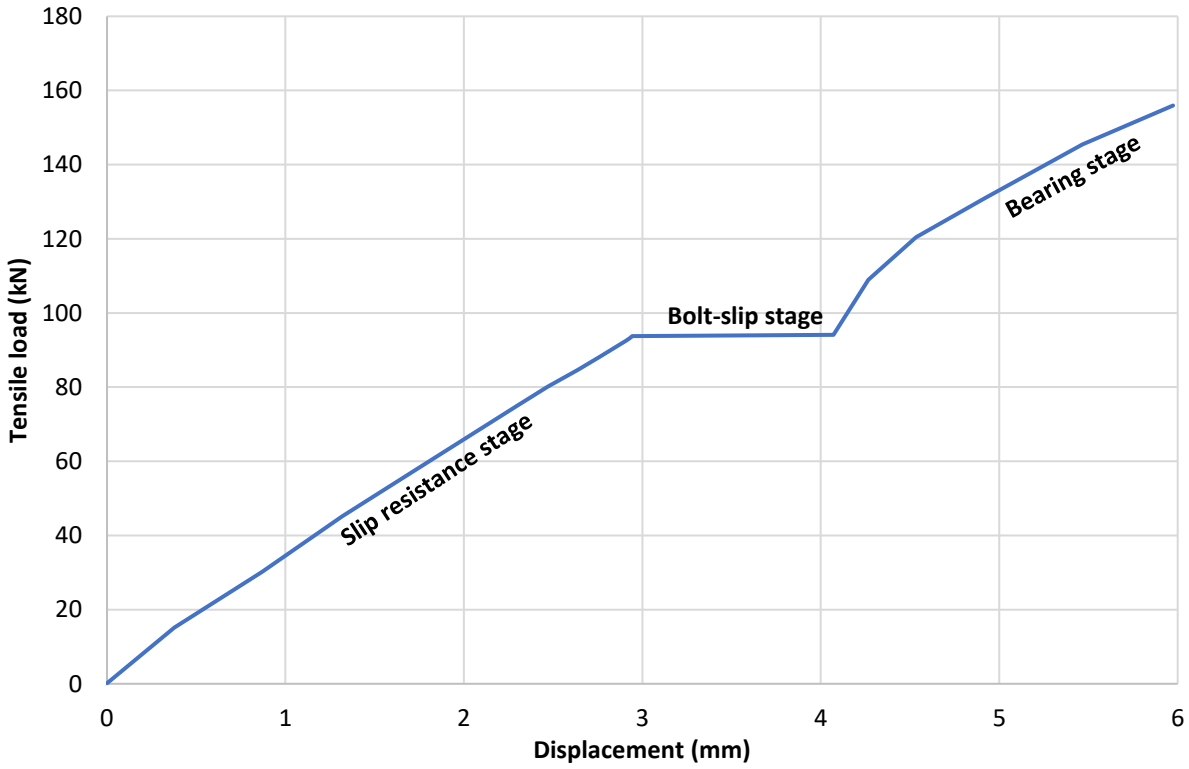
Tensile load (kN)
180
160
140
120
100
80
60
40
20
0
0
1
2
3
4
5
6
Displacement (mm)
Slip resistance stage
Bolt-slip stage
Bearing stage

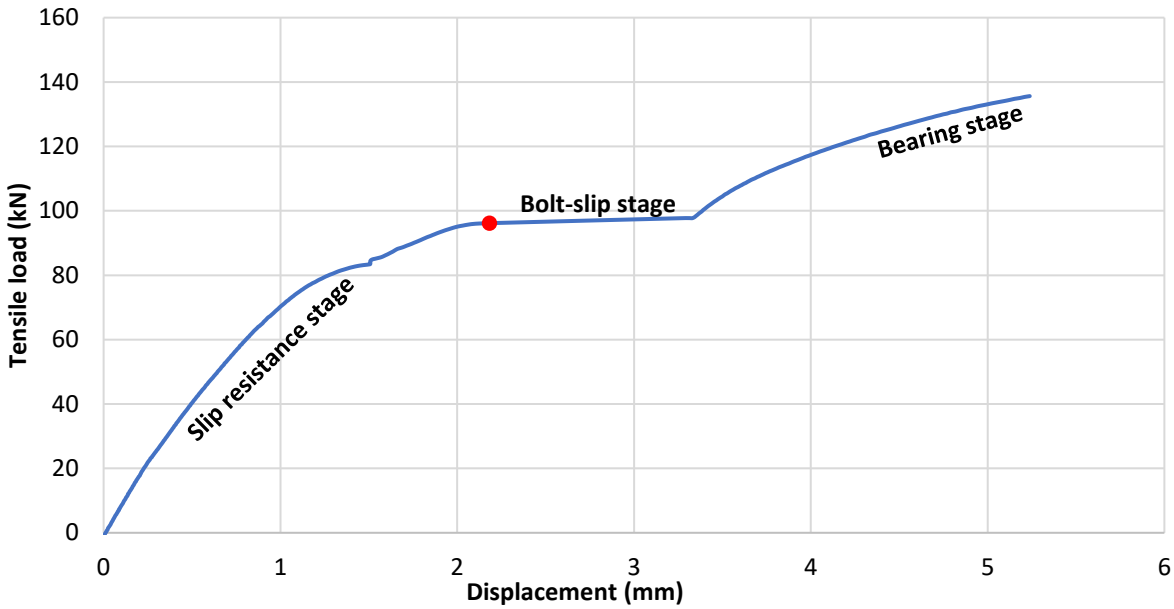

A325 High strength bolts and Class B surface finish specimens:

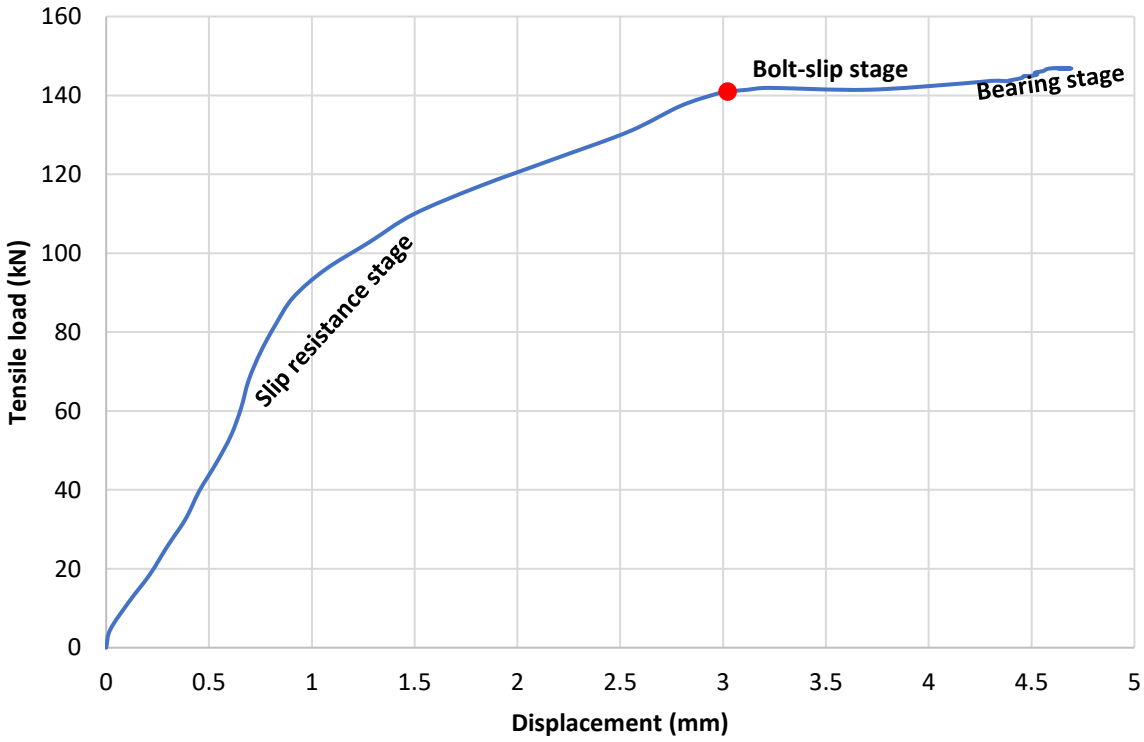

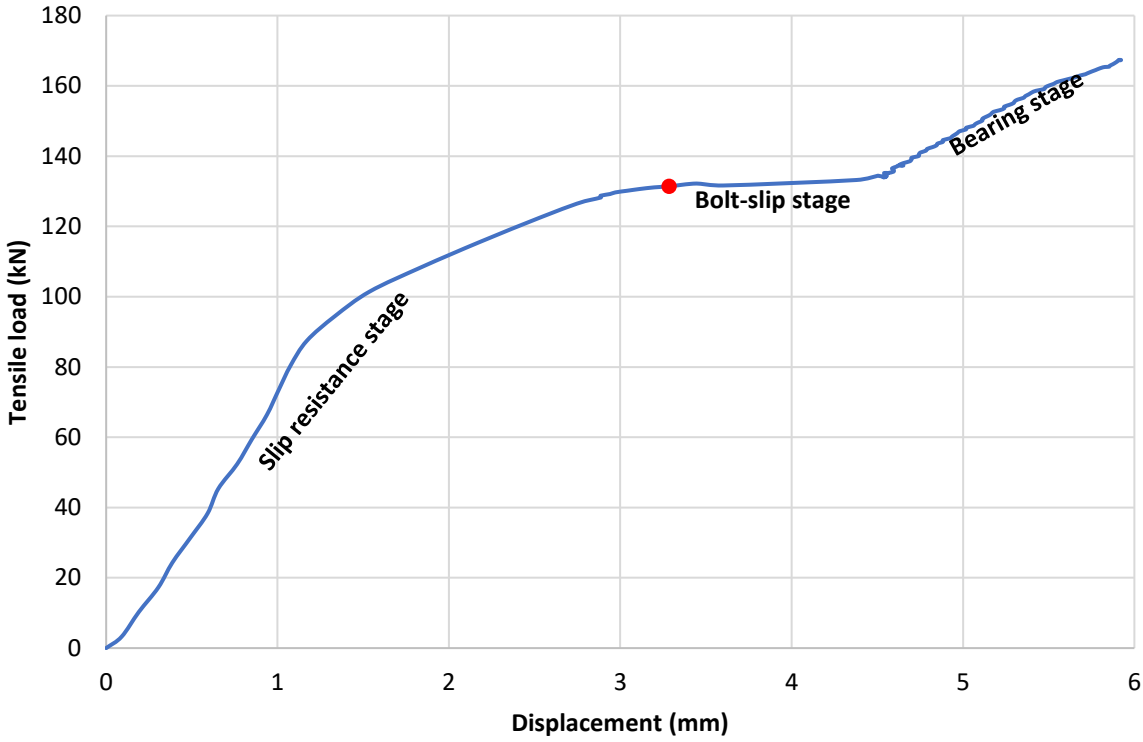
180
160
140
120
100
80
60
40
20
0
Tensile load (kN)
0
1
2
3
4
5
6
Displacement (mm)
Slip resistance stage
Bolt-slip stage
Bearing stage

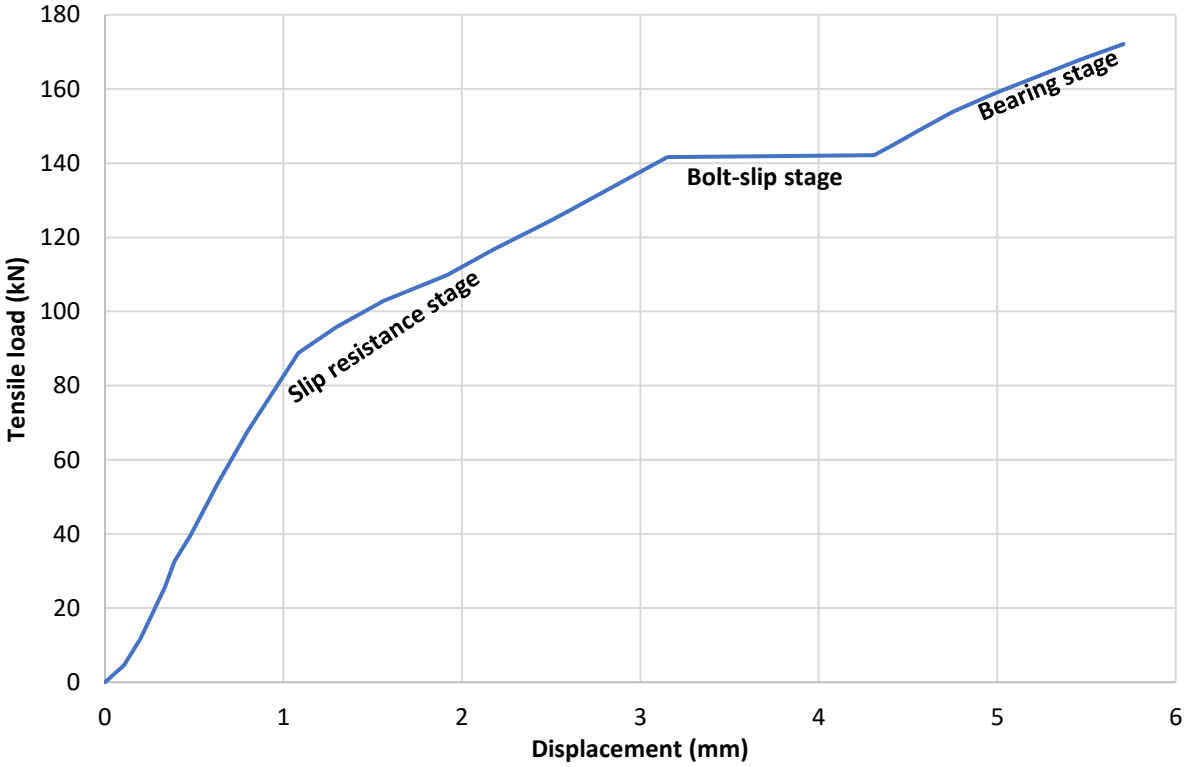
180
160
140
120
100
80
60
40
20
0
Tensile load (kN)
0
1
2
3
4
5
6
Displacement (mm)
Slip resistance stage
Bolt-slip stage
Bearing stage

C50LR Huck tension control bolts and Class B surface finish specimens:

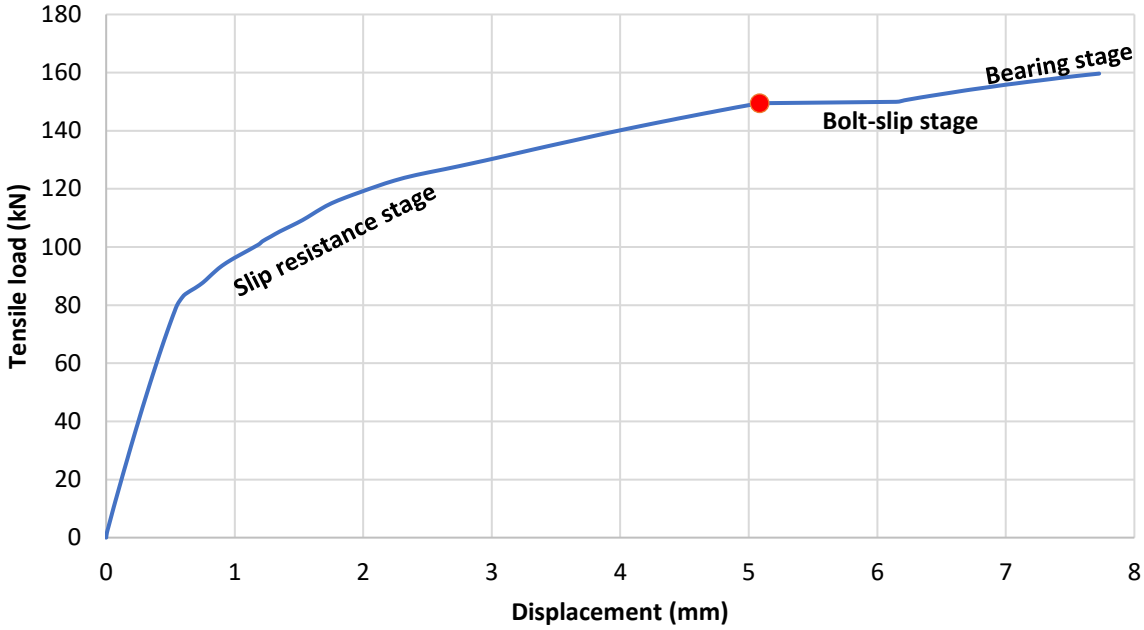

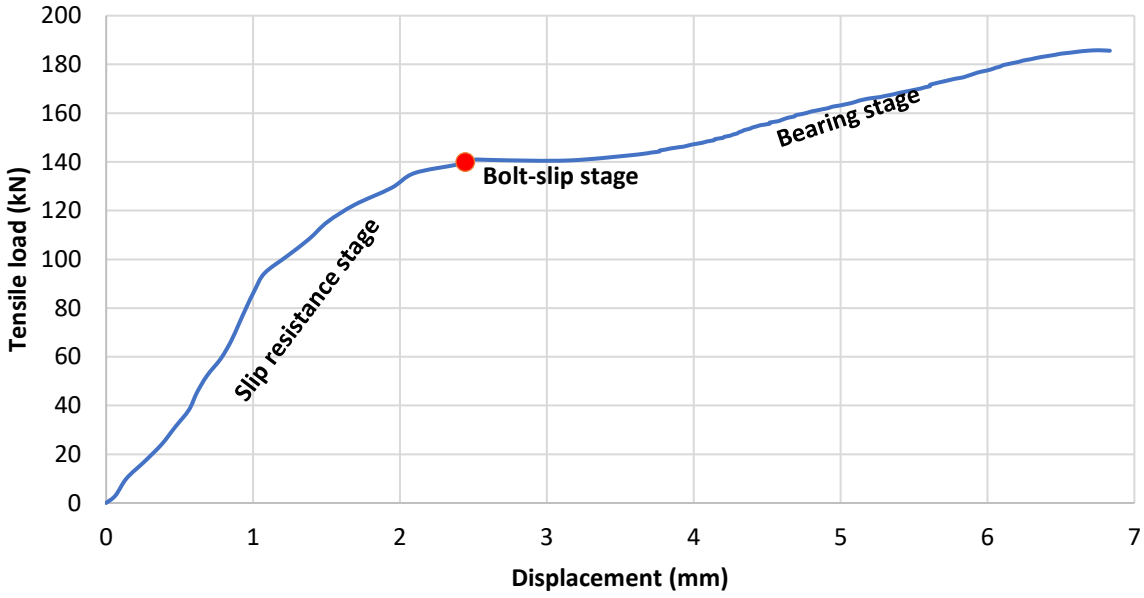

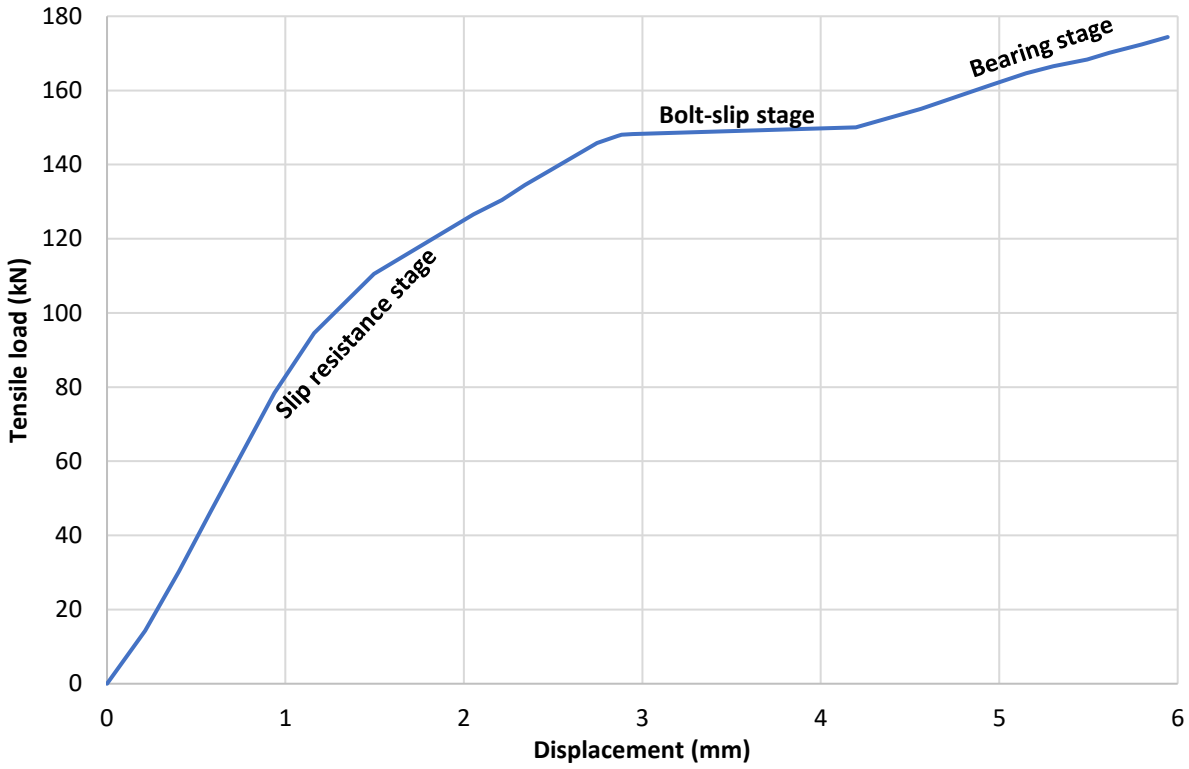
Tensile load (kN)
Displacement (mm)
Slip resistance stage
Bolt-slip stage
Bearing stage

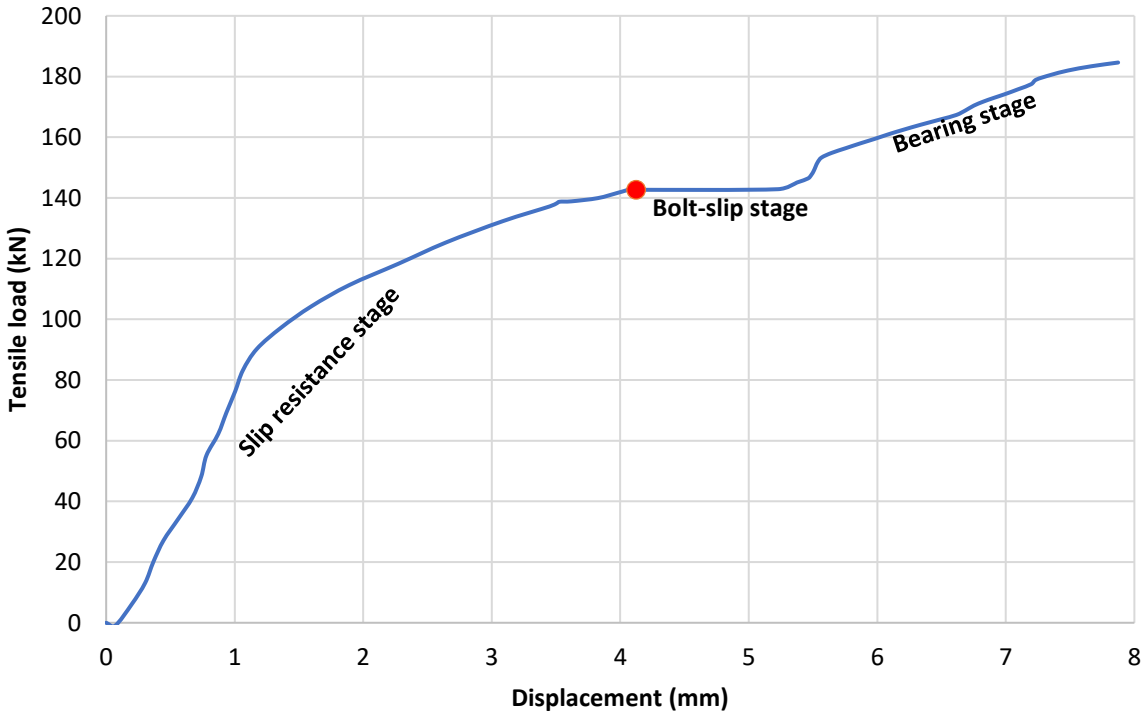
Tensile load (kN)
Displacement (mm)
Slip resistance stage
Bolt-slip stage
Bearing stage

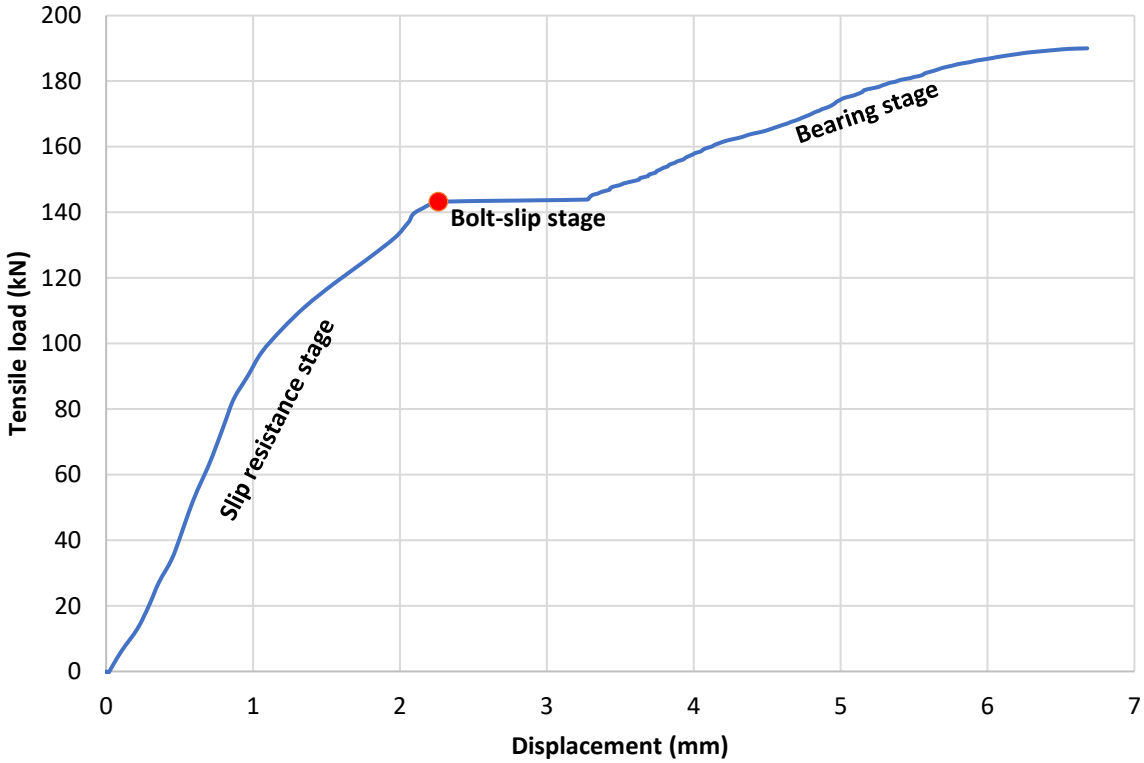
Tensile load (kN)
Displacement (mm)
Slip resistance stage
Bolt-slip stage
Bearing stage

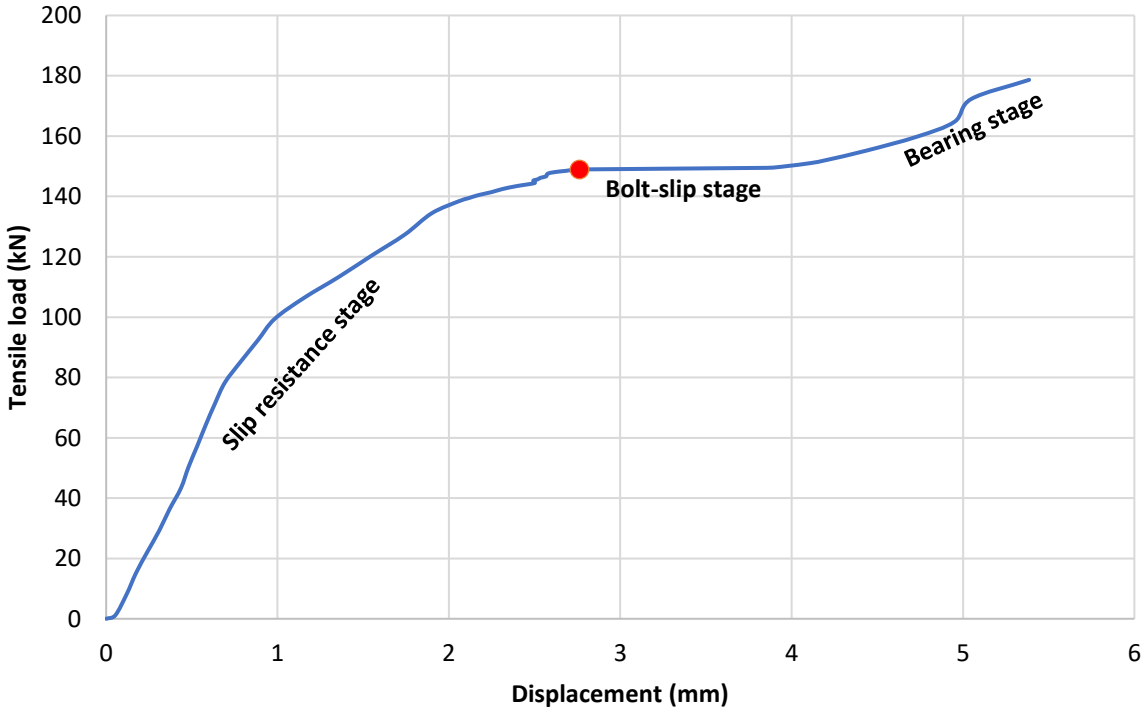
Tensile load (kN)
Displacement (mm)
Slip resistance stage
Bolt-slip stage
Bearing stage

APPENDIX F: STUDENT T-TEST SLIP RESISTANCE

Calculations of the Student t-test were done in order to determine whether the difference in slip resistance was statistically significant between samples made with A325 HSB and Class B surface finish and specimens made with C50LR Huck bolts and Class B surface finish.

	A325 HSB	C50LR Huck bolts
Number of samples (n)	3	6
Mean value Slip resistance (kN)	138.33	146.12
Standard Deviation (kN)	5.013	4.055
n-1	2	5
sd^2	25.129	16.441
Degrees of freedom	7	
Pooled Sd (Sp)	4.350	
1/n	0.333	0.167
t-statistic	-2.532	
-t0.05 (two tails)	-2.365	
95% confidence interval	-15.063	-0.514

In the population, the difference between the mean values of slip resistance of specimens made with A325 HSB and Class B surface finish and specimens made with C50LR Huck tension control bolts is statistically significant according to the Student t-test results. There is a 95% of confidence that the populations of these samples do not have similar mean values of slip resistance. Also, it can be said with 95% of confidence that the difference between the mean slip resistance of specimens made with A325 HSB and Class B surface finish and the mean slip resistance of samples assembled with C50LR Huck tension control bolts and Class B surface finish ranges between -15.063 and -0.514.

APPENDIX G: SLIP COEFFICIENT

	Slip coefficient (k_s)		
	A325 HSB		C50LR Huck bolts
	Class A	Class B	Class B
	0.246	0.446	0.470
	0.330	0.417	0.443
	0.294	0.442	0.472
	0.302		0.450
			0.451
			0.471
Mean value Slip coefficient (k_s)	0.293	0.435	0.459
Standard deviation	0.035	0.016	0.013
Coefficient of variation	11.86%	3.62%	2.77%

APPENDIX H: COPYRIGHT PERMISSION FOR FIGURE 2.7

SPRINGER NATURE LICENSE
TERMS AND CONDITIONS

Jan 04, 2019

This Agreement between University of Saskatchewan -- Pedro Cordova ("You") and Springer Nature ("Springer Nature") consists of your license details and the terms and conditions provided by Springer Nature and Copyright Clearance Center.

License Number	4502230255500
License date	Jan 04, 2019
Licensed Content Publisher	Springer Nature
Licensed Content Publication	Experimental Mechanics
Licensed Content Title	Identification of In Situ Frictional Properties of Bolted Assemblies with Digital Image Correlation
Licensed Content Author	J. de Crevoisier, N. Swiergiel, L. Champaney et al
Licensed Content Date	Jan 1, 2011
Licensed Content Volume	52
Licensed Content Issue	6
Type of Use	Thesis/Dissertation
Requestor type	academic/university or research institute
Format	print and electronic
Portion	figures/tables/illustrations
Number of figures/tables/illustrations	1
Will you be translating?	no
Circulation/distribution	<501
Author of this Springer Nature content	no
Title	Fretting fatigue in steel bolted connections.
Institution name	n/a
Expected presentation date	Dec 2018
Portions	Figure 3
Requestor Location	University of Saskatchewan 105 Administration Place Saskatoon, SK S7N 5A2 Canada Attn: University of Saskatchewan
Billing Type	Invoice
Billing Address	University of Saskatchewan 105 Administration Place Saskatoon, SK S7N 5A2 Canada Attn: University of Saskatchewan

Total 0.00 CAD

Terms and Conditions

Springer Nature Terms and Conditions for RightsLink Permissions

Springer Nature Customer Service Centre GmbH (the Licensor) hereby grants you a non-exclusive, world-wide licence to reproduce the material and for the purpose and requirements specified in the attached copy of your order form, and for no other use, subject to the conditions below:

1. The Licensor warrants that it has, to the best of its knowledge, the rights to license reuse of this material. However, you should ensure that the material you are requesting is original to the Licensor and does not carry the copyright of another entity (as credited in the published version).

   If the credit line on any part of the material you have requested indicates that it was reprinted or adapted with permission from another source, then you should also seek permission from that source to reuse the material.

2. Where **print only** permission has been granted for a fee, separate permission must be obtained for any additional electronic re-use.

3. Permission granted **free of charge** for material in print is also usually granted for any electronic version of that work, provided that the material is incidental to your work as a whole and that the electronic version is essentially equivalent to, or substitutes for, the print version.

4. A licence for 'post on a website' is valid for 12 months from the licence date. This licence does not cover use of full text articles on websites.

5. Where **'reuse in a dissertation/thesis'** has been selected the following terms apply: Print rights of the final author's accepted manuscript (for clarity, NOT the published version) for up to 100 copies, electronic rights for use only on a personal website or institutional repository as defined by the Sherpa guideline (www.sherpa.ac.uk/romeo/).

6. Permission granted for books and journals is granted for the lifetime of the first edition and does not apply to second and subsequent editions (except where the first edition permission was granted free of charge or for signatories to the STM Permissions Guidelines http://www.stm-assoc.org/copyright-legal-affairs/permissions/permissions-guidelines/), and does not apply for editions in other languages unless additional translation rights have been granted separately in the licence.

7. Rights for additional components such as custom editions and derivatives require additional permission and may be subject to an additional fee. Please apply to Journalpermissions@springernature.com/bookpermissions@springernature.com for these rights.

8. The Licensor's permission must be acknowledged next to the licensed material in print. In electronic form, this acknowledgement must be visible at the same time as the figures/tables/illustrations or abstract, and must be hyperlinked to the journal/book's homepage. Our required acknowledgement format is in the Appendix below.

9. Use of the material for incidental promotional use, minor editing privileges (this does not include cropping, adapting, omitting material or any other changes that affect the meaning, intention or moral rights of the author) and copies for the disabled are permitted under this licence.

10. Minor adaptations of single figures (changes of format, colour and style) do not require the Licensor's approval. However, the adaptation should be credited as shown in Appendix below.

Appendix — Acknowledgements:

For Journal Content:
Reprinted by permission from [**the Licensor**]: [**Journal Publisher** (e.g. Nature/Springer/Palgrave)] [**JOURNAL NAME**] [**REFERENCE CITATION** (Article name, Author(s) Name), [**COPYRIGHT**] (year of publication)

For **Advance Online Publication papers:**
Reprinted by permission from [**the Licensor**]: [**Journal Publisher** (e.g. Nature/Springer/Palgrave)] [**JOURNAL NAME**] [**REFERENCE CITATION** (Article name, Author(s) Name), [**COPYRIGHT**] (year of publication), advance online publication, day month year (doi: 10.1038/sj.[JOURNAL ACRONYM].)

For Adaptations/Translations:
Adapted/Translated by permission from [**the Licensor**]: [**Journal Publisher** (e.g. Nature/Springer/Palgrave)] [**JOURNAL NAME**] [**REFERENCE CITATION** (Article name, Author(s) Name), [**COPYRIGHT**] (year of publication)

Note: For any republication from the British Journal of Cancer, the following credit line style applies:

Reprinted/adapted/translated by permission from [**the Licensor**]: on behalf of Cancer Research UK: : [**Journal Publisher** (e.g. Nature/Springer/Palgrave)] [**JOURNAL NAME**] [**REFERENCE CITATION** (Article name, Author(s) Name), **[COPYRIGHT]** (year of publication)

For **Advance Online Publication** papers:
Reprinted by permission from The [**the Licensor**]: on behalf of Cancer Research UK: [**Journal Publisher** (e.g. Nature/Springer/Palgrave)] [**JOURNAL NAME**] [**REFERENCE CITATION** (Article name, Author(s) Name), [**COPYRIGHT**] (year of publication), advance online publication, day month year (doi: 10.1038/sj.[JOURNAL ACRONYM])

For Book content:
Reprinted/adapted by permission from [**the Licensor**]: [**Book Publisher** (e.g. Palgrave Macmillan, Springer etc) [**Book Title**] by [**Book author**(s)] [**COPYRIGHT**] (year of publication)

Other Conditions:

Version 1.1

APPENDIX I: COPYRIGHT PERMISSION FOR FIGURE 2.9

178 Rexdale Blvd.
Toronto, ON, M9W 1R3
Tel: 1-800-463-6727
www.csagroup.org

December 4, 2018

Mr. Pedro Cordova
University of Saskatchewan
105 Administration Place
Saskatoon, SK S7H 5J9

Email: plc831@mail.usask.ca

Dear Mr. Cordova,

This letter is in response to your request to reproduce copyrighted material from standard **CSA S16-14 – Design of steel structures** ("Standard"), owned by the Canadian Standards Association, (operating as "CSA Group"). We understand that you will be using this Standard for the purpose set out in the External Copyright Request Application dated December 4, 2018, as attached ("Purpose"). This arrangement is limited to this edition of the Standard and for the Purpose only.

The following notice and acknowledgement must be placed on the copyright notice page:

"With the permission of Canadian Standards Association, (operating as "CSA Group"), 178 Rexdale Blvd., Toronto, ON, M9W 1R3, material is reproduced from CSA Group's standard **CSA S16-14 – Design of steel structures.** This material is not the complete and official position of CSA Group on the referenced subject, which is represented solely by the Standard in its entirety. While use of the material has been authorized, CSA Group is not responsible for the manner in which the data is presented, nor for any representations and interpretations. No further reproduction is permitted. For more information or to purchase standard(s) from CSA Group, please visit store.csagroup.org or call 1-800-463-6727."

A copyright acknowledgement, (Source: Figure 1, **CSA S16-14 – Design of steel structures**. © 2014 Canadian Standards Association), should also appear adjacent to or underneath each instance of CSA Group's material that is reproduced. Please provide CSA Group with an electronic copy of the completed work for our files. Kindly forward this to copyright@csagroup.org.

I trust these terms satisfy your requirements. If I can be of any further assistance please do not hesitate to contact me.

Sincerely,

Patti Ensor
Manager, Licensing & Distribution
Tel. (416) 747-2629

Accepted and Agreed:

Signed Mr. Pedro Cordova

Signature: _____ Date: _____

Name: _____ Title: _____

APPENDIX J: COPYRIGHT PERMISSION FOR FIGURES 2.6, 2.11, 2.12 AND 2.15

ELSEVIER LICENSE
TERMS AND CONDITIONS

Jan 04, 2019

This Agreement between University of Saskatchewan -- Pedro Cordova ("You") and Elsevier ("Elsevier") consists of your license details and the terms and conditions provided by Elsevier and Copyright Clearance Center.

License Number	4502221053761
License date	Jan 04, 2019
Licensed Content Publisher	Elsevier
Licensed Content Publication	Tribology International
Licensed Content Title	Investigations on the fretting fatigue failure mechanism of bolted joints in high strength steel subjected to different levels of pre-tension
Licensed Content Author	Carlos Jiménez-Peña,Reza H. Talemi,Barbara Rossi,Dimitri Debruyne
Licensed Content Date	Apr 1, 2017
Licensed Content Volume	108
Licensed Content Issue	n/a
Licensed Content Pages	13
Start Page	128
End Page	140
Type of Use	reuse in a thesis/dissertation
Intended publisher of new work	other
Portion	figures/tables/illustrations
Number of figures/tables/illustrations	4
Format	both print and electronic
Are you the author of this Elsevier article?	No
Will you be translating?	No
Original figure numbers	Figure 3(b), Figure 6(c), Figure 7(a) and Figure 14(b).
Title of your thesis/dissertation	Fretting fatigue in steel bolted connections.
Expected completion date	Dec 2018
Estimated size (number of pages)	175
Requestor Location	University of Saskatchewan 105 Administration Place Saskatoon, SK S7N 5A2 Canada Attn: University of Saskatchewan
Publisher Tax ID	GB 494 6272 12

Total 0.00 CAD

Terms and Conditions

INTRODUCTION

1. The publisher for this copyrighted material is Elsevier. By clicking "accept" in connection with completing this licensing transaction, you agree that the following terms and conditions apply to this transaction (along with the Billing and Payment terms and conditions established by Copyright Clearance Center, Inc. ("CCC"), at the time that you opened your Rightslink account and that are available at any time at http://myaccount.copyright.com).

GENERAL TERMS

2. Elsevier hereby grants you permission to reproduce the aforementioned material subject to the terms and conditions indicated.
3. Acknowledgement: If any part of the material to be used (for example, figures) has appeared in our publication with credit or acknowledgement to another source, permission must also be sought from that source. If such permission is not obtained then that material may not be included in your publication/copies. Suitable acknowledgement to the source must be made, either as a footnote or in a reference list at the end of your publication, as follows:
"Reprinted from Publication title, Vol /edition number, Author(s), Title of article / title of chapter, Pages No., Copyright (Year), with permission from Elsevier [OR APPLICABLE SOCIETY COPYRIGHT OWNER]." Also Lancet special credit - "Reprinted from The Lancet, Vol. number, Author(s), Title of article, Pages No., Copyright (Year), with permission from Elsevier."
4. Reproduction of this material is confined to the purpose and/or media for which permission is hereby given.
5. Altering/Modifying Material: Not Permitted. However figures and illustrations may be altered/adapted minimally to serve your work. Any other abbreviations, additions, deletions and/or any other alterations shall be made only with prior written authorization of Elsevier Ltd. (Please contact Elsevier at permissions@elsevier.com). No modifications can be made to any Lancet figures/tables and they must be reproduced in full.
6. If the permission fee for the requested use of our material is waived in this instance, please be advised that your future requests for Elsevier materials may attract a fee.
7. Reservation of Rights: Publisher reserves all rights not specifically granted in the combination of (i) the license details provided by you and accepted in the course of this licensing transaction, (ii) these terms and conditions and (iii) CCC's Billing and Payment terms and conditions.
8. License Contingent Upon Payment: While you may exercise the rights licensed immediately upon issuance of the license at the end of the licensing process for the transaction, provided that you have disclosed complete and accurate details of your proposed use, no license is finally effective unless and until full payment is received from you (either by publisher or by CCC) as provided in CCC's Billing and Payment terms and conditions. If full payment is not received on a timely basis, then any license preliminarily granted shall be deemed automatically revoked and shall be void as if never granted. Further, in the event that you breach any of these terms and conditions or any of CCC's Billing and Payment terms and conditions, the license is automatically revoked and shall be void as if never granted. Use of materials as described in a revoked license, as well as any use of the materials beyond the scope of an unrevoked license, may constitute copyright infringement and publisher reserves the right to take any and all action to protect its copyright in the materials.
9. Warranties: Publisher makes no representations or warranties with respect to the licensed material.
10. Indemnity: You hereby indemnify and agree to hold harmless publisher and CCC, and their respective officers, directors, employees and agents, from and against any and all

claims arising out of your use of the licensed material other than as specifically authorized pursuant to this license.
11. No Transfer of License: This license is personal to you and may not be sublicensed, assigned, or transferred by you to any other person without publisher's written permission.
12. No Amendment Except in Writing: This license may not be amended except in a writing signed by both parties (or, in the case of publisher, by CCC on publisher's behalf).
13. Objection to Contrary Terms: Publisher hereby objects to any terms contained in any purchase order, acknowledgment, check endorsement or other writing prepared by you, which terms are inconsistent with these terms and conditions or CCC's Billing and Payment terms and conditions. These terms and conditions, together with CCC's Billing and Payment terms and conditions (which are incorporated herein), comprise the entire agreement between you and publisher (and CCC) concerning this licensing transaction. In the event of any conflict between your obligations established by these terms and conditions and those established by CCC's Billing and Payment terms and conditions, these terms and conditions shall control.
14. Revocation: Elsevier or Copyright Clearance Center may deny the permissions described in this License at their sole discretion, for any reason or no reason, with a full refund payable to you. Notice of such denial will be made using the contact information provided by you. Failure to receive such notice will not alter or invalidate the denial. In no event will Elsevier or Copyright Clearance Center be responsible or liable for any costs, expenses or damage incurred by you as a result of a denial of your permission request, other than a refund of the amount(s) paid by you to Elsevier and/or Copyright Clearance Center for denied permissions.

LIMITED LICENSE

The following terms and conditions apply only to specific license types:
15. **Translation**: This permission is granted for non-exclusive world **English** rights only unless your license was granted for translation rights. If you licensed translation rights you may only translate this content into the languages you requested. A professional translator must perform all translations and reproduce the content word for word preserving the integrity of the article.
16. **Posting licensed content on any Website**: The following terms and conditions apply as follows: Licensing material from an Elsevier journal: All content posted to the web site must maintain the copyright information line on the bottom of each image; A hyper-text must be included to the Homepage of the journal from which you are licensing at http://www.sciencedirect.com/science/journal/xxxxx or the Elsevier homepage for books at http://www.elsevier.com; Central Storage: This license does not include permission for a scanned version of the material to be stored in a central repository such as that provided by Heron/XanEdu.
Licensing material from an Elsevier book: A hyper-text link must be included to the Elsevier homepage at http://www.elsevier.com . All content posted to the web site must maintain the copyright information line on the bottom of each image.

Posting licensed content on Electronic reserve: In addition to the above the following clauses are applicable: The web site must be password-protected and made available only to bona fide students registered on a relevant course. This permission is granted for 1 year only. You may obtain a new license for future website posting.
17. **For journal authors:** the following clauses are applicable in addition to the above:
Preprints:
A preprint is an author's own write-up of research results and analysis, it has not been peer-reviewed, nor has it had any other value added to it by a publisher (such as formatting, copyright, technical enhancement etc.).
Authors can share their preprints anywhere at any time. Preprints should not be added to or enhanced in any way in order to appear more like, or to substitute for, the final versions of

articles however authors can update their preprints on arXiv or RePEc with their Accepted Author Manuscript (see below).
If accepted for publication, we encourage authors to link from the preprint to their formal publication via its DOI. Millions of researchers have access to the formal publications on ScienceDirect, and so links will help users to find, access, cite and use the best available version. Please note that Cell Press, The Lancet and some society-owned have different preprint policies. Information on these policies is available on the journal homepage.
Accepted Author Manuscripts: An accepted author manuscript is the manuscript of an article that has been accepted for publication and which typically includes author-incorporated changes suggested during submission, peer review and editor-author communications.
Authors can share their accepted author manuscript:

- immediately
  - via their non-commercial person homepage or blog
  - by updating a preprint in arXiv or RePEc with the accepted manuscript
  - via their research institute or institutional repository for internal institutional uses or as part of an invitation-only research collaboration work-group
  - directly by providing copies to their students or to research collaborators for their personal use
  - for private scholarly sharing as part of an invitation-only work group on commercial sites with which Elsevier has an agreement
- After the embargo period
  - via non-commercial hosting platforms such as their institutional repository
  - via commercial sites with which Elsevier has an agreement

In all cases accepted manuscripts should:

- link to the formal publication via its DOI
- bear a CC-BY-NC-ND license - this is easy to do
- if aggregated with other manuscripts, for example in a repository or other site, be shared in alignment with our hosting policy not be added to or enhanced in any way to appear more like, or to substitute for, the published journal article.

Published journal article (JPA): A published journal article (PJA) is the definitive final record of published research that appears or will appear in the journal and embodies all value-adding publishing activities including peer review co-ordination, copy-editing, formatting, (if relevant) pagination and online enrichment.
Policies for sharing publishing journal articles differ for subscription and gold open access articles:
Subscription Articles: If you are an author, please share a link to your article rather than the full-text. Millions of researchers have access to the formal publications on ScienceDirect, and so links will help your users to find, access, cite, and use the best available version.
Theses and dissertations which contain embedded PJAs as part of the formal submission can be posted publicly by the awarding institution with DOI links back to the formal publications on ScienceDirect.
If you are affiliated with a library that subscribes to ScienceDirect you have additional private sharing rights for others' research accessed under that agreement. This includes use for classroom teaching and internal training at the institution (including use in course packs and courseware programs), and inclusion of the article for grant funding purposes.
Gold Open Access Articles: May be shared according to the author-selected end-user license and should contain a CrossMark logo, the end user license, and a DOI link to the formal publication on ScienceDirect.
Please refer to Elsevier's posting policy for further information.

18. **For book authors** the following clauses are applicable in addition to the above: Authors are permitted to place a brief summary of their work online only. You are not allowed to download and post the published electronic version of your chapter, nor may you scan the printed edition to create an electronic version. **Posting to a repository:** Authors are permitted to post a summary of their chapter only in their institution's repository.
19. **Thesis/Dissertation**: If your license is for use in a thesis/dissertation your thesis may be submitted to your institution in either print or electronic form. Should your thesis be published commercially, please reapply for permission. These requirements include permission for the Library and Archives of Canada to supply single copies, on demand, of the complete thesis and include permission for Proquest/UMI to supply single copies, on demand, of the complete thesis. Should your thesis be published commercially, please reapply for permission. Theses and dissertations which contain embedded PJAs as part of the formal submission can be posted publicly by the awarding institution with DOI links back to the formal publications on ScienceDirect.

Elsevier Open Access Terms and Conditions
You can publish open access with Elsevier in hundreds of open access journals or in nearly 2000 established subscription journals that support open access publishing. Permitted third party re-use of these open access articles is defined by the author's choice of Creative Commons user license. See our open access license policy for more information.
Terms & Conditions applicable to all Open Access articles published with Elsevier:
Any reuse of the article must not represent the author as endorsing the adaptation of the article nor should the article be modified in such a way as to damage the author's honour or reputation. If any changes have been made, such changes must be clearly indicated.
The author(s) must be appropriately credited and we ask that you include the end user license and a DOI link to the formal publication on ScienceDirect.
If any part of the material to be used (for example, figures) has appeared in our publication with credit or acknowledgement to another source it is the responsibility of the user to ensure their reuse complies with the terms and conditions determined by the rights holder.
Additional Terms & Conditions applicable to each Creative Commons user license:
CC BY: The CC-BY license allows users to copy, to create extracts, abstracts and new works from the Article, to alter and revise the Article and to make commercial use of the Article (including reuse and/or resale of the Article by commercial entities), provided the user gives appropriate credit (with a link to the formal publication through the relevant DOI), provides a link to the license, indicates if changes were made and the licensor is not represented as endorsing the use made of the work. The full details of the license are available at http://creativecommons.org/licenses/by/4.0.
CC BY NC SA: The CC BY-NC-SA license allows users to copy, to create extracts, abstracts and new works from the Article, to alter and revise the Article, provided this is not done for commercial purposes, and that the user gives appropriate credit (with a link to the formal publication through the relevant DOI), provides a link to the license, indicates if changes were made and the licensor is not represented as endorsing the use made of the work. Further, any new works must be made available on the same conditions. The full details of the license are available at http://creativecommons.org/licenses/by-nc-sa/4.0.
CC BY NC ND: The CC BY-NC-ND license allows users to copy and distribute the Article, provided this is not done for commercial purposes and further does not permit distribution of the Article if it is changed or edited in any way, and provided the user gives appropriate credit (with a link to the formal publication through the relevant DOI), provides a link to the license, and that the licensor is not represented as endorsing the use made of the work. The full details of the license are available at http://creativecommons.org/licenses/by-nc-nd/4.0.
Any commercial reuse of Open Access articles published with a CC BY NC SA or CC BY NC ND license requires permission from Elsevier and will be subject to a fee.
Commercial reuse includes:

- Associating advertising with the full text of the Article
- Charging fees for document delivery or access
- Article aggregation
- Systematic distribution via e-mail lists or share buttons

Posting or linking by commercial companies for use by customers of those companies.

20. **Other Conditions**:

v1.9

APPENDIX K: COPYRIGHT PERMISSION FOR FIGURE 2.14

ELSEVIER LICENSE
TERMS AND CONDITIONS

Jan 04, 2019

This Agreement between University of Saskatchewan -- Pedro Cordova ("You") and Elsevier ("Elsevier") consists of your license details and the terms and conditions provided by Elsevier and Copyright Clearance Center.

License Number	4481681237655
License date	Dec 03, 2018
Licensed Content Publisher	Elsevier
Licensed Content Publication	Materials & Design
Licensed Content Title	An experimental investigation of the bolt clamping force and friction effect on the fatigue behavior of aluminum alloy 2024-T3 double shear lap joint
Licensed Content Author	T.N. Chakherlou,M.J. Razavi,A.B. Aghdam,B. Abazadeh
Licensed Content Date	Sep 1, 2011
Licensed Content Volume	32
Licensed Content Issue	8-9
Licensed Content Pages	9
Start Page	4641
End Page	4649
Type of Use	reuse in a thesis/dissertation
Intended publisher of new work	other
Portion	figures/tables/illustrations
Number of figures/tables/illustrations	1
Format	both print and electronic
Are you the author of this Elsevier article?	No
Will you be translating?	No
Original figure numbers	Figure 7
Title of your thesis/dissertation	Fretting fatigue in steel bolted connections.
Expected completion date	Dec 2018
Estimated size (number of pages)	175
Requestor Location	University of Saskatchewan 105 Administration Place Saskatoon, SK S7N 5A2 Canada Attn: University of Saskatchewan
Publisher Tax ID	GB 494 6272 12

Total 0.00 CAD

Terms and Conditions

INTRODUCTION

1. The publisher for this copyrighted material is Elsevier. By clicking "accept" in connection with completing this licensing transaction, you agree that the following terms and conditions apply to this transaction (along with the Billing and Payment terms and conditions established by Copyright Clearance Center, Inc. ("CCC"), at the time that you opened your Rightslink account and that are available at any time at http://myaccount.copyright.com).

GENERAL TERMS

2. Elsevier hereby grants you permission to reproduce the aforementioned material subject to the terms and conditions indicated.
3. Acknowledgement: If any part of the material to be used (for example, figures) has appeared in our publication with credit or acknowledgement to another source, permission must also be sought from that source. If such permission is not obtained then that material may not be included in your publication/copies. Suitable acknowledgement to the source must be made, either as a footnote or in a reference list at the end of your publication, as follows:
"Reprinted from Publication title, Vol /edition number, Author(s), Title of article / title of chapter, Pages No., Copyright (Year), with permission from Elsevier [OR APPLICABLE SOCIETY COPYRIGHT OWNER]." Also Lancet special credit - "Reprinted from The Lancet, Vol. number, Author(s), Title of article, Pages No., Copyright (Year), with permission from Elsevier."
4. Reproduction of this material is confined to the purpose and/or media for which permission is hereby given.
5. Altering/Modifying Material: Not Permitted. However figures and illustrations may be altered/adapted minimally to serve your work. Any other abbreviations, additions, deletions and/or any other alterations shall be made only with prior written authorization of Elsevier Ltd. (Please contact Elsevier at permissions@elsevier.com). No modifications can be made to any Lancet figures/tables and they must be reproduced in full.
6. If the permission fee for the requested use of our material is waived in this instance, please be advised that your future requests for Elsevier materials may attract a fee.
7. Reservation of Rights: Publisher reserves all rights not specifically granted in the combination of (i) the license details provided by you and accepted in the course of this licensing transaction, (ii) these terms and conditions and (iii) CCC's Billing and Payment terms and conditions.
8. License Contingent Upon Payment: While you may exercise the rights licensed immediately upon issuance of the license at the end of the licensing process for the transaction, provided that you have disclosed complete and accurate details of your proposed use, no license is finally effective unless and until full payment is received from you (either by publisher or by CCC) as provided in CCC's Billing and Payment terms and conditions. If full payment is not received on a timely basis, then any license preliminarily granted shall be deemed automatically revoked and shall be void as if never granted. Further, in the event that you breach any of these terms and conditions or any of CCC's Billing and Payment terms and conditions, the license is automatically revoked and shall be void as if never granted. Use of materials as described in a revoked license, as well as any use of the materials beyond the scope of an unrevoked license, may constitute copyright infringement and publisher reserves the right to take any and all action to protect its copyright in the materials.
9. Warranties: Publisher makes no representations or warranties with respect to the licensed material.
10. Indemnity: You hereby indemnify and agree to hold harmless publisher and CCC, and their respective officers, directors, employees and agents, from and against any and all

claims arising out of your use of the licensed material other than as specifically authorized pursuant to this license.
11. No Transfer of License: This license is personal to you and may not be sublicensed, assigned, or transferred by you to any other person without publisher's written permission.
12. No Amendment Except in Writing: This license may not be amended except in a writing signed by both parties (or, in the case of publisher, by CCC on publisher's behalf).
13. Objection to Contrary Terms: Publisher hereby objects to any terms contained in any purchase order, acknowledgment, check endorsement or other writing prepared by you, which terms are inconsistent with these terms and conditions or CCC's Billing and Payment terms and conditions. These terms and conditions, together with CCC's Billing and Payment terms and conditions (which are incorporated herein), comprise the entire agreement between you and publisher (and CCC) concerning this licensing transaction. In the event of any conflict between your obligations established by these terms and conditions and those established by CCC's Billing and Payment terms and conditions, these terms and conditions shall control.
14. Revocation: Elsevier or Copyright Clearance Center may deny the permissions described in this License at their sole discretion, for any reason or no reason, with a full refund payable to you. Notice of such denial will be made using the contact information provided by you. Failure to receive such notice will not alter or invalidate the denial. In no event will Elsevier or Copyright Clearance Center be responsible or liable for any costs, expenses or damage incurred by you as a result of a denial of your permission request, other than a refund of the amount(s) paid by you to Elsevier and/or Copyright Clearance Center for denied permissions.

LIMITED LICENSE

The following terms and conditions apply only to specific license types:
15. **Translation**: This permission is granted for non-exclusive world **English** rights only unless your license was granted for translation rights. If you licensed translation rights you may only translate this content into the languages you requested. A professional translator must perform all translations and reproduce the content word for word preserving the integrity of the article.
16. **Posting licensed content on any Website**: The following terms and conditions apply as follows: Licensing material from an Elsevier journal: All content posted to the web site must maintain the copyright information line on the bottom of each image; A hyper-text must be included to the Homepage of the journal from which you are licensing at http://www.sciencedirect.com/science/journal/xxxxx or the Elsevier homepage for books at http://www.elsevier.com; Central Storage: This license does not include permission for a scanned version of the material to be stored in a central repository such as that provided by Heron/XanEdu.
Licensing material from an Elsevier book: A hyper-text link must be included to the Elsevier homepage at http://www.elsevier.com . All content posted to the web site must maintain the copyright information line on the bottom of each image.

Posting licensed content on Electronic reserve: In addition to the above the following clauses are applicable: The web site must be password-protected and made available only to bona fide students registered on a relevant course. This permission is granted for 1 year only. You may obtain a new license for future website posting.
17. **For journal authors:** the following clauses are applicable in addition to the above:
Preprints:
A preprint is an author's own write-up of research results and analysis, it has not been peer-reviewed, nor has it had any other value added to it by a publisher (such as formatting, copyright, technical enhancement etc.).
Authors can share their preprints anywhere at any time. Preprints should not be added to or enhanced in any way in order to appear more like, or to substitute for, the final versions of

articles however authors can update their preprints on arXiv or RePEc with their Accepted Author Manuscript (see below).
If accepted for publication, we encourage authors to link from the preprint to their formal publication via its DOI. Millions of researchers have access to the formal publications on ScienceDirect, and so links will help users to find, access, cite and use the best available version. Please note that Cell Press, The Lancet and some society-owned have different preprint policies. Information on these policies is available on the journal homepage.
Accepted Author Manuscripts: An accepted author manuscript is the manuscript of an article that has been accepted for publication and which typically includes author-incorporated changes suggested during submission, peer review and editor-author communications.
Authors can share their accepted author manuscript:

- immediately
  - via their non-commercial person homepage or blog
  - by updating a preprint in arXiv or RePEc with the accepted manuscript
  - via their research institute or institutional repository for internal institutional uses or as part of an invitation-only research collaboration work-group
  - directly by providing copies to their students or to research collaborators for their personal use
  - for private scholarly sharing as part of an invitation-only work group on commercial sites with which Elsevier has an agreement
- After the embargo period
  - via non-commercial hosting platforms such as their institutional repository
  - via commercial sites with which Elsevier has an agreement

In all cases accepted manuscripts should:

- link to the formal publication via its DOI
- bear a CC-BY-NC-ND license - this is easy to do
- if aggregated with other manuscripts, for example in a repository or other site, be shared in alignment with our hosting policy not be added to or enhanced in any way to appear more like, or to substitute for, the published journal article.

Published journal article (JPA): A published journal article (PJA) is the definitive final record of published research that appears or will appear in the journal and embodies all value-adding publishing activities including peer review co-ordination, copy-editing, formatting, (if relevant) pagination and online enrichment.
Policies for sharing publishing journal articles differ for subscription and gold open access articles:
Subscription Articles: If you are an author, please share a link to your article rather than the full-text. Millions of researchers have access to the formal publications on ScienceDirect, and so links will help your users to find, access, cite, and use the best available version.
Theses and dissertations which contain embedded PJAs as part of the formal submission can be posted publicly by the awarding institution with DOI links back to the formal publications on ScienceDirect.
If you are affiliated with a library that subscribes to ScienceDirect you have additional private sharing rights for others' research accessed under that agreement. This includes use for classroom teaching and internal training at the institution (including use in course packs and courseware programs), and inclusion of the article for grant funding purposes.
Gold Open Access Articles: May be shared according to the author-selected end-user license and should contain a CrossMark logo, the end user license, and a DOI link to the formal publication on ScienceDirect.
Please refer to Elsevier's posting policy for further information.

18. **For book authors** the following clauses are applicable in addition to the above: Authors are permitted to place a brief summary of their work online only. You are not allowed to download and post the published electronic version of your chapter, nor may you scan the printed edition to create an electronic version. **Posting to a repository:** Authors are permitted to post a summary of their chapter only in their institution's repository.
19. **Thesis/Dissertation**: If your license is for use in a thesis/dissertation your thesis may be submitted to your institution in either print or electronic form. Should your thesis be published commercially, please reapply for permission. These requirements include permission for the Library and Archives of Canada to supply single copies, on demand, of the complete thesis and include permission for Proquest/UMI to supply single copies, on demand, of the complete thesis. Should your thesis be published commercially, please reapply for permission. Theses and dissertations which contain embedded PJAs as part of the formal submission can be posted publicly by the awarding institution with DOI links back to the formal publications on ScienceDirect.

Elsevier Open Access Terms and Conditions

You can publish open access with Elsevier in hundreds of open access journals or in nearly 2000 established subscription journals that support open access publishing. Permitted third party re-use of these open access articles is defined by the author's choice of Creative Commons user license. See our open access license policy for more information.
Terms & Conditions applicable to all Open Access articles published with Elsevier:
Any reuse of the article must not represent the author as endorsing the adaptation of the article nor should the article be modified in such a way as to damage the author's honour or reputation. If any changes have been made, such changes must be clearly indicated.
The author(s) must be appropriately credited and we ask that you include the end user license and a DOI link to the formal publication on ScienceDirect.
If any part of the material to be used (for example, figures) has appeared in our publication with credit or acknowledgement to another source it is the responsibility of the user to ensure their reuse complies with the terms and conditions determined by the rights holder.
Additional Terms & Conditions applicable to each Creative Commons user license:
CC BY: The CC-BY license allows users to copy, to create extracts, abstracts and new works from the Article, to alter and revise the Article and to make commercial use of the Article (including reuse and/or resale of the Article by commercial entities), provided the user gives appropriate credit (with a link to the formal publication through the relevant DOI), provides a link to the license, indicates if changes were made and the licensor is not represented as endorsing the use made of the work. The full details of the license are available at http://creativecommons.org/licenses/by/4.0.
CC BY NC SA: The CC BY-NC-SA license allows users to copy, to create extracts, abstracts and new works from the Article, to alter and revise the Article, provided this is not done for commercial purposes, and that the user gives appropriate credit (with a link to the formal publication through the relevant DOI), provides a link to the license, indicates if changes were made and the licensor is not represented as endorsing the use made of the work. Further, any new works must be made available on the same conditions. The full details of the license are available at http://creativecommons.org/licenses/by-nc-sa/4.0.
CC BY NC ND: The CC BY-NC-ND license allows users to copy and distribute the Article, provided this is not done for commercial purposes and further does not permit distribution of the Article if it is changed or edited in any way, and provided the user gives appropriate credit (with a link to the formal publication through the relevant DOI), provides a link to the license, and that the licensor is not represented as endorsing the use made of the work. The full details of the license are available at http://creativecommons.org/licenses/by-nc-nd/4.0.
Any commercial reuse of Open Access articles published with a CC BY NC SA or CC BY NC ND license requires permission from Elsevier and will be subject to a fee.
Commercial reuse includes:

- Associating advertising with the full text of the Article
- Charging fees for document delivery or access
- Article aggregation
- Systematic distribution via e-mail lists or share buttons

Posting or linking by commercial companies for use by customers of those companies.

20. **Other Conditions**:

v1.9

Questions? customercare@copyright.com or +1-855-239-3415 (toll free in the US) or +1-978-646-2777.

APPENDIX L: COPYRIGHT PERMISSION FOR FIGURE 2.19

ELSEVIER LICENSE
TERMS AND CONDITIONS

Jan 04, 2019

This Agreement between University of Saskatchewan -- Pedro Cordova ("You") and Elsevier ("Elsevier") consists of your license details and the terms and conditions provided by Elsevier and Copyright Clearance Center.

License Number	4481690900643
License date	Dec 03, 2018
Licensed Content Publisher	Elsevier
Licensed Content Publication	International Journal of Fatigue
Licensed Content Title	Fatigue of structures and secondary bending in structural elements
Licensed Content Author	J. Schijve,G. Campoli,A. Monaco
Licensed Content Date	Jul 1, 2009
Licensed Content Volume	31
Licensed Content Issue	7
Licensed Content Pages	13
Start Page	1111
End Page	1123
Type of Use	reuse in a thesis/dissertation
Intended publisher of new work	other
Portion	figures/tables/illustrations
Number of figures/tables/illustrations	1
Format	both print and electronic
Are you the author of this Elsevier article?	No
Will you be translating?	No
Original figure numbers	Figure 10
Title of your thesis/dissertation	Fretting fatigue in steel bolted connections.
Expected completion date	Dec 2018
Estimated size (number of pages)	175
Requestor Location	University of Saskatchewan 105 Administration Place Saskatoon, SK S7N 5A2 Canada Attn: University of Saskatchewan
Publisher Tax ID	GB 494 6272 12
Total	0.00 CAD

Terms and Conditions

INTRODUCTION

1. The publisher for this copyrighted material is Elsevier. By clicking "accept" in connection with completing this licensing transaction, you agree that the following terms and conditions apply to this transaction (along with the Billing and Payment terms and conditions established by Copyright Clearance Center, Inc. ("CCC"), at the time that you opened your Rightslink account and that are available at any time at http://myaccount.copyright.com).

GENERAL TERMS

2. Elsevier hereby grants you permission to reproduce the aforementioned material subject to the terms and conditions indicated.
3. Acknowledgement: If any part of the material to be used (for example, figures) has appeared in our publication with credit or acknowledgement to another source, permission must also be sought from that source. If such permission is not obtained then that material may not be included in your publication/copies. Suitable acknowledgement to the source must be made, either as a footnote or in a reference list at the end of your publication, as follows:
"Reprinted from Publication title, Vol /edition number, Author(s), Title of article / title of chapter, Pages No., Copyright (Year), with permission from Elsevier [OR APPLICABLE SOCIETY COPYRIGHT OWNER]." Also Lancet special credit - "Reprinted from The Lancet, Vol. number, Author(s), Title of article, Pages No., Copyright (Year), with permission from Elsevier."
4. Reproduction of this material is confined to the purpose and/or media for which permission is hereby given.
5. Altering/Modifying Material: Not Permitted. However figures and illustrations may be altered/adapted minimally to serve your work. Any other abbreviations, additions, deletions and/or any other alterations shall be made only with prior written authorization of Elsevier Ltd. (Please contact Elsevier at permissions@elsevier.com). No modifications can be made to any Lancet figures/tables and they must be reproduced in full.
6. If the permission fee for the requested use of our material is waived in this instance, please be advised that your future requests for Elsevier materials may attract a fee.
7. Reservation of Rights: Publisher reserves all rights not specifically granted in the combination of (i) the license details provided by you and accepted in the course of this licensing transaction, (ii) these terms and conditions and (iii) CCC's Billing and Payment terms and conditions.
8. License Contingent Upon Payment: While you may exercise the rights licensed immediately upon issuance of the license at the end of the licensing process for the transaction, provided that you have disclosed complete and accurate details of your proposed use, no license is finally effective unless and until full payment is received from you (either by publisher or by CCC) as provided in CCC's Billing and Payment terms and conditions. If full payment is not received on a timely basis, then any license preliminarily granted shall be deemed automatically revoked and shall be void as if never granted. Further, in the event that you breach any of these terms and conditions or any of CCC's Billing and Payment terms and conditions, the license is automatically revoked and shall be void as if never granted. Use of materials as described in a revoked license, as well as any use of the materials beyond the scope of an unrevoked license, may constitute copyright infringement and publisher reserves the right to take any and all action to protect its copyright in the materials.
9. Warranties: Publisher makes no representations or warranties with respect to the licensed material.
10. Indemnity: You hereby indemnify and agree to hold harmless publisher and CCC, and their respective officers, directors, employees and agents, from and against any and all claims arising out of your use of the licensed material other than as specifically authorized pursuant to this license.

11. No Transfer of License: This license is personal to you and may not be sublicensed, assigned, or transferred by you to any other person without publisher's written permission.
12. No Amendment Except in Writing: This license may not be amended except in a writing signed by both parties (or, in the case of publisher, by CCC on publisher's behalf).
13. Objection to Contrary Terms: Publisher hereby objects to any terms contained in any purchase order, acknowledgment, check endorsement or other writing prepared by you, which terms are inconsistent with these terms and conditions or CCC's Billing and Payment terms and conditions. These terms and conditions, together with CCC's Billing and Payment terms and conditions (which are incorporated herein), comprise the entire agreement between you and publisher (and CCC) concerning this licensing transaction. In the event of any conflict between your obligations established by these terms and conditions and those established by CCC's Billing and Payment terms and conditions, these terms and conditions shall control.
14. Revocation: Elsevier or Copyright Clearance Center may deny the permissions described in this License at their sole discretion, for any reason or no reason, with a full refund payable to you. Notice of such denial will be made using the contact information provided by you. Failure to receive such notice will not alter or invalidate the denial. In no event will Elsevier or Copyright Clearance Center be responsible or liable for any costs, expenses or damage incurred by you as a result of a denial of your permission request, other than a refund of the amount(s) paid by you to Elsevier and/or Copyright Clearance Center for denied permissions.

LIMITED LICENSE

The following terms and conditions apply only to specific license types:
15. **Translation**: This permission is granted for non-exclusive world **English** rights only unless your license was granted for translation rights. If you licensed translation rights you may only translate this content into the languages you requested. A professional translator must perform all translations and reproduce the content word for word preserving the integrity of the article.
16. **Posting licensed content on any Website**: The following terms and conditions apply as follows: Licensing material from an Elsevier journal: All content posted to the web site must maintain the copyright information line on the bottom of each image; A hyper-text must be included to the Homepage of the journal from which you are licensing at http://www.sciencedirect.com/science/journal/xxxxx or the Elsevier homepage for books at http://www.elsevier.com; Central Storage: This license does not include permission for a scanned version of the material to be stored in a central repository such as that provided by Heron/XanEdu.
Licensing material from an Elsevier book: A hyper-text link must be included to the Elsevier homepage at http://www.elsevier.com . All content posted to the web site must maintain the copyright information line on the bottom of each image.

Posting licensed content on Electronic reserve: In addition to the above the following clauses are applicable: The web site must be password-protected and made available only to bona fide students registered on a relevant course. This permission is granted for 1 year only. You may obtain a new license for future website posting.
17. **For journal authors:** the following clauses are applicable in addition to the above:
Preprints:
A preprint is an author's own write-up of research results and analysis, it has not been peer-reviewed, nor has it had any other value added to it by a publisher (such as formatting, copyright, technical enhancement etc.).
Authors can share their preprints anywhere at any time. Preprints should not be added to or enhanced in any way in order to appear more like, or to substitute for, the final versions of articles however authors can update their preprints on arXiv or RePEc with their Accepted Author Manuscript (see below).

If accepted for publication, we encourage authors to link from the preprint to their formal publication via its DOI. Millions of researchers have access to the formal publications on ScienceDirect, and so links will help users to find, access, cite and use the best available version. Please note that Cell Press, The Lancet and some society-owned have different preprint policies. Information on these policies is available on the journal homepage.
Accepted Author Manuscripts: An accepted author manuscript is the manuscript of an article that has been accepted for publication and which typically includes author-incorporated changes suggested during submission, peer review and editor-author communications.
Authors can share their accepted author manuscript:

- immediately
  - via their non-commercial person homepage or blog
  - by updating a preprint in arXiv or RePEc with the accepted manuscript
  - via their research institute or institutional repository for internal institutional uses or as part of an invitation-only research collaboration work-group
  - directly by providing copies to their students or to research collaborators for their personal use
  - for private scholarly sharing as part of an invitation-only work group on commercial sites with which Elsevier has an agreement
- After the embargo period
  - via non-commercial hosting platforms such as their institutional repository
  - via commercial sites with which Elsevier has an agreement

In all cases accepted manuscripts should:

- link to the formal publication via its DOI
- bear a CC-BY-NC-ND license - this is easy to do
- if aggregated with other manuscripts, for example in a repository or other site, be shared in alignment with our hosting policy not be added to or enhanced in any way to appear more like, or to substitute for, the published journal article.

Published journal article (JPA): A published journal article (PJA) is the definitive final record of published research that appears or will appear in the journal and embodies all value-adding publishing activities including peer review co-ordination, copy-editing, formatting, (if relevant) pagination and online enrichment.
Policies for sharing publishing journal articles differ for subscription and gold open access articles:
Subscription Articles: If you are an author, please share a link to your article rather than the full-text. Millions of researchers have access to the formal publications on ScienceDirect, and so links will help your users to find, access, cite, and use the best available version.
Theses and dissertations which contain embedded PJAs as part of the formal submission can be posted publicly by the awarding institution with DOI links back to the formal publications on ScienceDirect.
If you are affiliated with a library that subscribes to ScienceDirect you have additional private sharing rights for others' research accessed under that agreement. This includes use for classroom teaching and internal training at the institution (including use in course packs and courseware programs), and inclusion of the article for grant funding purposes.
Gold Open Access Articles: May be shared according to the author-selected end-user license and should contain a CrossMark logo, the end user license, and a DOI link to the formal publication on ScienceDirect.
Please refer to Elsevier's posting policy for further information.
18. **For book authors** the following clauses are applicable in addition to the above:
Authors are permitted to place a brief summary of their work online only. You are not

allowed to download and post the published electronic version of your chapter, nor may you scan the printed edition to create an electronic version. **Posting to a repository:** Authors are permitted to post a summary of their chapter only in their institution's repository.
19. **Thesis/Dissertation**: If your license is for use in a thesis/dissertation your thesis may be submitted to your institution in either print or electronic form. Should your thesis be published commercially, please reapply for permission. These requirements include permission for the Library and Archives of Canada to supply single copies, on demand, of the complete thesis and include permission for Proquest/UMI to supply single copies, on demand, of the complete thesis. Should your thesis be published commercially, please reapply for permission. Theses and dissertations which contain embedded PJAs as part of the formal submission can be posted publicly by the awarding institution with DOI links back to the formal publications on ScienceDirect.

Elsevier Open Access Terms and Conditions
You can publish open access with Elsevier in hundreds of open access journals or in nearly 2000 established subscription journals that support open access publishing. Permitted third party re-use of these open access articles is defined by the author's choice of Creative Commons user license. See our open access license policy for more information.
Terms & Conditions applicable to all Open Access articles published with Elsevier:
Any reuse of the article must not represent the author as endorsing the adaptation of the article nor should the article be modified in such a way as to damage the author's honour or reputation. If any changes have been made, such changes must be clearly indicated.
The author(s) must be appropriately credited and we ask that you include the end user license and a DOI link to the formal publication on ScienceDirect.
If any part of the material to be used (for example, figures) has appeared in our publication with credit or acknowledgement to another source it is the responsibility of the user to ensure their reuse complies with the terms and conditions determined by the rights holder.
Additional Terms & Conditions applicable to each Creative Commons user license:
CC BY: The CC-BY license allows users to copy, to create extracts, abstracts and new works from the Article, to alter and revise the Article and to make commercial use of the Article (including reuse and/or resale of the Article by commercial entities), provided the user gives appropriate credit (with a link to the formal publication through the relevant DOI), provides a link to the license, indicates if changes were made and the licensor is not represented as endorsing the use made of the work. The full details of the license are available at http://creativecommons.org/licenses/by/4.0.
CC BY NC SA: The CC BY-NC-SA license allows users to copy, to create extracts, abstracts and new works from the Article, to alter and revise the Article, provided this is not done for commercial purposes, and that the user gives appropriate credit (with a link to the formal publication through the relevant DOI), provides a link to the license, indicates if changes were made and the licensor is not represented as endorsing the use made of the work. Further, any new works must be made available on the same conditions. The full details of the license are available at http://creativecommons.org/licenses/by-nc-sa/4.0.
CC BY NC ND: The CC BY-NC-ND license allows users to copy and distribute the Article, provided this is not done for commercial purposes and further does not permit distribution of the Article if it is changed or edited in any way, and provided the user gives appropriate credit (with a link to the formal publication through the relevant DOI), provides a link to the license, and that the licensor is not represented as endorsing the use made of the work. The full details of the license are available at http://creativecommons.org/licenses/by-nc-nd/4.0.
Any commercial reuse of Open Access articles published with a CC BY NC SA or CC BY NC ND license requires permission from Elsevier and will be subject to a fee.
Commercial reuse includes:

- Associating advertising with the full text of the Article
- Charging fees for document delivery or access

- Article aggregation
- Systematic distribution via e-mail lists or share buttons

Posting or linking by commercial companies for use by customers of those companies.

20. **Other Conditions**:

v1.9

Questions? customercare@copyright.com or +1-855-239-3415 (toll free in the US) or +1-978-646-2777.

APPENDIX M: COPYRIGHT PERMISSION FOR FIGURE 2.20(a)

ELSEVIER LICENSE
TERMS AND CONDITIONS

Jan 04, 2019

This Agreement between University of Saskatchewan -- Pedro Cordova ("You") and Elsevier ("Elsevier") consists of your license details and the terms and conditions provided by Elsevier and Copyright Clearance Center.

License Number	4481691137340
License date	Dec 03, 2018
Licensed Content Publisher	Elsevier
Licensed Content Publication	Composites Science and Technology
Licensed Content Title	Effect of secondary bending on strength prediction of composite, single shear lap joints
Licensed Content Author	Johan Ekh,Joakim Schön
Licensed Content Date	May 1, 2005
Licensed Content Volume	65
Licensed Content Issue	6
Licensed Content Pages	13
Start Page	953
End Page	965
Type of Use	reuse in a thesis/dissertation
Intended publisher of new work	other
Portion	figures/tables/illustrations
Number of figures/tables/illustrations	1
Format	both print and electronic
Are you the author of this Elsevier article?	No
Will you be translating?	No
Original figure numbers	Figure 6
Title of your thesis/dissertation	Fretting fatigue in steel bolted connections.
Expected completion date	Dec 2018
Estimated size (number of pages)	175
Requestor Location	University of Saskatchewan 105 Administration Place Saskatoon, SK S7N 5A2 Canada Attn: University of Saskatchewan
Publisher Tax ID	GB 494 6272 12
Total	0.00 CAD

Terms and Conditions

INTRODUCTION

1. The publisher for this copyrighted material is Elsevier. By clicking "accept" in connection with completing this licensing transaction, you agree that the following terms and conditions apply to this transaction (along with the Billing and Payment terms and conditions established by Copyright Clearance Center, Inc. ("CCC"), at the time that you opened your Rightslink account and that are available at any time at http://myaccount.copyright.com).

GENERAL TERMS

2. Elsevier hereby grants you permission to reproduce the aforementioned material subject to the terms and conditions indicated.
3. Acknowledgement: If any part of the material to be used (for example, figures) has appeared in our publication with credit or acknowledgement to another source, permission must also be sought from that source. If such permission is not obtained then that material may not be included in your publication/copies. Suitable acknowledgement to the source must be made, either as a footnote or in a reference list at the end of your publication, as follows:
"Reprinted from Publication title, Vol /edition number, Author(s), Title of article / title of chapter, Pages No., Copyright (Year), with permission from Elsevier [OR APPLICABLE SOCIETY COPYRIGHT OWNER]." Also Lancet special credit - "Reprinted from The Lancet, Vol. number, Author(s), Title of article, Pages No., Copyright (Year), with permission from Elsevier."
4. Reproduction of this material is confined to the purpose and/or media for which permission is hereby given.
5. Altering/Modifying Material: Not Permitted. However figures and illustrations may be altered/adapted minimally to serve your work. Any other abbreviations, additions, deletions and/or any other alterations shall be made only with prior written authorization of Elsevier Ltd. (Please contact Elsevier at permissions@elsevier.com). No modifications can be made to any Lancet figures/tables and they must be reproduced in full.
6. If the permission fee for the requested use of our material is waived in this instance, please be advised that your future requests for Elsevier materials may attract a fee.
7. Reservation of Rights: Publisher reserves all rights not specifically granted in the combination of (i) the license details provided by you and accepted in the course of this licensing transaction, (ii) these terms and conditions and (iii) CCC's Billing and Payment terms and conditions.
8. License Contingent Upon Payment: While you may exercise the rights licensed immediately upon issuance of the license at the end of the licensing process for the transaction, provided that you have disclosed complete and accurate details of your proposed use, no license is finally effective unless and until full payment is received from you (either by publisher or by CCC) as provided in CCC's Billing and Payment terms and conditions. If full payment is not received on a timely basis, then any license preliminarily granted shall be deemed automatically revoked and shall be void as if never granted. Further, in the event that you breach any of these terms and conditions or any of CCC's Billing and Payment terms and conditions, the license is automatically revoked and shall be void as if never granted. Use of materials as described in a revoked license, as well as any use of the materials beyond the scope of an unrevoked license, may constitute copyright infringement and publisher reserves the right to take any and all action to protect its copyright in the materials.
9. Warranties: Publisher makes no representations or warranties with respect to the licensed material.
10. Indemnity: You hereby indemnify and agree to hold harmless publisher and CCC, and their respective officers, directors, employees and agents, from and against any and all claims arising out of your use of the licensed material other than as specifically authorized pursuant to this license.

11. No Transfer of License: This license is personal to you and may not be sublicensed, assigned, or transferred by you to any other person without publisher's written permission.
12. No Amendment Except in Writing: This license may not be amended except in a writing signed by both parties (or, in the case of publisher, by CCC on publisher's behalf).
13. Objection to Contrary Terms: Publisher hereby objects to any terms contained in any purchase order, acknowledgment, check endorsement or other writing prepared by you, which terms are inconsistent with these terms and conditions or CCC's Billing and Payment terms and conditions. These terms and conditions, together with CCC's Billing and Payment terms and conditions (which are incorporated herein), comprise the entire agreement between you and publisher (and CCC) concerning this licensing transaction. In the event of any conflict between your obligations established by these terms and conditions and those established by CCC's Billing and Payment terms and conditions, these terms and conditions shall control.
14. Revocation: Elsevier or Copyright Clearance Center may deny the permissions described in this License at their sole discretion, for any reason or no reason, with a full refund payable to you. Notice of such denial will be made using the contact information provided by you. Failure to receive such notice will not alter or invalidate the denial. In no event will Elsevier or Copyright Clearance Center be responsible or liable for any costs, expenses or damage incurred by you as a result of a denial of your permission request, other than a refund of the amount(s) paid by you to Elsevier and/or Copyright Clearance Center for denied permissions.

LIMITED LICENSE

The following terms and conditions apply only to specific license types:
15. **Translation**: This permission is granted for non-exclusive world **English** rights only unless your license was granted for translation rights. If you licensed translation rights you may only translate this content into the languages you requested. A professional translator must perform all translations and reproduce the content word for word preserving the integrity of the article.
16. **Posting licensed content on any Website**: The following terms and conditions apply as follows: Licensing material from an Elsevier journal: All content posted to the web site must maintain the copyright information line on the bottom of each image; A hyper-text must be included to the Homepage of the journal from which you are licensing at http://www.sciencedirect.com/science/journal/xxxxx or the Elsevier homepage for books at http://www.elsevier.com; Central Storage: This license does not include permission for a scanned version of the material to be stored in a central repository such as that provided by Heron/XanEdu.
Licensing material from an Elsevier book: A hyper-text link must be included to the Elsevier homepage at http://www.elsevier.com . All content posted to the web site must maintain the copyright information line on the bottom of each image.

Posting licensed content on Electronic reserve: In addition to the above the following clauses are applicable: The web site must be password-protected and made available only to bona fide students registered on a relevant course. This permission is granted for 1 year only. You may obtain a new license for future website posting.
17. **For journal authors:** the following clauses are applicable in addition to the above:
Preprints:
A preprint is an author's own write-up of research results and analysis, it has not been peer-reviewed, nor has it had any other value added to it by a publisher (such as formatting, copyright, technical enhancement etc.).
Authors can share their preprints anywhere at any time. Preprints should not be added to or enhanced in any way in order to appear more like, or to substitute for, the final versions of articles however authors can update their preprints on arXiv or RePEc with their Accepted Author Manuscript (see below).

If accepted for publication, we encourage authors to link from the preprint to their formal publication via its DOI. Millions of researchers have access to the formal publications on ScienceDirect, and so links will help users to find, access, cite and use the best available version. Please note that Cell Press, The Lancet and some society-owned have different preprint policies. Information on these policies is available on the journal homepage.
Accepted Author Manuscripts: An accepted author manuscript is the manuscript of an article that has been accepted for publication and which typically includes author-incorporated changes suggested during submission, peer review and editor-author communications.
Authors can share their accepted author manuscript:

- immediately
  - via their non-commercial person homepage or blog
  - by updating a preprint in arXiv or RePEc with the accepted manuscript
  - via their research institute or institutional repository for internal institutional uses or as part of an invitation-only research collaboration work-group
  - directly by providing copies to their students or to research collaborators for their personal use
  - for private scholarly sharing as part of an invitation-only work group on commercial sites with which Elsevier has an agreement
- After the embargo period
  - via non-commercial hosting platforms such as their institutional repository
  - via commercial sites with which Elsevier has an agreement

In all cases accepted manuscripts should:

- link to the formal publication via its DOI
- bear a CC-BY-NC-ND license - this is easy to do
- if aggregated with other manuscripts, for example in a repository or other site, be shared in alignment with our hosting policy not be added to or enhanced in any way to appear more like, or to substitute for, the published journal article.

Published journal article (JPA): A published journal article (PJA) is the definitive final record of published research that appears or will appear in the journal and embodies all value-adding publishing activities including peer review co-ordination, copy-editing, formatting, (if relevant) pagination and online enrichment.
Policies for sharing publishing journal articles differ for subscription and gold open access articles:
Subscription Articles: If you are an author, please share a link to your article rather than the full-text. Millions of researchers have access to the formal publications on ScienceDirect, and so links will help your users to find, access, cite, and use the best available version.
Theses and dissertations which contain embedded PJAs as part of the formal submission can be posted publicly by the awarding institution with DOI links back to the formal publications on ScienceDirect.
If you are affiliated with a library that subscribes to ScienceDirect you have additional private sharing rights for others' research accessed under that agreement. This includes use for classroom teaching and internal training at the institution (including use in course packs and courseware programs), and inclusion of the article for grant funding purposes.
Gold Open Access Articles: May be shared according to the author-selected end-user license and should contain a CrossMark logo, the end user license, and a DOI link to the formal publication on ScienceDirect.
Please refer to Elsevier's posting policy for further information.
18. **For book authors** the following clauses are applicable in addition to the above:
Authors are permitted to place a brief summary of their work online only. You are not

allowed to download and post the published electronic version of your chapter, nor may you scan the printed edition to create an electronic version. **Posting to a repository:** Authors are permitted to post a summary of their chapter only in their institution's repository.
19. **Thesis/Dissertation**: If your license is for use in a thesis/dissertation your thesis may be submitted to your institution in either print or electronic form. Should your thesis be published commercially, please reapply for permission. These requirements include permission for the Library and Archives of Canada to supply single copies, on demand, of the complete thesis and include permission for Proquest/UMI to supply single copies, on demand, of the complete thesis. Should your thesis be published commercially, please reapply for permission. Theses and dissertations which contain embedded PJAs as part of the formal submission can be posted publicly by the awarding institution with DOI links back to the formal publications on ScienceDirect.

Elsevier Open Access Terms and Conditions
You can publish open access with Elsevier in hundreds of open access journals or in nearly 2000 established subscription journals that support open access publishing. Permitted third party re-use of these open access articles is defined by the author's choice of Creative Commons user license. See our open access license policy for more information.
Terms & Conditions applicable to all Open Access articles published with Elsevier:
Any reuse of the article must not represent the author as endorsing the adaptation of the article nor should the article be modified in such a way as to damage the author's honour or reputation. If any changes have been made, such changes must be clearly indicated.
The author(s) must be appropriately credited and we ask that you include the end user license and a DOI link to the formal publication on ScienceDirect.
If any part of the material to be used (for example, figures) has appeared in our publication with credit or acknowledgement to another source it is the responsibility of the user to ensure their reuse complies with the terms and conditions determined by the rights holder.
Additional Terms & Conditions applicable to each Creative Commons user license:
CC BY: The CC-BY license allows users to copy, to create extracts, abstracts and new works from the Article, to alter and revise the Article and to make commercial use of the Article (including reuse and/or resale of the Article by commercial entities), provided the user gives appropriate credit (with a link to the formal publication through the relevant DOI), provides a link to the license, indicates if changes were made and the licensor is not represented as endorsing the use made of the work. The full details of the license are available at http://creativecommons.org/licenses/by/4.0.
CC BY NC SA: The CC BY-NC-SA license allows users to copy, to create extracts, abstracts and new works from the Article, to alter and revise the Article, provided this is not done for commercial purposes, and that the user gives appropriate credit (with a link to the formal publication through the relevant DOI), provides a link to the license, indicates if changes were made and the licensor is not represented as endorsing the use made of the work. Further, any new works must be made available on the same conditions. The full details of the license are available at http://creativecommons.org/licenses/by-nc-sa/4.0.
CC BY NC ND: The CC BY-NC-ND license allows users to copy and distribute the Article, provided this is not done for commercial purposes and further does not permit distribution of the Article if it is changed or edited in any way, and provided the user gives appropriate credit (with a link to the formal publication through the relevant DOI), provides a link to the license, and that the licensor is not represented as endorsing the use made of the work. The full details of the license are available at http://creativecommons.org/licenses/by-nc-nd/4.0.
Any commercial reuse of Open Access articles published with a CC BY NC SA or CC BY NC ND license requires permission from Elsevier and will be subject to a fee.
Commercial reuse includes:

- Associating advertising with the full text of the Article
- Charging fees for document delivery or access

- Article aggregation
- Systematic distribution via e-mail lists or share buttons

Posting or linking by commercial companies for use by customers of those companies.

20. **Other Conditions**:

v1.9

Questions? customercare@copyright.com or +1-855-239-3415 (toll free in the US) or +1-978-646-2777.

APPENDIX N: COPYRIGHT PERMISSION FOR FIGURE 2.20(b)

ELSEVIER LICENSE
TERMS AND CONDITIONS

Jan 04, 2019

This Agreement between University of Saskatchewan -- Pedro Cordova ("You") and Elsevier ("Elsevier") consists of your license details and the terms and conditions provided by Elsevier and Copyright Clearance Center.

License Number	4481691307022
License date	Dec 03, 2018
Licensed Content Publisher	Elsevier
Licensed Content Publication	Composites Part B: Engineering
Licensed Content Title	Secondary bending in multi fastener, composite-to-aluminium single shear lap joints
Licensed Content Author	Johan Ekh,Joakim Schön,L. Gunnar Melin
Licensed Content Date	Apr 1, 2005
Licensed Content Volume	36
Licensed Content Issue	3
Licensed Content Pages	14
Start Page	195
End Page	208
Type of Use	reuse in a thesis/dissertation
Intended publisher of new work	other
Portion	figures/tables/illustrations
Number of figures/tables/illustrations	1
Format	both print and electronic
Are you the author of this Elsevier article?	No
Will you be translating?	No
Original figure numbers	Figure 8
Title of your thesis/dissertation	Fretting fatigue in steel bolted connections.
Expected completion date	Dec 2018
Estimated size (number of pages)	175
Requestor Location	University of Saskatchewan 105 Administration Place Saskatoon, SK S7N 5A2 Canada Attn: University of Saskatchewan
Publisher Tax ID	GB 494 6272 12
Total	0.00 CAD

Terms and Conditions

INTRODUCTION

1. The publisher for this copyrighted material is Elsevier. By clicking "accept" in connection with completing this licensing transaction, you agree that the following terms and conditions apply to this transaction (along with the Billing and Payment terms and conditions established by Copyright Clearance Center, Inc. ("CCC"), at the time that you opened your Rightslink account and that are available at any time at http://myaccount.copyright.com).

GENERAL TERMS

2. Elsevier hereby grants you permission to reproduce the aforementioned material subject to the terms and conditions indicated.
3. Acknowledgement: If any part of the material to be used (for example, figures) has appeared in our publication with credit or acknowledgement to another source, permission must also be sought from that source. If such permission is not obtained then that material may not be included in your publication/copies. Suitable acknowledgement to the source must be made, either as a footnote or in a reference list at the end of your publication, as follows:
"Reprinted from Publication title, Vol /edition number, Author(s), Title of article / title of chapter, Pages No., Copyright (Year), with permission from Elsevier [OR APPLICABLE SOCIETY COPYRIGHT OWNER]." Also Lancet special credit - "Reprinted from The Lancet, Vol. number, Author(s), Title of article, Pages No., Copyright (Year), with permission from Elsevier."
4. Reproduction of this material is confined to the purpose and/or media for which permission is hereby given.
5. Altering/Modifying Material: Not Permitted. However figures and illustrations may be altered/adapted minimally to serve your work. Any other abbreviations, additions, deletions and/or any other alterations shall be made only with prior written authorization of Elsevier Ltd. (Please contact Elsevier at permissions@elsevier.com). No modifications can be made to any Lancet figures/tables and they must be reproduced in full.
6. If the permission fee for the requested use of our material is waived in this instance, please be advised that your future requests for Elsevier materials may attract a fee.
7. Reservation of Rights: Publisher reserves all rights not specifically granted in the combination of (i) the license details provided by you and accepted in the course of this licensing transaction, (ii) these terms and conditions and (iii) CCC's Billing and Payment terms and conditions.
8. License Contingent Upon Payment: While you may exercise the rights licensed immediately upon issuance of the license at the end of the licensing process for the transaction, provided that you have disclosed complete and accurate details of your proposed use, no license is finally effective unless and until full payment is received from you (either by publisher or by CCC) as provided in CCC's Billing and Payment terms and conditions. If full payment is not received on a timely basis, then any license preliminarily granted shall be deemed automatically revoked and shall be void as if never granted. Further, in the event that you breach any of these terms and conditions or any of CCC's Billing and Payment terms and conditions, the license is automatically revoked and shall be void as if never granted. Use of materials as described in a revoked license, as well as any use of the materials beyond the scope of an unrevoked license, may constitute copyright infringement and publisher reserves the right to take any and all action to protect its copyright in the materials.
9. Warranties: Publisher makes no representations or warranties with respect to the licensed material.
10. Indemnity: You hereby indemnify and agree to hold harmless publisher and CCC, and their respective officers, directors, employees and agents, from and against any and all claims arising out of your use of the licensed material other than as specifically authorized pursuant to this license.

11. No Transfer of License: This license is personal to you and may not be sublicensed, assigned, or transferred by you to any other person without publisher's written permission.
12. No Amendment Except in Writing: This license may not be amended except in a writing signed by both parties (or, in the case of publisher, by CCC on publisher's behalf).
13. Objection to Contrary Terms: Publisher hereby objects to any terms contained in any purchase order, acknowledgment, check endorsement or other writing prepared by you, which terms are inconsistent with these terms and conditions or CCC's Billing and Payment terms and conditions. These terms and conditions, together with CCC's Billing and Payment terms and conditions (which are incorporated herein), comprise the entire agreement between you and publisher (and CCC) concerning this licensing transaction. In the event of any conflict between your obligations established by these terms and conditions and those established by CCC's Billing and Payment terms and conditions, these terms and conditions shall control.
14. Revocation: Elsevier or Copyright Clearance Center may deny the permissions described in this License at their sole discretion, for any reason or no reason, with a full refund payable to you. Notice of such denial will be made using the contact information provided by you. Failure to receive such notice will not alter or invalidate the denial. In no event will Elsevier or Copyright Clearance Center be responsible or liable for any costs, expenses or damage incurred by you as a result of a denial of your permission request, other than a refund of the amount(s) paid by you to Elsevier and/or Copyright Clearance Center for denied permissions.

LIMITED LICENSE

The following terms and conditions apply only to specific license types:
15. **Translation**: This permission is granted for non-exclusive world **English** rights only unless your license was granted for translation rights. If you licensed translation rights you may only translate this content into the languages you requested. A professional translator must perform all translations and reproduce the content word for word preserving the integrity of the article.
16. **Posting licensed content on any Website**: The following terms and conditions apply as follows: Licensing material from an Elsevier journal: All content posted to the web site must maintain the copyright information line on the bottom of each image; A hyper-text must be included to the Homepage of the journal from which you are licensing at http://www.sciencedirect.com/science/journal/xxxxx or the Elsevier homepage for books at http://www.elsevier.com; Central Storage: This license does not include permission for a scanned version of the material to be stored in a central repository such as that provided by Heron/XanEdu.
Licensing material from an Elsevier book: A hyper-text link must be included to the Elsevier homepage at http://www.elsevier.com . All content posted to the web site must maintain the copyright information line on the bottom of each image.

Posting licensed content on Electronic reserve: In addition to the above the following clauses are applicable: The web site must be password-protected and made available only to bona fide students registered on a relevant course. This permission is granted for 1 year only. You may obtain a new license for future website posting.
17. **For journal authors:** the following clauses are applicable in addition to the above:
Preprints:
A preprint is an author's own write-up of research results and analysis, it has not been peer-reviewed, nor has it had any other value added to it by a publisher (such as formatting, copyright, technical enhancement etc.).
Authors can share their preprints anywhere at any time. Preprints should not be added to or enhanced in any way in order to appear more like, or to substitute for, the final versions of articles however authors can update their preprints on arXiv or RePEc with their Accepted Author Manuscript (see below).

If accepted for publication, we encourage authors to link from the preprint to their formal publication via its DOI. Millions of researchers have access to the formal publications on ScienceDirect, and so links will help users to find, access, cite and use the best available version. Please note that Cell Press, The Lancet and some society-owned have different preprint policies. Information on these policies is available on the journal homepage.
Accepted Author Manuscripts: An accepted author manuscript is the manuscript of an article that has been accepted for publication and which typically includes author-incorporated changes suggested during submission, peer review and editor-author communications.
Authors can share their accepted author manuscript:

- immediately
  - via their non-commercial person homepage or blog
  - by updating a preprint in arXiv or RePEc with the accepted manuscript
  - via their research institute or institutional repository for internal institutional uses or as part of an invitation-only research collaboration work-group
  - directly by providing copies to their students or to research collaborators for their personal use
  - for private scholarly sharing as part of an invitation-only work group on commercial sites with which Elsevier has an agreement
- After the embargo period
  - via non-commercial hosting platforms such as their institutional repository
  - via commercial sites with which Elsevier has an agreement

In all cases accepted manuscripts should:

- link to the formal publication via its DOI
- bear a CC-BY-NC-ND license - this is easy to do
- if aggregated with other manuscripts, for example in a repository or other site, be shared in alignment with our hosting policy not be added to or enhanced in any way to appear more like, or to substitute for, the published journal article.

Published journal article (JPA): A published journal article (PJA) is the definitive final record of published research that appears or will appear in the journal and embodies all value-adding publishing activities including peer review co-ordination, copy-editing, formatting, (if relevant) pagination and online enrichment.
Policies for sharing publishing journal articles differ for subscription and gold open access articles:
Subscription Articles: If you are an author, please share a link to your article rather than the full-text. Millions of researchers have access to the formal publications on ScienceDirect, and so links will help your users to find, access, cite, and use the best available version.
Theses and dissertations which contain embedded PJAs as part of the formal submission can be posted publicly by the awarding institution with DOI links back to the formal publications on ScienceDirect.
If you are affiliated with a library that subscribes to ScienceDirect you have additional private sharing rights for others' research accessed under that agreement. This includes use for classroom teaching and internal training at the institution (including use in course packs and courseware programs), and inclusion of the article for grant funding purposes.
Gold Open Access Articles: May be shared according to the author-selected end-user license and should contain a CrossMark logo, the end user license, and a DOI link to the formal publication on ScienceDirect.
Please refer to Elsevier's posting policy for further information.
18. **For book authors** the following clauses are applicable in addition to the above:
Authors are permitted to place a brief summary of their work online only. You are not

allowed to download and post the published electronic version of your chapter, nor may you scan the printed edition to create an electronic version. **Posting to a repository:** Authors are permitted to post a summary of their chapter only in their institution's repository.
19. **Thesis/Dissertation**: If your license is for use in a thesis/dissertation your thesis may be submitted to your institution in either print or electronic form. Should your thesis be published commercially, please reapply for permission. These requirements include permission for the Library and Archives of Canada to supply single copies, on demand, of the complete thesis and include permission for Proquest/UMI to supply single copies, on demand, of the complete thesis. Should your thesis be published commercially, please reapply for permission. Theses and dissertations which contain embedded PJAs as part of the formal submission can be posted publicly by the awarding institution with DOI links back to the formal publications on ScienceDirect.

Elsevier Open Access Terms and Conditions
You can publish open access with Elsevier in hundreds of open access journals or in nearly 2000 established subscription journals that support open access publishing. Permitted third party re-use of these open access articles is defined by the author's choice of Creative Commons user license. See our open access license policy for more information.
Terms & Conditions applicable to all Open Access articles published with Elsevier:
Any reuse of the article must not represent the author as endorsing the adaptation of the article nor should the article be modified in such a way as to damage the author's honour or reputation. If any changes have been made, such changes must be clearly indicated.
The author(s) must be appropriately credited and we ask that you include the end user license and a DOI link to the formal publication on ScienceDirect.
If any part of the material to be used (for example, figures) has appeared in our publication with credit or acknowledgement to another source it is the responsibility of the user to ensure their reuse complies with the terms and conditions determined by the rights holder.
Additional Terms & Conditions applicable to each Creative Commons user license:
CC BY: The CC-BY license allows users to copy, to create extracts, abstracts and new works from the Article, to alter and revise the Article and to make commercial use of the Article (including reuse and/or resale of the Article by commercial entities), provided the user gives appropriate credit (with a link to the formal publication through the relevant DOI), provides a link to the license, indicates if changes were made and the licensor is not represented as endorsing the use made of the work. The full details of the license are available at http://creativecommons.org/licenses/by/4.0.
CC BY NC SA: The CC BY-NC-SA license allows users to copy, to create extracts, abstracts and new works from the Article, to alter and revise the Article, provided this is not done for commercial purposes, and that the user gives appropriate credit (with a link to the formal publication through the relevant DOI), provides a link to the license, indicates if changes were made and the licensor is not represented as endorsing the use made of the work. Further, any new works must be made available on the same conditions. The full details of the license are available at http://creativecommons.org/licenses/by-nc-sa/4.0.
CC BY NC ND: The CC BY-NC-ND license allows users to copy and distribute the Article, provided this is not done for commercial purposes and further does not permit distribution of the Article if it is changed or edited in any way, and provided the user gives appropriate credit (with a link to the formal publication through the relevant DOI), provides a link to the license, and that the licensor is not represented as endorsing the use made of the work. The full details of the license are available at http://creativecommons.org/licenses/by-nc-nd/4.0.
Any commercial reuse of Open Access articles published with a CC BY NC SA or CC BY NC ND license requires permission from Elsevier and will be subject to a fee.
Commercial reuse includes:

- Associating advertising with the full text of the Article
- Charging fees for document delivery or access

- Article aggregation
- Systematic distribution via e-mail lists or share buttons

Posting or linking by commercial companies for use by customers of those companies.

20. **Other Conditions**:

v1.9

Questions? customercare@copyright.com or +1-855-239-3415 (toll free in the US) or +1-978-646-2777.

APPENDIX O: COPYRIGHT PERMISSION FOR FIGURE 2.21

ELSEVIER LICENSE
TERMS AND CONDITIONS

Jan 04, 2019

This Agreement between University of Saskatchewan -- Pedro Cordova ("You") and Elsevier ("Elsevier") consists of your license details and the terms and conditions provided by Elsevier and Copyright Clearance Center.

License Number	4481691482503
License date	Dec 03, 2018
Licensed Content Publisher	Elsevier
Licensed Content Publication	Engineering Failure Analysis
Licensed Content Title	Effect of torque tightening on the fatigue strength of bolted joints
Licensed Content Author	José María Mínguez,Jeffrey Vogwell
Licensed Content Date	Dec 1, 2006
Licensed Content Volume	13
Licensed Content Issue	8
Licensed Content Pages	12
Start Page	1410
End Page	1421
Type of Use	reuse in a thesis/dissertation
Intended publisher of new work	other
Portion	figures/tables/illustrations
Number of figures/tables/illustrations	1
Format	both print and electronic
Are you the author of this Elsevier article?	No
Will you be translating?	No
Original figure numbers	Figure 4
Title of your thesis/dissertation	Fretting fatigue in steel bolted connections.
Expected completion date	Dec 2018
Estimated size (number of pages)	175
Requestor Location	University of Saskatchewan 105 Administration Place Saskatoon, SK S7N 5A2 Canada Attn: University of Saskatchewan
Publisher Tax ID	GB 494 6272 12
Total	0.00 CAD

Terms and Conditions

INTRODUCTION

1. The publisher for this copyrighted material is Elsevier. By clicking "accept" in connection with completing this licensing transaction, you agree that the following terms and conditions apply to this transaction (along with the Billing and Payment terms and conditions established by Copyright Clearance Center, Inc. ("CCC"), at the time that you opened your Rightslink account and that are available at any time at http://myaccount.copyright.com).

GENERAL TERMS

2. Elsevier hereby grants you permission to reproduce the aforementioned material subject to the terms and conditions indicated.
3. Acknowledgement: If any part of the material to be used (for example, figures) has appeared in our publication with credit or acknowledgement to another source, permission must also be sought from that source. If such permission is not obtained then that material may not be included in your publication/copies. Suitable acknowledgement to the source must be made, either as a footnote or in a reference list at the end of your publication, as follows:
"Reprinted from Publication title, Vol /edition number, Author(s), Title of article / title of chapter, Pages No., Copyright (Year), with permission from Elsevier [OR APPLICABLE SOCIETY COPYRIGHT OWNER]." Also Lancet special credit - "Reprinted from The Lancet, Vol. number, Author(s), Title of article, Pages No., Copyright (Year), with permission from Elsevier."
4. Reproduction of this material is confined to the purpose and/or media for which permission is hereby given.
5. Altering/Modifying Material: Not Permitted. However figures and illustrations may be altered/adapted minimally to serve your work. Any other abbreviations, additions, deletions and/or any other alterations shall be made only with prior written authorization of Elsevier Ltd. (Please contact Elsevier at permissions@elsevier.com). No modifications can be made to any Lancet figures/tables and they must be reproduced in full.
6. If the permission fee for the requested use of our material is waived in this instance, please be advised that your future requests for Elsevier materials may attract a fee.
7. Reservation of Rights: Publisher reserves all rights not specifically granted in the combination of (i) the license details provided by you and accepted in the course of this licensing transaction, (ii) these terms and conditions and (iii) CCC's Billing and Payment terms and conditions.
8. License Contingent Upon Payment: While you may exercise the rights licensed immediately upon issuance of the license at the end of the licensing process for the transaction, provided that you have disclosed complete and accurate details of your proposed use, no license is finally effective unless and until full payment is received from you (either by publisher or by CCC) as provided in CCC's Billing and Payment terms and conditions. If full payment is not received on a timely basis, then any license preliminarily granted shall be deemed automatically revoked and shall be void as if never granted. Further, in the event that you breach any of these terms and conditions or any of CCC's Billing and Payment terms and conditions, the license is automatically revoked and shall be void as if never granted. Use of materials as described in a revoked license, as well as any use of the materials beyond the scope of an unrevoked license, may constitute copyright infringement and publisher reserves the right to take any and all action to protect its copyright in the materials.
9. Warranties: Publisher makes no representations or warranties with respect to the licensed material.
10. Indemnity: You hereby indemnify and agree to hold harmless publisher and CCC, and their respective officers, directors, employees and agents, from and against any and all claims arising out of your use of the licensed material other than as specifically authorized pursuant to this license.

11. No Transfer of License: This license is personal to you and may not be sublicensed, assigned, or transferred by you to any other person without publisher's written permission.
12. No Amendment Except in Writing: This license may not be amended except in a writing signed by both parties (or, in the case of publisher, by CCC on publisher's behalf).
13. Objection to Contrary Terms: Publisher hereby objects to any terms contained in any purchase order, acknowledgment, check endorsement or other writing prepared by you, which terms are inconsistent with these terms and conditions or CCC's Billing and Payment terms and conditions. These terms and conditions, together with CCC's Billing and Payment terms and conditions (which are incorporated herein), comprise the entire agreement between you and publisher (and CCC) concerning this licensing transaction. In the event of any conflict between your obligations established by these terms and conditions and those established by CCC's Billing and Payment terms and conditions, these terms and conditions shall control.
14. Revocation: Elsevier or Copyright Clearance Center may deny the permissions described in this License at their sole discretion, for any reason or no reason, with a full refund payable to you. Notice of such denial will be made using the contact information provided by you. Failure to receive such notice will not alter or invalidate the denial. In no event will Elsevier or Copyright Clearance Center be responsible or liable for any costs, expenses or damage incurred by you as a result of a denial of your permission request, other than a refund of the amount(s) paid by you to Elsevier and/or Copyright Clearance Center for denied permissions.

LIMITED LICENSE

The following terms and conditions apply only to specific license types:
15. **Translation**: This permission is granted for non-exclusive world **English** rights only unless your license was granted for translation rights. If you licensed translation rights you may only translate this content into the languages you requested. A professional translator must perform all translations and reproduce the content word for word preserving the integrity of the article.
16. **Posting licensed content on any Website**: The following terms and conditions apply as follows: Licensing material from an Elsevier journal: All content posted to the web site must maintain the copyright information line on the bottom of each image; A hyper-text must be included to the Homepage of the journal from which you are licensing at http://www.sciencedirect.com/science/journal/xxxxx or the Elsevier homepage for books at http://www.elsevier.com; Central Storage: This license does not include permission for a scanned version of the material to be stored in a central repository such as that provided by Heron/XanEdu.
Licensing material from an Elsevier book: A hyper-text link must be included to the Elsevier homepage at http://www.elsevier.com . All content posted to the web site must maintain the copyright information line on the bottom of each image.

Posting licensed content on Electronic reserve: In addition to the above the following clauses are applicable: The web site must be password-protected and made available only to bona fide students registered on a relevant course. This permission is granted for 1 year only. You may obtain a new license for future website posting.
17. **For journal authors:** the following clauses are applicable in addition to the above:
Preprints:
A preprint is an author's own write-up of research results and analysis, it has not been peer-reviewed, nor has it had any other value added to it by a publisher (such as formatting, copyright, technical enhancement etc.).
Authors can share their preprints anywhere at any time. Preprints should not be added to or enhanced in any way in order to appear more like, or to substitute for, the final versions of articles however authors can update their preprints on arXiv or RePEc with their Accepted Author Manuscript (see below).

If accepted for publication, we encourage authors to link from the preprint to their formal publication via its DOI. Millions of researchers have access to the formal publications on ScienceDirect, and so links will help users to find, access, cite and use the best available version. Please note that Cell Press, The Lancet and some society-owned have different preprint policies. Information on these policies is available on the journal homepage.
Accepted Author Manuscripts: An accepted author manuscript is the manuscript of an article that has been accepted for publication and which typically includes author-incorporated changes suggested during submission, peer review and editor-author communications.
Authors can share their accepted author manuscript:

- immediately
  - via their non-commercial person homepage or blog
  - by updating a preprint in arXiv or RePEc with the accepted manuscript
  - via their research institute or institutional repository for internal institutional uses or as part of an invitation-only research collaboration work-group
  - directly by providing copies to their students or to research collaborators for their personal use
  - for private scholarly sharing as part of an invitation-only work group on commercial sites with which Elsevier has an agreement
- After the embargo period
  - via non-commercial hosting platforms such as their institutional repository
  - via commercial sites with which Elsevier has an agreement

In all cases accepted manuscripts should:

- link to the formal publication via its DOI
- bear a CC-BY-NC-ND license - this is easy to do
- if aggregated with other manuscripts, for example in a repository or other site, be shared in alignment with our hosting policy not be added to or enhanced in any way to appear more like, or to substitute for, the published journal article.

Published journal article (JPA): A published journal article (PJA) is the definitive final record of published research that appears or will appear in the journal and embodies all value-adding publishing activities including peer review co-ordination, copy-editing, formatting, (if relevant) pagination and online enrichment.
Policies for sharing publishing journal articles differ for subscription and gold open access articles:
Subscription Articles: If you are an author, please share a link to your article rather than the full-text. Millions of researchers have access to the formal publications on ScienceDirect, and so links will help your users to find, access, cite, and use the best available version.
Theses and dissertations which contain embedded PJAs as part of the formal submission can be posted publicly by the awarding institution with DOI links back to the formal publications on ScienceDirect.
If you are affiliated with a library that subscribes to ScienceDirect you have additional private sharing rights for others' research accessed under that agreement. This includes use for classroom teaching and internal training at the institution (including use in course packs and courseware programs), and inclusion of the article for grant funding purposes.
Gold Open Access Articles: May be shared according to the author-selected end-user license and should contain a CrossMark logo, the end user license, and a DOI link to the formal publication on ScienceDirect.
Please refer to Elsevier's posting policy for further information.
18. **For book authors** the following clauses are applicable in addition to the above:
Authors are permitted to place a brief summary of their work online only. You are not

allowed to download and post the published electronic version of your chapter, nor may you scan the printed edition to create an electronic version. **Posting to a repository:** Authors are permitted to post a summary of their chapter only in their institution's repository.
19. **Thesis/Dissertation**: If your license is for use in a thesis/dissertation your thesis may be submitted to your institution in either print or electronic form. Should your thesis be published commercially, please reapply for permission. These requirements include permission for the Library and Archives of Canada to supply single copies, on demand, of the complete thesis and include permission for Proquest/UMI to supply single copies, on demand, of the complete thesis. Should your thesis be published commercially, please reapply for permission. Theses and dissertations which contain embedded PJAs as part of the formal submission can be posted publicly by the awarding institution with DOI links back to the formal publications on ScienceDirect.

Elsevier Open Access Terms and Conditions
You can publish open access with Elsevier in hundreds of open access journals or in nearly 2000 established subscription journals that support open access publishing. Permitted third party re-use of these open access articles is defined by the author's choice of Creative Commons user license. See our open access license policy for more information.
Terms & Conditions applicable to all Open Access articles published with Elsevier:
Any reuse of the article must not represent the author as endorsing the adaptation of the article nor should the article be modified in such a way as to damage the author's honour or reputation. If any changes have been made, such changes must be clearly indicated.
The author(s) must be appropriately credited and we ask that you include the end user license and a DOI link to the formal publication on ScienceDirect.
If any part of the material to be used (for example, figures) has appeared in our publication with credit or acknowledgement to another source it is the responsibility of the user to ensure their reuse complies with the terms and conditions determined by the rights holder.
Additional Terms & Conditions applicable to each Creative Commons user license:
CC BY: The CC-BY license allows users to copy, to create extracts, abstracts and new works from the Article, to alter and revise the Article and to make commercial use of the Article (including reuse and/or resale of the Article by commercial entities), provided the user gives appropriate credit (with a link to the formal publication through the relevant DOI), provides a link to the license, indicates if changes were made and the licensor is not represented as endorsing the use made of the work. The full details of the license are available at http://creativecommons.org/licenses/by/4.0.
CC BY NC SA: The CC BY-NC-SA license allows users to copy, to create extracts, abstracts and new works from the Article, to alter and revise the Article, provided this is not done for commercial purposes, and that the user gives appropriate credit (with a link to the formal publication through the relevant DOI), provides a link to the license, indicates if changes were made and the licensor is not represented as endorsing the use made of the work. Further, any new works must be made available on the same conditions. The full details of the license are available at http://creativecommons.org/licenses/by-nc-sa/4.0.
CC BY NC ND: The CC BY-NC-ND license allows users to copy and distribute the Article, provided this is not done for commercial purposes and further does not permit distribution of the Article if it is changed or edited in any way, and provided the user gives appropriate credit (with a link to the formal publication through the relevant DOI), provides a link to the license, and that the licensor is not represented as endorsing the use made of the work. The full details of the license are available at http://creativecommons.org/licenses/by-nc-nd/4.0.
Any commercial reuse of Open Access articles published with a CC BY NC SA or CC BY NC ND license requires permission from Elsevier and will be subject to a fee.
Commercial reuse includes:

- Associating advertising with the full text of the Article
- Charging fees for document delivery or access

- Article aggregation
- Systematic distribution via e-mail lists or share buttons

Posting or linking by commercial companies for use by customers of those companies.

20. **Other Conditions**:

v1.9

Questions? customercare@copyright.com or +1-855-239-3415 (toll free in the US) or +1-978-646-2777.

APPENDIX P: COPYRIGHT PERMISSION FOR FIGURE 2.10

LIMITED CONSENT AGREEMENT FOR COMMERCIAL REPRINTING OF PROTECTED WORKS

Note to Author(s): Please complete all information in Part I and sign and date this agreement in Part III.

Mail to: AISC, 130 E. Randolph St., Suite 2000, Chicago, IL 60601-6204, Attn: Rachel Jordan
Or e-mail to: jordan@aisc.org

Date: 9th of January/2019

PART I: [to be completed by the Author]

The American Institute of Steel Construction ("AISC"), hereby grants a limited, non-transferable, non-exclusive consent to:

Pedro Cordova

[name(s) of Author(s)]

plc831@mail.usask.ca

[address/e-mail/fax number for corresponding author]

(the "Author") to reprint the following copyrighted publications (the "Reprinted Material") titled:

A fatigue primer for structural engineers

[name of the AISC publication from which the Reprinted Material is to be taken]

The portions to be copied are as follows:

Figure 46

[list of pages and/or portions thereof that make up the Reprinted Material]

This limited consent is expressly subject to the following terms and conditions:

1. Limited Use.
   The Reprinted Material is to appear unchanged in text in a publication or standard, password-protected internet-based course, or online posting entitled:
   M.Sc. Thesis title: Fretting fatigue in steel bolted connections
   [name of Publication in which the Reprinted Material will appear; if internet-based course or online posting, please also provide URL]
   (the "Publication"), to be published and distributed by:
   University of Saskatchewan
   [name of Publisher]
   and may not be used or reprinted for any other purpose. This Consent does not authorize any other use beyond the terms of this agreement.

2. Publication.
   The approximate publication date is:
   16th of January 2019
   [date of Publication]
   (the "Publication Date"), and the probable selling price to the public is:
   $0.00

[selling price of Publication in U.S. Dollars per copy]

PART II: [to be completed by AISC]

3. Reproduction Fee.
   AISC requires no payment or royalty for reproduction of the Reprinted Materials, as designated and in consideration of the rights granted herein.

4. Author's Covenants.
   The Author agrees (i) to give full credit to AISC, in the form specified in Section 5 below; (ii) to restrict the use of the Reprinted Material to the Publication; and (iii) if at any time a new edition of the Publication is contemplated, to secure further permission from AISC to use the Reprinted Material therein.

5. Attribution of Ownership.
   The Author shall cause an appropriate notice of the AISC's copyright in the Reprinted Material and the following form of credit to be printed on the copyright page of every copy of the Publication or on each page in which a quotation from the Reprinted Material appears:

   "Copyright © American Institute of Steel Construction
   Reprinted with permission. All rights reserved."

6. Duration of Limited Consent.
   Failure to keep the Publication in print/posted on the internet shall result in the reversion of this right and termination of this limited consent without notice.

PART III: [to be completed by the Author and AISC]
Signed:

[enter signature(s) of Author(s)] [enter date (month day, year)]

American Institute of Steel Construction